UNIVERSITÀ DI PARMA

UNIVERSITÀ DEGLI STUDI DI PARMA

DOTTORATO DI RICERCA IN
"*Scienze Chimiche*"

CICLO XXXII

Calix[6]arene derivatives as tools to tune the properties of their bound guests

Coordinatore:
Chiar.mo Prof. Roberto Corradini

Tutore:
Chiar.mo Prof. Arturo Arduini

Dottorando: Margherita Bazzoni

Anni 2016/2019

Abstract

This PhD dissertation focuses on the potentiality of *host-guest* chemistry as tool to modulate the physical and chemical properties of chemical species through intermolecular interactions. Initially, the ability of tris(*N*-phenylureido) calix[6]arene *hosts* to enhance the reactivity of threaded *N*-alkylpyridylpyridinium salts towards nucleophilic substitutions was exploited to obtain sophisticated molecular architectures. In particular, [3]rotaxanes composed by two non-palindrome calix[6]arene *hosts* and a threaded bisviologen-based dumbbell may exist in three different orientational isomers. The supramolecular assisted approach allowed to obtain all the possible orientational isomers of the [3]rotaxanes with good yields and high control on the reciprocal orientation of the components. Then, the synthesis of a two-stations-two-gates oriented catenane was carried out to examine the possibility to use this MIM as a prototype of a unidirectional rotatory molecular motor. A further significant study explored the influence of the complexation inside a tris(*N*-phenylureido)-calix[6]arene *host* on the spectroscopic behavior of stilbazolium salts, particularly focusing on the role played by the orientation of these *guests* inside the cavity. Lastly, the properties of new bis(*N*-phenylureido)- and bis(*N*-phenylthioureido)-calix[6]arene *hosts* were explored. The impact of the modification of the number/type and geometrical arrangement of the functional groups at the upper rim on the conformation and complexation ability of the *hosts* was investigated.

Contents

Preface

Supramolecular chemistry was born in the '60s, [1] when the importance of the environment on the properties of molecules became the focus of research.[2] This scientific area studies and exploits non-covalent interactions between chemical species to create assemblies endowed with new exciting properties. [3] Artificial nano-sized structures with important applications in drug development, sensing, catalysis could be obtained tailoring the geometrical arrangement of the components.[4, 5] The weak, non-covalent interactions that lead to the formation of self-assembled supramolecular structures may have dramatic effects on the properties of the involved chemical species. Indeed, such interactions impact on the potential energy of the complex and thus its stucture, geometry and properties.[6]. The possibility to exploit the formation of supramolecular assemblies to tune the outcome of chemical reactions is already well studied in literature. Aside from supramolecular catalysis[7] and supramolecular protecting groups, the supramolecular assistance to the synthesis of mechanically interlocked species is gaining increasing interest. This last aspect allows synthesis of supramolecular assemblies with full control of the geometrical organisation of their components, and with good yields. Such ideal control on the components' arrangement inside the supramolecule is crucial to obtain systems characterised by specific stimuli-responsive functions. As an example, intermolecular interactions may have a significant impact on the spectroscopic properties of the involved species, making *host-guest* chemistry a highly convenient tool to create new photo-responsive devices and to tune their stimuli triggered behaviour.
After a brief introduction, this thesis presents research works regarding the calix[6]arene derivatives employed as tools to tune the properties of their bound *guests*. More specifically:

- Chapter 2 is focused on the supramolecularly assisted synthesis of calix[6]arene-based oriented [3]rotaxanes, exploiting the spontaneous self-assembly of the components and the supramolecular assistance given by calixarene wheel to the reactions taking place on the axle. (to form the axle)
- Chapter 3 describes the synthesis of a calix[6]arene-based oriented catenane, characterised by the presence of two stations and two gates

on its track rim, that should allow unidirectional reciprocal movement between the two rings.

- Chapter 4 studies the influence that the complexation inside the non-palindromic cavity of a calix[6]arene *host* has on the spectroscopic behaviour of stilbazonium salts, focusing in particular on the role played by the orientation of the *guest*.

- Chapter 5 investigates the role played by the number, reciprocal orientation and nature of the binding sites at the upper rim of a calix[6]arene *host* on its adopted conformation and binding abilities.

Bibliography

(1) Vicens, J.; Vicens, Q. *J. Incl. Phenom. Macrocycl. Chem.* **2009**, *65*, 221–235.

(2) *Analytical methods in supramolecular chemistry*; Schalley, C. A., Ed.; Wiley-VCH: 2007.

(3) Gale, P. A. *Philosophical Transactions of the Royal Society of London. Series A: Mathematical, Physical and Engineering Sciences* **2000**, *358*, ed. by Thompson, J. M. T., 431–453.

(4) Bhalla, V. *Reson* **2018**, *23*, 277–290.

(5) Gale, P. A.; Steed, J. W., *Supramolecular Chemistry: From Molecules to Nanomaterials*; Wiley-VCH: 2012.

(6) Hobza, P.; Müller-Dethlefs, K., *Non-covalent Interactions: Theory and Experiment*; RSC Publishing: 2010.

(7) Raynal, M.; Ballester, P.; Vidal-Ferran, A.; van Leeuwen, P. W. N. M. *Chem. Soc. Rev.* **2014**, *43*, 1660–1733.

Chapter 1

Introduction

The progress made in the last 50 years in the field of supramolecular chemistry led to impressive systems such as molecules capable of mimic life by self-replication,[1] mixtures of molecules able to self-assemble into racks, ribbons or rosettes,[2] up to the development of the so-called molecular machines. According to Jean-Marie Lehn, supramolecular chemistry can be described as "chemistry beyond the molecule".[3] This scientific area studies and exploits non-covalent interactions between chemical species, like hydrogen bonds, Van der Waals, electrostatic, and $\pi - \pi$ interactions, to create assemblies of two or more components.[4] The control of the arrangement of the components, with the highest degree of precision possible, allows the creation of artificial nano-sized structures with important applications in drug development, sensors, catalysis, nanoscience, molecular devices, etc.[5] These aggregates have new properties and functionalities different from those of the single components.[3–6] Molecular recognition is a fundamental principle of supramolecular chemistry. It is based on the geometrical and electronic complementarity between the involved species and leads to the formation of *host-guest* complexes.[6] A *host* is usually described as a large molecule or aggregate endowed with a central hole or cavity that possesses convergent binding sites. A *guest* could be an ion, a neutral species, or a more complex molecule that exhibits one or more binding sites that are divergent and complementary with respect to those of the *host*.[7] The complex formation is driven by the free energy gain due to the intermolecular interactions that lead to aggregation. These interactions may also modify

the physical, optical and electrochemical properties of either the *guest*, the *host* or both. Based on this, the principles and methods of supramolecular chemistry may represent important tools to tune the reactivity and the desired properties of the *guests*.[8, 9] Supramolecular chemistry is extensively employed by nature to exploit a wide number of biological functions. In particular, enzymes are valuable examples of supramolecular catalysts and of how intermolecular interactions can drive a reaction along the desired pathways. The first step, in both enzymatic and supramolecular catalysis, is the recognition of the substrate guided by specific intermolecular interactions that collocates it close to the catalytic site. The correct orientation of the substrate is crucial to maximize the catalytic effect, generally due to the stabilisation of the transition state of the reaction. Another key factor in catalysis is the turnover, which is the release of the product at the end of a catalytic reaction. In the case of natural enzymes, product inhibition was progressively avoided thanks to evolution. For supramolecular catalysis, the receptor inhibition is instead a crucial factor to be considered during the design of the system. However, in some cases, the increased affinity of the macrocyclic receptor toward its modified substrate after the reaction, can be an important benefit. Indeed, the product of a supramolecularly assisted reaction could be the desired target of the synthesis. This is the case, for example, of some Mechanically Interlocked Molecules (MIMs) such as rotaxanes, catenanes and knots[10], synthesised using an active template approach.[11] MIMs are interlocked systems in which two or more species become connected, not *via* chemical bonds but because they are threaded through or around one another forming a single entity. The number of component species is indicated between square brackets before the name. Interesting examples of the supramolecularly assisted approach to the synthesis of MIMs were recently reported in the literature for the preparation of complexed assemblies.[11–13] They are based on the spontaneous preorganisation of the components along with the assistance of one of them to the reaction that leads to the final MIM or complex. This recently developed approach allowed the synthesis of complex molecular assemblies with full control on the reciprocal orientation of the components and higher yields with respect to the passive template approach. This latter is based on spontaneous self-assembly followed by a capping or clipping reaction. Other notable examples of supramolecular systems are the biological molecular motors that

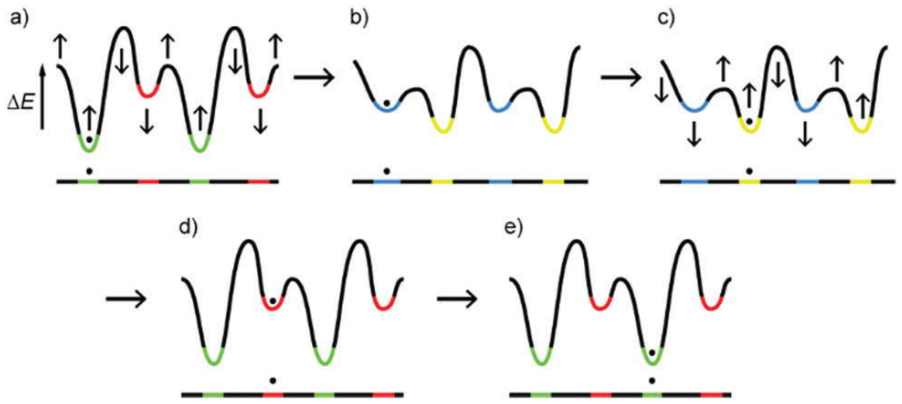

Figure 1.1: Example of a ratchet mechanism. Adapted from ref.[15]. ©The Royal Society of Chemistry, 2017.

have inspired synthetic chemists in the development of artificial molecular machines.[14] These are supramolecular systems in which a suitable external stimulus can promote the relative motion between the components [15] that results in the production of work. In molecular motors, the work carried out during the movement is not cancelled when the system comes back, after a work cycle, to its original state. In this context, the trajectory of the motion is of fundamental importance: only when the initial and return movements are carried out following two different paths the work will not be cancelled. For example, in a catenane the unidirectional rotary motion of the wheel along the tracking macrocycle allows the return of the moving macrocycle to its starting station without the loss of the accomplished work. Contrarywise, in a rotaxane, the work produced during the translation of the wheel from its starting station to the second one is wiped out when the wheel comes back to the starting station, following the same but reverse trajectory. To drive a system out of equilibrium, fundamental and challenging is the possibility to control the trajectory/directionality of the movement.[15]

The directional motion in molecular motors is achieved by exploiting the random thermal fluctuations steered by a ratchet-like mechanism. An energy ratchet can be seen as a periodic series of pairs of energy maxima and minima. The component starts from an energy minimum and, upon

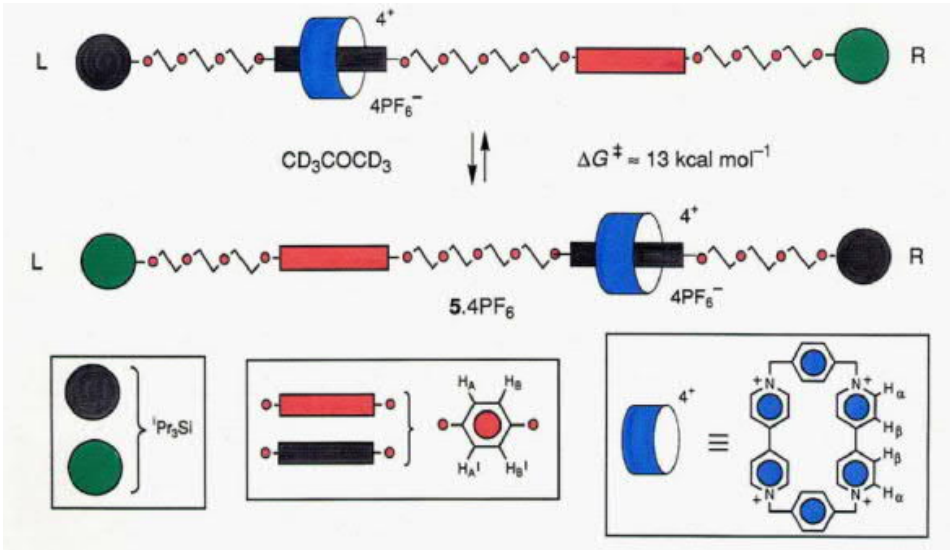

Figure 1.2: The first example of a molecular shuttle based on a [2]rotaxane. Adapted from ref.[16] ©The American Chemical Society, 1991.

the increasing of that minimum's energy and the lowering of the adjacent maximum, it changes position due to its Brownian motion combined with the new surface energy (see figure 1.1).[15] Controlling the change in the relative height of maxima and minima, the direction of the movement can be controlled. The achievement of directional transport at the molecular level requires: i) that the components that are moving one with respect to the other have to remain attached for the whole operation cycle, ii) the existence of a preferential direction for the motion, iii) the possibility to repeat the work cycle that leads to the motion, and iv) the restoration of the initial state at the end of the work cycle, travelling back to the original position along a different trajectory (*vide supra*). MIMs such as rotaxanes and catenanes, briefly introduced above, have been extensively studied as prototypes of molecular machines. Indeed, the mechanical bond restricts the movement between the components in specific directions and permits large-amplitude displacement in other directions. The synthesis of MIMs is generally based on the use of template methods that exploit recognition motifs to guide the blocking or catenation reactions.

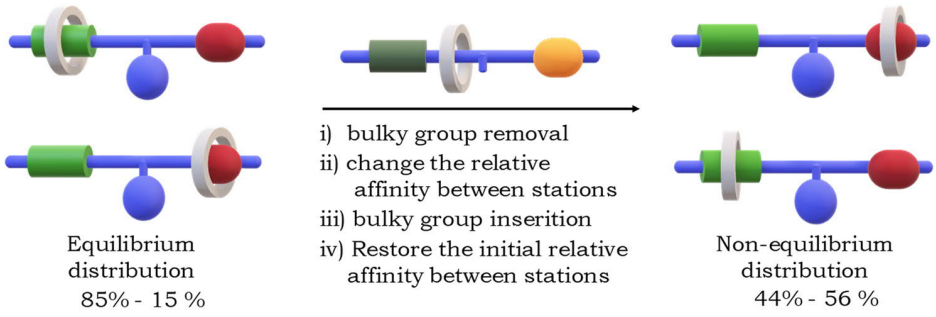

Figure 1.3: Rachet motion mechanism in a [2]rotaxane.

In 1991 Stoddart's group reported the first example of [2]rotaxane molecular shuttle, see figure 1.2. The system presents a temperature-dependent shuttling movement of the macrocyclic component between the two identical stations present on the axle.[16] Three years later, the same group reported the first stimuli-responsive molecular shuttle in which a pH change switches the preferential position of the macrocycle.[17] These preliminary findings paved the way for the synthesis of a large number of switches driven by stimuli of different nature such as pH and temperature variation or electrochemical and light-based inputs. However, the development of molecular motors also needs the introduction of a ratchet mechanism. The Leigh group developed the first system endowed with these features.[18] They prepared a [2]rotaxane characterised by two binding sites on the axle (figure 1.3). The important feature of this system is the possibility to control i)the relative binding affinities of the two sites through the isomerisation of a station and pH variation, and ii) the exchange between the two stations using a bulky group acting as gate. Such arrangement allows to create a non-equilibrium distribution of the two positional isomers of the pseudorotaxane.

This is an example of how the ratchet mechanism applied to a rotaxane allows to create a macrocycle distribution, along the axles, away from equilibrium. However, if the ring cannot dethread the axle from the opposite end with respect to the one used for the threading, the system will reach a steady-state that will not allow to further perform work. To obtain a real molecular motor is thus necessary to design a system in which the

unidirectional motion of a component along the other, obtained through a ratchet mechanism, can be continuously perpetrated. The unidirectional rotatory motion in a catenane is a suitable solution. The first example of control of rotatory motion in a catenane was reported by Sauvage et al. in 1994.[19] In the following decade, the same group reported other examples, but in none of these systems the rotatory motion was unidirectional. Calix[n]arenes are synthetic polyphenolic macrocycles easily obtainable in high yield from the base-catalysed condensation between p-*tert*-buthylphenol and formaldehyde.[20, 21] Tuning the reaction conditions, it is possible to selectively obtain calixarenes with the desired number of phenolic units (4, 6 or 8). Because of the possibility of the intra-annular interconversion of the phenolic unis, calix[n]arenes may adopt several conformations in solution and in the solid-state. In the so-called cone conformation, all the phenolic nuclei are oriented on the same side. Therefore, for a convention, it is possible to identify as the *Upper rim* the one functionalised with the *tert*-butyl groups and as the *Lower rim* the one bearing the hydroxyl groups. These *hosts* have attracted great interest thanks to the high versatility of the post-synthesis functionalisation of their scaffold on both rims.[20, 22, 23] In 2000, Arduini et al. reported the first example of a calix[6]arene used as a wheel for the formation of pseudorotaxanes and rotaxanes.[24] Such *host*, the tris-(N-phenylureido)calix[6]arene **Woct** (see figure 1.4), was characterised by the presence of three phenylureido groups at the upper rim and three methoxy groups and three octyloxy chains in alternate position at the lower rim.

In a solution of weakly polar solvents (chloroform, dichloromethane, benzene or toluene), this calixarene derivative assumes a cone conformation on the NMR time scale, as witnessed by the pattern of signals found in its ^{1}H spectrum taken in $CDCl_3$ (see figure 1.5c). The methylene bridging groups resonate as a pair of doublets with geminal coupling at 3.5 (6 pseudo-equatorial protons) and 4.5 ppm (6 pseudo-axial protons). The methoxy groups resonate as a broad signal at 2.9 ppm since, on the NMR time scale, they are oriented inward the aromatic cavity. The chosen *guests* were, respectively, an N,N'-4,4'-bispyridinium salt functionalised with two octyl chains (**DOV**) for the formation of the pseudorotaxane, and two ω-hydroxydodecyl chains, then stoppered with a diphenylacetate moiety, for the rotaxane. In figure 1.5, is reported the stack plot comparing the

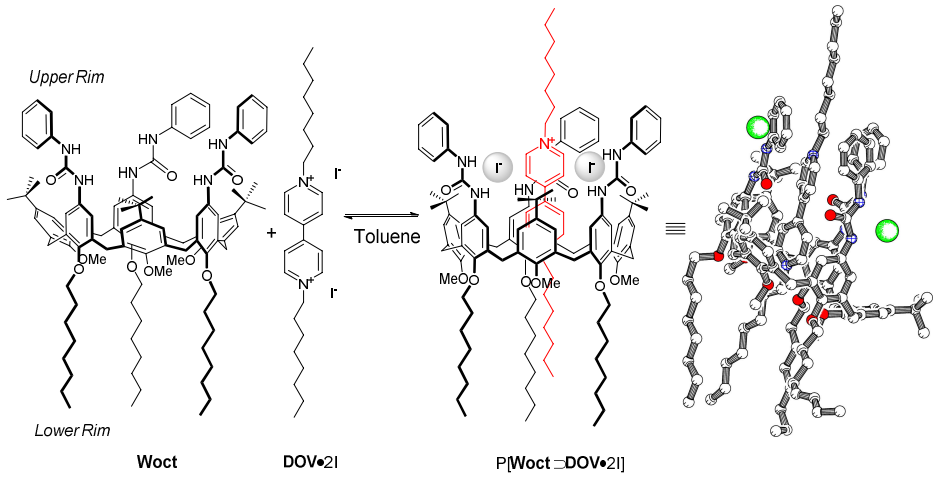

Figure 1.4: Self-assembly in weakly polar solvents such as toluene, benzene or chloroform of a triphenylureido calix[6]arene-based wheel (**Woct**) and an N,N'-dioctyl viologen axle (**DOV·2I**) and X-rays solid-state structure of the resulting pseudorotaxane complex **P[Woct⊃DOV·2I⁻]**.

^{1}H NMR spectra of the wheel **Woct**, the pseudorotaxane complex, and the free axle. Upon complexation, all the signals of the guest are upfield shifted (see figure 1.5b) because of the shielding effect exerted by the electron-rich cavity of the calixarene host.

Thus, the ability of the calixarene **Woct** to take up viologen salts in weakly polar solvent and to form pseudorotaxane structures was demonstrated, and an apparent association constant with a logK $\sim 6 \div 7$ was calculated through UV/vis measurements.[25] This type of complex is stabilised by a plethora of non-covalent intermolecular interactions, as witnessed by the analysis of some X-rays structures.[24, 26] The wheel and the axle are held together by the cooperative action of $\pi - \pi, CH - \pi$ and charge transfer (CT) interactions, but of particular importance in the stabilisation of the complex is the formation of six hydrogen bonds between the three phenylureido groups of the host and the two counteranions of the salt. The association constant is indeed affected by nature of the counteranions of the *guest*, and it increases with more coordinating anion.[25] In the last two decades, calix[6]arene derivatives such as the tris-

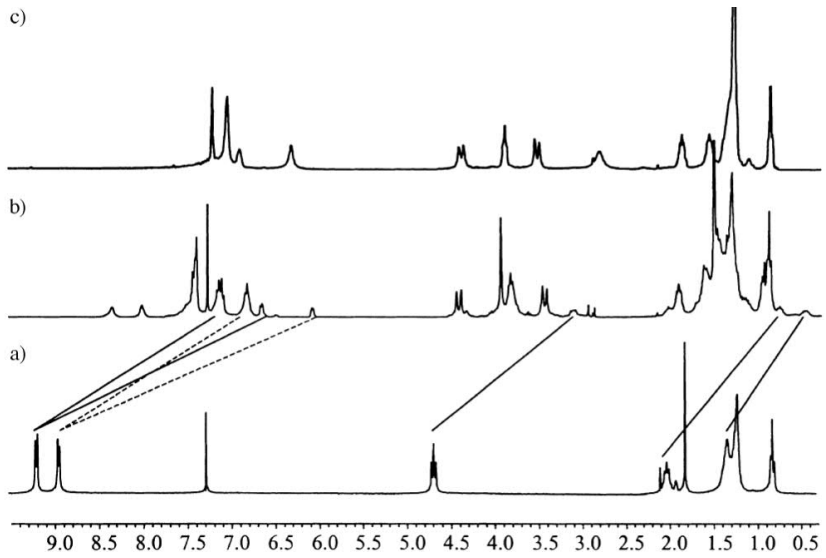

Figure 1.5: ^{1}H NMR stack plot (400 MHz) showing a) **DOV**$\cdot$**2**$^-$] in 10%$CDCl_3/CD_3CN$; b) the pseudorotaxane complex and c) the triphenylureido calix[6]arene wheel **Woct** in $CDCl_3$

(N-phenylureido)calix[6]arene **Woct** and its homologous **WEtOEt**, which possess three ethoxyethyl chains on the lower rim instead of the octyl ones, have been exploited as host for the construction of MIMs.[27, 28] The ability of viologen salts to thread the wheel was thus exploited to obtain pseudorotaxanes complexes that, by using the passive template approach eventually led to the synthesis of rotaxanes and catenanes.[24, 29–35] It is important to consider that these non-palindrome hosts have two different accesses to the aromatic cavity, that is through either its larger upper rim or the smaller lower one. Key insights on the directionality of the threading of viologen axles in the calix[6]arene wheel were then acquired through a series of studies.[35–37] Indeed, it was verified that in apolar solvents the threading of viologen salts into the cavity of **WEtOEt** (see figure 1.6) occurs selectively through the upper rim,[35, 36] while in more polar solvents such as acetonitrile or methanol, it occurs through both the cavity accesses.[35]

This behaviour could be explained considering that: i) the orientation assumed, on the NMR time scale, by the methoxy groups at the lower

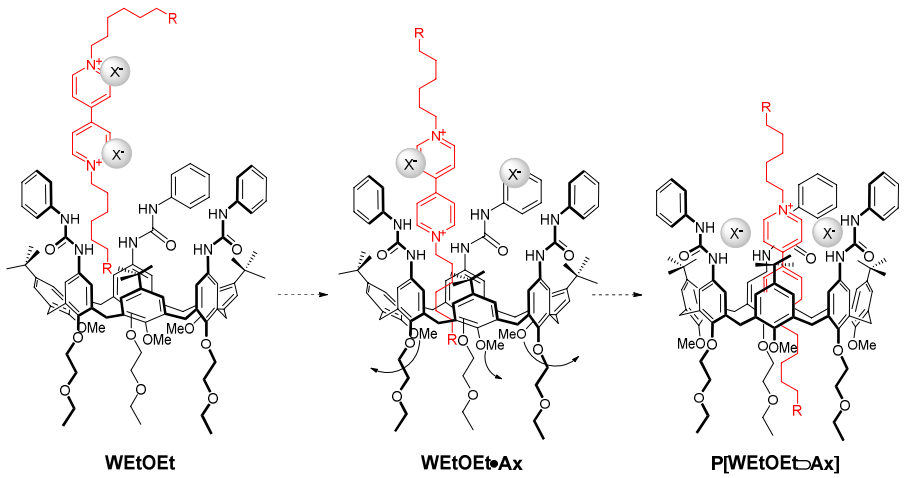

Figure 1.6: Possible threading mechanism of a viologen-based non-symmetric axle in a triphenylureido calix[6]arene-based wheel **WEtOEt**: the three phenylurea moieties present on the calix[6]arene aromatic cavity coordinate the viologen counteranions by hydrogen bonding, thus pivoting threading of the dicationic axle from the upper rim of the wheel (see text).

rim, partially closes the access to the cavity; ii) in the same solvents the viologen salts are barely soluble and are present as tight ions pairs that have to be separated before the complexation; iii) the phenylureido groups that, as good hydrogen bonding donor sites, assume a crucial role in the separation of the ion pairs, are at the *host* upper rim. When the axle is functionalised with two alkyl chains of different lengths, it threads the wheel preferentially with its shorter/less hindered alkyl chain. Moreover, when the difference in the length of the two chains is bigger than seven carbon atoms,[38] or when one of the chains ends with a bulky group,[36] the selective formation of only one of the orientational isomers is observed. Putting all these findings together, the unidirectional transit of an asymmetric viologen salt through the cavity of **WEtOEt** governed by light and solvent was achieved.([39]) In particular, a viologen axle functionalised with a hydroxyl-ending hexyl chain on one side and with a photoisomerisable stilbene on the other was equilibrated with the wheel in a low polar medium. The spontaneous threading, that happens selectively through the upper rim

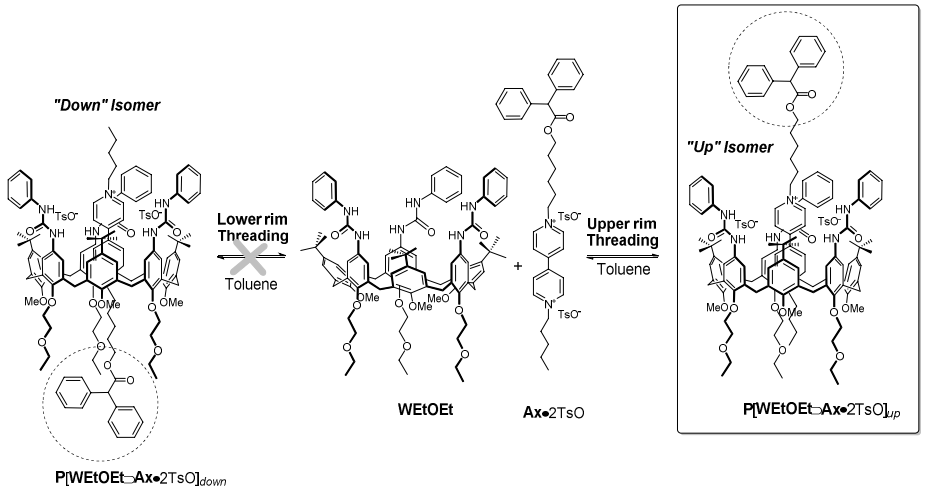

Figure 1.7: Formation of the two possible pseudorotaxane isomers derived from the calix[6]arene wheel **WetOEt** and a non-symmetric axle carrying only one stopper.

and with the less hindered hexyl chain, leads to the formation of only one orientational isomer of the complex. After the stoppering of the hexyl chain with diphenylacetylchloride, the addition of DMSO (polar solvent) induces the dethreading of the axle that can only occur with the stilbene passing through the lower rim of **WEtOEt**.

Important results on the use of simple alkoxy calix[6]arene hosts for the synthesis of oriented assemblies were reported from the group of Neri and coworkers. The threading of alkylbenzylammonium salt with weakly coordinating anion in the calixarene cavity leads to the formation of two different orientational isomers of the pseudorotaxanes, indicated in fig 1.8 as endo-alkyl and endo-benzyl. The endo-alkyl/endo-bezyl ratio can be tuned changing the length of the alkyl chain.[40]

Since calix[6]arene-based *hosts* in cone conformation are non symmetric, in the presence of an asymmetric *guest*, the reciprocal orientation of the components in the supramolecular assembly is of fundamental importance. The directional threading is a useful tool to selectively synthesise only one isomer of the oriented rotaxane (or pseudorotaxane), but has the important drawback that it does not allow the synthesis of the op-

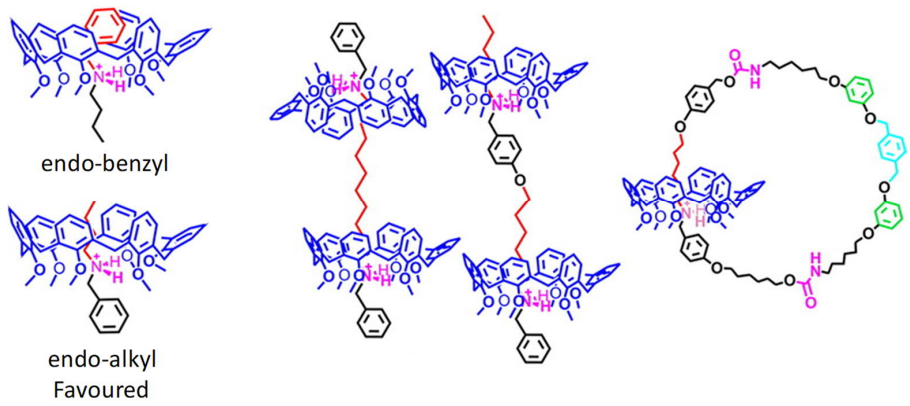

Figure 1.8: Oriented calix[6]arene based architectures achieved by Neri group exploiting the "endo-alkyl" rule. Partially adapted with permission from ref.[40], Copyright ©2013 American Chemical Society.

posite isomer. Recently, the ability of **Woct** and **WEtOEt** to complex N-alkylpyridylpyridnium salts was demonstrated.[41, 42] The ability of this class of *guests* to thread the wheel from both its upper and lower rims allows the formation of both the orientational pseudorotaxane isomers, even if the salt alkyl chain ends with a bulky group. Through a UV-vis titration, an association constant with a logK$\sim 4 \div 5$ was determined. Alkylation reaction carried out on the pyridine moiety of an N-alkylpyridyl pyridinium salt requires harsher conditions compared with those for 4,4'-bipyridine. This is due to the positive charge present on the alkylated pyridinium ring that reduces the nucleophilicity of the pyridine non-alkylated nitrogen atom. However, the inclusion of the salt into an electron-rich cavity stabilises its positive charge, thus leading to an enhancement of its reactivity. Based on these findings, the new supramolecular assisted approach for the synthesis of oriented rotaxane was developed.[32] It was in fact verified that the alkylation of a pyridylpyridinium salt carried out inside the cavity of a calixarene *host* leads to the spontaneous formation of only one orientational isomer of the final (pseudo)rotaxane. In particular, the orientational isomer having the alkyl chain initially present on the salt in the proximity of the *host* lower rim is exclusively formed, while the alkyl chain deriving from the used alkylating agent is now always found at the *host* upper rim.

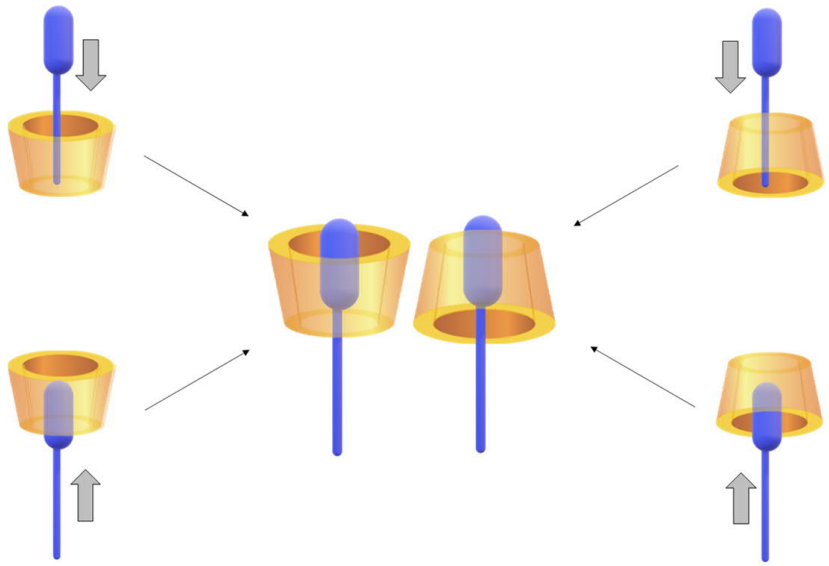

Figure 1.9: Graphical representation of the two possible orientational pseudorotaxane isomers and the four threading processes derived from a calix[6]arene wheel and a pyridylpyridinium salt.

The orientational outcome of the reaction is explained considering that the **Up** isomer of the starting complex has the free nitrogen atom better exposed to the bulk and in the proximity of the phenylureido groups at the upper rim of the wheel.[32, 41, 42] These groups, through their coordination with the incipient anion deriving from the alkylating agent leaving group, play a fundamental role in the acceleration of the reaction. This new synthetic strategy allowed the synthesis of new oriented (pseudo)rotaxanes, not accessible through the *threading* and *capping* approach.[31, 41, 42]

Bibliography

(1) *Analytical methods in supramolecular chemistry*; Schalley, C. A., Ed.; Wiley-VCH: 2007.

(2) Dodziuk, H., *Introduction to Supramolecular Chemistry*; Springer: 2007.

(3) Lehn, J.-M. *Angew. Chem. Int. Ed.* **1988**, *27*, 89–112.

(4) Gale, P. A. *Philosophical Transactions of the Royal Society of London. Series A: Mathematical, Physical and Engineering Sciences* **2000**, *358*, ed. by Thompson, J. M. T., 431–453.

(5) Bhalla, V. *Reson* **2018**, *23*, 277–290.

(6) Lehn, J.-M., *Supramolecular Chemistry: Concepts and Perspectives*; Wiley-VCH: 1995.

(7) Gale, P. A.; Steed, J. W., *Supramolecular Chemistry: From Molecules to Nanomaterials*; Wiley-VCH: 2012.

(8) Raynal, M.; Ballester, P.; Vidal-Ferran, A.; van Leeuwen, P. W. N. M. *Chem. Soc. Rev.* **2014**, *43*, 1660–1733.

(9) Maiti, B.; Abramov, A.; Pérez-Ruiz, R.; Díaz Díaz, D. *Acc. Chem. Res.* **2019**, *52*, 1865–1876.

(10) Schill, G.; Blomquist, A., *Catenanes, Rotaxanes, and Knots*; Organic Chemistry; A Series of Monographs; Elsevier Science: 2017.

(11) Crowley, J. D.; Hänni, K. D.; Lee, A.-L.; Leigh, D. A. *J. Am. Chem. Soc.* **2007**, *129*, 12092–12093.

(12) Crowley, J. D.; Goldup, S. M.; Lee, A.-L.; Leigh, D. A.; McBurney, R. T. *Chem. Soc. Rev.* **2009**, *38*, 1530–1541.

(13) Aucagne, V.; Hänni, K. D.; Leigh, D. A.; Lusby, P. J.; Walker, D. B. *J. Am. Chem. Soc.* **2006**, *128*, 2186–2187.

(14) Drexler, K. E., *Engines of Creation*; Anchor Press/Doubleday: 1986.

(15) Kassem, S.; Leeuwen, T. v.; S. Lubbe, A.; R. Wilson, M.; L. Feringa, B.; A. Leigh, D. *Chem. Soc. Rev.* **2017**, *46*, 2592–2621.

(16) Anelli, P. L.; Spencer, N.; Stoddart, J. F. *J. Am. Chem. Soc.* **1991**, *113*, 5131–5133.

(17) Bissell, R. A.; Córdova, E.; Kaifer, A. E.; Stoddart, J. F. *Nature* **1994**, *369*, 133–137.

(18) Chatterjee, M. N.; Kay, E. R.; Leigh, D. A. *J. Am. Chem. Soc.* **2006**, *128*, 4058–4073.

(19) Nierengarten, J. F.; Dietrich-Buchecker, C. O.; Sauvage, J. P. *J. Am. Chem. Soc.* **1994**, *116*, 375–376.

(20) Gutsche, C. D., *Calixarenes Revisited*; RSC Publishing: 1998.

(21) Parker, D., *Macrocycle Synthesis: A Practical Approach*; Oxford University Press: 1996.

(22) *Calixarenes 2001*; Asfari, M.-Z., Böhmer, V., Harrowfield, J., Vicens, J., Eds.; Springer Netherlands: 2001.

(23) Vicens, J.; Böhmer, V., *Calixarenes: A Versatile Class of Macrocyclic Compounds*; Springer Science & Business Media: 2012.

(24) Arduini, A.; Ferdani, R.; Pochini, A.; Secchi, A.; Ugozzoli, F. *Angew. Chem. Int. Ed.* **2000**, *39*, 3453–3456.

(25) Credi, A.; Dumas, S.; Silvi, S.; Venturi, M.; Arduini, A.; Pochini, A.; Secchi, A. *J. Org. Chem.* **2004**, *69*, 5881–5887.

(26) Ugozzoli, F.; Massera, C.; Arduini, A.; Pochini, A.; Secchi, A. *CrystEngComm* **2004**, *6*, 227–232.

(27) Arduini, A.; Orlandini, G.; Secchi, A.; Credi, A.; Silvi, S.; Venturi, M. In *Calixarenes and Beyond*, Neri, P., Sessler, J. L., Wang, M.-X., Eds.; Springer International Publishing: Cham, 2016, pp 761–781.

(28) Arduini, A.; Orlandini, G.; Secchi, A.; Credi, A.; Silvi, S.; Venturi, M. In *Reference Molecule in Chemistry, Molecular Sciences and Chemical Engineering*; Elsevier: 2014, pp 1–26.

(29) Bazzoni, M.; Zanichelli, V.; Casimiro, L.; Massera, C.; Credi, A.; Secchi, A.; Silvi, S.; Arduini, A. *Eur. J. Org. Chem.* **2019**, *2019*, 3513–3524.

(30) Zanichelli, V.; Dallacasagrande, L.; Arduini, A.; Secchi, A.; Ragazzon, G.; Silvi, S.; Credi, A. *Molecules* **2018**, *23*, 1156–1168.

(31) Zanichelli, V.; Bazzoni, M.; Arduini, A.; Franchi, P.; Lucarini, M.; Ragazzon, G.; Secchi, A.; Silvi, S. *Chem. Eur. J.* **2018**, *24*, 12370–12382.

(32) Zanichelli, V.; Ragazzon, G.; Arduini, A.; Credi, A.; Franchi, P.; Orlandini, G.; Venturi, M.; Lucarini, M.; Secchi, A.; Silvi, S. *Eur. J. Org. Chem.* **2016**, *2016*, 1033–1042.

(33) Orlandini, G.; Zanichelli, V.; Secchi, A.; Arduini, A.; Ragazzon, G.; Credi, A.; Venturi, M.; Silvi, S. *Supramol. Chem.* **2016**, *28*, 427–435.

(34) Arduini, A.; Bussolati, R.; Credi, A.; Pochini, A.; Secchi, A.; Silvi, S.; Venturi, M. *Tetrahedron* **2008**, *64*, 8279–8286.

(35) Arduini, A.; Ciesa, F.; Fragassi, M.; Pochini, A.; Secchi, A. *Angew. Chem. Int. Ed.* **2005**, *44*, 278–281.

(36) Arduini, A.; Calzavacca, F.; Pochini, A.; Secchi, A. *Chem. Eur. J.* **2003**, *9*, 793–799.

(37) Arduini, A.; Bussolati, R.; Credi, A.; Faimani, G.; Garaudée, S.; Pochini, A.; Secchi, A.; Semeraro, M.; Silvi, S.; Venturi, M. *Chem. Eur. J.* **2009**, *15*, 3230–3242.

(38) Arduini, A.; Bussolati, R.; Credi, A.; Secchi, A.; Silvi, S.; Semeraro, M.; Venturi, M. *J. Am. Chem. Soc.* **2013**, *135*, 9924–9930.

(39) Arduini, A.; Bussolati, R.; Credi, A.; Monaco, S.; Secchi, A.; Silvi, S.; Venturi, M. *Chem. Eur. J.* **2012**, *18*, 16203–16213.

(40) Ciao, R.; Talotta, C.; Gaeta, C.; Margarucci, L.; Casapullo, A.; Neri, P. *Org. Lett.* **2013**, *15*, 5694–5697.

(41) Zanichelli, V.; Ragazzon, G.; Orlandini, G.; Venturi, M.; Credi, A.; Silvi, S.; Arduini, A.; Secchi, A. *Org. Biomol. Chem.* **2017**, *15*, 6753–6763.

(42) Orlandini, G.; Ragazzon, G.; Zanichelli, V.; Secchi, A.; Silvi, S.; Venturi, M.; Arduini, A.; Credi, A. *Chem. Commun.* **2017**, *53*, 6172–6174.

Chapter 2

Synthesis of Calix[6]arene-based Oriented [3]-Rotaxanes

2.1 Introduction

In the last decades, countless examples of working devices and molecular machines prototypes, whose functioning under the action of external stimuli is governed by non-covalent interactions, have been proposed.[1–5] The ability to control the reciprocal orientation of the components of interlocked structures could allow to obtain systems capable of stimuli-promoted unidirectional movement. This represents a fundamental achievement for the realisation of switches and unidirectional rotary and linear motors. Several of these examples rely on the use of the so-called Mechanically Interlocked Molecules (MIMs), such as rotaxanes and catenanes.[6] MIMs are synthetically challenging targets, mainly because of the inherent difficulty in arranging in space two or more independent species to have the predictable formation of the desired mechanical bonds. The first step for the synthesis of MIMs is, usually, the formation of a pseudorotaxane precursor. The self-assembly of the components favors their correct mutual arrangement that leads eventually to the formation of a rotaxane upon the insertion of bulky substituents (stoppers) at the termini of the axle. This synthetic strategy, sometimes indicated either as *capping* [7] or *thread-*

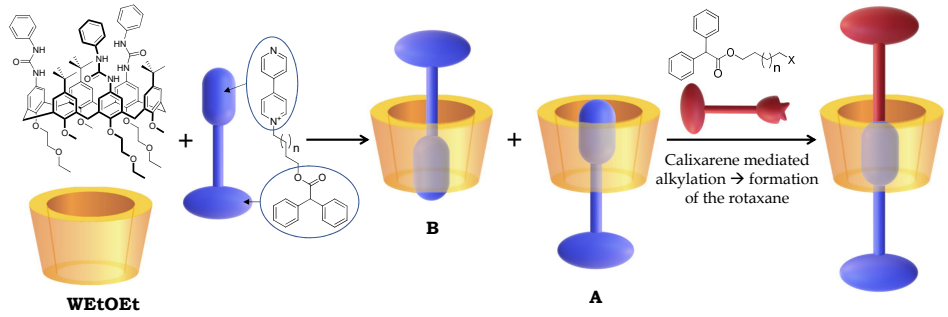

Figure 2.1: Schematic representation of the active template approach for the calix[6]arene-based rotaxanes synthesis used in this study. The yellow cartoon represents the calix[6]arene **WEtOEt**, while the blue and red pin-shaped ones indicate the pyridylpyridinium axle and the stoppering alkylating agent, respectively.

ing/stoppering, belongs to the more general category of the so-called passive template methods,[8] which allowed the synthesis of MIMs with sophisticated molecular architectures.[9] Leigh and co-workers introduced a new strategy defined as active template method [10] in which a reactive unit embedded in the macrocycle, typically a metal ion, both pivots the organisation of the components and mediates the formation of the covalent bonds. A growing number of different metal-catalysed reactions have been exploited for the realisation of rotaxanes and catenanes.[10–14] This latter approach in which the reactions exclusively proceed through a threaded intermediate allows the formation of several otherwise inaccessible mechanically connected macromolecules. Recently, our research group developed an efficient calix[6]arene-based oriented pseudorotaxanes and rotaxanes synthesis through an active template approach.[15, 16] Indeed, the engulfment of a positively charged pyridylpyridinium salt inside the π-rich cavity of a calix[6]arene-based wheel (**WEtOEt**, see figure 2.1) leads to two pseudorotaxanes isomers that differ for the orientation of the axle inside the wheel. It was verified that the axle pyridine ring is alkylated faster when it is included in the calixarene wheel with the arrangement of the orientational pseudorotaxane isomer **A**with respect to **B** and the free axle. [15]

The alkylation of the complexed substrates leads to the formation of pseudorotaxanes and rotaxanes with faster kinetics and higher yields compared to the threading and capping procedures exploited so far. More im-

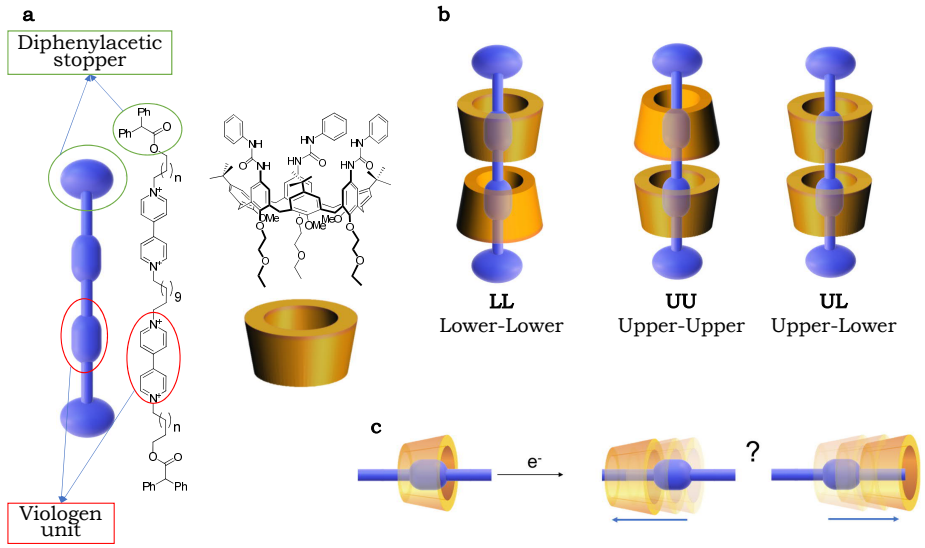

Figure 2.2: Schematic representation of a)the dumbbell component and the calix[6]arene wheel used for the [3]rotaxanes b)the three [3]rotaxane orientational isomers that can be synthesised by two **WEtOEt** wheels and a bis-viologen axle (top), c) two possible slipping direction for the movement of a wheel along its axle, upon reduction of the viologen station (bottom).

portant, this supramolecular-assisted strategy represents a useful tool for the efficient synthesis of calix[6]arene-based MIMs otherwise not accessible through the threading-capping approach. Moreover, it allows full control of the mutual orientation of the non-symmetric components.[15–17] A further task in this context would be the synthesis of oriented [3]rotaxanes (see figure 2.2 *c* and *b*) to evaluate the shuttling direction of its calixarene macrorings along their axle. In particular an enticing objective would be to establish whether the wheels movement takes place preferentially from their upper or lower rims and to investigate the role played by their reciprocal orientation. To this aim, the design and synthesis of oriented calix[6]arene based [3]rotaxanes characterised by a tetracationic bis-viologen salt as the dumbbell and two calix[6]arene units as the wheels have been carried out.

2.2 Results and Discussion

Due to the asymmetry of **WEtOEt**, the complexation of two wheels along a tetra-cationic dumbbell could in principle lead to the formation of three different orientational isomers: i) the upper rims of the two wheels are facing each other (**UU**), ii) the lower rim of the two wheels are facing each other (**LL**), iii) the upper rim of the first wheel faces the lower rim of the second one (**UL**) (see figure 2.2b).

Due to the complexity of the systems presented in this chapter, the following labelling scheme will be used: **P** indicates a pseudorotaxane, **R** a rotaxane, while the $\boldsymbol{C_nC_nC_n}$ code between square brackets indicates the length of the three alkyl chain composing the thread/dumbbell. The subscript **UU**, **LL** or **UL** after the square bracket indicates the reciprocal orientation of the two wheels as specified above. The label $\boldsymbol{R[C_6C_{12}C_6]_{UU}}$ would, for example, denote a [3]rotaxane composed by two calix[6]arene wheels faced through their upper rims and threaded by a dumbbell having a C12 alkyl spacer between the two bis-pyridinium units (bipy) and two external C6 alkyl spacers. The key features needed for the axial component are: i) a suitable length of the alkyl chain that spans the two viologen units in order to avoid steric hindrance between the two macrocycles, ii) an appropriate distance between the viologen units and the termini of the axle since a too short linker for the phenylacetic stopper may prevent the translational movement of the two wheels upon reduction of the viologen units. To check all these critical issues, the synthesis of a series of [3]rotaxanes using the passive template approach was initially tackled using the *threading* and *capping* strategy.

2.2.1 Synthesis of [3]rotaxanes (passive template method)

The chosen axles **5a,b** and **6a,b** are characterised by an inner spacer of variable length (C6 or C12) between the two viologen units, and by two terminal arms (C6 or C12) bearing a hydroxy moiety, required for the final capping with the diphenylacetyl stoppers. These axles were synthesised according to scheme 2.1. First, the reaction of the α,ω-diols **1a,b** with 0.9 or 2 equivalents of tosyl chloride leads to the monotosylate **3a,b** and ditosylate **2a,b**, respectively (see scheme 2.1). The reaction of **3a,b** with a stoichiometric excess of 4,4'-bipyridine in refluxing acetonitrile afforded the

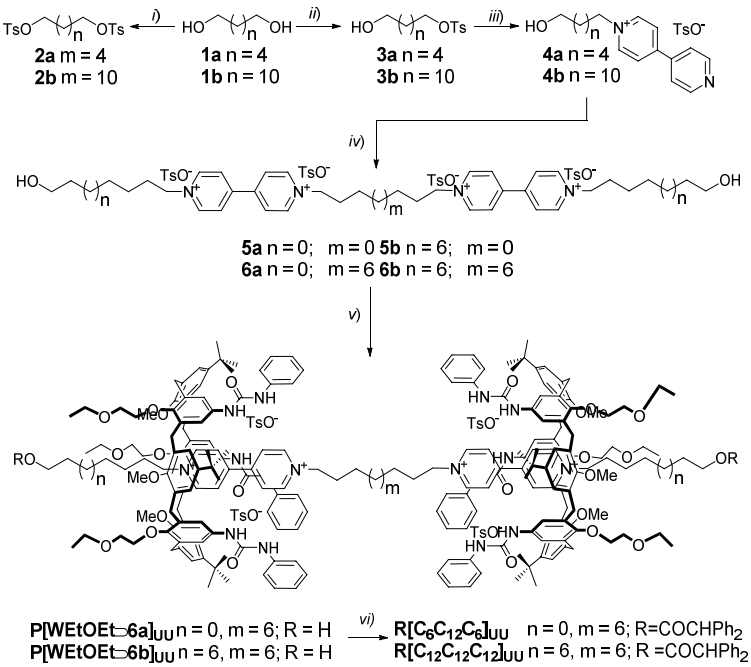

Scheme 2.1: Reagents and conditions: i) TsCl (2 eq.), DCM, DIMAP, Et_3N, rt; ii) TsCl (0.9 eq.), DCM, DIMAP, Et_3N, rt; iii) 4,4'-bipy (2 eq.), CH_3CN, reflux, 4 d; iv) **2a,b**, CH_3CN, reflux, 4 d; v) **WEtOEt** (2 eq.), C_6D_6 or toluene , RT, 24 h; vi) $Ph_2CHCOCl$, Et_3N, toluene, RT, 16 h.

pyridyl pyridinium salts **4a,b**, which were finally converted into the desired tetracationic axles **5a,b** and **6a,b** by their reaction with **2a,b** in refluxing acetonitrile for four days. The identity of the axles was confirmed through ^{1}H NMR and ESI-MS measurements. The NMR characterisation of these axles was carried out in CD_3OD for solubility reasons. As an example, the ^{1}H NMR spectrum of **6b** (***C*$_{12}$*C*$_{12}$*C*$_{12}$**) (see Figure 2.3c) shows, as diagnostic signals a multiplet centred at $\delta = 4.72$ ppm relative to the eight protons of the four methylene groups α and *12* linked to the pyridinium moieties and a triplet at $\delta = 3.54$ for the four protons of the two hydroxymethyl groups *1* (see figure 2.3 for the labeling). The two bipyridinium units resonate as two doublets, each integrating for eight protons, at $\delta = 9.24$ and 8.65 ppm, while the aromatic protons of the four tosylate counteranions

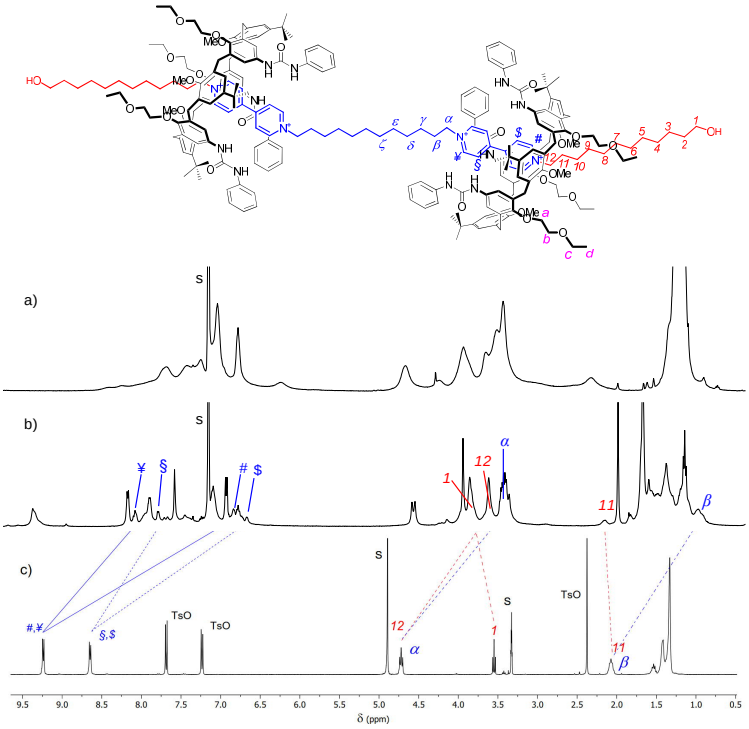

Figure 2.3: ^{1}H NMR (400 MHz) stack plot of a) **WEtOEt** in C_6D_6; b) [3]pseudorotaxane ***P*[*WEtOEt* ⊃ *6b*]*UU*** in C_6D_6 and c) axle **6b** in CD_3OD; the most essential protons assignments were indicated with letters, numbers and symbols in the graphical sketch above the stack.

resonate as two doublets at δ = 7.69 and 7.24 ppm while the singlet at δ = 2.37 ppm was assigned at their methyl groups. The synthesis of the desired [3]rotaxanes using the passive template approach, briefly discussed in the introductory part, is based on the formation of [3]pseudorotaxane complexes between **WEtOEt** and axles **5a,b** and **6a,b** (see scheme 2.1). In weakly polar solvents such as chloroform, toluene or benzene, the threading process of an asymmetric N,N'-dialkyl viologen-based axles inside the cavity of **WEtOEt** is unidirectional and takes place exclusively from the wheel upper rim (see scheme 2.1).[18] Based on the axles structure, it is possible to hypothesise that the threading processes would, therefore, exclusively yield [3]pseudorotaxane orientational isomers in which the two upper rims

of the calix[6]arene wheels face each other (**UU**). In separated experiments, the synthesised axles were suspended in deuterated benzene with a two-fold amount of **WEtOEt**. After stirring at room temperature for 24 h, the mixtures of the two threading experiments carried out with the axles endowed with the shorter (C6) inner spacer (**5a,b**), were still heterogeneous. The undissolved salt was removed from the mixtures by filtration to yield pale orange homogeneous solutions. The following ^{1}H NMR measurements carried out in C_6D_6 revealed the presence in the upfield region of the spectra of some signals witnessing the formation of axle-wheel(s) threaded species. However, because of the general broadness of the signals, mostly due to a non-negligible amount of uncomplexed wheel, it was not possible to assess the stoichiometry and the geometry of these threaded species. Such findings, however, support the hypothesis that a non-quantitative complexation of the axles occurs in solution. More interesting results came from the analysis of the experiments carried out with the axles having the longer C12 inner spacer (**6a,b**). The relative suspensions turned homogeneous and deep red after a few hours of stirring. This coloring of the solution is generally considered as a nacked eye indication of pseudorotaxane.[19] The NMR spectra collected for these threading experiments, confirmed the complexation since they show the typical pattern of signals belonging to a pseudorotaxane complex having the calix[6]arene **WEtOEt** as the wheel and an N,N'-dialkylviologen salt as the axle.[20, 21] The threading process between **6b** (see Figure 2.3b) and two **WEtOEt** wheels was witnessed in the ^1HNMR spectrum by the minor fluxionality of the macrocycle skeleton on the NMR time-scale (cf. figure 2.3a and b). In fact, upon threading, the axial and equatorial methylene protons of the macrocycle give rise to an AX system and resonate as two doublets at $\delta = 4.57$ and 3.38 ppm (the latter partially overlapped). This pattern is not visible in the spectrum of the free wheel, and it is also an indication that, after threading, the calix[6]arene macrocycle adopts, on the NMR time scale, a cone conformation with the three phenylureas oriented on the same side of the macrocycle. Other observations witnessing the threading of **6b** and the formation of a [3]pseudorotaxane complex are the symmetry of the spectrum and the ratio between the integral of the two components (1:2) as well as the splitting of the resonances relative to the bipyridinium units and the nearby methylene groups. As discussed before, the two pairs of protons labelled as ¥ and #,

and as $ and § (see figure 2.3 for labelling), are chemically equivalent in the free axle and resonates as a pair of doublets at $\delta = 9.24$ (¥, #) and 8.65 ($, §) ppm. Upon threading in **WEtOEt**, these protons experience a different magnetic environment due to the anisotropic effect of the calixarene cavity. Such an effect greatly upfield-shifts their resonances at $\delta = 8.05$ (¥), 7.79 (§), 6.83 (#) and 6.68 ($) ppm. Although less evident, such effect is also experienced by the methylene protons α and *12* that are upfield-shifted of *ca.* 1 ppm (see figure 2.3) and split into two resonances at $\delta = 3.61$ and 3.45 ppm. For the methylene groups *11* and β the split in two resonances is even more extensive with the second of these methylene groups yielding a very broad signal at *ca.* 1 ppm. The NMR results are in agreement with the hypothesis that the threading of the axle **6b** takes place selectively through the upper rim for both the wheels, leading to a [3]pseurotaxanes in which the two upper rims are facing each other. Similar results were obtained in the experiment carried out using **6a** as the axle. These results suggest that: i) in axles **5a,b** the C6 inner spacer is too short to provide a correct placement of the wheels around the bipyridinium stations because of the possible steric hindrance between the phenylureas of the two facing macrocycles; ii) the pattern of signals and their symmetric distribution found in the NMR spectra of the experiments with **6a,b** suggest that the relative arrangement of the two calix[6]arene wheels with respect the thread is **UU**. Based on these findings, the synthesis of the [3]rotaxanes was carried out using the axles endowed with the C12 inner spacer. In separated experiments, a suspension of axle **6a** or **6b** and two equivalent of **WEtOEt** in toluene was stirred to give a homogeneous and red-colored solution. The stoppering of the protruding ω-hydroxyalkyl arms with triethylamine and diphenylacetyl chloride, led to the corresponding mechanical interlocked molecule through the formation of new ester bonds (see scheme 2.1). After chromatographic separation, [3]rotaxanes $\boldsymbol{R[C_6C_{12}C_6]_{UU}}$ and $\boldsymbol{R[C_{12}C_{12}C_{12}]_{UU}}$ were isolated in 15%, and 21% of yield, respectively. NMR and HR-MS measurements confirmed the identity of these novel MIMs.

As an example, in Figure 2.4 have been reported the ^{1}H and 2D HSQC spectra of $\boldsymbol{R[C_6C_{12}C_6]_{UU}}$ taken in $CDCl_3$. The outcome of the capping reaction, with the formation of a diphenylacetic ester moiety, is evidenced by the appearance of the singlet at $\delta = 5.02$ ppm, assigned to the methine proton of the diphenylacetic stopper. This signal integrates for more than

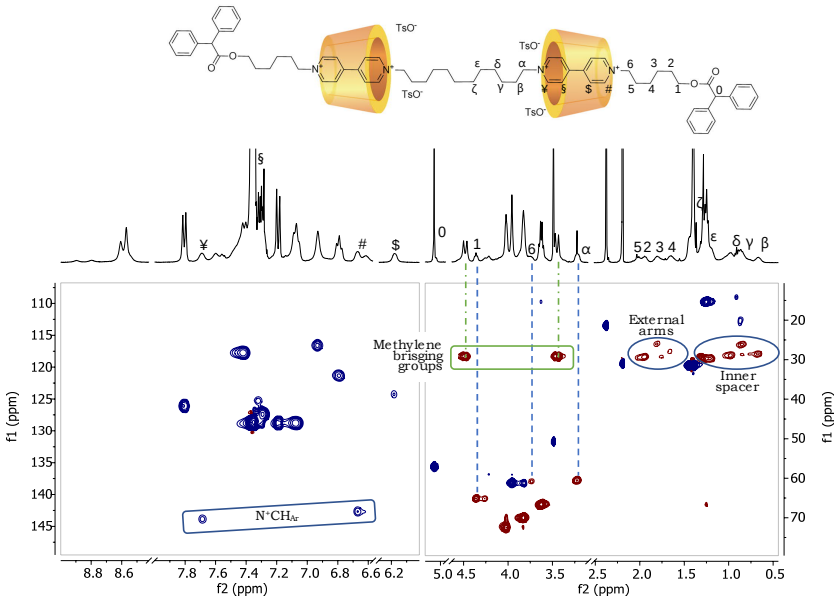

Figure 2.4: 2D edited HSQC spectrum of [3]rotaxane $\boldsymbol{R[C_6C_{12}C_6]_{UU}}$. The cross-peaks with blue contours indicate CH couplings relative to tertiary and primary carbons, while those with reddish contours the CH couplings of secondary carbons

two protons since the diphenylacetate salts are difficult to remove from the product. As expected, in analogy to the corresponding pseudorotaxanes, also in the spectrum of $\boldsymbol{R[C_6C_{12}C_6]_{UU}}$, the signals of the thread are upfield-shifted due to the inclusion inside the cavities of the *hosts*. In particular, the signals relative to the proton # and ¥ resonate now at δ = 6.67 and 7.69 ppm, the methylene protons α and *6* are upfield-shifted of *ca.* 1 ppm and split into two resonances at δ = 3.22 and 3.74 ppm. The alkyl chain starting from the methylene α, labelled in the spectrum as $\alpha, \beta, \gamma, \delta, \epsilon$ and ζ, and identified thanks to a 2D-TOCSY experiment, is symmetric and strongly influenced by the shielding effect of the phenylureido groups of the wheels. These findings confirm that the two wheels are oriented with the two upper rims facing each other. HR-MS measurements (ORBITRAP LQ) finally confirmed the formation of both [3]rotaxanes. The mass spectrum of $\boldsymbol{R[C_6C_{12}C_6]_{UU}}$ shows a very intense doubly charged (z = 2) peak at m/z = 2171.14411 given by the adduct generated by the tetra-charged rotaxane and two tosylate counter-anions, while the spectrum of $\boldsymbol{R[C_{12}C_{12}C_{12}]_{UU}}$ displays a triply charged intense peak at m/z = 1446.48779, which was assigned to the adduct formed by the [3]rotaxane with one tosylate as counterion. In conclusion, these preliminary studies showed that a C6 spacer for the inner alkyl chain of the axle does not favor the formation of the [3]pseudorotaxane structure. Moreover, it was demonstrated that with axles having a C12 inner spacer, the *threading* and *capping* strategy lead to the exclusive formation of the **UU** oriented [3]rotaxanes.

2.2.2 Synthesis of [3]rotaxanes (active template method)

As briefly discussed in the introduction, the active template method allows the preparation of calix[6]arene-based interlocked molecules overcoming the limit of the threading directionality, which is the main disadvantage for the *threading* and *capping* strategy. On these premises, the goal of the ensuing part of this study was to investigate the robustness and high modularity of this method for the synthesis of **UU**, **LL**, and **UL**-type [3]rotaxanes (see figure 2.2 and 2.5). To this aim, two sets of [3]rotaxane orientational isomers based on $\boldsymbol{C_6C_{12}C_6}$ and $\boldsymbol{C_{12}C_{12}C_{12}}$ dumbbells, respectively, were devised. Indeed, based on the results discussed above, C12 inner spacer was used, while two different alkyl chains (C6 and C12) were exploited as the linkers

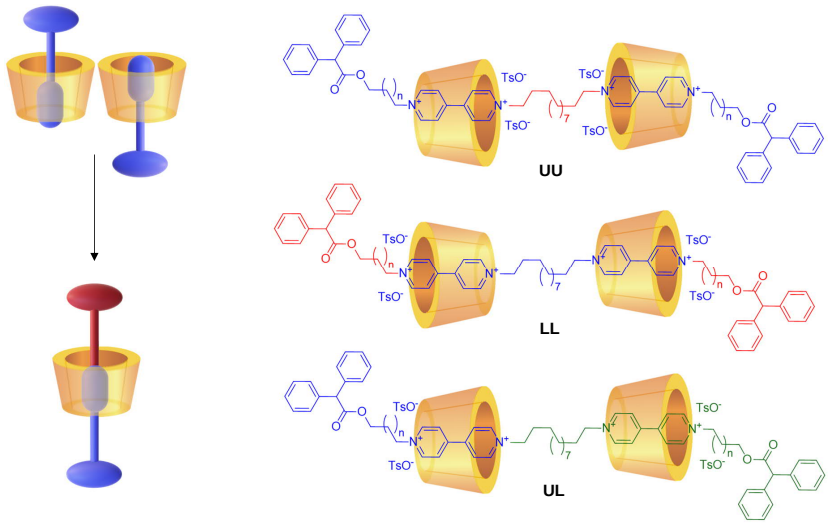

Figure 2.5: schematic representation of the [3]rotaxane orientational isomers.

between the viologen units and the diphenyl acetic stoppers. The members of each set differ only for the orientation of the wheels with respect the dumbbell (**UU**, **LL**, and **UL**), while among the sets each type of orientational isomer differs for the length (C6 and C12) of the linkers between the viologen units and the diphenyl acetic stoppers. Initially, it was necessary to identify the suitable dumbbell components (DC) necessaries for the obtainment of the desired orientational [3]rotaxane isomer. With this aim, it is important to consider that, based on the studies discussed above,[15, 16] the alkyl chain initially present on the N-alkyl-4,4'-pyridylpyridinium salt will be in proximity of the lower rim of the *host* at the end of the [3]rotaxane supramolecular assisted synthesis.

From figure 2.5 is possible to note that in the **UU** isomer, the alkyl chains ending with the bulky groups are in proximity of the lower rim of the wheels, so a pyridylpyridinium salt bearing an alkyl chain ending with the stopper had to be synthesised. On the other hand, in the **LL** isomer, the alkyl spacer that spans the two viologen units is in the proximity of the lower rim of the wheels. The needed starting semi-axis, in this case, posses two pyridylpyridinium units spanned by a C12 alkyl chain. The retrosynthetic

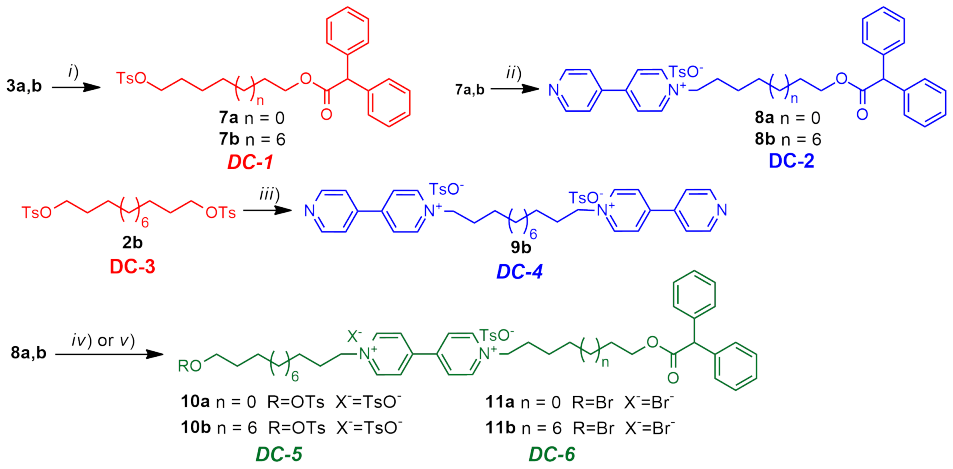

Scheme 2.2: Reagents and conditions: i) $Ph_2CHCOCl$, Et_3N, DCM, RT; ii) 4,4'-bipy (2 eq.), CH_3CN, reflux, 24 h; iii) 4,4'-bipy (2.5 eq.), CH_3CN, reflux, 24 h; iv) **2b** (5 eq), CH_3CN, reflux, 7 d; v)1,12-dibromododecane (5 eq), CH_3CN, reflux, 7 d.

analysis for the synthesis of the **UL** isomers, which are the only asymmetric compounds of the sets, evidence that to obtain the desired orientation is needed to break the dumbbell asymmetrically. The hypothesised starting dumbbell components (**DC-1-6**) for the synthesis of the three orientational [3]rotaxane isomers are reported in Scheme 2.2. For the synthesis of **7a,b**, that represents the first dumbbell component (**DC-1**), the monotosylate **3a,b** were reacted with diphenylacetyl chloride in dichloromethane in the presence of triethylamine as proton scavenger. These tosylates were then converted in **8a,b** (**DC-2**) through their reaction with a stoichiometric excess (2 eq.) of 4,4'-bipyridine in refluxing acetonitrile. The synthesis of the bis-pyridylpyridinium ditosylate **9b**, that represents the dumbbell component containing the C12 inner spacer (**DC-4**), was accomplished similarly to **DC-2** but using the ditosylate **2b** as the starting reagent. It is worth to note that **2b** will be used later as a dumbbell component (**DC-3**). For the synthesis of the new viologen salts **10a,b** (**DC-5**), the ditosylate **2b** was reacted with **8a,b** in a 5:1 stoichiometric ratio. The reaction carried out in refluxing dry acetonitrile for seven days, afforded the desired salts in 28% and 80% yields. The same procedure, but using 1,12-dibromododecane as alkylating agent, was followed for the synthesis of **11a,b** (**DC-6**) obtained

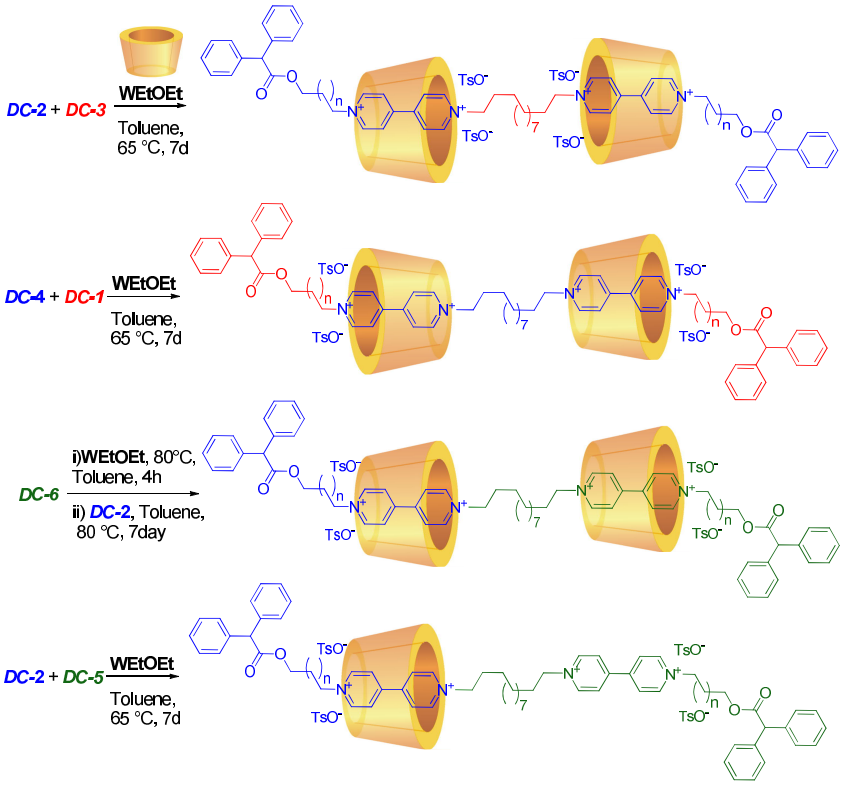

Scheme 2.3: schematic representation of the synthesis of the [3]rotaxanes: the components of the axles are colored according to their labels.

in 52% and 47% yields, respectively. Maximise the complexation of the dumbbell components is fundamental for a successful synthesis of the [3]rotaxane isomers, since the obtainment of the desired product/geometry is strictly related to the supramolecularly assisted alkylation occurring inside the calix[6]arene cavity. The active template approach was initially applied to the synthesis of [3]rotaxanes $\boldsymbol{R[C_6C_{12}C_6]_{UU}}$ and $\boldsymbol{R[C_{12}C_{12}C_{12}]_{UU}}$, previously prepared with the *threading* and *capping* strategy in low yields. To this aim, in separated experiments, the appropriate pyridylpyridinium salt **8a,b** (**DC-2**) was equilibrated in toluene with a stoichiometric excess of **WEtOEt** and stirred at room temperature for 30 min (see scheme 2.3). The solution turned orange and homogeneous, confirming the complexation of the unsoluble semi-axis inside the wheel. The ditosylate **2b** was then added, and the solution was stirred at 65 °C for seven days until it turned dark red.

The products of these reactions were purified through chromatographic separation on silica gel (see experimental). Due to the presence in the reac-

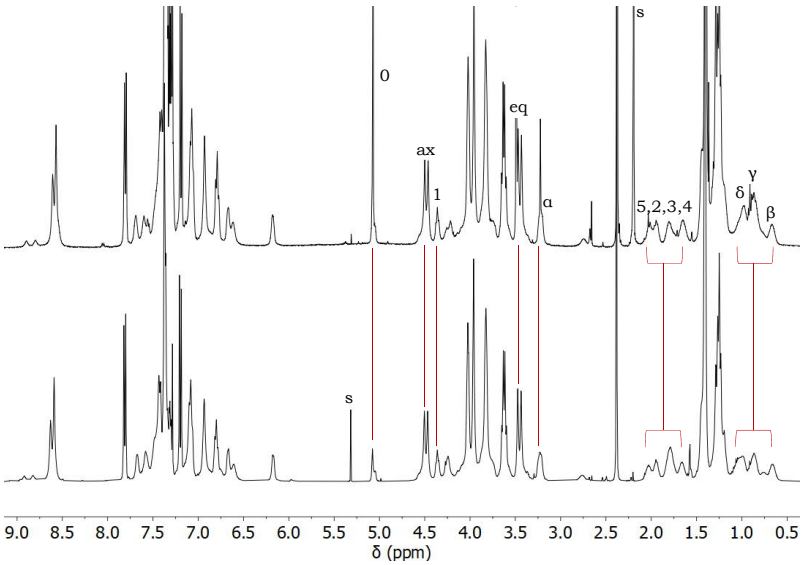

Figure 2.6: ^{1}H NMR stack plot (400 MHz, $CDCl_3$, 298 K) of the oriented [3]rotaxane $\boldsymbol{R[C_6C_{12}C_6]_{UU}}$ synthesised via i) *threading* and *capping* method (top), ii) supramolecular-assisted method (bottom).

tion mixture of partially reacted species, **WEtOEt** was released from the unstoppered psuedorotaxane complexes during the chromatographic purification, and it was present in all the isolated fractions. For this reason, it was necessary to perform a second chromatographic purification that allowed to obtain the [3]rotaxane $\boldsymbol{R[C_6C_{12}C_6]_{UU}}$ and $\boldsymbol{R[C_{12}C_{12}C_{12}]_{UU}}$ as pure compounds in 62% and 43% yield, respectively. They were characterised through HR-MS and NMR spectroscopy. The stack plot reported in figure 2.6 shows that for $\boldsymbol{R[C_6C_{12}C_6]_{UU}}$ the ^{1}H NMR spectra acquired in $CDCl_3$ on the products obtained using the *threading* and *capping* strategy and the supramolecular-assisted synthesis are perfectly overlapping, except for the signal of the methine proton of the diphenylacetic stopper (labelled as "0"), and resonating at *ca.* 5 ppm. In the spectrum of $\boldsymbol{R[C_6C_{12}C_6]_{UU}}$, deriving from the supramolecular-assisted reaction, this signal, resonating at $\delta = 5.07$ ppm (see figure 2.6, top), integrates correctly for two protons. In the spectrum of $\boldsymbol{R[C_6C_{12}C_6]_{UU}}$ isolated from the *threading/capping* reaction, this signal is always too intense (see figure 2.6, bottom) because of purification problems (vide supra). Further evidence of the orientation of the two wheels with respect to the dumbbell arises from 1D and 2D ROESY experiments that show correlations between the protons *2*, *3*, *4*, and *5* of the dumbbell and the methoxy group at the lower rim of the wheel resonating at $\delta = 3.96$ ppm. Others significant correlations are those between the dumbbell methylene groups β, δ, γ and the phenylureido groups at the upper rim of the wheel. Similar results were also obtained for the corresponding [3]rotaxane $\boldsymbol{R[C_{12}C_{12}C_{12}]_{UU}}$. HR-MS measurements (see figure 2.7) confirmed the identity of the two products. In the mass spectrum recorded for $\boldsymbol{R[C_{12}C_{12}C_{12}]_{UU}}$, the most abundant peak is a tetra charged one at m/z = 1042.86438 D in good agreement with the calculated mass of the product (see figure 2.7, bottom). For $\boldsymbol{R[C_6C_{12}C_6]_{UU}}$, the mass spectrum shows the presence of a doubly charged peak at m/z = 2172.66105 D and a triply charged one at 1391.43024 D corresponding to the calculated mass of the adduct with two tosylates and one tosylate, respectively (see figure 2.7, top). Summarising, the supramolecular assisted strategy here reported allowed to obtain $\boldsymbol{R[C_6C_{12}C_6]_{UU}}$ with better yields and higher purity (more facile purification) with respect to the *threading* and *capping*.

For the synthesis of the [3]rotaxane isomers $\boldsymbol{R[C_{12}C_{12}C_{12}]_{LL}}$ and $\boldsymbol{R[C_6C_{12}C_6]_{LL}}$, the bis-pyridylpyridinium ditosylate **9b** (**DC-4**) and a

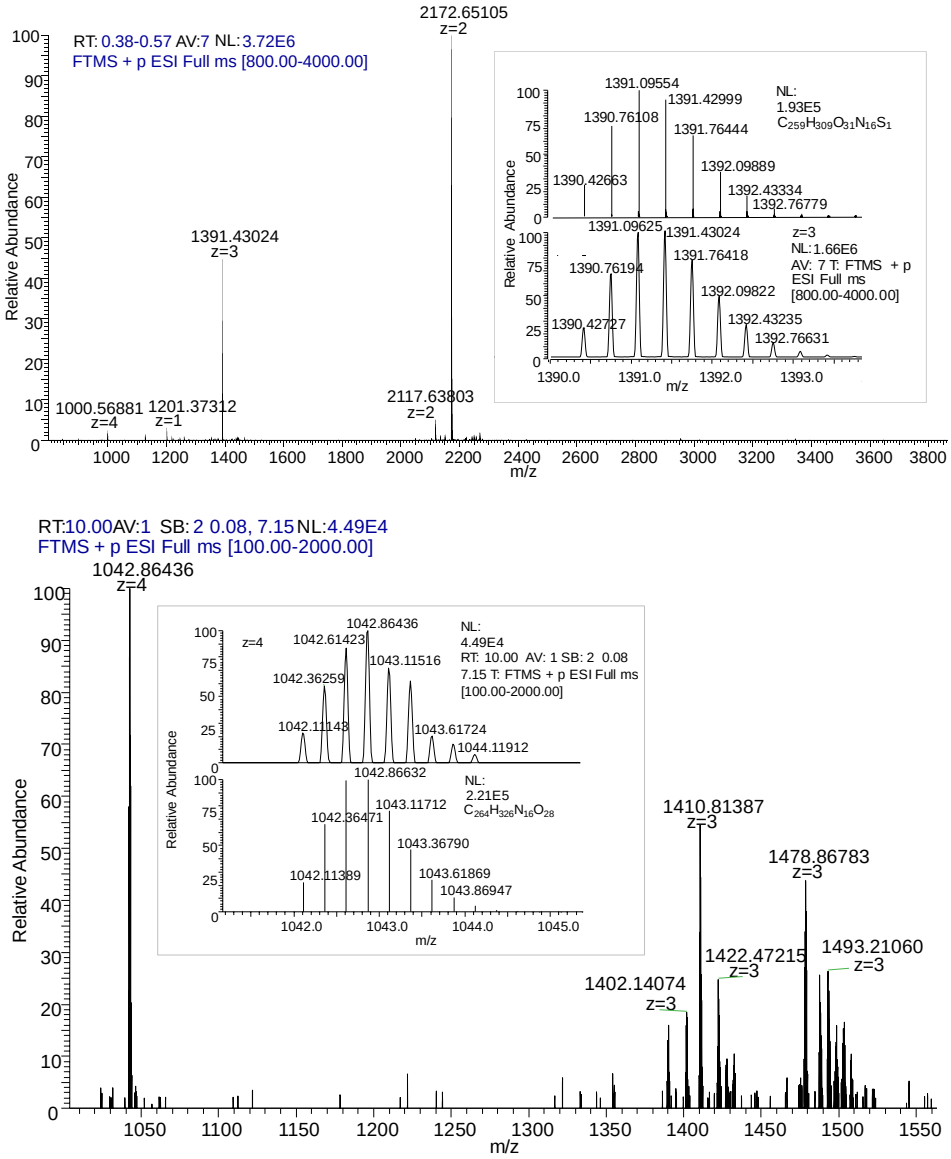

Figure 2.7: HR-MS spectra of $\boldsymbol{R[C_{12}C_{12}C_{12}]_{UU}}$ (bottom) and $\boldsymbol{R[C_6C_{12}C_6]_{UU}}$ (top). In the inset, the experimental isotopic distribution is compared with the calculated one.

stoichiometric excess of **WEtOEt** were equilibrated in toluene (see scheme 2.3). The suspension was stirred at room temperature for 30 min. until it turns orange colored and homogeneous. After the addition of the alkylating agent **7a** or **7b** (**DC-1**), the resulting reaction mixture was stirred for seven days at 65°C. The rotaxanes $\boldsymbol{R[C_{12}C_{12}C_{12}]_{LL}}$ and $\boldsymbol{R[C_6C_{12}C_6]_{LL}}$ were isolated in 38 and 50 % yields through the chromatographic separation described above. The obtained products were characterised through HR-MS and NMR measurements.

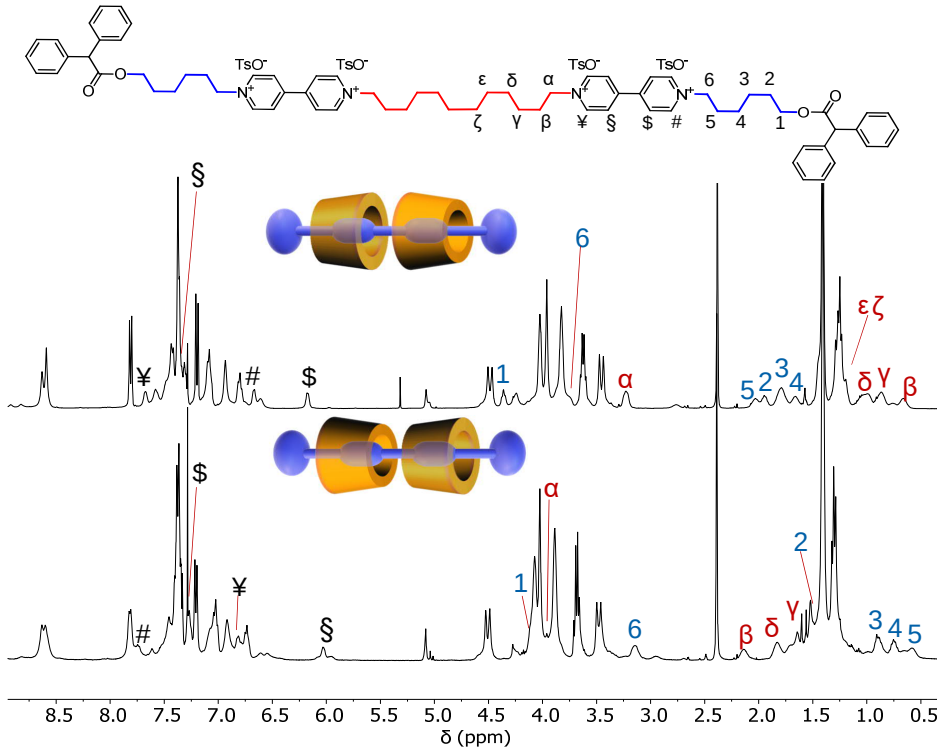

Figure 2.8: ^{1}H NMR stack plot (400 MHz, $CDCl_3$) of [3]rotaxane $\boldsymbol{R[C_6C_{12}C_6]_{UU}}$ (top) and $\boldsymbol{R[C_6C_{12}C_6]_{LL}}$ (bottom).

In figure 2.8 is reported the ^{1}H NMR stack plot comparing the spectra of the [3]rotaxane isomers $\boldsymbol{R[C_6C_{12}C_6]_{LL}}$ (bottom) and $\boldsymbol{R[C_6C_{12}C_6]_{UU}}$ (top). As found for the spectrum $\boldsymbol{R[C_6C_{12}C_6]_{UU}}$, also the spectrum of $\boldsymbol{R[C_6C_{12}C_6]_{LL}}$ shows high symmetry with a pattern of peaks in agreement

with the formation of a [3]rotaxane compound in which the wheels adopt the same orientation with respect the dumbbell. Some differences between the two spectra were present, and they were analysed through a series of 2D NMR measurements. A 2D HSQC experiment allowed to identify the resonance of the methylene group adjacent to the diphenyl acetic stopper *1* at F2/F1 = 4.09/65.1 ppm. Starting from this signal, with the help of a 2D TOCSY experiment (see Figure 2.9), the whole spin system of the C6/C12 alkyl chains was recognised.

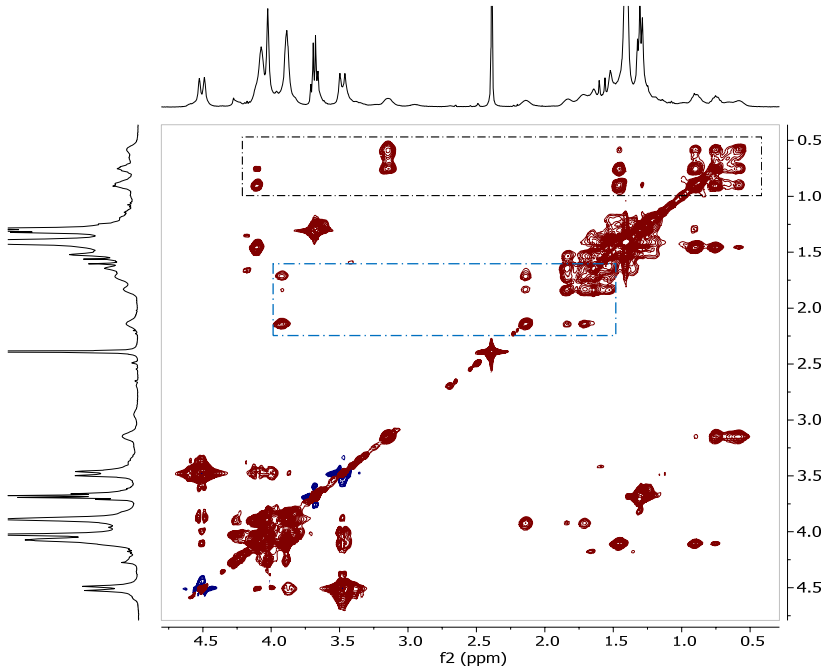

Figure 2.9: ^{1}H ^{1}H 2D TOCSY (400 MHz, $CDCl_3$ of $\boldsymbol{R[C_6C_{12}C_6]_{LL}}$ (expanded region 0.25-4.75 ppm). In dark dashed rectangle is evidenced the spin system of the C6 alkyl chain (methylene groups *1-6*), while in the blue dashed rectangle have been highlighted some of the correlations for the C12 alkyl chain with methylene groups $\alpha - \zeta$

It is important to note that in this new [3]rotaxane isomer, the signals of the alkyl chains that separate the viologen units and the stoppering bulky groups are significantly more upfield shifted than for $\boldsymbol{R[C_6C_{12}C_6]_{UU}}$. As an example, protons of methylene *6* resonate at $\delta \sim 3.8$ ppm for the **UU**

isomer, while the same signal is found at $\delta \sim 3.2$ ppm in the spectrum of **LL** ($\Delta\delta \sim$ -0.6 ppm). The other methylene groups of this chain resonate between 1.5 and 2.1 ppm in the **UU** isomer, and they are upfield shifted between 0.5 and 1.3 ppm in the **LL** one. These findings are an indication that in $\boldsymbol{R[C_6C_{12}C_6]_{LL}}$ the two C6 alkyl chains connecting the stoppers with the viologen units are surrounded, as expected, by the phenylureido groups of the calix[6]arene wheels, thus experiencing an anisotropic shielding effect. For the same reason, but with the opposite effect, the resonances of the methylene groups of the C12 inner spacer ($\alpha - \zeta$) in the spectrum of $\boldsymbol{R[C_6C_{12}C_6]_{LL}}$ are downfield-shifted with respect to the same resonance in $\boldsymbol{R[C_6C_{12}C_6]_{UU}}$. Indeed, in the latter isomer, this chain was wrapped by the two facing aromatic cavities, while in **LL**, it is found in the proximity of the wheels lower rims. The ROESY experiments allowed to identify correlations between the methylene groups *3*, *4* and *5* of the *guest* and the protons of the phenylureido groups of the wheel resonating at δ 6.73 and 7.02 ppm. These ROE correlations explain the above chemical shift comparison, indicating that effectively the phenylureas exert a shielding effect on the methylene protons indicated as *3*, *4* and *5*. Overall these findings confirm that the $\boldsymbol{R[C_6C_{12}C_6]_{LL}}$ isomer, obtained through the supramolecular-assisted reaction, has the hypothesised and desired dumbbell/wheels geometrical arrangement, with the lower rims of the two wheels facing each other. Similar results were also gained for $\boldsymbol{R[C_{12}C_{12}C_{12}]_{LL}}$.

The HR-MS measurements confirmed the identity of the two products. In the mass spectrum of $\boldsymbol{R[C_{12}C_{12}C_{12}]_{LL}}$, the most abundant peak correspond to a tetra charged species at m/z = 1042.61365 D in good agreement with the calculated mass of the product. For $\boldsymbol{R[C_6C_{12}C_6]_{LL}}$, the mass spectrum shows the presence of a doubly charged peak at m/z=2172.09505 D, and a triply charged at 1391.64973 D corresponding to the calculated mass of the adduct with two tosylates and one tosylate, respectively.

For the synthesis of the asymmetric [3]rotaxane isomer $\boldsymbol{R[C_6C_{12}C_6]_{UL}}$, the viologen salt **10a** (**DC-5**), the pyridylpyridinium tosylate **8a** (**DC-2**) and the wheel **WEtOEt** were mixed in toluene (see scheme 2.3). After stirring at room temperature for 30 min, the original suspension turned orangish but not completely homogeneous. The reaction mixture was then stirred at 65°C for seven days, and it turned dark red. However, a considerable amount of insoluble residue was still present in the reaction mixture,

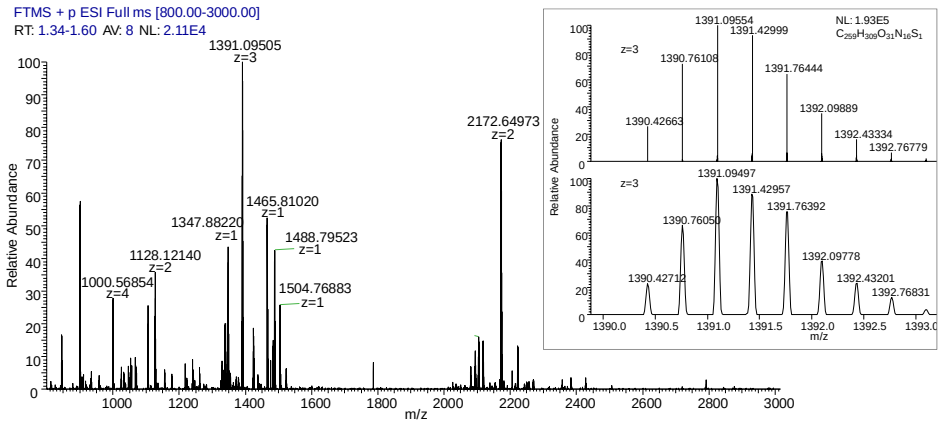

Figure 2.10: HR-MS spectrum of $\boldsymbol{R[C_6C_{12}C_6]_{LL}}$, in the inset, the experimental isotopic distribution is compared with the calculated one.

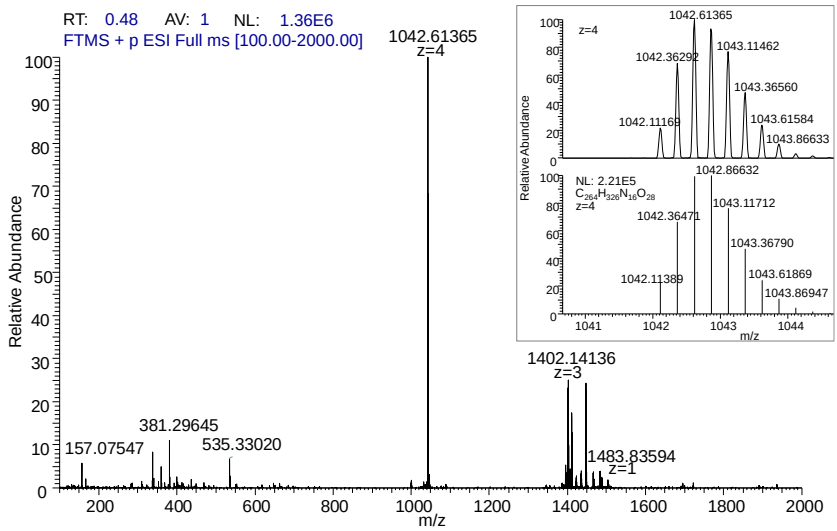

Figure 2.11: HR-MS spectrum of $\boldsymbol{R[C_{12}C_{12}C_{12}]_{LL}}$, in the inset, the experimental isotopic distribution is compared with the calculated one.

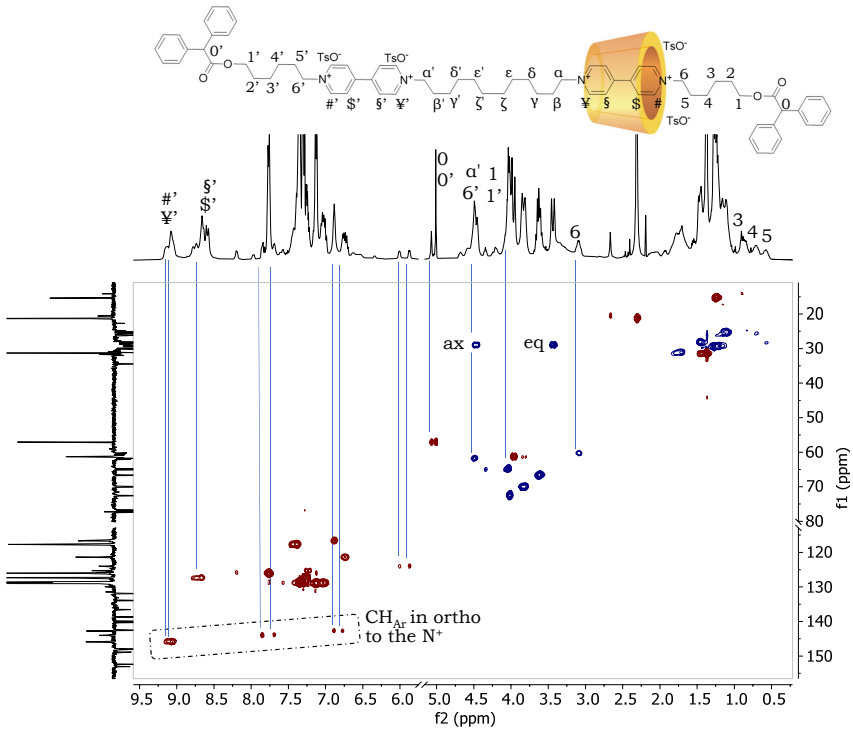

Figure 2.12: ^{1}H and 2D HSQC spectra (600 MHz, 25°C, $CDCl_3$) of **2*R*[*C*$_6$*C*$_{12}$*C*$_6$]**.

and its chromatographic purification presented more difficulties than the separations accomplished for the four rotaxanes already isolated. Indeed, the red compound present in the reaction mixture did not elute with the eluent used so far. To isolate this product, it was necessary to add to the eluent a 1% V/V of a saturated aqueous solution of sodium tosylate. The ESI MS spectrum of the obtained product show two main peaks at m/z = 902.7 and m/z = 1440.0 that are not in agreement with the calculated mass of the desired product. They instead fit with the mass of a [2]rotaxane constituted by the whole thread and a single wheel. In particular, the two peaks correspond to a doubly charged adduct with two tosylates, and to a triply charged species, that is the adduct with one tosylate. The 2D HSQC NMR spectrum of the isolated product is reported in figure 2.12, and the signals are labeled according to the sketch above it. In the aromatic region of the HSQC spectrum, at F1 ∼145 ppm, are easily recognisable three sets of correlations relative to the aromatic CH in ortho to the positively charged nitrogen nucleus of the pyridinium rings. Two of these correlations are found in F2 at ∼6.8 and ∼7.8 ppm and are due to the viologen unit threaded inside the cavity. The third pair of correlations, at F2 ∼9.1 ppm, is due to the same protons of the viologen unit not threaded inside the cavity of the *host*. This characterisation surprisingly led to the finding that the isolated product was the [2]rotaxane $\mathbf{2}\boldsymbol{R}[\boldsymbol{C_6C_{12}C_6}]$ represented in scheme 2.3. A 2D TOCSY spectrum (see figure 2.13) allowed to identify the alkyl chain of *guest* in proximity of the upper rim of the wheel.

To verify that this reactivity problem was not due to an excess of steric hindrance between the two wheels, the synthesis of the corresponding [3]rotaxane $\boldsymbol{R}[\boldsymbol{C_{12}C_{12}C_{12}}]_{\boldsymbol{UL}}$, with the longer C12 alkyl chains, was attempted in the same conditions. Also in this case, the [2]rotaxane $\mathbf{2}\boldsymbol{R}[\boldsymbol{C_{12}C_{12}C_{12}}]$ represented in scheme 2.3 was exclusively isolated in appreciable yields. Its HR-MS spectrum shows two main peaks at m/z = 901.21649 and 1523.84290 D corresponding to the product that had lost one proton and to the adduct with two tosylates, respectively. This behavior strongly suggests that only one of the two semiaxes reacts inside the wheel. Considering that the treading of **8a** and **8b** inside the wheel **WEtOEt** has been verified in previous studies in identical conditions,[16] it has been hypothesised that this lack of reactivity could be due to unsuccessful threading of **10a** and **10b** in the wheel. Indeed, this salt has to thread via its long C12 alkyl chain ending

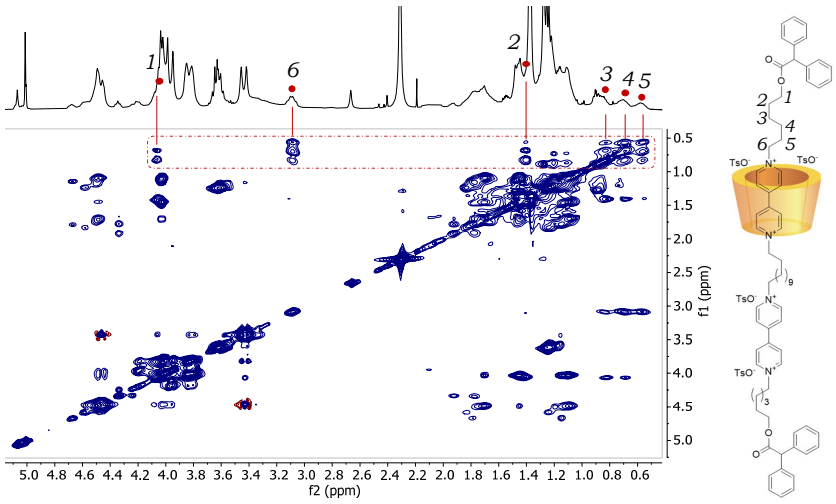

Figure 2.13: 2D TOCSY spectrum of $\mathbf{2}\boldsymbol{R}[\boldsymbol{C_6C_{12}C_6}]$ ($CDCl_3$, 400 MHz, 298 K), expanded region 0.4 - 5.2 ppm. In the red dashed rectangle, the correlations corresponding to the alkyl chain *1-6*.

with the *p*-toluensulfonyl group.

To reduce the steric hindrance of this chain, the new salts **11a** and **11b**, bearing a bromide as a leaving group, have been synthesised in 52% and 47% yields according to scheme 2.2. In two separate experiments, **11a** and **11b** have been then equilibrated with **WEtOEt** in toluene at room temperature for one hour. Since after this period, the solution was still uncolored, and the salt not dissolved yet. Therefore, the reaction mixture was heated at 80°C to facilitate the complexation. After four hours of heating, the reaction turned red-colored and homogeneous. The pyridylpyridinium salt **8a** (or **8b**) was added, and the reaction was further stirred for seven days at 80°C. The reaction mixtures were purified through column chromatography as described above for the other [3]rotaxanes. In this way, the desired oriented [3]rotaxanes $\boldsymbol{R}[\boldsymbol{C_6C_{12}C_6}]_{\boldsymbol{UL}}$ and $\boldsymbol{R}[\boldsymbol{C_{12}C_{12}C_{12}}]_{\boldsymbol{UL}}$ were obtained in 42 and 40 % yield, respectively. The two products were characterised by HR-MS and NMR measurements.

The HR-MS spectra of $\boldsymbol{R}[\boldsymbol{C_6C_{12}C_6}]_{\boldsymbol{UL}}$ and $\boldsymbol{R}[\boldsymbol{C_{12}C_{12}C_{12}}]_{\boldsymbol{UL}}$ are reported in figure 2.15. In both cases two main peaks are present: a double

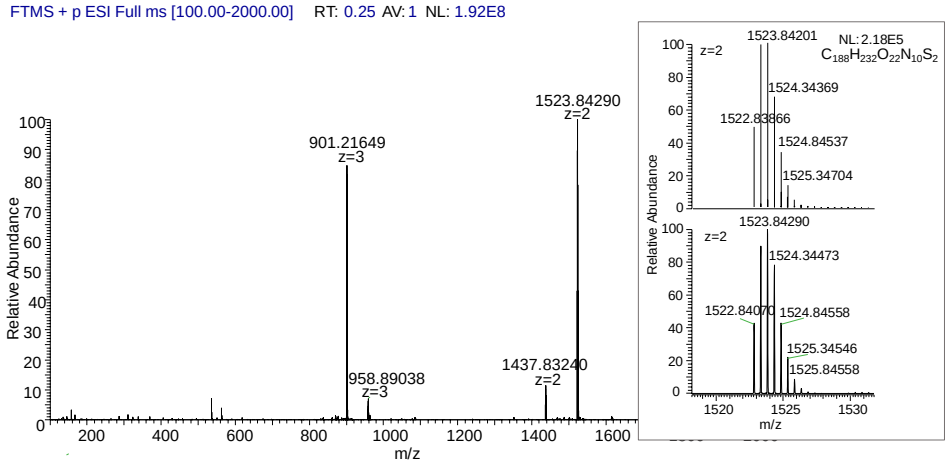

Figure 2.14: HR-MS spectrum of $\mathbf{2}\boldsymbol{R}[\boldsymbol{C_{12}C_{12}C_{12}}]$, in the inset, the experimental isotopic distribution is compared with the calculated one.

charged species at m/z = 2172.65186 and 2256.74351 D, respectively, corresponding to the adduct with two tosylates, and a triply charged species at m/z = 1391.09607 and 1447.49140 D, corresponding to the adduct with one tosylate. Moreover, in both spectra is present a tetra charged species at m/z = 1000.56866 and 1042.61467 D, corresponding to the rotaxanes without the anions. The ^{1}H NMR stack plot comparing the spectrum of $\boldsymbol{R}[\boldsymbol{C_6C_{12}C_6}]_{\boldsymbol{UL}}$ (middle) with the spectra of its two orientational isomers, $\boldsymbol{R}[\boldsymbol{C_6C_{12}C_6}]_{\boldsymbol{UU}}$ (top) and $\boldsymbol{R}[\boldsymbol{C_6C_{12}C_6}]_{\boldsymbol{LL}}$ (bottom) is reported in figure 2.16. The pattern of peaks in the three spectra is similar, indirectly confirming that $\boldsymbol{R}[\boldsymbol{C_6C_{12}C_6}]_{\boldsymbol{UL}}$ is a [3]rotaxane. However, the different reciprocal orientation of the [3]rotaxane components generates significant discrepancies between the three spectra. The spectrum of $\boldsymbol{R}[\boldsymbol{C_6C_{12}C_6}]_{\boldsymbol{UL}}$ (see figure 2.16, middle) is characterised by a higher number of signals that reflects the asymmetry of this compound with respect to its isomers. Particularly significative in this context is the analysis of the multiplets generated by the diasterotopic protons of the macrocycles bridging methylene groups. In the spectra of the more symmetric [3]rotaxane orientational isomers $\boldsymbol{R}[\boldsymbol{C_6C_{12}C_6}]_{\boldsymbol{UU}}$ (see figure 2.16, top) and $\boldsymbol{R}[\boldsymbol{C_6C_{12}C_6}]_{\boldsymbol{LL}}$ (see figure 2.16, bottom) these methylene groups originate an AX system of two

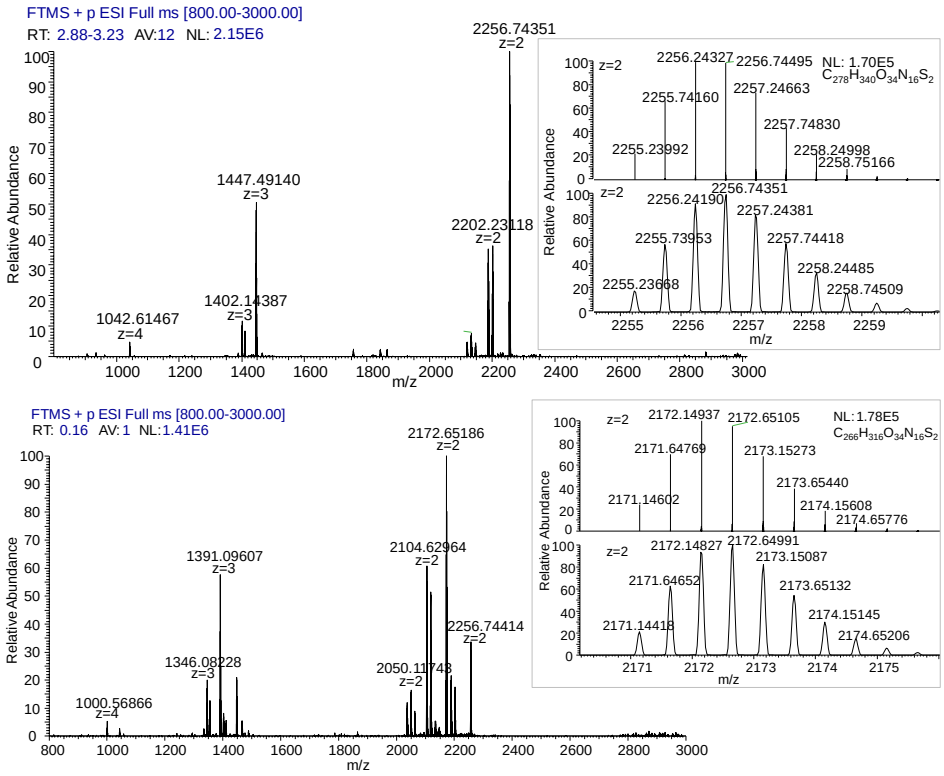

Figure 2.15: HR-MS of $\boldsymbol{R[C_6C_{12}C_6]_{UL}}$ at the bottom and $\boldsymbol{R[C_{12}C_{12}C_{12}]_{UL}}$ on top. In the inset, the experimental isotopic distribution is compared with the calculated one.

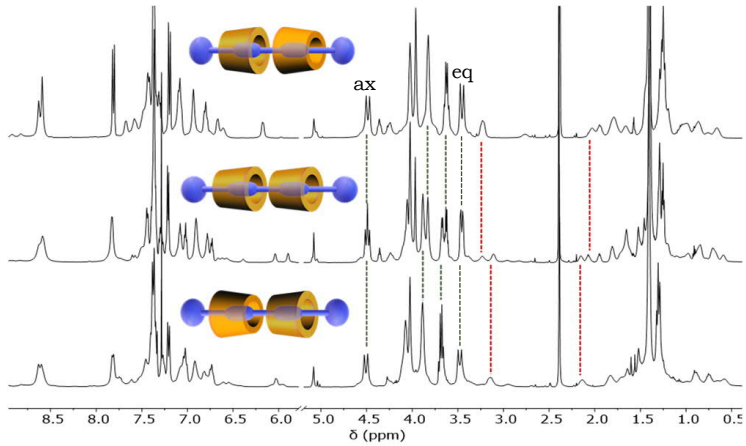

Figure 2.16: ^{1}H NMR stack plot (400 MHz, $CDCl_3$, 298 K) of the oriented [3]rotaxane $\boldsymbol{R}[\boldsymbol{C_6C_{12}C_6}]_{\boldsymbol{UU}}$ (top), $\boldsymbol{R}[\boldsymbol{C_6C_{12}C_6}]_{\boldsymbol{UL}}$ (middle) and $\boldsymbol{R}[\boldsymbol{C_6C_{12}C_6}]_{\boldsymbol{LL}}$ (bottom).

well-recognisable doublets with geminal coupling at $\delta \sim 3.5$ (equatorial protons) and 4.5 ppm (axial protons, see figure 2.16 top and bottom). Because of the asymmetry, in the spectrum of $\boldsymbol{R}[\boldsymbol{C_6C_{12}C_6}]_{\boldsymbol{UL}}$ the equatorial and axial protons of the bridging methylene groups yield two pairs of doublets each. Indeed, being both the wheels oriented in the same direction with respect to the dumbbell, the lower rim of one macrocycle experiences a different magnetic environment with respect to the one of the other. The same happens for the upper rim. As a result, the bridging methylene groups of the two wheels becomes magnetically different giving rise to two pairs of doublets. In the spectrum, these doublets resonate at similar but not identical chemical shifts and thus are visible as two merged doublets (see figure 2.16, middle). All the synthesised rotaxane will be employed for electrochemical studies to explore the role of the reciprocal orientation of the rotaxane components on its behavior in response to the application of external stimuli.

2.3 Conclusion

The study discussed in this chapter demonstrated the robustness and versatility of our supramolecular-assisted approach. Indeed it allowed the synthesis of a series of calix[6]arene-based [3]rotaxane with excellent control on the reciprocal orientation among the components. Through careful choice of the starting molecular components, it is possible to selectively obtain the desired orientational isomer (**UU**, **LL** or **UL**) of the [3]rotaxane. This result is crucial especially considering that the chromatographic separation of the three orientational isomers would be difficult or not possible because of their similar Rf with all the tested chromatographic conditions. Through this synthetic approach it would be possible to introduce in the dumbbell a large variety of functional groups (*e.g.* stations or stoppers) to address specific functionalities to the resulting compound.

2.4 Experimental

Materials: All solvents were dried using standard procedures; all other reagents were of reagent grade quality obtained from commercial suppliers and used without further purification. Melting points are uncorrected. NMR spectra were recorded at 600, 400, and 300 MHz for ^{1}H and 100 MHz for ^{13}C. Chemical shifts are expressed in ppm (δ) using the residual solvent signal as internal reference (7.16 ppm for C_6H_6; 7.26 ppm for $CDCl_3$ and 3.31 for CH_3OH). Mass spectra were recorded in the ESI mode. Compounds **WEtOEt**,[22] **2a,b**,[21] **3a**,[23] **3b**,[17] **4a**,[24] **4b**,[25] **7a**,[26] **7b**,[16] **8a**,[26] **8b**,[16] were synthesised according to published procedures.

Synthetic Procedures

General procedure for the synthesis of the bis-viologen axles 5a,b and 6a,b. In a sealed 100 mL glass autoclave, a solution of the appropriate salt **4a,b** (0.6 mmol) and ditosylate **2a,b** (0.3 mmol) in dry acetonitrile (40 mL) was refluxed under vigorous stirring for 4 days. Afterwards, the solution was evaporated to dryness under reduced pressure.

Axle 5a: the solid residue of the evaporation was recrystallised from CH_3OH/CH_3CN to afford 0.3 g of **5a** as a white solid powder (67%). ^{1}H

NMR (CD_3OD, 400 MHz) δ = 9.3-9.2 (m, 8H), 8.60 (d, 8H, ^3J = 6.4 Hz), 7.69 (d, 8H, ^3J = 8.0 Hz), 7.24 (d, 8H, ^3J = 8.0 Hz), 4.8-4.7 (m, 8H), 3.57 (t, 4H, ^3J = 6.4 Hz), 2.35 (s, 12H), 2.2-2.0 (m, 8H), 1.6-1.4 (m, 18H). ^{13}C NMR (100 MHz): δ = 150.6, 149.7, 149.6, 145.7, 145.6, 143.9, 142.4, 140.4, 128.6, 128.4, 126.8, 126.8, 126.5, 125.6, 125.3, 70.3, 61.8, 61.5, 61.3, 31.9, 31.1, 30.6, 29.2, 25.8, 25.6, 25.4, 25.0, 24.9, 20.1; MS (ESI): m/z: 1111.8 $[M- TsO]^+$.

Axle 5b: the solid residue of the evaporation was triturated with CH_3CN to afford 0.3 g of **5b** as a white solid powder (65%). ^1H NMR (CD_3OD, 400 MHz) δ = 9.3 - 9.2 (m, 8H), 8.62 (d, 8H, ^3J = 6.4 Hz), 7.69 (d, 8H, ^3J = 8.0 Hz), 7.24 (d, 8H, ^3J = 8.0 Hz), 4.8-4.7 (m, 8H), 3.55 (t, 4H, ^3J = 6.8 Hz), 2.36 (s, 12H), 2.2-2.0 (m, 8H), 1.6 - 1.3 (m, 40H). ^{13}C NMR (100 MHz): δ = 149.8, 149.7, 145.7, 145.6, 142.3, 140.3, 128.6, 126.9, 126.9, 125.6, 61.9, 61.6, 61.5, 32.3, 31.2, 30.6, 29.4, 29.3, 29.2, 29.1, 28.8, 25.8, 25.6, 24.9, 20.0; MS (ESI): m/z: 1279.1 $[M-TsO]^+$.

Axle 6a: the solid residue of the evaporation was triturated with CH_3CN to afford 0.3 g of product **6a** as a white solid powder (63%). M.p. = 156-158 °C. ^1H NMR (CD_3OD, 400 MHz) δ = 9.25 (d, 8H, ^3J = 5.6 Hz), 8.66 (d, 8H, ^3J = 6.4 Hz), 7.70 (d, 8H, ^3J = 8.4 Hz), 7.25 (d, 8H, ^3J = 8.0 Hz), 4.8 - 4.7 (m, 8H), 3.57 (t, 4H, ^3J = 5.6 Hz), 2.37 (s, 12H), 2.1 - 2.0 (m, 8H), 1.5 - 1.3 (m, 28H). ^{13}C NMR (100 MHz): δ = 149.8, 145.6, 142.3, 140.3, 128.5, 126.9, 125.5, 61.9, 61.8, 61.2, 31.8, 31.2, 31.1, 29.2, 29.1, 28.8, 25.8, 25.7, 25.6, 25.0, 19.9. MS (ESI): m/z: 1195.9 $[M-TsO]^+$.

Axle 6b: the solid residue of the evaporation was recrystallised from CH_3OH/CH_3CN to afford 0.3 g of **6b** as a white solid powder (62%). M.p. = 196-198 °C; ^1H NMR (CD_3OD, 400 MHz) δ = 9.25 (d, 8H, ^3J = 6.8 Hz), 8.66 (d, 8H, ^3J = 6.4 Hz), 7.70 (d, 8H, ^3J = 8.0 Hz), 7.25 (d, 8H, ^3J = 8.0 Hz), 4.72 (t, 8H, ^3J = 7.6 Hz), 3.55 (t, 4H, ^3J = 7.0 Hz) 2.37 (s, 12H), 2.1 (br. s, 8H), 2.0-1.9 (m, 4H), 1.53 (t, 4H, ^3J = 6.8 Hz), 1.5 - 1.3 (m, 48H). ^{13}C NMR (100 MHz): δ = 149.8, 145.6, 142.3, 140.3, 128.5, 126.9, 70.5, 61.9, 61.6, 32.2, 31.2, 29.3, 29.2, 29.1, 28.8, 28.7, 25.8, 25.5, 19.9. MS (ESI): m/z: 341.6 $[M-3TsO]^{3+}$.

Semiaxle 9b: in a 100 mL round bottomed flask a solution **2b** (0.50 g, 0.98 mmol) and a stoichiometric excess of 4,4'-bipyridyl (0.38 g, 0.45 mmol) in dry CH_3CN (40 mL) was refluxed under stirring for 24 h. The solution was then evaporated to dryness under reduced pressure. The solid residue was then recrystallised from CH_3OH to afford 0.46 g of **9b** as a white solid (57 %). ^{1}H NMR (CD_3OD, 400 MHz) δ = 9.11 (d, 4H, ^{3}J = 6.3 Hz), 8.84 (d, 4H, ^{3}J = 4.6 Hz), 8.51 (d, 4H, ^{3}J = 4.0 Hz), 7.99 (d, 4H, ^{3}J = 6.2 Hz), 7.71 (d, 4H, ^{3}J = 6.7 Hz), 7.23 (d, 4H ^{3}J = 7.1), 4.68 (t, 4H, ^{3}J = 7.5 Hz), 2.37 (s, 6H), 2.13 - 2.00 (m, 4H), 1.5-1.3 (m, 16H). MS (ESI): m/z: 240.1 $[M\text{-}2TsO]^{2+}$.

General procedure for the synthesis of the viologen axles 10a,b, and 11a,b: in a sealed 100 mL glass autoclave, a solution of the appropriate salt **8a,b** and a stoichiometric excess of the alkylating agent in dry CH_3CN (40 mL) were refluxed under vigorous stirring for 7 days. The solution was then cooled to room temperature to allow the precipitation of the desired product upon standing.

Axle 10a: 0.3 mmol of **8a** and 1.5 mmol of **2b**. The precipitation led to 103 mg of **10a** isolated as a white solid (28 %). ^{1}H NMR (CD_3OD, 400 MHz) δ = 9.24 (d, 4H, ^{3}J = 6.8 Hz), 8.64 (d, 4H, ^{3}J = 7.2 Hz), 7.78 (d, 2H, ^{3}J = 8.4 Hz), 7.69 (d, 4H, ^{3}J = 8.0 Hz), 7.45 (d, 2H, ^{3}J = 8.0 Hz), 7.32 - 7.21 (m, 14H), 5.09 (s, 1H), 4.73 (t, 2H, ^{3}J = 7.6 Hz), 4.67 (t, 2H, ^{3}J = 7.4 Hz), 4.17 (t, 2H, ^{3}J = 6.4 Hz), 4.02 (t, 2H, ^{3}J = 6.2 Hz), 2.46 (s, 3H), 2.37 (s, 6H), 2.10 - 1.90 (m, 4H), 1.67 - 1.59 (m, 4H), 1.5-1.3 (m, 20H). ^{13}C NMR (100 MHz): δ = 172.9, 149.9, 145.7, 142.2, 140.3, 138.9, 129.7, 128.5, 128.3, 128.2, 127.6, 126.9, 126.9, 125.5, 70.7, 64.4, 61.9, 61.7, 56.9, 31.1, 30.9, 29.1, 29.0 (three resonances), 28.7, 28.5, 28.4, 27.9, 25.8, 25.1, 25.0, 20.2, 20.0. MS (ESI): m/z: 395.9 $[M\text{-}2TsO]^{2+}$.

Axle 10b: 0.35 mmol of **8b** and 1.75 mmol of **2b**. The precipitation led to 343 mg of **10b** isolated as a white solid (80 %). ^{1}H NMR (CD_3OD, 400 MHz) δ = 9.23 (d, 4H, ^{3}J = 6.7 Hz), 8.64 (d, 4H, ^{3}J = 6.5 Hz), 7.78 (d, 2H, ^{3}J = 8.3 Hz), 7.69 (d, 4H, ^{3}J = 8.1 Hz), 7.45 (d, 2H, ^{3}J = 8.1 Hz), 7.35 - 7.20 (m, 14H), 5.09 (s, 1H), 4.72 (t, 4H, ^{3}J = 7.5 Hz), 4.16 (t, 2H, ^{3}J = 6.4 Hz), 4.02 (t, 2H, ^{3}J = 6.2 Hz), 2.46 (s, 3H), 2.37 (s, 6H), 2.12 - 2.03 (m, 4H),

1.66 - 1.56 (m, 4H), 1.5-1.2 (m, 32H). ^{13}C NMR (100 MHz): δ = 172.9, 149.8, 145.6, 142.2, 140.3, 138.9, 129.7, 128.5, 128.3, 128.2, 127.6, 126.9, 126.9, 125.5, 70.7, 64.8, 61.9, 60.0, 31.2, 29.2, 29.1(three resonances), 29.0 (two resonances), 28.8, 28.7, 28.5, 28.4, 28.2, 25.8(two resonances), 25.4, 25.0, 20.2, 20.0. MS (ESI): m/z: 395.9 $[M\text{-}2TsO]^{2+}$.

Axle 11a: 0.28 mmol of **8a** and 1.4 mmol of 1,12-dibromododecane. The precipitation led to 150 mg of **11a** isolated as a pale yellow solid (52 %). ^{1}H NMR (CD_3OD, 600 MHz) δ = 9.27 (d, 2H, ^{3}J = 6.5 Hz), 9.24 (d, 2H, ^{3}J = 6.7 Hz), 8.63 - 8.69 (m, 4H), 7.68 (d, 1H, ^{3}J = 8.1 Hz), 7.20 - 7.33 (m, 11H), 5.07 (s, 1H), 4.74 (t, 2H, ^{3}J = 7.6 Hz), 4.69 (t, 2H, ^{3}J = 7.5 Hz), 4.16 (t, 2H, ^{3}J = 6.5 Hz), 3.43 (t, 2H, ^{3}J = 6.7 Hz), 2.36 (s, 1.5H), 2.13 - 2.06 (m, 2H), 2.05 - 1.99 (m, 2H), 1.80 - 1.86 (m, 2H), 1.69-1.63 (m, 2H), 1.5-1.3 (m, 20H). MS (ESI): m/z: 350.3 $[M\text{-}2X]^{2+}$.

Axle 11b: 0.32 mmol of **8b** and 1.6 mmol of 1,12-dibromododecane. The precipitation led to 130 mg of **11b** isolated as a pale yellow solid (47 %). ^{1}H NMR (CD_3OD, 600 MHz) δ = 9.27 (d, 4H, ^{3}J = 6.2 Hz), 8.67 (d, 4H, ^{3}J = 5.6 Hz), 7.67 (d, 1H, ^{3}J = 8.2 Hz), 7.20 - 7.33 (m, 11H), 5.07 (s, 1H), 4.74 (t, 4H, ^{3}J = 7.6 Hz), 4.14 (t, 2H, ^{3}J = 6.5 Hz), 3.43 (t, 2H, ^{3}J = 6.7 Hz), 2.36 (s, 1H), 2.13 - 2.06 (m, 4H), 1.79 - 1.89 (m, 2H), 1.63-1.57 (m, 2H), 1.5-1.2 (m, 32H). ^{13}C NMR (100 MHz): δ = 171.4, 150.0, 145.8, 139.0, 128.5, 128.4, 128.2, 127.0, 126.9, 125.6, 64.9, 62.0, 57.0, 33.1, 32.6, 31.2, 29.2 (four resonances), 29.1 (two resonances), 28.8, 28.5, 27.8, 25.9, 25.0, 20.0. MS (ESI): m/z: 392.2 $[M\text{-}2X]^{2+}$.

General procedure for the synthesis of the [3]Rotaxanes UU with the passive template method: a suspension of the appropriate axle **6a,b** (0.03 mmol) and wheel **WEtOEt** (0.1 g, 0.06 mmol) in toluene (10 mL) was stirred for 24 h at room temperature for **6a** and at reflux for **6b**. When the mixture turned in a red homogeneous solution, diphenylacetyl chloride (0.03 g, 0.12 mmol) and triethylamine (0.03g, 0.12 mmol) were added. After stirring at RT for 16 h, the solvent was evaporated to dryness under reduced pressure. The red solid residue from the evaporation was purified through chromatographic separation (DCM:MeOH = 95:5). The

product was then dissolved in dichloromethane and washed twice with an aqueous solution of NaOTs and twice with distilled water.

***R*[$C_6C_{12}C_6$]$_{UU}$:** 0.05 g (15 %) as a red solid compound. HR-MS (ESI, Orbitrap LQ) calculated for $C_{266}H_{316}N_{16}O_{34}S_2$ m/z (z = 2): 271.14602 (24 %), 2171.64769 (70 %), 2172.14937 (100 %), 2172.65105 (95 %), 2173.15273 (68 %), 2173.65440 (39 %), 2174.15608 (18 %), 2174.65776 (7 %); Found: 271.14348 (21 %), 2171.64532 (64 %), 2172.14235 (99 %), 2172.664861 (100 %), 2173.15003 (80 %), 2173.65187 (53 %), 2174.15217 (30 %), 2174.65623 (13 %).

***R*[$C_{12}C_{12}C_{12}$]$_{UU}$:** 0.07 g (21 %) as red solid compound. HR-MS (ESI, Orbitrap LQ) calculated for $C_{278}H_{340}N_{16}O_{34}S_2$ m/z (z = 2): 2255.23992 (22 %), 2255.74160 (67 %), 2256.24327 (100 %), 2256.74495 (99 %), 2257.246632 (74 %), 2257.74830 (44 %), 2258.24998 (22 %), 2258.75166 (9 %); Found: 2255.23668 (18 %), 2255.74953 (58 %), 2256.24190 (93 %), 2256.74351 (100 %), 2257.246381 (83 %), 2257.74418 (59 %), 2258.24485 (34 %), 2258.74509 (17 %).

General procedure for the synthesis of the [3]Rotaxanes UU with the active template method: in a sealed glass tube, the appropriate semiaxis **8a,b** was suspended in 2 mL of dry toluene, wheel **WEtOEt** and the alkylating agents **2b** were added. The mixture was stirred at room temperature for half an hour until the complete dissolution of the reagents. After stirring at 65 °C for 7 days, the solvent was evaporated under reduced pressure. The crude mixture was then purified through column chromatography (Hex:EtOAc:MeOH = 60:35:5). The purified product was then dissolved in 2 mL of dichloromethane and a solution of AgOTs in ethanol (20 mL) was added. The mixture was stirred for 2 hours, then the solvent was evaporate to dryness under reduced pressure. The solid residue was taken up in dichloromethane and filtered to remove the silver salts.

***R*[$C_6C_{12}C_6$]$_{UU}$:** Reagents: **8a** (90 mg, 0.144 mmol), **WEtOEt** (220 mg, 0.150 mmol), **2b** (31 mg, 0.060 mmol). ***R*[$C_6C_{12}C_6$]$_{UU}$** was obtained as a red solid in 62 % yield. HR-MS (ESI, Orbitrap LQ) calculated for $C_{266}H_{316}N_{16}O_{34}S_2$ m/z (z = 2): 271.14602 (24 %), 2171.64769 (70 %),

2172.14937 (100 %), 2172.65105 (95 %), 2173.15273 (68 %), 2173.65440 (39 %), 2174.15608 (18 %), 2174.65776 (7 %); Found: 271.14727 (21 %), 2171.64984 (64 %), 2172.14021 (97 %), 2172.65105 (100 %), 2173.15302 (80 %), 2173.65450 (55 %), 2174.15436 (31 %), 2174.65442 (15 %).

***R*[$C_{12}C_{12}C_{12}$]$_{UU}$:** Reagents: **8b** (86 mg, 0.122 mmol), **WEtOEt** (187 mg, 0.127 mmol), **2b** (26 mg, 0.051 mmol). ***R*[$C_{12}C_{12}C_{12}$]$_{UU}$** was obtained as a red solid in 43 % yield. HR-MS (ESI, Orbitrap LQ) calculated for $C_{271}H_{333}N_{16}O_{31}S$ m/z (z = 3): 1446.4892 (20 %), 1446.8236 (61 %), 1447.1580 (95 %), 1447.4924 (100 %), 1447.8267 (80 %), 1448.1610 (53 %), 1448.4952 (29 %), 1448.8295 (14 %); Found: 1446.4878 (17 %), 1446.8230 (63 %), 1447.1573 (97 %), 1447.4916 (100 %), 1447.8258 (81 %), 1448.1599 (54 %), 1448.4940 (30 %), 1448.8286 (13 %);

General procedure for the synthesis of the [3]Rotaxanes LL with the active template method: in a sealed glass tube, the appropriate semiaxis **9b** was suspended in 2 mL of dry toluene, wheel **WEtOEt**, and the opportune alkylating agent **7a,b** were added. The mixture was stirred at room temperature for half an hour until the complete dissolution of the reagents. After stirring at 65 °C for 7 days the solvent was evaporated under reduced pressure. The crude mixture was then purified through column chromatography (Hex:EtOAc:MeOH = 60:35:5). The purified product was then dissolved in 2 mL of dichloromethane and a solution of AgOTs in ethanol (20 mL) was added. The mixture was stirred for 2 hours, then the solvent was evaporated to dryness under reduced pressure. The solid residue was taken up in dichloromethane and filtered to remove the silver salts.

***R*[$C_6C_{12}C_6$]$_{LL}$:** Reagents: **7a** (50 mg, 0.106 mmol), **WEtOEt** (170 mg, 0.116 mmol), **9b** (35 mg, 0.043 mmol). ***R*[$C_6C_{12}C_6$]$_{LL}$** was obtained as a red solid in 50 % yield. HR-MS (ESI, Orbitrap LQ) calculated for $C_{259}H_{309}N_{16}O_{31}S_1$ m/z (z = 3): 1390.42663 (26 %), 1390.76108 (72 %), 1391.09554 (100 %), 1391.42999 (92 %), 1391.76444 (64 %), 1392.09889 (36 %), 1392.43334 (16 %), 1392.76779 (7 %), 1393.10224 (2 %); Found: 1390.42712 (23 %), 1390.76050 (66 %), 1391.09497 (100 %), 1391.42957 (89

%), 1391.76392 (76 %), 1392.09778 (39 %), 1392.43201 (23 %), 1392.76831(13 %), 1393.09827 (4 %).

***R*[$C_{12}C_{12}C_{12}$]$_{LL}$:** Reagents: **7b** (80 mg, 0.144 mmol), **WEtOEt** (220 mg, 0.150 mmol), **9b** (48 mg, 0.058 mmol). ***R*[$C_{12}C_{12}C_{12}$]$_{LL}$** was obtained as a red solid in 38 % yield. HR-MS (ESI, Orbitrap LQ) calculated for $C_{264}H_{326}N_{16}O_{28}$ m/z (z = 4): 1042.11389 (23 %), 1042.36471 (67 %), 1042.6155 (99 %), 1042.86632 (100 %), 1043.11712 (76 %), 1043.36790 (47 %), 1043.61869 (24 %), 1043.86947 (11 %); Found: 1042.11169(22 %), 1042.36292 (69 %), 1042.61365 (100 %), 1042.86543 (94 %), 1043.11462 (77 %), 1043.36560(47 %), 1043.61584 (24 %), 1043.86633(11 %).

General procedure for the synthesis of the [3]Rotaxanes UL with the active template method. in a sealed glass tube the appropriate viologen salt **11a,b** was suspended in 2 mL of dry toluene, wheel **WEtOEt** was added, and the mixture was stirred at 80 °C for 4 hours. The solution was then cooled to room temperature and the opportune semiaxle **8a,b** was added. After stirring at RT for 30 min, the mixture was reacted at 80 °C for 7 days. The solvent was evaporated under reduced pressure and the crude mixture was purified trough column chromatography (Hex:EtOAc:MeOH = 60:35: 5). The purified product was then dissolved in 2 mL of dichloromethane and a solution of AgOTs in ethanol (20 mL) was added. The mixture was stirred for 2 hours, then the solvent was evaporate to dryness under reduced pressure. The solid residue was taken up in dichloromethane and filtered to remove the silver salts.

***R*[$C_6C_{12}C_6$]$_{UL}$:** Reagents: **11a** (50 mg, 0.055 mmol), **WEtOEt** (258 mg, 0.176 mmol), **8a** (48 mg, 0.077 mmol). ***R*[$C_6C_{12}C_6$]$_{UL}$** was obtained as a red solid in 42 % yield. HR-MS (ESI, Orbitrap LQ) calculated for $C_{266}H_{316}N_{16}O_{34}S_2$ m/z (z = 2): 271.14602 (24 %), 2171.64769 (70 %), 2172.14937 (100 %), 2172.65105 (95 %), 2173.15273 (68 %), 2173.65440 (39 %), 2174.15608 (18 %), 2174.65776 (7 %); Found: 271.14418 (21 %), 2171.64652 (63 %), 2172.14827 (94 %), 2172.64991 (100 %), 2173.15087 (82 %), 2173.65132 (55 %), 2174.15145 (30 %), 2174.65206 (14 %).

***R*[$C_{12}C_{12}C_{12}$]$_{UL}$:** Reagents: **11b** (55 mg, 0.055 mmol), **WEtOEt** (258 mg, 0.176 mmol), **8b** (54.4 mg, 0.077 mmol). ***R*[$C_{12}C_{12}C_{12}$]$_{UL}$** was obtained as a red solid in 40 % yield. HR-MS (ESI, Orbitrap LQ) calculated for $C_{278}H_{340}N_{16}O_{34}S_2$ m/z (z = 2): 2255.23992 (22 %), 2255.74160 (67 %), 2256.24327 (100 %), 2256.74495 (99 %), 2257.246632 (74 %), 2257.74830 (44 %), 2258.24998 (22 %), 2258.75166 (9 %); Found: 2255.23668 (18 %), 2255.74953 (58 %), 2256.24190 (93 %), 2256.74351 (100 %), 2257.246381 (83 %), 2257.74418 (59 %), 2258.24485 (34 %), 2258.74509 (17 %).

General procedure for the synthesis of the [2]Rotaxanes with the active template method: in a sealed glass tube the appropriate viologen salt **10a,b** was suspended in 2 mL of dry toluene, wheel **WEtOEt**, and the appropriate semiaxle **8a,b** were added. The mixture was stirred at room temperature for half an hour until the complete dissolution of the reagents. After stirring at 65 °C for 7 days the solvent was evaporated under reduced pressure. The crude mixture was purified trough column chromatography (Hex:EtOAc:MeOH = 60:35:5 + 1 % $TsONa_{aq}$). The purified product was then dissolved in 2 mL of dichloromethane and a solution of AgOTs in ethanol (20 mL) was added. The mixture was stirred for 2 hours, then the solvent was evaporated to dryness under reduced pressure. The solid residue was taken up in dichloromethane and filtered to remove the silver salts.

2*R*[$C_6C_{12}C_6$] : Reagents: **10a** (33 mg, 0.029 mmol), **WEtOEt** (171 mg, 0.116 mmol), **8a** (24 mg, 0.038 mmol). **2*R*[$C_6C_{12}C_6$]** was obtained as a red solid in 35 % yield. MS (ESI): m/z = 902.7 $[M\text{-}3TsO]^{3+}$, 1440.0 $[M\text{-}2TsO]^{2+}$

2*R*[$C_{12}C_{12}C_{12}$] : Reagents: **10b** (69 mg, 0.057 mmol), **WEtOEt** (250 mg, 0.171 mmol), **8b** (40 mg, 0.080 mmol). **2*R*[$C_{12}C_{12}C_{12}$]** was obtained as a red solid in 32 % yield. HR-MS (ESI, Orbitrap LQ) calculated for $C_{188}H_{232}N_{10}O_{22}S_2$ m/z (z = 2): 1522.83866 (48%), 1523.34028 (98%), 1523.84201 (100%), 1524.34369 (67%), 1524.84537 (34%), 1525.34704 (13%), 1525.84872 (5%); Found: 1522.84070 (44%), 1523.34237 (89%), 1523.84290 (100%), 1524.34473 (78%), 1524.84558 (45%), 1525.34546 (23%), 1525.84558 (8%)

Bibliography

(1) Kassem, S.; Leeuwen, T. v.; S. Lubbe, A.; R. Wilson, M.; L. Feringa, B.; A. Leigh, D. *Chem. Soc. Rev.* **2017**, *46*, 2592–2621.

(2) *Molecular Machines and Motors: Recent Advances and Perspectives*; Credi, A., Silvi, S., Venturi, M., Eds.; Topics in Current Chemistry; Springer International Publishing: 2014.

(3) Kay, E. R.; Leigh, D. A.; Zerbetto, F. *Angew. Chem. Int. Ed.* **2007**, *46*, 72–191.

(4) *Molecular Machines*; Kelly, T. R., Ed.; Springer-Verlag: Berlin Heidelberg, 2005.

(5) Balzani, V.; Credi, A.; Venturi, M. *Chem. Eur. J.* **2002**, *8*, 5524–5532.

(6) Sauvage, J.-P.; Dietrich-Buchecker, C., *Molecular Catenanes, Rotaxanes and Knots*; Wiley-VCH: 1999.

(7) Wu, J.; Leung, K. C.-F.; Stoddart, J. F. *Proceedings of the National Academy of Sciences* **2007**, *104*, 17266–17271.

(8) Griffiths, K. E.; Stoddart, J. F. *Pure and Applied Chemistry* **2008**, *80*, 485–506.

(9) Hubin, T. J.; Busch, D. H. *Coordination Chemistry Reviews* **2000**, *200-202*, 5–52.

(10) Crowley, J. D.; Goldup, S. M.; Lee, A.-L.; Leigh, D. A.; McBurney, R. T. *Chem. Soc. Rev.* **2009**, *38*, 1530–1541.

(11) Goldup, S. M.; Leigh, D. A.; Long, T.; McGonigal, P. R.; Symes, M. D.; Wu, J. *J. Am. Chem. Soc.* **2009**, *131*, 15924–15929.

(12) Sato, Y.; Yamasaki, R.; Saito, S. *Angew. Chem. Int. Ed.* **2009**, *48*, 504–507.

(13) Aucagne, V.; Hänni, K. D.; Leigh, D. A.; Lusby, P. J.; Walker, D. B. *J. Am. Chem. Soc.* **2006**, *128*, 2186–2187.

(14) Saito, S.; Takahashi, E.; Nakazono, K. *Org. Lett.* **2006**, *8*, 5133–5136.

(15) Orlandini, G.; Ragazzon, G.; Zanichelli, V.; Secchi, A.; Silvi, S.; Venturi, M.; Arduini, A.; Credi, A. *Chem. Commun.* **2017**, *53*, 6172–6174.

(16) Zanichelli, V.; Ragazzon, G.; Orlandini, G.; Venturi, M.; Credi, A.; Silvi, S.; Arduini, A.; Secchi, A. *Org. Biomol. Chem.* **2017**, *15*, 6753–6763.

(17) Zanichelli, V.; Bazzoni, M.; Arduini, A.; Franchi, P.; Lucarini, M.; Ragazzon, G.; Secchi, A.; Silvi, S. *Chem. Eur. J.* **2018**, *24*, 12370–12382.

(18) Arduini, A.; Bussolati, R.; Credi, A.; Secchi, A.; Silvi, S.; Semeraro, M.; Venturi, M. *J. Am. Chem. Soc.* **2013**, *135*, 9924–9930.

(19) Credi, A.; Dumas, S.; Silvi, S.; Venturi, M.; Arduini, A.; Pochini, A.; Secchi, A. *J. Org. Chem.* **2004**, *69*, 5881–5887.

(20) Arduini, A.; Bussolati, R.; Credi, A.; Pochini, A.; Secchi, A.; Silvi, S.; Venturi, M. *Tetrahedron* **2008**, *64*, 8279–8286.

(21) Arduini, A.; Bussolati, R.; Credi, A.; Faimani, G.; Garaudée, S.; Pochini, A.; Secchi, A.; Semeraro, M.; Silvi, S.; Venturi, M. *Chem. Eur. J.* **2009**, *15*, 3230–3242.

(22) González, J. J.; Ferdani, R.; Albertini, E.; Blasco, J. M.; Arduini, A.; Pochini, A.; Prados, P.; Mendoza, J. d. *Chem. Eur. J.* **2000**, *6*, 73–80.

(23) Tatsuta, K.; Nakagawa, A.; Maniwa, S.; Kinoshita, M. *Tetrahedron Lett.* **1980**, *21*, 1479–1482.

(24) Burns, D. H.; Chan, H.; Miller, J. D.; Jayne, C. L.; Eichhorn, D. M. *J. Org. Chem.* **2000**, *65*, 5185–5196.

(25) Fear, E. J. P.; Thrower, J.; Veitch, J. *J. Chem. Soc.* **1958**, 1322–1325.

(26) Arduini, A.; Ciesa, F.; Fragassi, M.; Pochini, A.; Secchi, A. *Angew. Chem. Int. Ed.* **2005**, *44*, 278–281.

Chapter 3

Synthesis and Characterisation of a Two-stations Two-gates Calix[6]arene-based Catenane

3.1 Introduction

Catenanes are a class of mechanically interlocked molecules (MIMs)[1] characterised by two or more entwined macrocyclic structures, which cannot be separated without breaking a chemical bond. An essential property of these compounds is the potential ability of their rings to move with respect to one another upon the application of suitable external stimuli. The possibility to control this movement is a key factor for the realisation of prototypes of rotatory motors. Indeed, to obtain a molecular motor, it is necessary a system in which the unidirectional motion of a component along the other could be perpetrated continuously. This could be obtained through a ratchet mechanism.[2] In order to have reciprocal movement between the two rings, catenanes have to satisfy some fundamental structural requirements: i) the whole system should have sufficient freedom degrees to allow

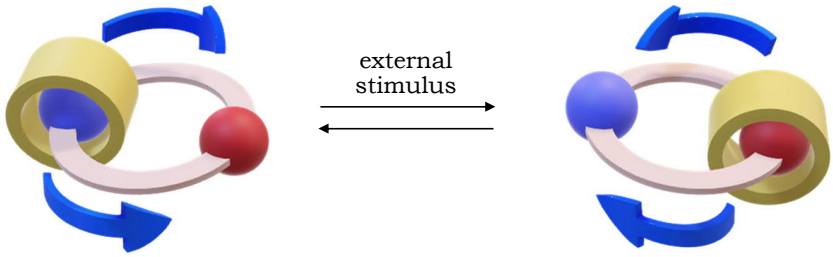

Figure 3.1: In a [2]catenane containing two different recognition sites on one ring, the relative rotation of the rings is achieved upon switching off and on the primary recognition site with an external stimulus. As the clockwise and anticlockwise directions are equally probable, no repetitive unidirectional circumrotation can be obtained.

one of the rings to move along the other; ii) one of the rings must contain at least "two stations" in its structure, whose affinities for some structural features present in the other macrocyclic ring are different (see figure 3.1); iii) the affinities between the complementary sites of the interlocked rings must be switchable or in someway modifiable through the application of suitable external stimuli.

The first example of control of the rotatory motion in a catenane was reported by Sauvage et al. in 1994.[3] in the following decade, the same group reported other examples, but in none of these systems the rotatory motion is unidirectional. In most of the examples of molecular shuttles based on [2]catenanes present in the literature,[4, 5] the unidirectional circumrotation of one ring with respect to another is obtained through a series of successive and orthogonal chemical transformations carried out on one or both the rings. As a straightforward example of these systems, Leigh and co-workers have shown the possibility to induce a unidirectional sequential rotation in a [2]catenane consisting of one small ring moving around a larger one (see Figure 3 -2).[6] The small ring moves in discrete steps between different binding sites located on the larger ring. The movement is driven by light, heat, or chemical stimuli that change the relative affinity of the small ring for the different binding sites.

The first example of calix[6]arene-based [2]catenane was reported by Neri et al. in 2013.[7] A few years later, our research group synthesised the catenane depicted in scheme 3.1.[7, 8] The synthesis exploited the template

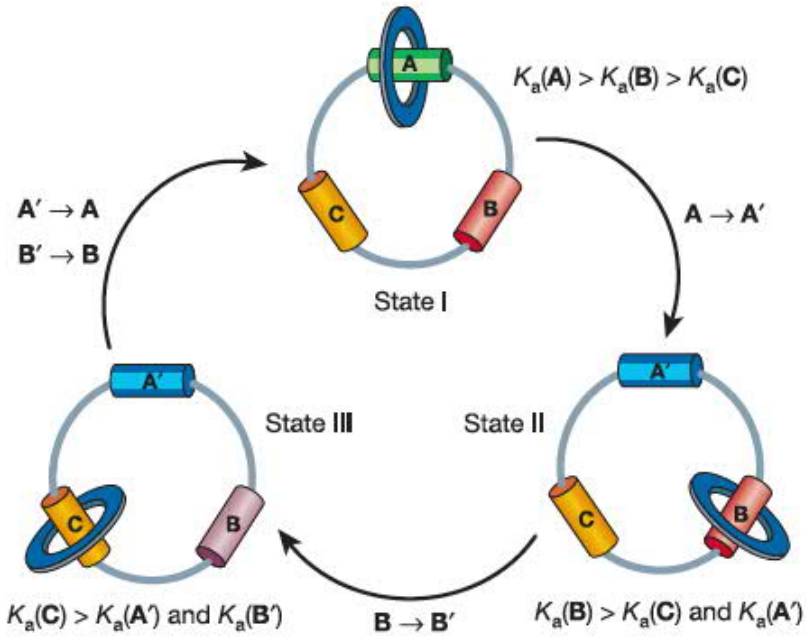

Figure 3.2: Schematic representation of the movement induced by external stimuli of a macrocycle through three different recognition sites in a [2]catenane. The larger macrocycle contains three stations labelled as A, B and C, each with different affinities (association constant, K_a) for the smaller macrocycle. Adapted from ref. [6], copyright © Nature publishing group.

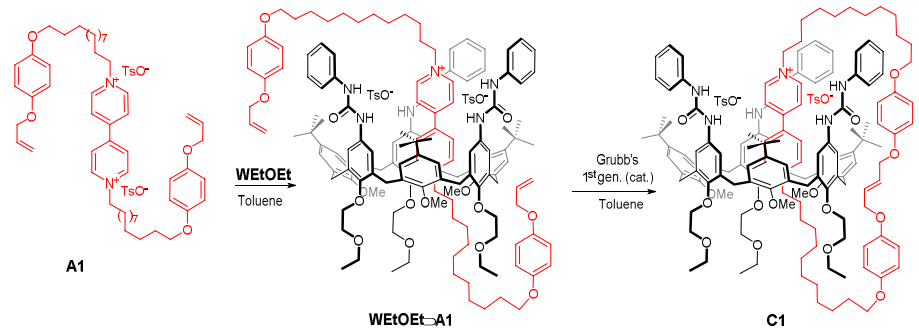

Scheme 3.1: A single-station asymmetric calix[6]arene-based [2]catenane (see ref. [6]).

effect of a [2]pseudorotaxane complex formed between **WEtOEt** and symmetric viologen-based axle (**A1**) characterised by two long alkyl arms, each terminating with an allyloxyphenyl group.

A Ring-Closing Metathesis (RCM) reaction catalysed by a 1^{st} gen. Grubbs catalyst was then used to clip the axle around the calix[6]arene wheel, giving the desired interwoven compound **C1**. Compound **C1** is an example of single-station [2]catenane for which a possible directional movement of the shuttling calix[6]arene wheel, potentially occurring upon reduction of the viologen station, cannot be evidenced since the track of the second ring is symmetrical. Moreover, this structure lacks of a second station capable of promoting the shift of the wheel from the reduced viologen station. On these bases, a second [2]catenane **C2** was thereafter designed and prepared (see scheme 3.2).[9] It consists of a "track" ring endowed with two distinct recognition sites, a bipyridinium and an ammonium unit, and of **WEtOEt** as the "shuttling" ring. By exploiting, as usual, the ability of the calix[6]arene to directionally thread appropriate non-symmetric axles (**A2**), an oriented pseudorotaxane was assembled and converted into the corresponding oriented catenane **C2** through an intramolecular RCM reaction catalysed by a 2^{nd} gen. Grubbs catalyst.

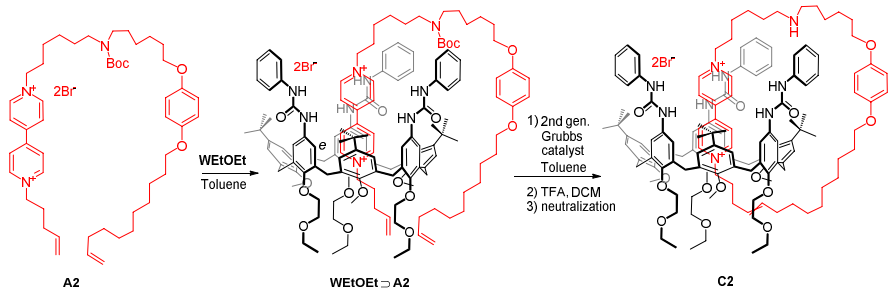

Scheme 3.2: A two-station oriented calix[6]arene-based [2]catenane (see ref. 8).

3.2 Results and Discussion

The two-station track ring present in [2]catenanes **C2** cannot adequately discriminate if the shuttling movement of **WEtOEt** may occur preferentially clockwise or counterclockwise. The tools used to trigger and evaluate the wheel movement (EPR and cyclic voltammetry) may indeed discriminate only between the starting and the arrival stations, but not the directionality of this movement. To obtain such relevant information, the track ring must contain some "gates", or functional groups, which may change their molecular geometry (*i.e.* cis-trans isomerism) upon the application of selected stimuli. According to the geometry adopted, a gate can allow or not the shuttling of the calix[6]arene wheel between the two stations. The insertion of gates and stations alternately in the track ring, should allow to control the direction of the shuttling movement of **WEtOEt**. Indeed, according to the non-hindrance (NH) or hindrance (H) status of each gate, the wheel may only move clockwise or counterclockwise, as depicted in figure 3.3. Therefore, when a gate is open, (NH) the shuttling kinetic will exclusively depend on the propensity of the wheel to move in that direction along the track.

The studies presented above evidenced that the length of the track ring must be at least of 30 carbon atoms to allow free motion of **WEtOEt** along it. Moreover, if the starting axle is too short, the cyclisation of the axial component will be disfavored due to excessive torsion needed for the two chains to react. On the other hand, an axle too long will result in excessive mobility of the two chains that will decrease the probability of

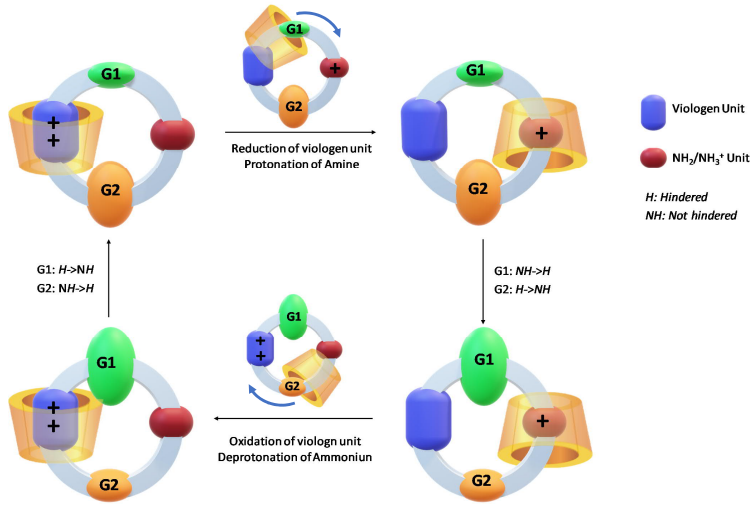

Figure 3.3: Schematic representation of the possible shuttling motions of **WEtOEt** along a two-station-two-gates track ring

an intramolecular ring-closing reaction. Based on these premises, the axle **22** depicted in figure 3.4 was designed. It is based on two stations: i) viologen core (V) and ii) ammonium moiety (N) and characterised by an azobenzene unit as the primary "gate" (**G1**), which is interposed between the V- and N- stations through two C6 alkyl spacers. The azobenzene unit was selected thanks to its extensively documented properties of cis-trans photoisomerisation.[10] Both the stations are also functionalised with a ω-hydroxyl C6 alkyl chain. The idea to use the OH group as the reactive axle endings, was due to the well-known propensity of this functional group to undergo mild protection and deprotection procedures.

Moreover, the OH group allows fast esterification reactions in high yields with a plethora of commercially available acids or derivatives. The axle **22** was designed to allow the facile introduction in the track ring of the resulting [2]catenane of any secondary gate (**G2**) in the form of difunctional acid derivatives. Most important, this introduction is always accomplished in the final stage of the catenation reaction. This increases the versatility and modularity of the method (see figure 3.4). Since the designed axle **22** is not symmetric, and the wheel **WEtOEt** is not palindrome, the final catenation

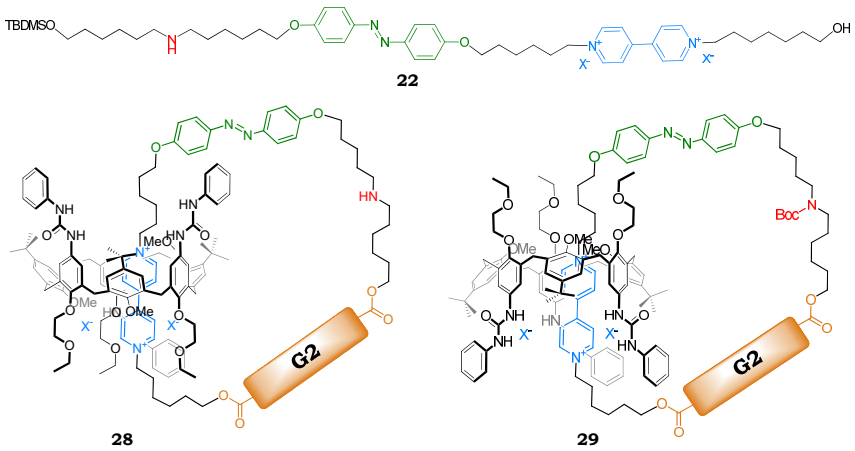

Figure 3.4: Schematic representation of axle **22** and the two possible [2]catenane orientational isomers **28** and **29** deriving from the ring-closing reaction between pseudorotaxane **WEtOEt⊃22** and a generic difunctional unit containing the gate **G2**.

reaction may potentially afford the two orientational [2]catenane isomers, **28** and **29** reported in figure 3.4. As stated in the previous chapters, however, in low polarity solvents such as chloroform or toluene, the threading of a viologen salt in **WEtOEt** always occurs selectively through the upper rim of the macrocycle and with the less hindered alkyl chain. The synthesis of the orientational isomer indicated as **25** in figure 3.5 can be thus achieved for threading and clipping of axle **22**, while to synthesise the opposite isomer **24**, it would be necessary to adopt the supramolecular-assisted strategy previously described.

Axle **22** and wheel **WEtOEt** were thus identified as the candidates for the formation of two orientational pseudorotaxane isomers to be used as precursors for the synthesis of the desired [2]catenane isomers **28** and **29** through a clipping reaction with a proper gate unit **G2**. Since pseudorotoxane complexes are not isolable through chromatographic separations, it was decided to synthesise and characterise the two relative oriented [2]rotaxane isomers **24** and **25** shown in figure 3.5.

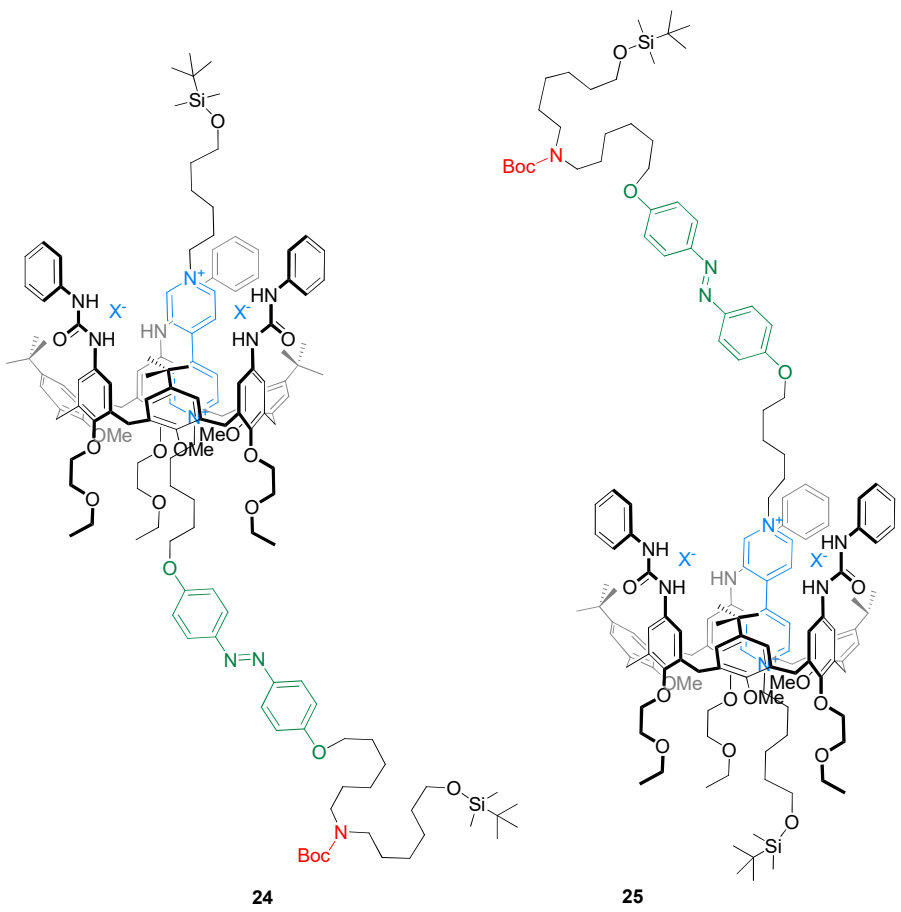

Figure 3.5: Schematic representation of the oriented [2]rotaxane isomers **25** and **24** used as a precursor for the synthesis of [2]catenanes **29** and **28**

3.2.1 Synthesis of Axle 22

The preparation of axle **22** required several synthetic steps. Through a retrosynthetic analysis, compounds **14** and **17** were identified as the proper precursors. The synthesis of **14** started from the commercially available 6-aminohexan-1-ol (see scheme 3.3). The N-Boc-protected derivative **12** was synthesised in quantitative yield by reacting the 6-amino-1-hexanol with di-tert-butyl dicarbonate (Boc_2O) in 1:2 stoichiometric ratio. The reaction was carried out in refluxing anhydrous THF for 24 hours. The product **12** is a colourless oil, identified by ^1H NMR spectroscopy. In the following step, the hydroxyl group of **12** was protected with the tert-butyl-dimethyl silyl group (TBDMS). The alcohol protection reaction, which leads to the formation of **13** in 81 % yield, was carried out in dry dichloromethane at room temperature for 24 hours using the tert-butyl-dimethyl silyl chloride (TBDMS-Cl) and 4-dimethylaminopyridine (DMAP) as the catalyst. Triethylamine was added to the reaction mixture as the scavenger of the hydrochloric acid released in the reaction. The TBDMS group was selected to protect the amino alcohol OH group because of its good stability to the basic condition necessary in few following synthetic steps. Moreover, thanks to its high steric hindrance, this PG can also act as the axle stopper in the rotaxane formation. Compound **13** was then converted into the desired Boc-protected O-protected intermediate **14**. The reaction was carried out under inert atmosphere in dry DMF and using sodium hydride as the base to deprotonate the NH group of **13**. A large stoichiometric excess of 1,6-dibromohexane (1:3) was used to promote the formation of the monosubstitution product. Compound **14** was purified by chromatographic separation as colourless oil in 70 % yield. Its identity was confirmed through NMR and MS measurements (see experimental part).

The second intermediate for the preparation of axle **22** is the azobenzene precursor **17**, whose synthesis is depicted in scheme 3.3. The first strategy applied to obtain this precursor was an attempt to monoalkylate the known 4,4'-dihydroxy azobenzene[11] with 6-hydroxyhexyl tosylate. To favour the formation of the monoalkylated product, a stoichiometric defect of the alkylating agent (1:0.5) was used. However, this strategy led to the almost exclusive formation of the dialkylated product, likely because of the higher solubility and reactivity of the monoalkylated adduct compared to that of the reactant. To overcome this problem, the monoalkylated

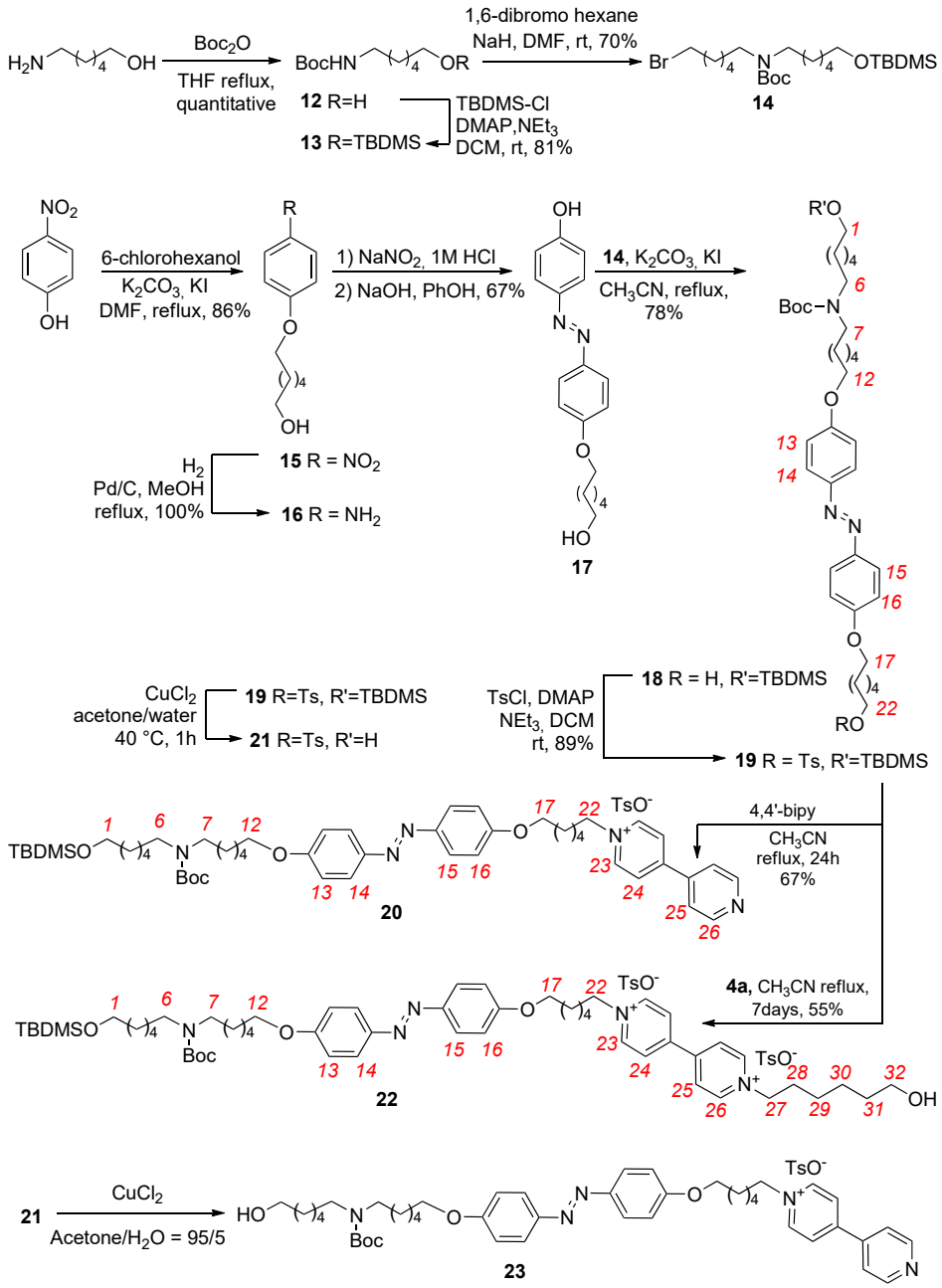

Scheme 3.3: Synthesis of axle **22** and semi-axle **20** and **23**

azobenzene derivative **17** was synthesised starting from the commercially available p-nitrophenol using the three-step procedure described in scheme 3.3. In the first step of the procedure, the nitro derivative **15** was synthesised by reacting p-nitrophenol with 6-chlorohexan-1-ol in refluxing dry DMF for 24 hours, using K_2CO_3 as base and KI as the catalyst.[12] After reaction workup, **15** is obtained as a pure yellow solid in 86 % of yield. The nitro group of **15** was then quantitatively reduced to obtain **16** using hydrazine monohydrate as hydrogen source and Pd/C as catalyst in refluxing methanol for 24 h. The synthesis of the azobenzene intermediate **17** was finally carried out through a diazotisation reaction. The diazonium chloride salt is produced by dissolving **16** in a 1 M solution of HCl and adding a solution of sodium nitrite in water. The subsequent electrophilic aromatic substitution reaction of the diazonium salt with phenol in a basic solution (NaOH) finally led to the desired azocompound **17** in 70 % of overall yield. After the NMR product identification, the alkylation of **17** with **14** carried out in refluxing dry acetonitrile using K_2CO_3 as the base and KI as the catalyst, gave **18** as a waxy yellow solid in 78 % of yield. The identity of **18** was verified by NMR and MS measurements.

In the following step, the terminal hydroxyl group of **18** was transformed into a good leaving group by its reaction with p-toluenesulfonyl chloride in dry dichloromethane and using DMAP and triethylamine as the catalyst and the proton scavenger, respectively. After chromatographic separation, the resulting tosylate **19** was isolated as a yellow solid in 89 % yield. This compound is the starting building block for the synthesis of both the orientational isomers of the [2]catenane. Indeed, it was then reacted in refluxing dry acetonitrile with i) 4,4'-bipyridine for 48 h to give the semi-axle **20** in 65 % yield, and then with ii) the pyridylpyridinium salt **4a** for seven days, to obtain axle **22** in 55 % yield. All the intermediates up to **20** and **22** were fully characterised through NMR and MS measurements. The ^{1}H-NMR spectra of semi-axle **20** and axle **22** have been reported in the stack plot of figure 3.6. The two spectra share all the signals deriving from the TBDMS and Boc PGs (at 0.07, 0.90 and 1.45 ppm), from the aliphatic protons of the inner methylene groups of the alkyl spacers (in the 1.2 - 2.2 ppm range) and from the methyl group of the tosylate anion (at 2.35 ppm). In the mid-field region of the spectra (from 3 to 5 ppm), it is observed the presence of several triplets, more or less overlapped. These signals were

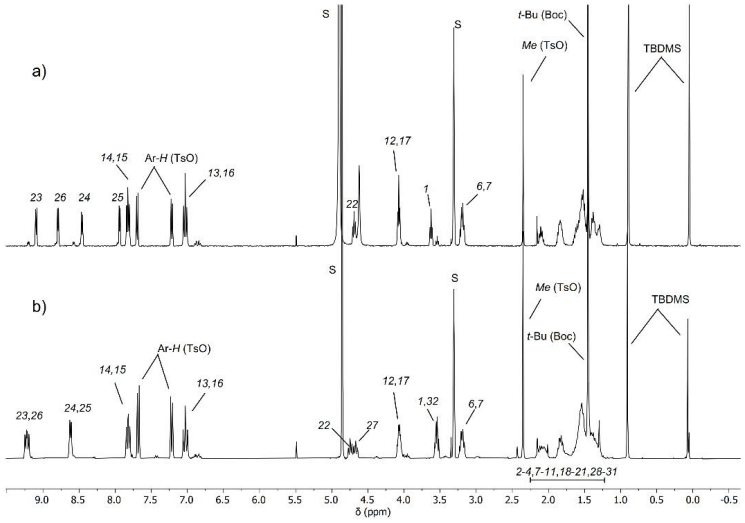

Figure 3.6: ^{1}H NMR stack plot (400 MHz, CD_3OD) of a) semi-axle **20** and b) axle **22**. For the proton assignment and labelling see text and scheme 3.3

assigned to the several methylene groups adjacent to the V- and N-station and the azobenzene unit of the axles. At *ca.* 3.2 ppm two overlapped triplets, overall integrating for 4 protons, are visible. They were assigned to the methylene protons adjacent to the N-station and labelled as *6* and *7* in scheme 3.3. The methylene group *1*, adjacent to the TBDMS-protected terminal hydroxyl group, resonates as a well-defined triplet centered at 3.62 ppm in **20** (see figure 3.6a), while in axle **22** it is overlapped with the triplet assigned to methylene *31* (see figure 3.6b). The two methylene groups *12* and *17*, adjacent to the azobenzene unit, give rise to a triplet at 4.08 ppm in **20**, and to a multiplet at *ca.* 4 ppm in **22**. Finally, the protons of the methylene group adjacent to the V-station, resonate in **20** as a single triplet integrating for two protons at 4.69 ppm (*22*), while in **22** as two close but distinct triplets at 4.67 (*22*) and 4.75 (*27*) ppm. In the downfield region of the spectra are visible the two doublets relative to the aromatic portion of the tosylate anion at 7.21 and 7.68 ppm. The different substitution of the azobenzene unit makes the aromatic protons in ortho to the alkoxy substituents, labelled in scheme 3.3 as *13* and *16*, chemically different. The same applies to protons *14* and *15*, in ortho to the azo group. As a con-

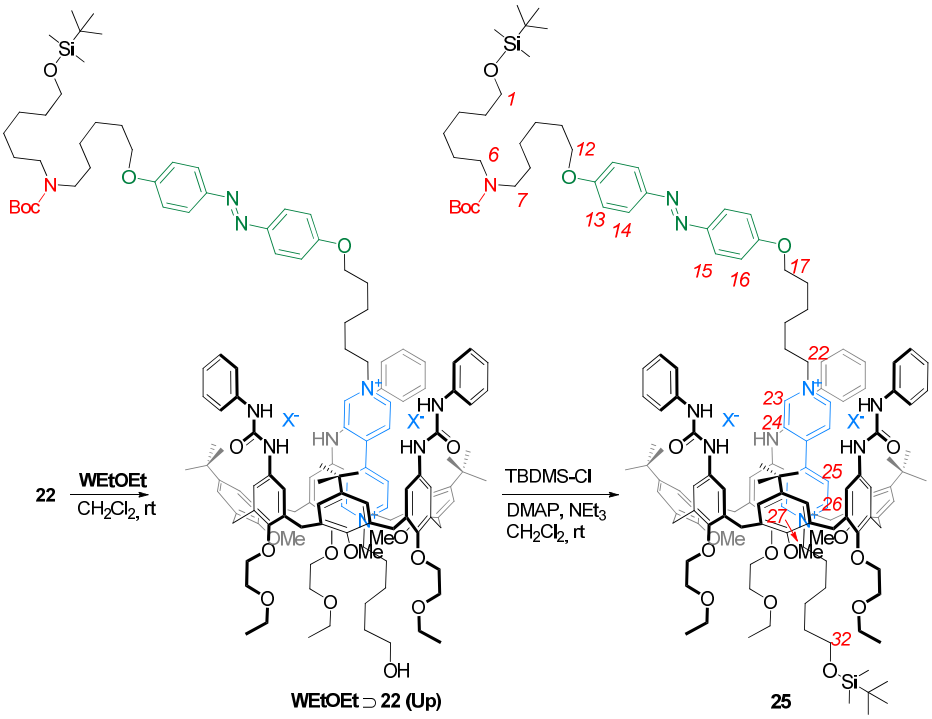

Scheme 3.4: Synthesis of the oriented [2]rotaxane isomer **25** through the procedure of threading and capping

sequence, each pair of these coupled protons gives rise to two overlapped doublets centered at 7.02 for protons *13* and *16* and a similar system at 7.82 ppm for protons *14* and *15*. In both spectra, such pattern is identical (see figure 3.6). The most significant difference in the spectra of **20** and **22** is found in the pattern of signals yielded by the two pyridine aromatic rings of the V-station. The higher symmetry of this system in **22** generates two overlapped doublets at *ca.* 9.2 ppm for protons in ortho to the positively charged nitrogen, *i.e.* the protons labelled as *23* and *26*, while the less deshielded protons *24* and *25* resonate as a doublet at 8.62 ppm. In **20**, the V-station is alkylated only to one pyridine ring. This generates a pattern of four doublets: 9.10, 8.79, 8.46 and 7.94 ppm for protons *23*, *26*, *24* and *25*, respectively.

The equilibration of **22** with **WEtOEt** in dichloromethane at room temperature led to the formation of the single oriented pseudorotaxane isomer **WEtOEt⊃22** (see scheme 3.4), in which the hydroxyl termini of the axle is in proximity of the lower rim of the wheel. Indeed, in low polarity solvent, the threading of N,N'-dialkylviologen salts selectively occurs always with either the less hindered[13, 14] or the shortest alkyl chain through the upper rim of the calix[6]arene wheel. The red colour of the resulting solution, given by the charge transfer interaction between the electron-poor axis and the electron-rich calixarene cavity, confirmed the formation of the pseudorotaxane complex. The reaction of the terminal hydroxyl group, protruding from the wheel lower rim, with the bulky TBDMS-Cl, in presence of triethylamine as the base and DMAP as the catalyst, led to the formation of the orientational [2]rotaxane isomer **25** in 44 % yield (see scheme 3.4). The resulting mechanically interlocked molecule can be purified and isolated through column chromatography and, most important, it allows to confirm the hypothesised reciprocal orientation of the two molecular components through a series of NMR measurements. Such orientation should indeed represent an indirect proof of the orientation of the final catenane.

The ^{1}H NMR spectrum of rotaxane **25** taken in CD_2Cl_2 has been reported in figure 3.7b. With respect to the free wheel **WEtOEt**, it is interesting to note that **25** gives rise to a better-resolved pattern of signals. This usually indicates an increment of the rigidity of the macrocycle due to the formation of the MIM (*cf.* figure 3.7a and b). This hypothesis is also confirmed by the sharpening and the downfield shift of the signal relative to the wheel methoxy groups (from *ca.* 2.9 to 3.98 ppm). Indeed, because of the axle threading, the methoxy groups are ejected from the cavity and resonate at lower fields. Other diagnostic signals that confirm the threading and blocking of **22** inside the cavity of **WEtOEt** are: i) the large upfield shift of the signals relative to protons of the pyridinium rings (from 9.3 - 8.6 to *ca.* 7.7 - 5.9 ppm, *cf.* figure 3.7b and figure 3.7c) that, being included inside the aromatic cavity, became broader and shifted to higher field; ii) the appearance of two broad signals for the NH protons of the *host* phenylureido group at 8.9 and 8.6 ppm, which are hydrogen-bonded to the thread counteranions (tosylate); iii) the upfield shift of the methylene protons *22* and *27* from *ca.* 4.8 and 4.7 to 3.2 and 3.9 ppm, respectively (In the spectrum of **25** these resonances become very broad, and they are recognised

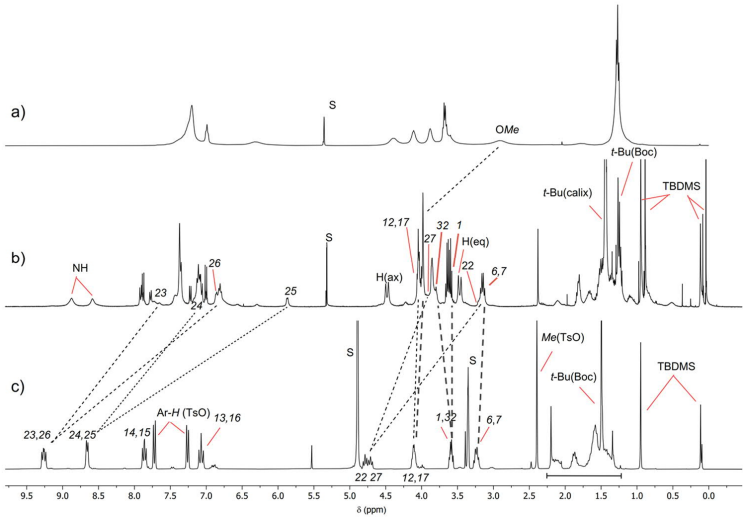

Figure 3.7: ^{1}H NMR stack plot (400 MHz, 298 K) of a) wheel **WEtOEt** and b) [2]rotaxane **23** in CD_2Cl_2, and of c) axle **22** in CD_3OD. For the proton assignment and labelling see text and Scheme 3.

only through the analysis of the HSQC spectrum). The different extent of the shift of these two signals (*ca.* 1.6 and 0.8 ppm) is due to the well-known geometry of inclusion of the V-station in the calix[6]arene wheel. Methylene labelled as *27* protrudes from the cavity, while *22* experiences a large anisotropic effect due also to the phenylureas present on the wheel upper rim. It is also worth to observe that the two singlets due to the tert-butyl and methyl groups of the TBDMS protecting groups are split because of the asymmetry of the rotaxane (one of the protecting groups is close to the upper rim of the wheel, while the other one is close to the lower rim). The signals relative to methylene groups labelled as *1* and *32* are split into to resonances now at 3.59 ppm (*1*) and 3.79 ppm (*32*). Very important for the identification of the signals, was the identification of the 2D TOCSY correlations between *22* and *17*, *1* and *6*, *27* and *32*. Moreover, the signals *22* and *17* have TOCSY correlations with the four upfield shifted methylene groups resonating at 0.52 ppm (*21*), 0.84 ppm (*20*), 1.86 ppm (*19*) and 1.66 ppm (*18*). These findings confirm that this portion of the *guest* is close to the phenylureido groups at the upper rim of **WEtOEt** and it is

strongly influenced by its shielding effect.

3.2.2 Synthesis of the Rotaxane 24

As anticipated above, the synthesis of the other orientational [2]rotaxane isomer **24**, through the *threading* and *capping* strategy, is not feasible. Indeed, it would require an axial component with the TBDMS stopper on the shorter alkyl chain of the V-station and with the free OH ending on the opposite longer alkyl chain. Nevertheless, even in this condition, the threading of a so hindered long alkyl chain would be unfavoured. Based on these considerations, a different strategy, called "supramolecular-assisted alkylation"[15] was used for the synthesis of **24**.

The opportune pyridylpyridinium salt **20** and **WEtOEt** were equilibrated in dry toluene in 1:1.5 ratio (see scheme 3.5). Previous studies of our research group[15–17] have indeed demonstrated that pyridylpiridinium salts, such as **20**, can thread the **WEtOEt** macrocycle from both the upper and the lower rim leading to the formation of both the two possible pseudorotaxane orientational isomers in solution. However, the isomer with the alkyl chain protruding from the lower rim has, for stability reasons, its positively charged pyridinium rim deeply engulfed inside the calixarene cavity. Thus, its non-alkylated pyridine nitrogen atom is more nucleophilic. As a consequence, this isomer is more reactive toward the further alkylation of the free nitrogen atom. Indeed, after the equilibration of **WEtOEt** with **20** for 24 h, the monotosylate **3a** was added to the reaction mixture and left to react for seven days at 70 °C.

The obtained pseudorotaxane isomer **WEtOEt⊃22** (**Down**) was then converted in a [2]rotaxane by reacting the hydroxyl termini of thread **22** with TBDMS-Cl (see scheme 3.5). The rotaxane **24** was isolated as a red solid compound through a column chromatography separation with a 47 % overall yield for the last two steps. The ^{1}H NMR spectrum of rotaxane **24** taken in CD_2Cl_2 is reported in the stack plot of figure 3.8. To check the difference between the signals assignment of rotaxane **25** and **24** their spectra were gathered in the stack plot of figure 3.9. Even though the overall pattern of signals in the two spectra is very similar, there are few notable differences: i) the signals assigned to the bispyridinium core (protons labelled as *23-26* in schemes 3.4 and 3.5) are swapped. This is in agreement with the hypothesis that in the two rotaxanes the orientation of

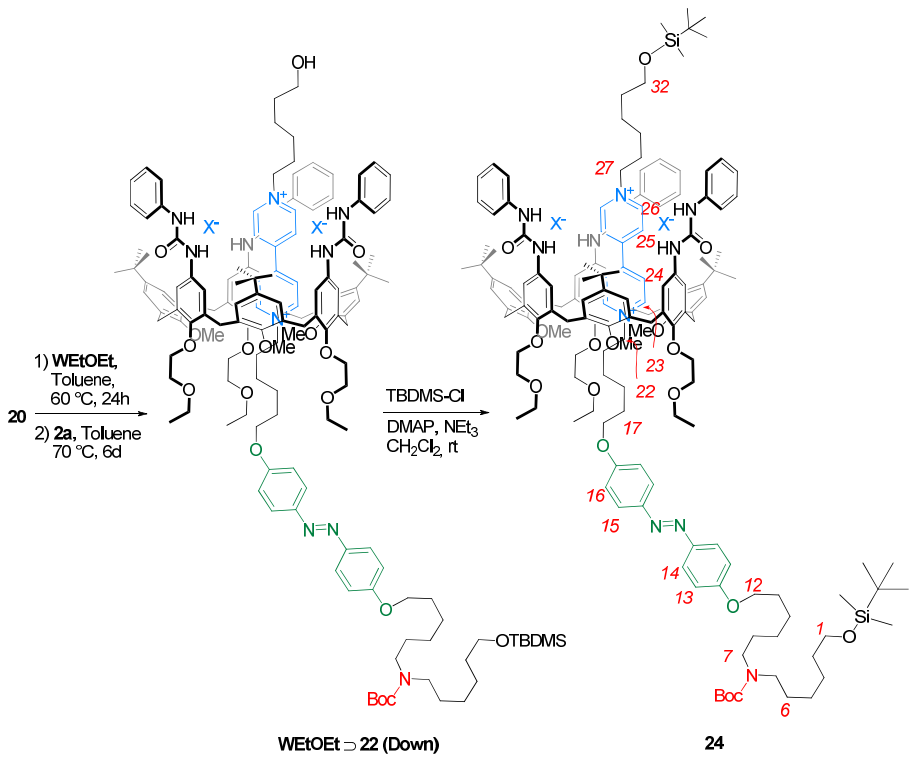

Scheme 3.5: Synthesis of the oriented [2]rotaxane isomer **24** and the oriented pseudorotaxane **WEtOEt⊃22** (**Down**) through the supramolecular-assisted approach.

the thread inside the wheel is opposite.

For rotaxane **25**, in which the azobenzene unit is oriented toward the *host* upper rim, the signals relative to the methylene protons *12* and *17* are slightly upfield-shifted (*ca.* 0.2 ppm) with respect the same signals in **24**. This could reflect the fact that the azobenzene unit is still affected by the anisotropic shielding effect of the calix[6]arene cavity. Since the determined molecular ion for the two compounds is identical (see figure 3.10), these differences are an indirect proof that the two compounds are isomers of the assembly.

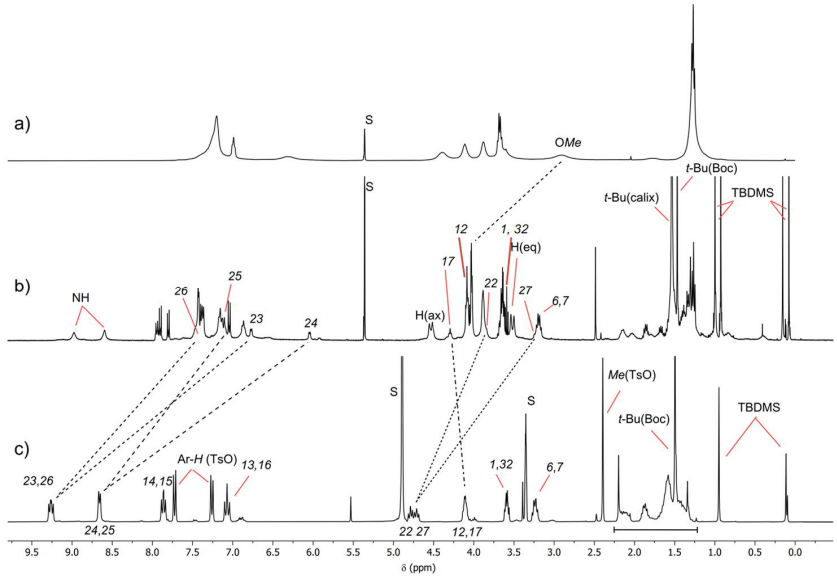

Figure 3.8: ^{1}H NMR stack plot (400 MHz) of a) wheel **WEtOEt** and b) [2]rotaxane 24 in CD_2Cl_2, and of c) axle **22** in CD_3OD. For the protons' labelling see scheme 3.5

3.2.3 Synthesis of the Clipping Agent 27

As specified in the introduction to this chapter, the synthesis of the target catenane requires a final catenation reaction with a suitable "clipping agent". This latter must be a difunctional compound capable to quickly react with the re-established OH groups of the thread, and possibly capable to behave as a gate. The trans-stilbene acyl chloride derivative **27** depicted in scheme 3.6 was selected as a useful model of the clipping agent. The esterification reaction with the thread hydroxyl termini should not affect the stability of the pseudorotaxane as, in contrast, it may occur with base-catalysed reactions. Moreover, once clipped on the catenane thread, its unsaturation can be isomerised. **27** was synthesised by the two-step procedure illustrated in scheme 3.6.

Its precursor, the dibenzoic acid **26**, was prepared according to a procedure reported in the literature.[18] The 4-bromo benzoic acid is reacted triethoxyethyl vinyl silane in a Heck/Hiyama coupling reaction catalysed by $Pd(OAc)_2$. The reaction is carried out in a NaOH solution at 140 °C for

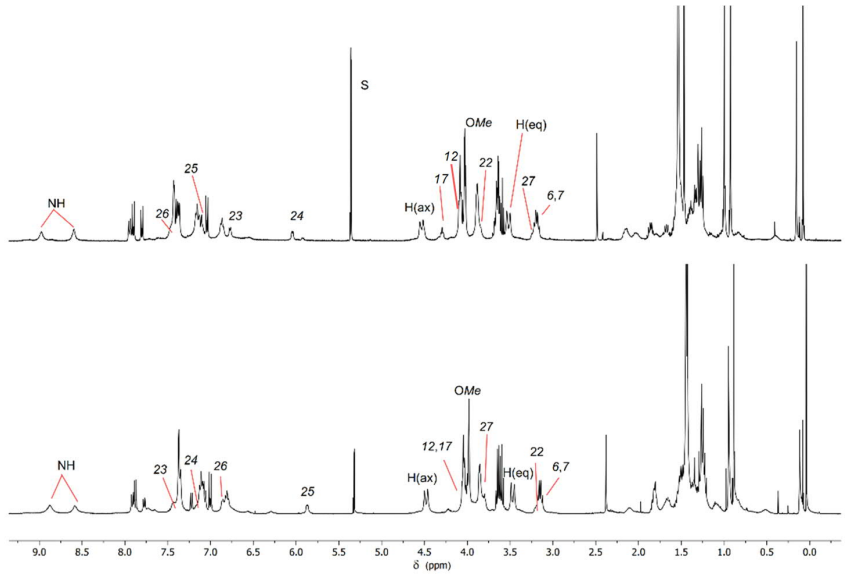

Figure 3.9: ^{1}H NMR stack plot of (400 MHz, CD_2Cl_2) of the [2]rotaxane orientational isomers **24** (top) and **25** (bottom).

5 hours; after acidification of the solution, product **26** is isolated by precipitation in a 73 % yield. The carboxylic functions were then transformed into the more reactive acyl chloride to have a faster and milder clipping reaction. It is worth to note that the final catenation reaction must be carried out in weakly polar media to avoid the scrambling of the thread in the pseudorotaxane. The conversion of **26** to **27** was accomplished with thionyl chloride in DMF at 70 °C for 24 h. The acyl chloride was isolated quantitatively as a yellow solid compound.

3.2.4 Synthesis of the Catenane 28

The catenation reaction was carried out on the oriented pseudorotaxane isomer **WEtOEt⊃23** (**Down**) (see scheme 3.6). For the preparation of this complex, the semiaxle **23** was synthesised from the deprotected azobenzene derivative **21** (see scheme 3.3). This latter was obtained from **19** removing the TBDMS PG using $CuCl_2$ in a water / acetone mixture. This deprotection reaction is very mild and does not affect the azobenzene and the

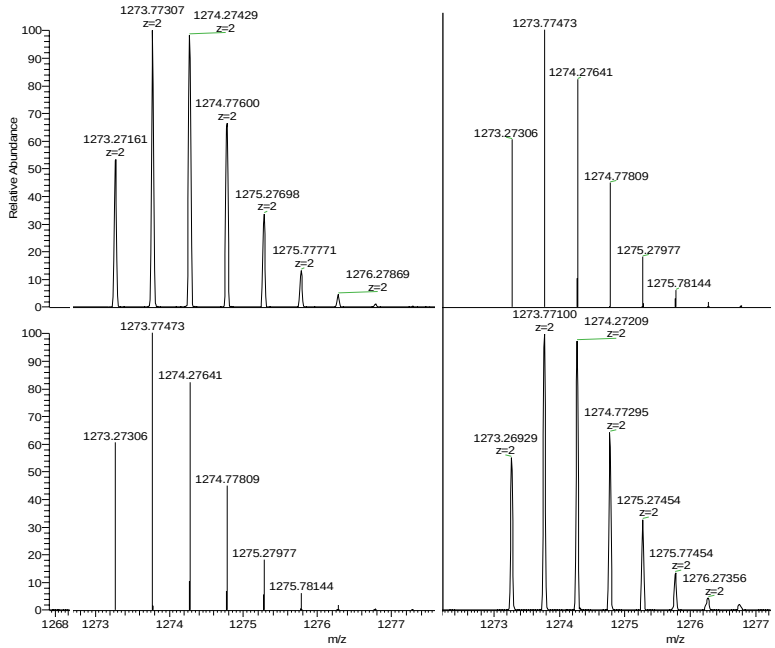

Figure 3.10: HR-MS spectra of the [2]rotaxane orientational isomers **25** (top left) and **24** (down right) with the corresponding theoretical isotopic distributions in the same column.

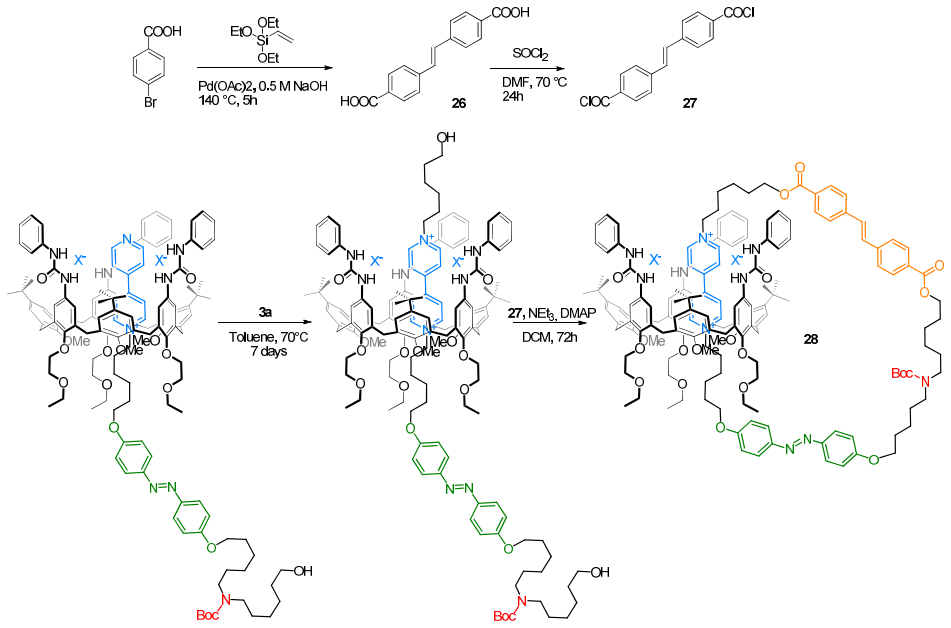

Scheme 3.6: Synthesis of the clipping agent **27** and of the oriented [2]catenane **28**

BOC PG of **19**. All the attempts performed to remove this PG using more usual deprotecting agents such as KF or TBAF determined the semi-axle decomposition. Then the oriented pseudorotaxane complex was prepared in a similar way to rotaxane **24** through the supramolecular-assisted reaction. Semi-axle **23** was equilibrated with a stoichiometric excess of **WEtOEt** in toluene, then tosylate **3a** was added (see scheme 3.6). After solvent evaporation, the so obtained pseudoroxatane was taken up in dry dichloromethane up to a 10^{-3} M concentration. In previous studies, this concentration was indeed identified as suitable to avoid/minimise the intermolecular reaction.[8, 9] A solution of **27** in the same solvent was then added, along with DMAP as catalyst and triethylamine as base. After 72 h of reaction at room temperature and removal of the solvent under reduced pressure, the [2]catenane **28** was isolated through preparative TLC and characterised through MS and NMR measurements.

The ^{1}H NMR spectrum taken in $CDCl_3$ (see figure 3.11, top), despite a general broadness, present similar features with the spectrum of rotaxane

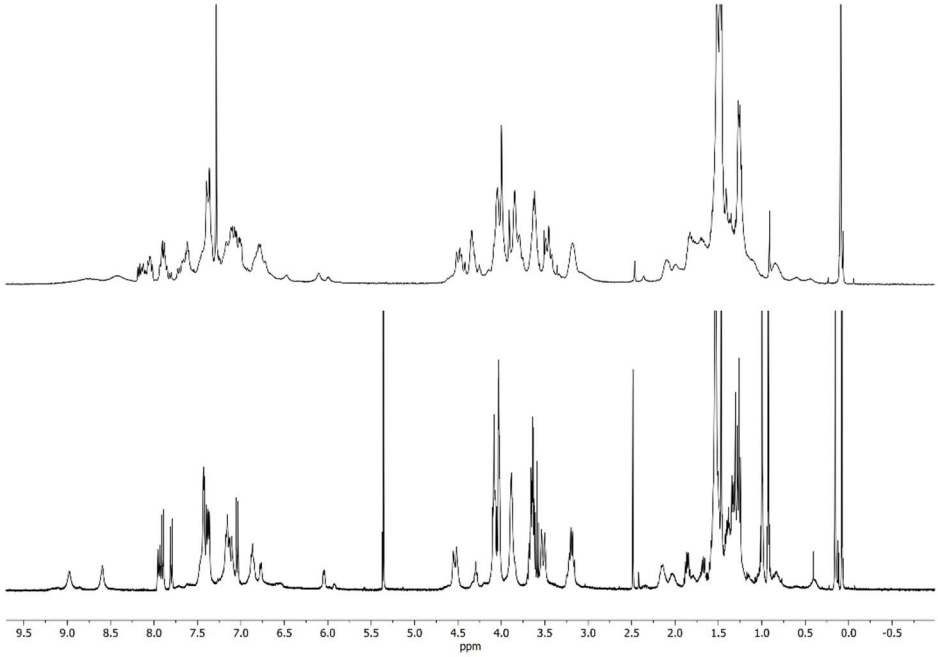

Figure 3.11: ^{1}H NMR stack plot of (400 MHz, 298 K) of the oriented [2]catenane **28** in $CDCl_3$ (top), and of [2]rotaxane orientational isomers **24** in CD_2Cl_2 (bottom).

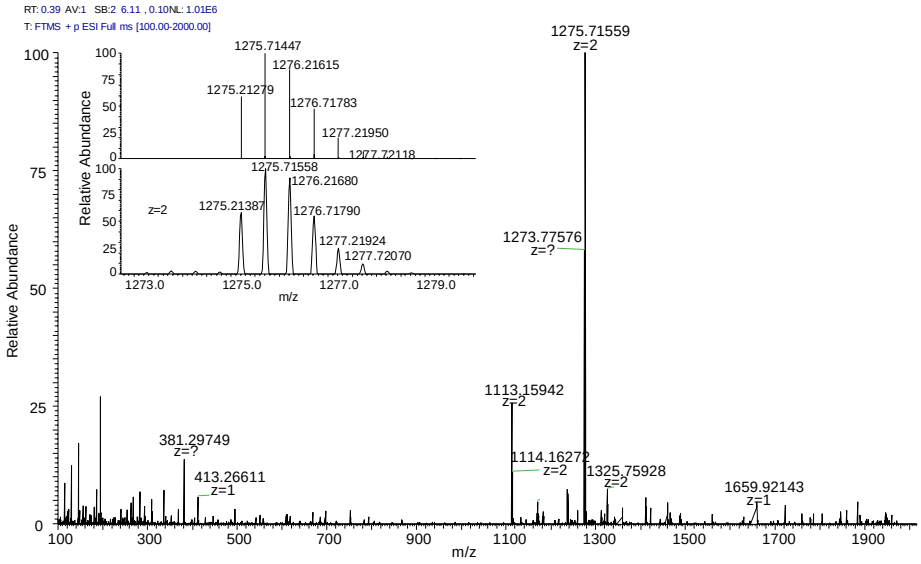

Figure 3.12: HR-MS spectra of the [2]catenane **28** with a double charged peak at 1275.71559 (z = 2). In the inset, the experimental isotopic distribution is compared with the calculated one.

24 (see figure 3.11, bottom), with which it shares the same orientation of the azobenzene unit with respect the macrocycle rims. Moreover, in the downfield region of the spectrum (at δ >8 ppm) are now present aromatic resonances not found in the spectrum of **24**. These new resonances are reasonably assigned to the aromatic portion of the stilbene gate just introduced. The general higher complexity of the spectrum of **28** is likely due to the cyclisation reaction that introduces a further element of asymmetry in the molecular system. As an example, the bridging methylene groups of the calix[6]arene macrocycle of **28** do not resonate as a typical AX system of two doublets with germinal coupling for the equatorial and axial diasterotopic protons, as found instead in 24. Nevertheless, the HR-MS spectrum (see figure 3.12) highlights the presence of a doubly charged peak at m/z = 1275.71559 D in good agreement with the calculated mass for **28**.

3.3 Experimental

Materials All solvents were dried using standard procedures; all other reagents were of reagent grade quality, obtained from commercial suppliers and were used without further purification. NMR spectra were recorded at 400 MHz for ^{1}H and 100 MHz for ^{13}C. Melting points are uncorrected. Chemical shifts are expressed in ppm (δ) using the residual solvent signal as internal reference (7.16 ppm for C_6H_6; 7.26 ppm for $CHCl_3$ and 3.31 for CH_3OH). Mass spectra were recorded in ESI mode. Compounds **12**,[19] **13**, [20] **15**, [21] **16**, [22] **17**, [12] and the stilbene unit.[23] were synthesised according to published procedures.

Synthetic procedures

tert-butyl(6-bromohexyl)(6-((tert-butyldimethylsilyl)oxy)hexyl) carbamate (14) In a 100 mL two necks round bottomed flask, **13** (1.0 g, 3.02 mmol) was dissolved in 20 mL of dry DMF under inert atmosphere. Sodium hydride (0.16 g, 6.67 mmol) was added, and the reaction mixture was stirred at RT for 1 h, then 1,6-dibromohexane (1.38 mL, 9.06 mmol) was added and the solution was stirred for 4 h. After quenching the reaction by addition of iced water, the organic phase was diluted with dichloromethane (150 mL) and washed with water (3x200 mL), then dried with anhydrous sodium sulfate and evaporated to dryness under reduced pressure. The oily residue was purified through column chromatography on silica gel (hexane/dichloromethane = 20/80) to yield 1.0 g of **14** (70 %) as colorless oil. ^{1}H NMR (400 MHz, $CDCl_3$): δ (ppm) = 3.59 (t, 2H, ^{3}J = 6.5 Hz), 3.39 (t, 2H, ^{3}J = 6.8 Hz), 3.14 - 3.13 (br.s, 4 H), 1.88 - 1.81 (m, 2 H), 1.50 - 1.44 (m, 17H), 1.31 - 1.28 (m, 6H), 0.88 (s, 9H), 0.03 (s, 6H). ^{13}C NMR (100 MHz, $CDCl_3$): δ (ppm) = 155.6, 78.9, 78.8, 63.1, 47.0, 46.8, 33.6, 32.8, 32.7, 28.7 (two resonances), 27.9, 26.7, 26.0, 25.9 (two resonances), 18.3, 5.3. ESI-MS(+): m/z = 518 $[M+Na]^+$, 534 $[M+K]^+$.

Azobenzene derivative (18) In a 100 mL round bottomed flask **17** (0.58 g, 1.85 mmol) and K_2CO_3 (0.31 g, 2.24 mmol) were dissolved in 30 mL of dry acetonitrile. The mixture was stirred 10 minutes at RT, then **14** (1 g, 2.02 mmol) and KI (cat.) were added and the reaction was refluxed 48

h. The solvent was evaporated under reduced pressure, the crude mixture was taken up with ethyl acetate (100 mL). The resulting organic phase was treated in an iced bath with a 10 % w/v solution of HCl up to neutrality, and then washed twice with distilled water (2x150 mL), dried with anhydrous sodium sulfate and evaporated to dryness under reduced pressure. The chromatographic separation on silica gel (hexane/ethyl acetate = 50/50) afforded **18** (78 %) as a yellow solid. M.p. = 70.8 - 71.1 °C. ^{1}H NMR (300 MHz, $CDCl_3$): δ (ppm) = 7.91 (4H, d, ^{3}J = 8.9 Hz), 7.01 (br.s, d, 4H, ^{3}J = 7.8), 4.05 (q, 4H, ^{3}J = 6.4 Hz), 3.69 (t, 2H, ^{3}J = 6.5 Hz), 3.61 (t, 2H, ^{3}J = 6.4 Hz), 3.24 - 3.12 (m, 4H), 1.93 - 1.77 (m, 4H), 1.70 - 1.45, 1.44-1.25 and 1.47 (2m, s, 37H), 0.91 (s, 9H), 0.06 (s, 6H). ^{13}C NMR (100 MHz, $CDCl_3$): δ (ppm) = 161.2, 146.9, 124.4, 114.7, 68.2, 63.2, 62.9, 47.0, 32.8, 32.7, 29.2, 28.5, 26.7 (two resonances), 26.0, 25.9, 25.7, 25.6, 5.2. ESI-MS(+): m/z = 728.

Azobenzene derivative (19) In a 50 mL round bottomed flask, 7 (0.90 g, 1.24 mmol), triethylamine (0.155 mL, 1.57 mmol) and DMAP (cat.) were dissolved in 30 mL of dichloromethane. The reaction mixture was cooled using an external ice bath and 4-methylbenzenesulfonylclhoride (0.20 g, 1.07 mmol) was added. The reaction mixture was stirred for 24 h at RT, then the organic phase was washed with distilled water (2x100 mL), dried with sodium sulfate and evaporate to dryness under reduced pressure. The residue was purified by column chromatography on silica gel (hexane/ethyl acetate = 9/1) to yield 0.97 g of **19** (89 %) as a yellow solid. M.p. = 81.9 - 83.2 °C. ^{1}H NMR (300 MHz, $CDCl_3$): δ (ppm) = 7.89 (d, 4H, ^{3}J = 8.8 Hz), 7.82 (d, 2H, ^{3}J = 8.2 Hz), 7.36 (d ,2H, ^{3}J = 7.4 Hz), 7.01 and 6.98 (2d, 4H, ^{3}J = 8.8 Hz), 4.06 (q, 4H, ^{3}J = 6.4 Hz), 4.02 (t, 2H, ^{3}J = 6.4 Hz), 3.61 (t, 2H, ^{3}J = 6.4 Hz), 3.2 - 3.1 (br.s, q, 4H), 2.46 (s, 3H), 1.92 - 1.66 (2m, 6H), 1.62 - 1.22 and 1.47 (m and s, 30H), 0.91 (s, 9H), 0.06 (s, 6H). ^{13}C NMR (100 MHz, $CDCl_3$): δ (ppm) = 161.4, 161.2, 155.7, 146.5, 144.7, 133.2, 129.8, 127.9, 124.5, 114.7 (two resonances), 79.1, 77.2, 70.5, 68.2, 68.0, 46.9, 32.7, 29.2, 29.0, 28.8, 28.5, 26.6, 25.9, 25.7, 25.5, 25.2, 21.7.

Pyridylpyridinium derivative (20) In a 50 mL round bottomed flask, **19** (0.30 g, 0.34 mmol) and 4,4‘-bipyridyl (0.05 g, 0.35 mmol) were dissolved in 20 mL of dry acetonitrile. The resulting reaction mixture was refluxed for

48 h. After this period the solvent was evaporated under reduced pressure and the crude residue purified by precipitation from ethyl acetate yielding 0.23 g of **20** (65 %) as a yellow solid. M.p. = 116.6-117.2 °C. ^{1}H NMR (300 MHz, $CDCl_3$): δ (ppm) = 9.05 (d, 2H, ^{3}J = 6.7 Hz), 8.79 (d, 2H, ^{3}J = 5.9 Hz), 8.44 (d, 2H, ^{3}J = 6.7 Hz), 7.93 (d, 2H, ^{3}J = 6.1 Hz), 7.84 (d, 2H, ^{3}J = 8.6 Hz), 7.82 (d, 2H, ^{3}J = 8.6 Hz), 7.7 (d, 2H, ^{3}J = 8.1 Hz); 7.21 (d, 2H, ^{3}J = 8.1 Hz), 7.04 (d, 2H, ^{3}J = 8.4 Hz), 7.02 (d, 2H, ^{3}J = 8.4 Hz), 4.68 (t, 2H, ^{3}J = 7.4 Hz), 4.07 (t, 4H, ^{3}J = 6.2 Hz), 3.64 (t, 2H, ^{3}J = 6.2 Hz), 3.21 (q, 4H, ^{3}J = 6.8 Hz), 2.37 (s, 3H), 2.16-2.01 (m, 2H), 1.9 - 1.74 (m, 4H), 1.69 - 1.22 and 1.47 (m and s, 29H), 0.91 (s, 9H), 0.06 (s, 6H). ESI-MS (+): m/z = 866.5 $[M\text{-}TsO]^+$.

Azobenzene derivative (21) In a 25 mL round bottom flask, **19** (0.30 g, 0.34 mmol) was dissolved in 10 mL of acetone / water = 95/5. $CuCl_2$ (0.03 mmol) was added and the mixture was heated at 50°C for 2 hours. Upon cooling to room temperature, the crude reaction mixture was filtered trhough a PAD of silica gel to remove the copper salts and dried under reduced pressure to yield **21** quantitatively.

Axle (22) In a sealed glass autoclave, a solution of **4a** (0.10 g, 0.23 mmol) and **19** (0.21 g, 0.23 mmol) in acetonitrile (10 mL) was refluxed for 7 days. After cooling to room temperature, the reaction mixture was evaporated to dryness under reduced pressure. Recrystallisation of the solid residue from acetonitrile afforded **22** (53 %) as an orange solid. M.p = 180-184°C. ^{1}H NMR (300 MHz, $CDCl_3$): δ (ppm) = 9.28 and 9.24 (2d, 4H, ^{3}J = 6.7 and 6.5 Hz), 8.66 (d, 4H, ^{3}J = 6 Hz), 7.87 and 7.85 (2d, 4H, ^{3}J = 7 and 6.9 Hz), 7.72 (d, 4H, ^{3}J = 8.1 Hz), 7.26 (d, 4H, ^{3}J = 8.1 Hz), 7.09 and 7.05 (2d, 4H, ^{3}J = 8.1 Hz), 4.79 (t, 2H, ^{3}J = 7.6 Hz), 4.71 (t, 2H, ^{3}J = 7.6 Hz) 4.15 - 4.05 (m, 4H), 3.63 - 3.54 (m, 4H), 3.24 (br.s, q, 4H), 2.39 (s, 6H), 2.2 - 2.0 (m, 4H), 1.94 - 1.80 (m, 4H), 1.72 - 1.28 and 1.49 (m and s, 32H), 0.95 (s, 9H), 0.11 (s, 6H).

Pyridylpyridinium derivative (23) . In a 50 mL round bottom flask, **21** (0.12 g, 0.152 mmol) and 4,4‘-bipyridyl (0.04 g, 0.23 mmol) were dissolved in 20 mL of dry acetonitrile. The resulting reaction mixture was refluxed for 48 h. After this period the solvent was evaporated under re-

duced pressure and the crude residue purified by precipitation from ethyl acetate yielding 0.08 g of **23** (59 %) as a yellow solid. ^{1}H NMR (300 MHz, $CDCl_3$): δ (ppm) = 9.09 (d, 2H, ^{3}J = 6.8 Hz), 8.79 (d, 2H, ^{3}J = 6.0 Hz), 8.45 (d, 2H, ^{3}J = 9.8 Hz), 7.95 (d, 2H, ^{3}J = 5.8 Hz), 7.86 - 7.81 (m, 4H), 7.70 (d, 2H, ^{3}J = 8.2 Hz), 7.22 (d, 2H, ^{3}J = 8.0 Hz), 7.06 - 7.01 (m, 4H), 6.69 (t, 2H, ^{3}J = 7.5 Hz), 4.08 (t, 4H, ^{3}J = 7.5 Hz), 3.55 (t, 2H, ^{3}J = 6.5 Hz), 3.24 - 3.18 (m, 4H), 2.34 (s, 3H), 2.13 - 2.08 (m, 2H), 1.88 - 1.81 (m, 4H), 1.7 - 1.2 (m, 27H).

Rotaxane (24) In a 25 mL round bottomed flask, **WetOEt** (0.040 g, 0.02 ml) and **22** (0.030 g, 0.02 mmol) were dissolved in 5 mL of dry dichloromethane. The resulting solution was stirred for 2 h at RT, then, tert-butyl-di-methyl-silyl-chloride (0.044 g, 0.03 mmol), triethylamine (0.03 mL, 0.03 mmol), and DMAP (cat.) were added. The reaction mixture was stirred for 24 h at RT, then diluted with dichloromethane and the resulting organic phase washed twice with distilled water (2x50 mL), dried over sodium sulfate and evaporate to dryness under reduced pressure. The solid residue was purified by column chromatography on silica gel (DCM/MeOH = 96:4) to afford 0.025 g of rotaxane **24** (44 %) as a reddish solid. HR-MS calculated for $[C_{153}H_{211}N_{11}O_{18}Si_2]^{2+}$ m/z = 1273.2731 (60 %), 1273.7747 (100.0 %), 1274.2764 (82 %), 1274.7781 (26 %); Found: 1273.2693 (55 %), 1273.7710 (100 %), 1274.2721 (90 %), 1274.7730 (60 %), 1275.2745 (30 %).

Rotaxane 25 In a sealed glass autoclave, **20** (0.124 g, 0.012 mmol) and **WetOEt** (0.263 g, 0.018 mmol) were equilibrated in dry toluene for 24 h at 60 °C, then 6-hydroxyhexyl-p-toluensulfonate (0.033 g, 0.12 mmol) was added and the reaction was stirred at 70 °C for 6 days. Upon cooling to RT, triethylamine (0.03 mL, 0.29 mmol), tert-butyl-dimethyl-silylchloride (0.044 g, 0.29 mmol) and DMAP (cat.) were added and the mixture was stirred for 24 h at RT. After this period, the solvent was evaporated under reduced pressure, and the solid residue was solubilised in 50 mL of dichloromethane. The organic phase was washed twice with distilled water (2x50 mL), dried with sodium sulfate and evaporated to dryness under reduced pressure. The solid residue was purified by column chromatography on silica gel (Dichloromethane / Methanol = 95:5) to afford 0.162 g of rotaxane **25** (47 %) as a reddish solid. HR-MS calculated

for $C_{153}H_{211}N_{11}O_{18}Si_2]^{2+}$ m/z = 1273.2731 (60 %), 1273.7747 (100.0 %), 1274.2764 (82 %), 1274.7781 (26 %); Found: 1273.2716 (55 %), 1273.7731 (100.0 %), 1274.2749 (90 %), 1274.7760 (60 %), 1275.2770 (30 %).

Catenane 28 In a 5 mL round bottom flask, **WEtOEt** (0.36 g, 0.24 mmol), **23** (0.15 g, 0.16 mmol) and **3a** (0.05 g, 0.18 mmol) were equilibrated in 3 mL of toluene. The reaction was heated at 70°C for seven days. After evaporation of the solvent, the mixture was taken up with dry dichloromethane to obtain a $10^{-3}M$ solution and **27** was added. HR-MS calculated for $C_{157}H_{191}N_{11}O_{20}]^{2+}$ m/z = 1275.21279 (59 %), 1275.71447 (100 %), 1276.21615 (83 %), 1276.71783 (46 %), 1277.21950 (20 %), 1277.72118 (8 %); Found: 1275.21387 (59 %), 1275.71558 (100 %), 1276.21680 (91 %), 1276.71790 (53 %), 1277.21924 (23 %), 1277.7207 (9 %).

Bibliography

(1) Forgan, R. S.; Sauvage, J.-P.; Stoddart, J. F. *Chem. Rev.* **2011**, *111*, 5434–5464.

(2) Kassem, S.; Leeuwen, T. v.; S. Lubbe, A.; R. Wilson, M.; L. Feringa, B.; A. Leigh, D. *Chem. Soc. Rev.* **2017**, *46*, 2592–2621.

(3) Nierengarten, J. F.; Dietrich-Buchecker, C. O.; Sauvage, J. P. *J. Am. Chem. Soc.* **1994**, *116*, 375–376.

(4) Gil-Ramírez, G.; Leigh, D. A.; Stephens, A. J. *Angew. Chem. Int. Ed.* **2015**, *54*, 6110–6150.

(5) Lewis, J. E. M.; Galli, M.; Goldup, S. M. *Chem. Commun.* **2016**, *53*, 298–312.

(6) Leigh, D. A.; Wong, J. K. Y.; Dehez, F.; Zerbetto, F. *Nature* **2003**, *424*, 174–179.

(7) Gaeta, C.; Talotta, C.; Mirra, S.; Margarucci, L.; Casapullo, A.; Neri, P. *Org. Lett.* **2013**, *15*, 116–119.

(8) Orlandini, G.; Zanichelli, V.; Secchi, A.; Arduini, A.; Ragazzon, G.; Credi, A.; Venturi, M.; Silvi, S. *Supramol. Chem.* **2016**, *28*, 427–435.

(9) Zanichelli, V.; Dallacasagrande, L.; Arduini, A.; Secchi, A.; Ragazzon, G.; Silvi, S.; Credi, A. *Molecules* **2018**, *23*, 1156–1168.

(10) Merino, E.; Ribagorda, M. *Beilstein J. Org. Chem.* **2012**, *8*, 1071–1090.

(11) Paris, E.; Bigi, F.; Cauzzi, D.; Maggi, R.; Maestri, G. *Green Chem.* **2018**, *20*, 382–386.

(12) Kunitake, T.; Okahata, Y.; Shimomura, M.; Yasunami, S.; Takarabe, K. *J. Am. Chem. Soc.* **1981**, *103*, 5401–5413.

(13) Arduini, A.; Calzavacca, F.; Pochini, A.; Secchi, A. *Chem. Eur. J.* **2003**, *9*, 793–799.

(14) Arduini, A.; Ciesa, F.; Fragassi, M.; Pochini, A.; Secchi, A. *Angew. Chem. Int. Ed.* **2005**, *44*, 278–281.

(15) Orlandini, G.; Ragazzon, G.; Zanichelli, V.; Secchi, A.; Silvi, S.; Venturi, M.; Arduini, A.; Credi, A. *Chem. Commun.* **2017**, *53*, 6172–6174.

(16) Zanichelli, V.; Ragazzon, G.; Orlandini, G.; Venturi, M.; Credi, A.; Silvi, S.; Arduini, A.; Secchi, A. *Org. Biomol. Chem.* **2017**, *15*, 6753–6763.

(17) Zanichelli, V.; Bazzoni, M.; Arduini, A.; Franchi, P.; Lucarini, M.; Ragazzon, G.; Secchi, A.; Silvi, S. *Chem. Eur. J.* **2018**, *24*, 12370–12382.

(18) Gordillo, Á.; Jesús, E. d.; López-Mardomingo, C. *Chem. Commun.* **2007**, 4056–4058.

(19) Fisher, B. F.; Gellman, S. H. *J. Am. Chem. Soc.* **2016**, *138*, 10766–10769.

(20) Yoritate, M.; Meguro, T.; Matsuo, N.; Shirokane, K.; Sato, T.; Chida, N. *Chem. Eur. J.* **2014**, *20*, 8210–8216.

(21) Yoshino, T.; Mamiya, J.-i.; Kinoshita, M.; Ikeda, T.; Yu, Y. *Molecular Crystals and Liquid Crystals* **2007**, *478*, 233/[989]–243/[999].

(22) Carrigan, C. N.; Bartlett, R. D.; Esslinger, C. S.; Cybulski, K. A.; Tongcharoensirikul, P.; Bridges, R. J.; Thompson, C. M. *J. Med. Chem.* **2002**, *45*, 2260–2276.

(23) Arduini, A.; Bussolati, R.; Credi, A.; Monaco, S.; Secchi, A.; Silvi, S.; Venturi, M. *Chem. Eur. J.* **2012**, *18*, 16203–16213.

Chapter 4

Encapsulation of Stilbazolium Guests in Calix[6]arene Hosts: a New Tool for Tunable Fluorescent-devices

4.1 Introduction

The first member of the class of cyanine dyes was discovered more than one century ago by G. Williams.[1] Cyanine dyes are characterised by the presence of two nitrogen centers: the first, positively charged, is spanned from the second, neutral, by a conjugated chain of carbon atoms (see figure 4.1).[2] These dyes generally have an all-trans geometry in their stable form, but occasional photoisomerisation can take place. Because of their highly conjugated structure, cyanine dyes have high extinction coefficients ($>10^5 M^{-1} cm^{-1}$). Their optical properties, such as extinction and fluorescence, can be tuned through a careful choice of the substituents attached to the nitrogen and by changing the length and the rigidity of the polymethine chain. The non-linear optical (NLO) properties, the solvatochromism, the photoisomerisation and the photodimerisation of this class of dyes[3] have

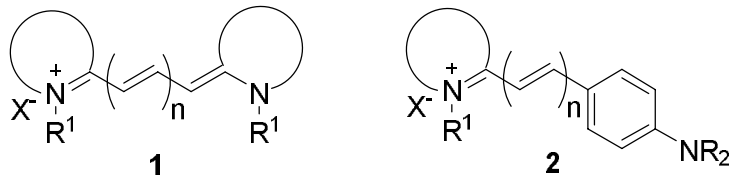

Figure 4.1: General structure of cyanine (1) and hemicyanine (2) dyes; the derivatives of 2 with the shortest bridge (n = 1) are often indicated either as styryl dyes or styryl cyanine dyes (see text)

been studied for more than 20 years, leading to various applications such as spectral sensitisers in large band-gap semiconductor materials, laser gain materials, probes for biological systems and light-harvesting systems.[2]

Stilbazolium salts are organic dyes belonging to the class of cationic styryl cyanines (see figure 4.1), which are usually obtained via condensation of 2/4-methyl pyridinium salt with a properly substituted benzaldehyde derivative in the presence of a base. Stilbazolium salts are widely studied thanks to their two-photon absorption in the near IR range (NIR). Optical materials with this feature are of great interest for application in 3D fluorescence microscopy, up-converted lasing, data processing, and bioimaging. Micro/nanolasers are of great importance in science and technology thanks to their ability to deliver intense coherent light signals at the micro/nanoscale.[4, 5] In this context, the development of innovative optical materials to be used as gain media plays a fundamental role in expanding the micro/nanolasers capabilities and performances.[6] Up to now, the most important gain materials for the micro/nanolasers construction are based on inorganic semiconductors thanks to their high stability and optoelectronic properties. The drawbacks presented by these materials derives from complicated and costly processing, limited spectral tunability, brittleness and the lack of flexibility.[7] Organic semiconductor-based lasers have attracted great interest in the last decades since they allow to overcome some of the drawbacks listed above. They are prepared with straightforward fabrication processes and, most important, they allow femtosecond pulse generation, the broadband optical amplification and can be used to tune the lasing frequency.[8] The principal limitation in the use of organic dyes as gain media, including the styryl cyanines, is the aggregation-caused

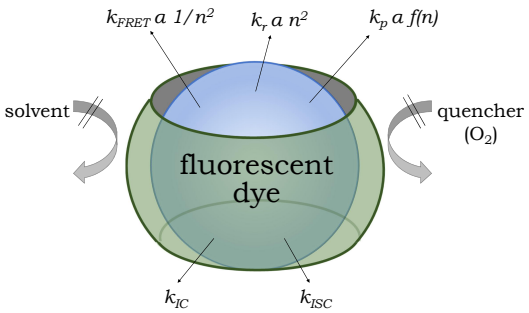

Figure 4.2: Illustration of the role played by the complexation into a molecular container on the deactivation of singlet excited states. The container protects the dye from solvent induces quenching and quenchers and influences the rate constants of other deactivation pathways.[9]

quenching (ACQ) effect that avoids their direct use as solid-state gain media.

To overcome the ACQ problem, the development of organic solid-state laser is nowadays based on the encapsulation of the dye molecules into a matrix able to spatially separate them.[4, 7] Initially, the dyes were encapsulated as *guests* in polymers, sol-gel glasses and molecular/ionic crystals. However, due to the absence of specific interactions between the matrix and the dye molecules, these latters are spatially separated, and thus the quenching mechanism is avoided, only in dilute systems. In recent years, ordered porous compounds and macrocyclic *hosts* are attracting great interest as new *host* materials. Their ability to spatially confine the *guest* through non-covalent intermolecular interactions allowed the use of higher dyes concentrations without quenching problems. This led to higher optical gain intensity and hence increased laser output power.[4] The confinement of a chromophore into a *host* cavity changes its environment drastically, and this inevitably affects the physical/chemical properties of the *guest* (see figure 4.2). The inclusion of a dye molecule into a *host* may become an important tool to modulate its optical properties. Indeed, the de-excitation pathways, as well as the excited states, are really sensitive to the microenvironment. Internal conversion (IC), one of the most important non-radiative de-excitation pathways, together with many other similar de-excitation pathways, is slowed down upon the inclusion of dyes into *hosts*

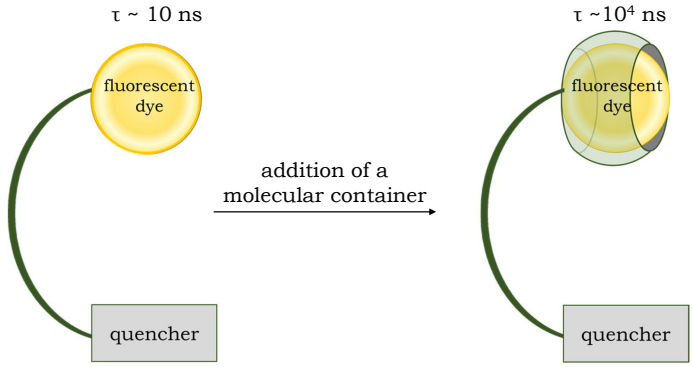

Figure 4.3: schematic representation of the role played by the complexation inside an opportune macrocyclic *host* on the enhancement of the life-time (τ) of the excited state of a dye in the presence of a quencher.

molecules. Indeed, the geometrical confinement of the *guest* inside the *host* cavity restricts the rotational and vibrational motions and often reduce the polarity of the microenvironment with respect to the bulk (the majority of organic dyes are water-soluble).[9, 10]

Recently, *host-guest* composite materials have been exploited to construct high-performance organic microlasers since they combine the properties of both the *host* and the *guest* with new functionalities carried by the supramolecular interactions. The more common *host* materials present in the literature are the ordered porous materials such as silica, zeolite, and MOF. An alternative is to encapsulate the dyes in synthetic organic macrocycles such as cyclodextrins, calixarenes or cucurbiturils.[4, 9, 11] The encapsulation of dyes in macrocyclic compounds has been exploited in applications for microlasers, fluorescent sensors, biomedical applications, catalysis, functional materials, electronic devices, pharmaceuticals, drug formulations and delivery, nanomedicines, and many others.[10] A really important bioassay is the time-resolved fluorescence (TRF). Differently from the rare earth metal ions used so far, the TRF assays based on organic dyes are completely compatible with the solid-phase synthesis of oligonucleotides and peptides. Improvement in TRF measurements can be achieved by exploiting supramolecular radiative decay engineering to lengthen the life-time of the excited state (see figure 4.3).[12]

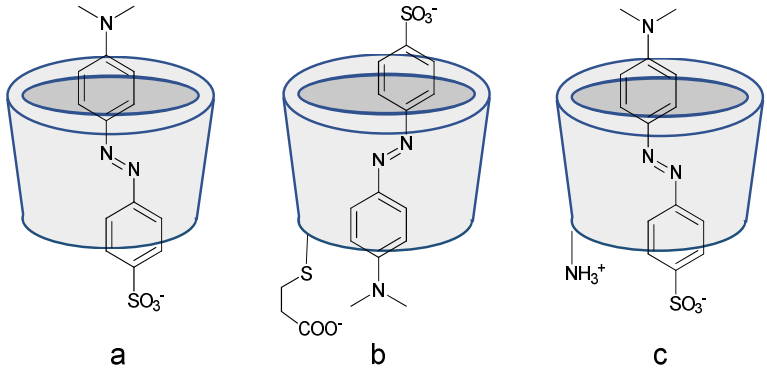

Figure 4.4: complexes between variably substituted cyclodextrins and methyl orange a) β**CD**/**MO**, b) anionic sodium heptakis[6-deoxy-6-(3-thiopropionate)]-β**CD**/**MO**, c) cationic heptakis(6-deoxy-6-amino)-β**CD** hydrochloride/**MO**.[13]

Relatively less explored and of fundamental importance is the tuning of the spectroscopic properties of a dye in function of its geometrical arrangement inside the cavity of the *host* material. Almost all the examples reported in the literature are about systems in which only one orientation of the *guest* is taken into account; however, the different orientations of a *guest* inside the same *host* cavity could originate assemblies with different spectroscopic behavior. In this context, the possibility to employ a hollow and non-palindrome synthetic macrocyclic receptor that possesses different functionalities on the accesses of its cavity can be potentially exploited to orient the dye inside the macrocycle itself. A few examples of this approach are known in the literature. Among them, Mourtzis et al.[13] reported an interesting example of cyclodextrin (**CD**) *hosts* in which the functionalities present on the macrocycle rims are modified to tune the directional threading of Methyl Orange (**MO**) (see Figure 4.4). Although the complexation properties of these systems have been studied using NMR, the spectroscopic properties of the enclosed dye as a function of its orientation have not been studied yet. The calix[6]arene wheel **WEtOEt**, introduced in the previous chapters, like the cyclodextrins, is a non-palindrome *host*, and the directionality of the threading process of viologen and pyridylpyridinium-based *guests* has been widely studied.[14, 15] To verify whether the orientation of a monocationic axle with respect to the two chemically different rims of

WEtOEt could be exploited as a tool to address specific spectroscopic responses, the complexation properties of this *host* toward a series of stilbazolium dyes will be addressed in this chapter.

4.2 Results and Discussion

A series of stilbazolium dyes were synthesised according to scheme 4.1. 4-Dimethylamino benzaldehyde was reacted with 4-picoline in the presence of KOH to yield the styrilpyridine **S1**.[16] The reaction of compound **S1** with the appropriate alkylating agents allowed to synthesise the desired library of dyes reported in scheme 4.1. All the stilbazolium salts were obtained in high yields as tosylates. This anion was chosen because it can be used as tracing counteranion in NMR studies, and it has high coordinating power toward hydrogen bond donating moieties.

Initially, the binding ability of **WEtOEt** was evaluated toward the stilbazolium salt **SC18N**. Preliminary UV-Vis data were collected at 298 K in dichloromethane titrating a $1.3 \cdot 10^{-5} M$ solution of **SC18N** with a $0.8 \cdot 10^{-3} M$ solution of **WEtOEt** (see figure 4.5). In this solvent and at this concentration, the *guest* presents an intense absorption band centered at $\lambda \sim 508$ nm ($\varepsilon \sim 4.3 \cdot 10^4 M^{-1} cm^{-1}$). Upon the addition of incremental aliquots of the *host* solution (see experimental part), a progressive red-shift of the **SC18N** band was observed together with a reduction of its extinction. The presence of two distinct isosbestic points at $\lambda \sim 310$ and 450 nm in the collection of spectra of figure 4.5 is in agreement with the hypothesis of two absorbing species that are present in solution. For a 1:1 binding model, an apparent binding constant with a $logK_{1:1} = 4.23 \pm 0.08$ was calculated through the fitting of the absorbance in the 280 – 650 nm range for different [H]/[G] values with the SPECFIT/32 software.[17]

4.2.1 NMR Characterisation of the WEtOEt/SC18N Complex

Preliminaries NMR studies were carried out by mixing stoichiometric amounts of **WEtOEt** and **SC18N** in deuterated chloroform. The ^{1}H NMR spectrum of the resulting homogeneous solution, acquired at 400 MHz, displays a pattern of signals that differs from the spectra of the separated compo-

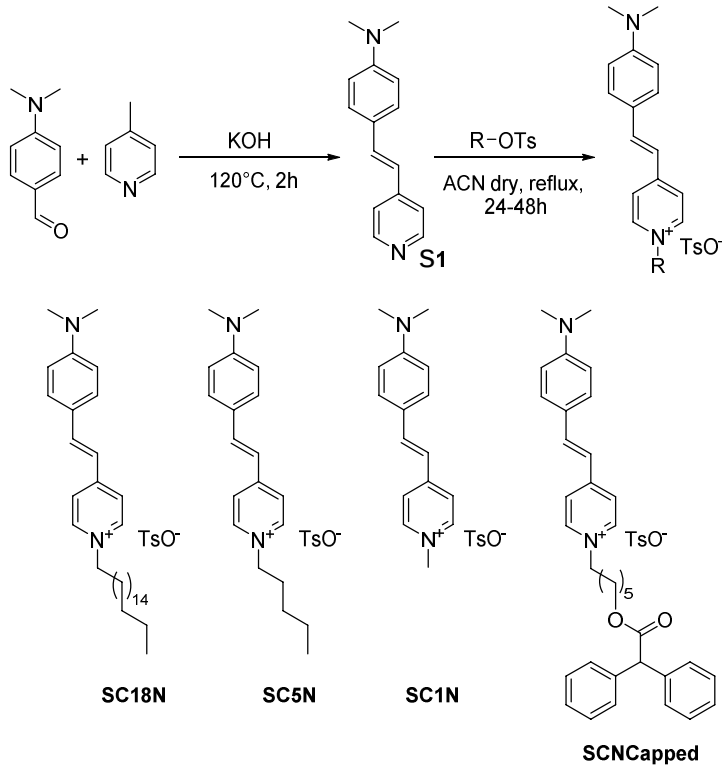

Scheme 4.1: Schematic representation of the synthesis of stilbazolium salts (top), from the left stilbazolium salt **SC18N**, **SC5N**, **SC1N** and **SCNCapped** (bottom).

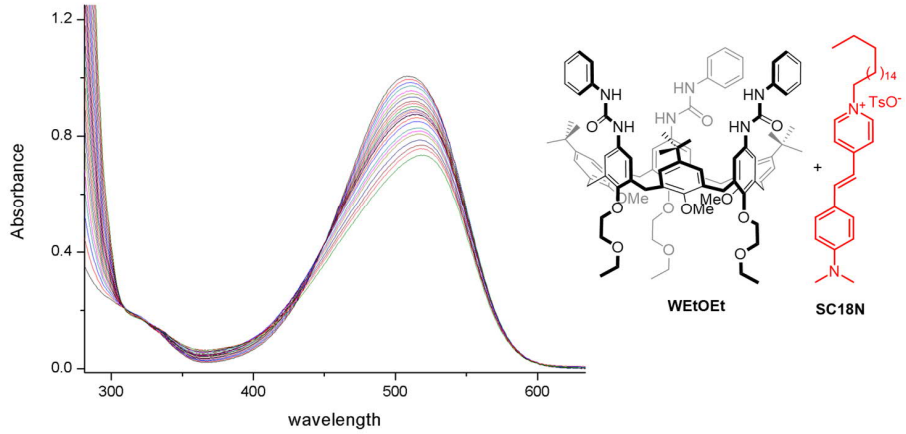

Figure 4.5: UV/vis absorption spectra (dichloromethane, 298 K) of **SC18N** upon titration with **WEtOEt**.

nents as shown in the stack of figure 4.6. A series of 2D NMR experiments (COSY, TOCSY, HSQC, and ROESY) were carried out to investigate the composition of the mixture. In particular, the heterocorrelated 2D HSQC spectrum reported in figure 4.7 allowed to identify some of the *host* and *guest* signals, such as those in the 3.2 - 5 ppm region, which are related to the ethoxyethyl chains and the methylene bridging groups of the *host*. In particular, the broad signals at ca. 4.5 and 3.5 ppm indicate that the bridging methylene group of the calix[6]arene macrocycle are diasterotopic and thus the calix[6]arene macrocycle prevalently adopts a pseudocone conformation on the NMR timescale. At 2.3 ppm is present a singlet due to the methyl group of the *p*-toluensulfonate, used as counteranion for the *guest*. The downfield shift of the signal of methoxy groups of the *host* from 2.9 ppm to ca. 4 ppm suggests that the methoxy groups are ejected from the cavity due to the complexation of the *guest*.[18]

Important indications of the complexation of the *guest* are also given by the general upfield shift of its resonances. The appearance of several new signals in the up-field region of the spectrum of the 1:1 mixture (see figure 4.6, middle), between 0 and 1 ppm, is consistent with the hypothesis that a portion of the *guest* alkyl chain is shielded by the aromatic cavity of the *host*. Such behavior strongly supports the hypothesis that the stilbazolium

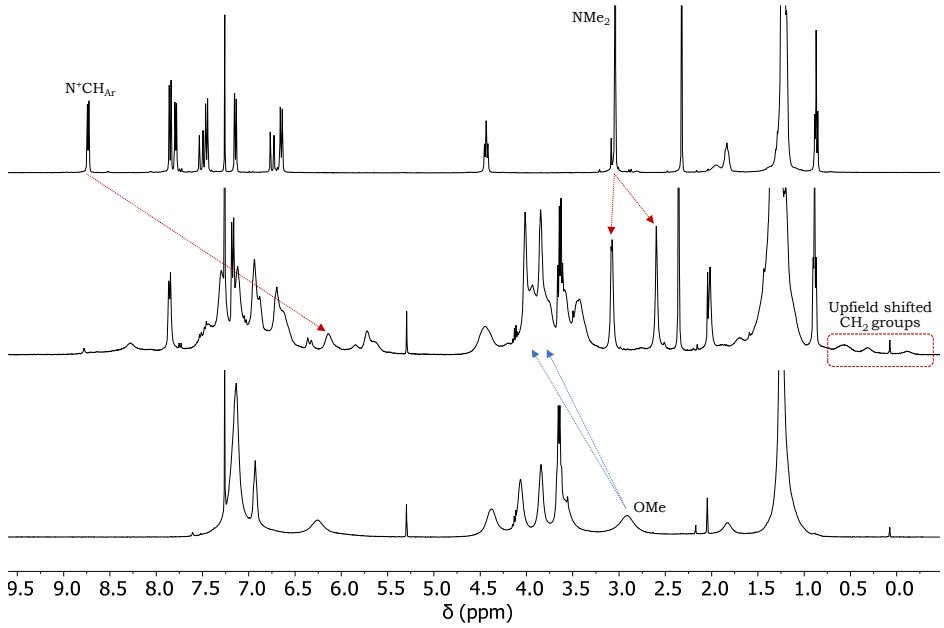

Figure 4.6: stack plot (400 MHz, $CDCl_3$, 298 K) of **SC18N** (top), 1:1 mixture (middle), and **WEtOEt** (bottom).

guest is complexed inside the aromatic cavity of the *host*. The aromatic region of the spectrum is crowded with broad and overlapped signals and thus of difficult interpretation. Interestingly, in the ^{1}H and HSQC spectra of the mixture, the NMe_2 group of **SC18N** gives rise to two main signals at δ = 3.07 and 2.59 ppm. This group, present on the aromatic portion of the *guest* (see scheme 4.2), is thus experiencing two different magnetic environments that might depend on several scenarios such as i) a different orientation of the *guest* inside the *host* cavity, ii) different conformations adopted by the surrounding *host* cavity, iii) the presence of free *guest* and iv) to an exocavity complexation. The latter two hypotheses were rejected because the exocavity complexation is not supported by the observed chemical shift of the methoxy groups (*vide supra*). Furthermore, the analysis of the 2D heterocorrelated spectrum excludes the presence of free *guest* in the solution. If present, it would have given a diagnostic cross-peak at F_2, F_1 = 8.7; 140.0 ppm for the protons of the pyridinium ring in 2- and 6-position,

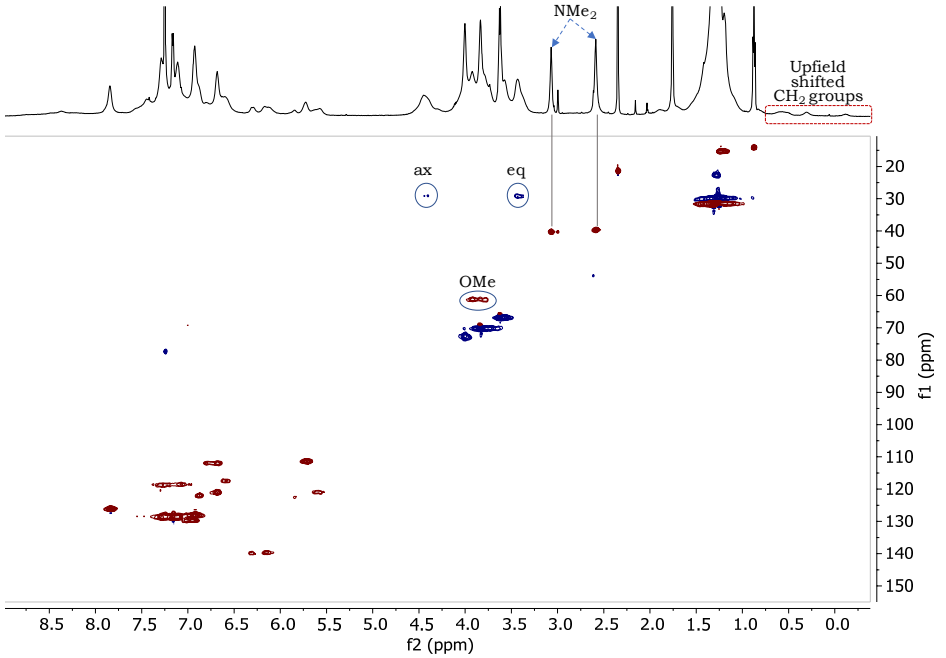

Figure 4.7: 2D HSQC ($CDCl_3$, 298 K, 600 MHz) of the 1:1 mixture of **WEtOEt** and **SC18N**.

which is instead not present.

Due to the superimposition of several *host/guest* signals in the aromatic region, the NMR characterisation in chloroform did not allow full identification of the species present in solution. Better results were obtained using C_6D_6 as the solvent. Indeed, thanks to the aromatic solvent-induced shift (ASIS) effect,[19] a better splitting of the aromatic signals was observed. An important first observation was that, when the 1:1 *host/guest* mixture was prepared, the relative intensity of the two signals of the dimethylamino group, now resonating at $\delta = 2.3$ and 2.5 ppm, varied appreciably with time. In contrast, no significant variation for the signals of the *host* was observed. These findings strongly support the hypothesis that the two dimethylamino signals are not related to conformational changes of the *host*, but rather to the presence in solution of two different complex species in slow equilibrium on the NMR timescale. In a previous study, it was

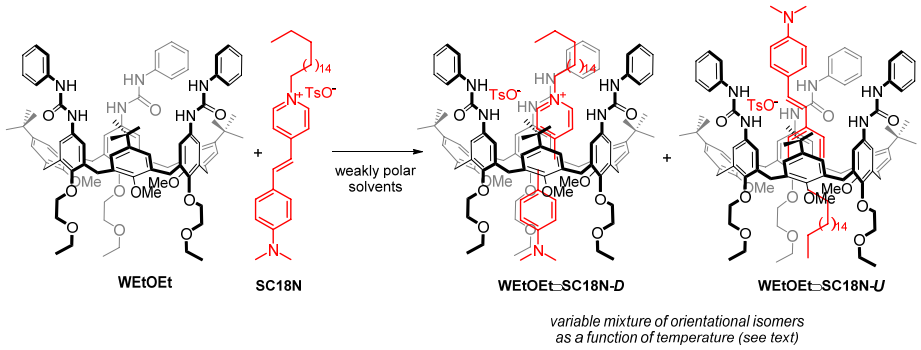

Scheme 4.2: Schematic representation of the complexes formed between stilbazolium tosylate **SC18N** and the calix[6]arene wheel **WEtOEt**.

shown that pyridylpyridinium salts forms with the **WEtOEt** wheel two orientational pseudorotaxane isomers.[14, 15] It is thus reasonable to assume that also **SC18N**, which shares with the aforementioned pyridylpyridinium salts several structural similarities, can generate two orientational pseudorotaxane isomers (see scheme 4.2). These isomers are due to the two possible geometrical arrangements of **SC18N** with respect to the non-palindrome cavity of the *host*. Considering the asimmetry of these *guests*, the formation of the two orientational isomers could be tentatively explained taking into account two different threading mechanisms. In the first hypothesis, the *guest* threads only one rim of the wheel but with both its ending (NMe_2 group and C18 alkyl chain); in the second case the *guest* threads both rims of the wheel but using only one extremity. In scheme 4.2, it is indicated as **WEtOEt⊃SC18N-*D***, the orientational isomer (**Down**) having the dimethylamino group oriented downward with respect to the phenylurea groups present on the *host* upper rim. The corresponding **WEtOEt⊃SC18N-*U***, or **Up**, isomer presents its dimethylamino group positioned at the *host* upper rim.

A series of 1D and 2D NMR experiments were carried out at different temperatures to assess the geometrical arrangement of the two orientational pseudorotaxane isomers present in solution. Interestingly, the variable temperature experiment (figure 4.8) shows that the ratio and the broadness of the two NMe_2 signals change with the temperature. Among the several

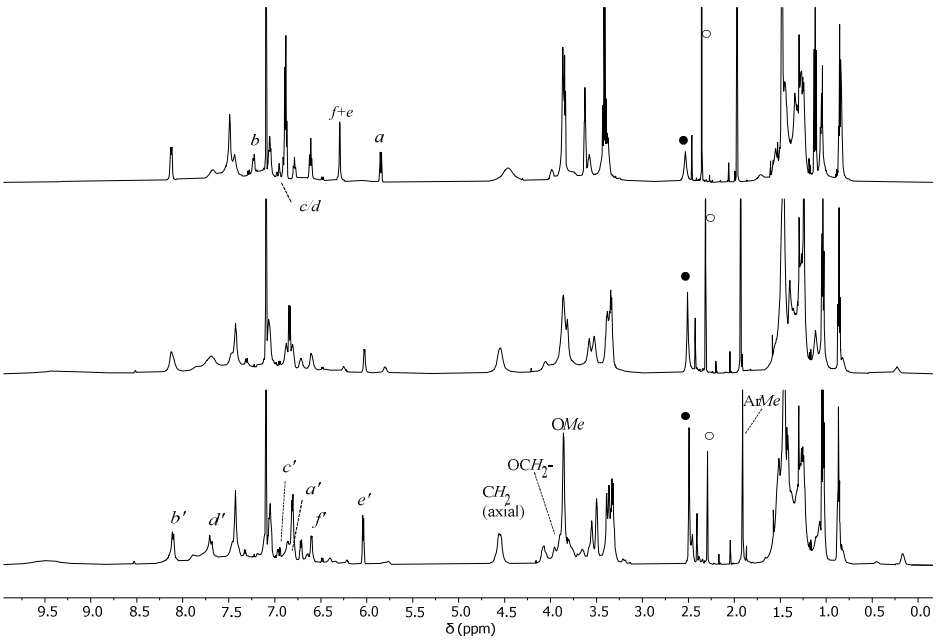

Figure 4.8: ^{1}H NMR stack plot (600 MHz, C_6D_6) of the 1:1 mixture between **WEtOEt** and **SC18N** taken at different temperatures (top: 333 K, middle: 298 K, bottom: 280 K) showing the different intensities of the dimethylamino signals resonating at 2.6 (•) and 2.4 ppm (○). The signals labeling of the spectrum at T = 280 K (bottom) is relative to the protons assignment of the **Down** isomer (see text and sketch of figure 4.9), while the labeling for the spectrum at T = 333 K (top) is relative to the protons assignment of the **Up** isomer (see text and sketch of figure 4.11).

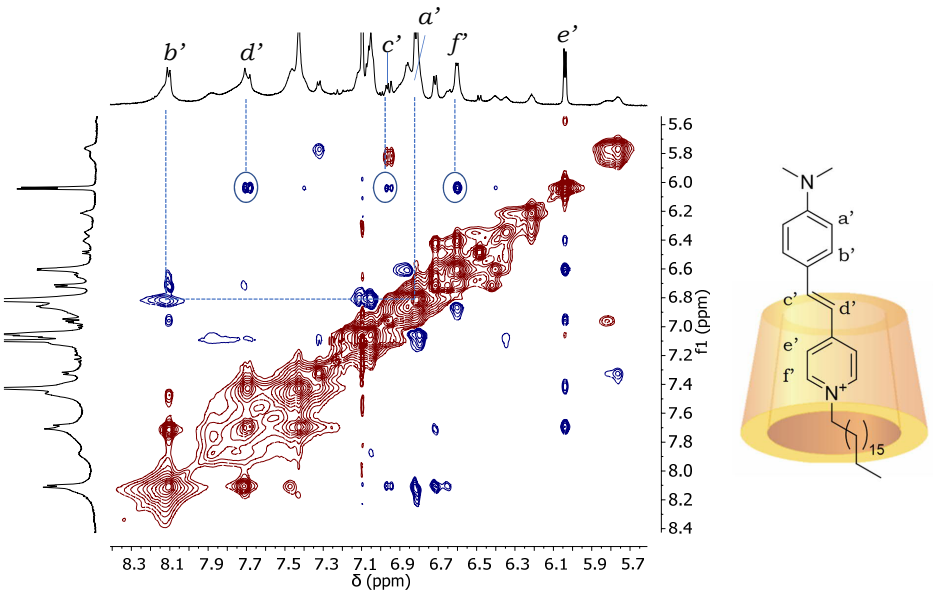

Figure 4.9: 2D ROESY spectrum (C_6D_6, 600 MHz, T = 280 K, τ_m = 200 ms) of the 1:1 mixture between **WEtOEt** and **SC18N**, expanded aromatic region. The signals labeling is relative to the protons assignment of the **Down** isomer (see the sketch on the right).

temperatures investigated, the spectrum taken at T = 280 K was identified as the more suitable for the assignment of the *guest* signals in the orientational isomer **Down**. In figure 4.9, it has been reported an expansion of the aromatic portion of the 2D-ROESY spectrum in which it is possible to identify all the aromatic protons of the *guest*. Starting from the doublet at $\delta = 6.03$ ppm, previously identified through 2D COSY and HSQC experiments as the proton *e'* in the meta position of the pyridinium ring, are visible the ROE correlations with: i) the two olefinic protons *d'* and *c'*, resonating at $\delta = 7.71$ and 6.97 ppm, respectively; ii) the proton *f'* in the ortho position of the pyridinium ring at $\delta = 6.60$ ppm.

The analysis of the COSY spectrum allowed us to identify the proton *a'* of the *guest* aniline ring at ca. 6.8 ppm (for the *guest* protons labeling and assignment see also the sketch in figure 4.9). The identification of the signals relative to protons *c'* and *d'* was also supported from the results of a selective 1D ROESY experiment (see figure 4.10), carried out by irradi-

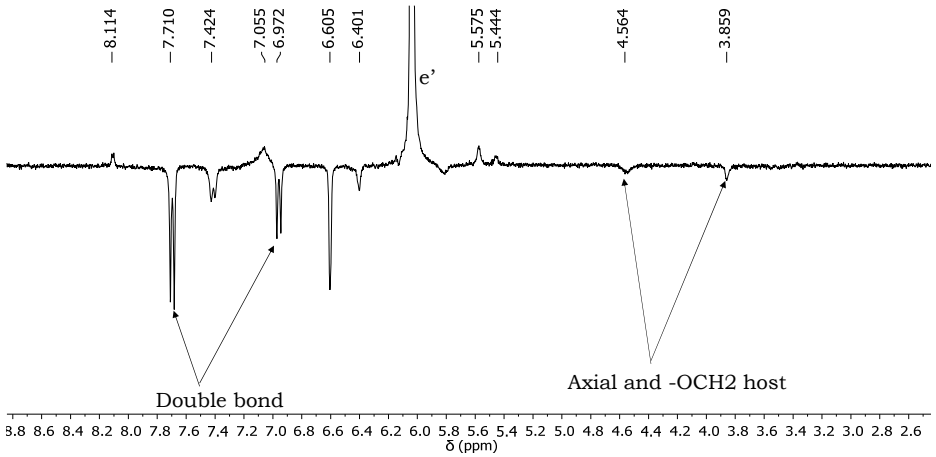

Figure 4.10: 1D selective ROE experiment (C_6D_6, 600 MHz, T = 280 K, τ_m = 200 ms) carried out on the 1:1 mixture between **WEtOEt** and **SC18N** by irradiating the *guest* signal (*e'*) at δ = 6.03 ppm.

ating the signal of proton *e'* at δ = 6.03 ppm. Interestingly, this spectrum shows also correlations with the signals at δ = 4.56 and 3.89 ppm assigned, respectively, to the diasterotopic axial bridging methylene protons of the calix[6]arene macrocycle and the OCH_2 protons present at its lower rim. At this temperature, the intensity of the signals relative to the **Up** isomer is not intense enough to allow their correct identification. The ^{1}H spectrum acquired at T = 333 K instead shows intense and sharp signals for the **Up** isomer. Indeed, the analysis of a series of 2D experiments (HSQC, COSY, ROESY) carried out at this temperature allowed the identification of all the aromatic protons of the *guest* in the **Up** isomer. The assignment of the *guest* signals is reported in the expansion of the aromatic portion of the 2D ROESY spectrum depicted in figure 4.11.

All these experiments allowed to identify the two sets of signals for the two orientations of the *guest* in the pseudorotaxane complexes. To complete the characterisation of the geometrical arrangement of the *guest* component in the two orientational pseudorotaxane isomers, a further series of selective 1D ROESY experiments was performed (see figure 4.12 and 4.13). As shown in figure 4.12, several ROE correlations were observed for the two dimethylamino signals. The signal at δ = 2.6 ppm correlates with

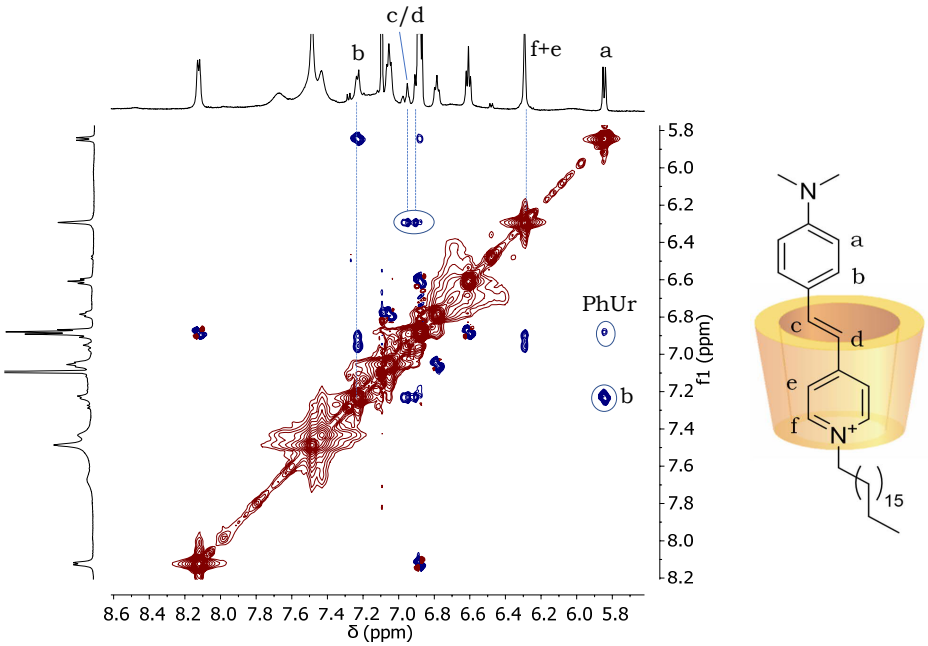

Figure 4.11: 2D ROESY spectrum (C_6D_6, 600 MHz, T = 333 K, τ_m = 200 ms) of the 1:1 mixture between **WEtOEt** and **SC18N**, expanded aromatic region. The signals labeling is relative to the protons assignment of the **Up** isomer (see the sketch on the right).

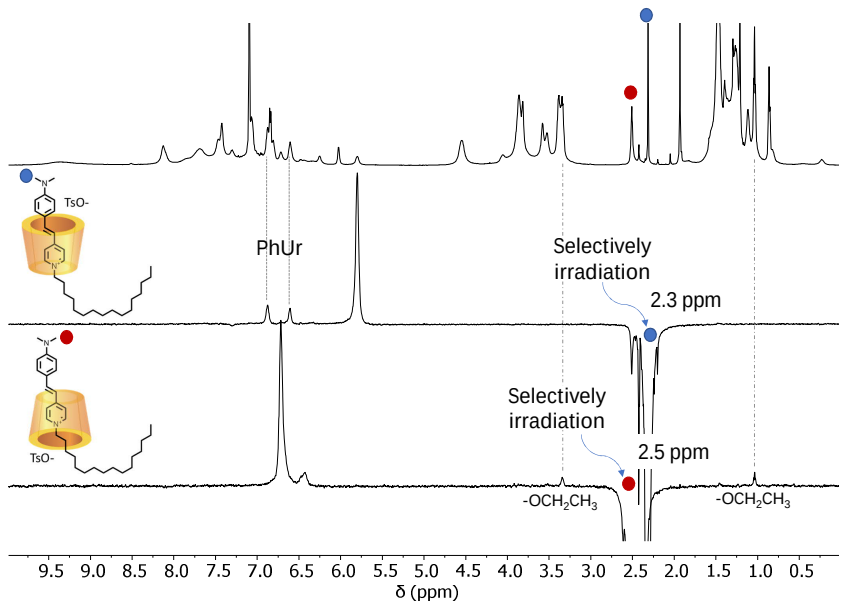

Figure 4.12: Stack plot (600 MHz, C_6D_6, T = 298 K) of (top) ^{1}H NMR spectrum of the 1:1 mixture of **WEtOEt** and **SC18N**, and the 1D Selective ROE experiments (τ_m = 200 ms) carried out by irradiating the NMe_2 signals at 2.5 (middle) and 2.3 ppm (bottom).

the signals of the ethoxyethyl chains at the *host* lower rim at δ = 3.3 and 1.0 ppm. These correlations are consistent with the orientational isomer indicated as **Down**. The more upfield-shifted signal at δ = 2.4 ppm shows instead correlations with the resonances of the phenylureido groups at the *host* upper rim, consistently with the isomer indicated as **Up**.

Moreover, a 1D selective ROESY experiment (figure 4.13) carried out irradiating the cluster of *host* signals relative to part of the ethoxyethyl chains, to the OMe groups, and to the diasterotopic equatorial bridging methylene groups (CH_2eq), shows correlations in the aromatic region with the signals of the proton *b'* at 8.10 ppm, *c'* at 6.95 ppm and *d'* at 7.70 ppm. All these resonances belong to the **Down** isomer. All these findings are in agreement with the hypothesised structure of the complexes and are also supported by the molecular mechanics minimised (MMFF94 force field) structures reported in figure 4.14.

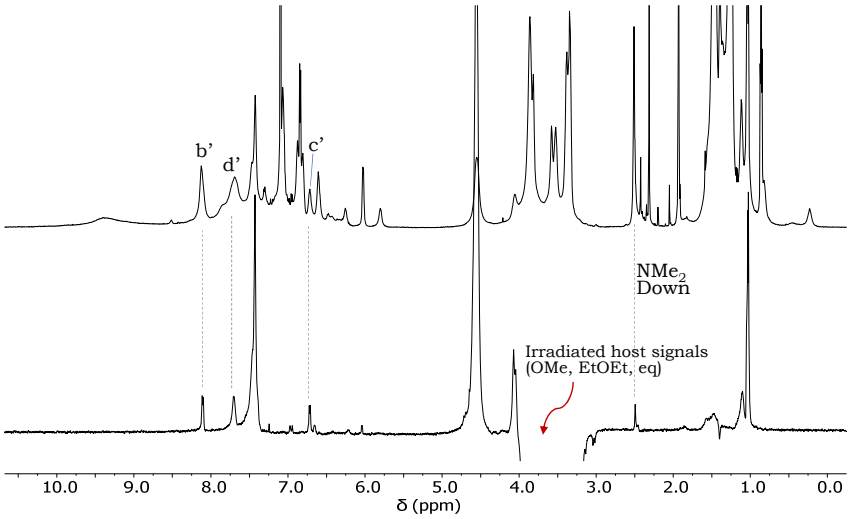

Figure 4.13: stack plot of the ^{1}H NMR spectrum (600 MHz, C_6D_6, T = 280 K) of the 1:1 mixture between **WEtOEt** and **SC18N** (top), and 1D selective ROESY (τ_m = 200 ms) spectrum (bottom) carried out by irradiating the cluster of *host* signals centered at 3.6 ppm (see text for further details).

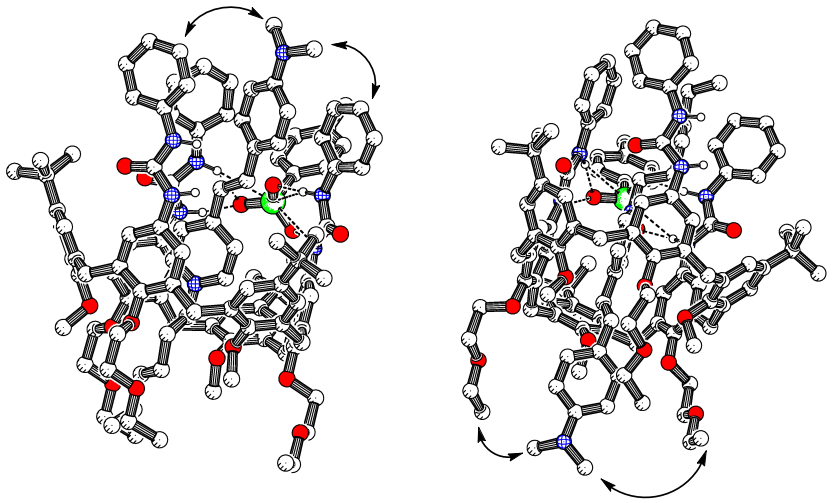

Figure 4.14: Molecular mechanics minimised structures (MMFF94 force field) of the two orientational isomers **Up** (left) and **Down** (right) of the complex between **WEtOEt** and **SC18N**. The ROE correlations of figure 4.12 are indicated with double-headed arrows.

4.2.2 Kinetic Experiments

As previously specified, in deuterated benzene, the equilibration process between the two orientational pseudorotaxane isomer is sufficiently slow to be monitored by NMR. To confirm the evolution of the system with time, some kinetic experiments at different temperatures have been performed. A preliminary experiment was carried out at room temperature (T = 298 K) following the variation of intensity of the two NMe_2 signals after the mixing of the components until the attainment of a steady-state in which the intensity of the signal no longer appreciably varies. This experiment evidenced an increase in the abundance of the **Up** isomer with a decrease of the **Down**. To verify the reversibility of the process, the same sample was kept in the fridge at *ca.* 277 K for 48 h and the following measure at 298 K again showed a ratio between the **Up** to **Down** signals close to the initial one. Based on this preliminary experiment, three kinetic follow up at T = 288, 298 and 333 K were performed. The first kinetic experiment was accomplished at 288 K. To this aim, the probe spectrometer was stabilised at the correct temperature, and a previously prepared sample of the 1:1 mixture was removed from the fridge, kept in hand until it was melted, gently shaken and then introduced into the probe. A total of 29 ^{1}H spectra were recorded with the same acquisition parameters. The superposition of the spectra collected in figure 4.15 shows that there is no significant variation of the chemical shift of the signals with time. The instrumental stability was highlighted, for example, by the resonance of the deuterated solvent residual signal that does not change appreciably with time (see inset of figure 4.15).

The expanded region collected in figure 4.16 shows that any significant variation of the sum of the integrals of the two NMe_2 signals was observed for the first 16 spectra recorded. The average value and its standard deviation are 2.216 ± 0.014. Similarly, no significant integral variation was observed for the following 13 spectra, but its average value is slightly smaller (2.179 ± 0.011). A similar systematic decrease is also observed for other *guest* signals and is likely due to a spectrometer instability.

The most significant insights obtained from this first kinetic experiment were a slow increase with time of the intensity of the signal at 2.37 ppm (**Up**) with a corresponding decrease of the signal at 2.56 ppm (**Down**). The fitting of the intensity variation of the former signal, reported in figure

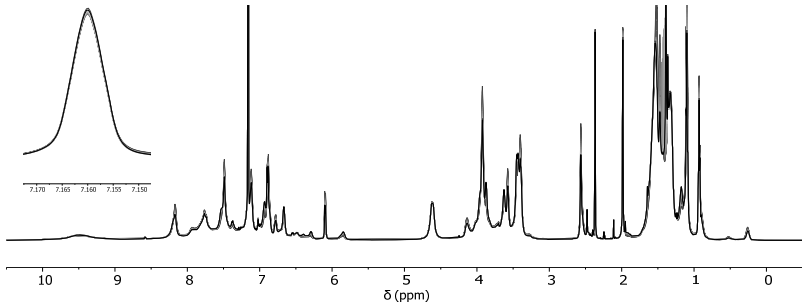

Figure 4.15: Superimposed spectra of the kinetic experiment at T = 288 K (C_6D_6, 600 MHz). The inset shows the signal of the solvent that did not undergo appreciable chemical shift variation for all the experiments.

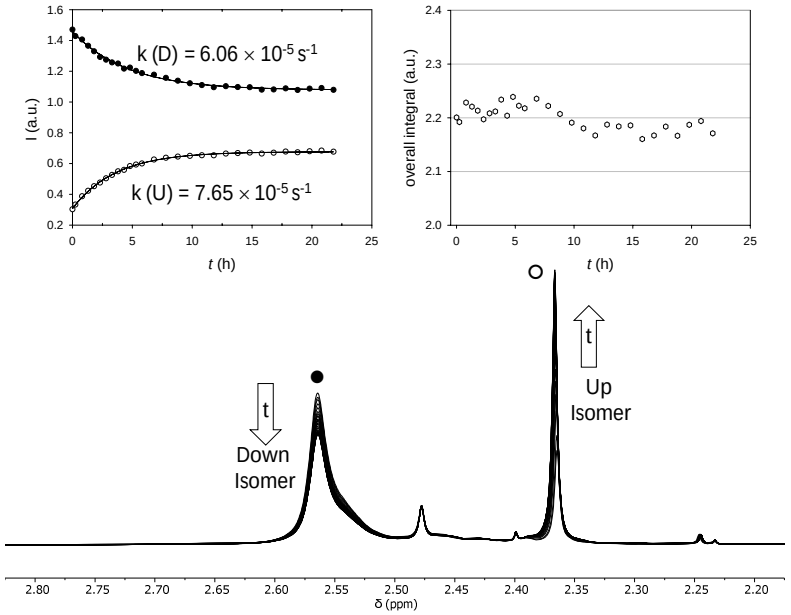

Figure 4.16: Variation of the intensities with time at T = 288 K of the N,N-dimethylamino signals of the orientational isomers **Down** (left) and **Up** (right). The plot on the right shows the variation of the overall integral intensity with time. The variation of the intensity of the two signals was fitted with a three-parameter exponential; the results are indicated on the relative plot on the left.

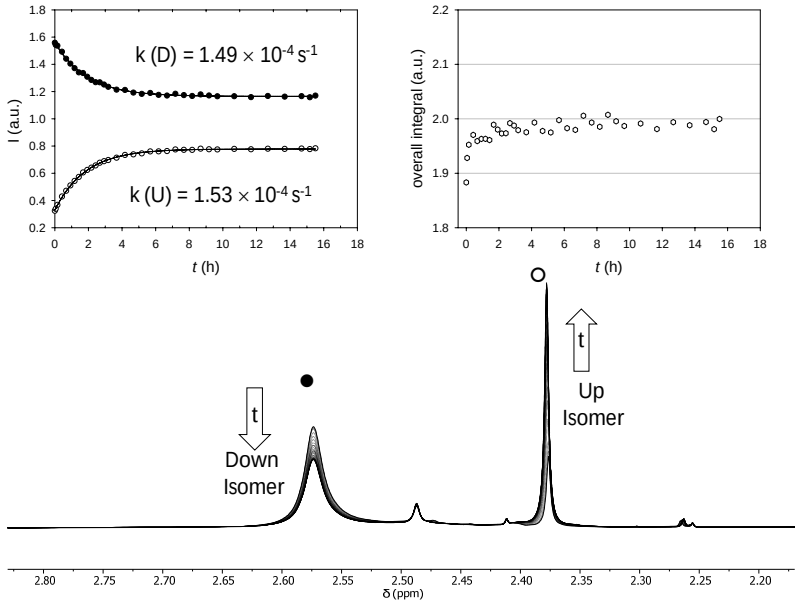

Figure 4.17: Variation of the intensities with time at T = 298 K of the N,N-dimethylamino signals of the orientational isomers **Down** (left) and **Up** (right). The plot on the right shows the variation of the overall integral intensity with time. The variation of the intensity of the two signals was fitted with a three-parameter exponential; the results are indicated on the relative plot on the left.

4.16, is in agreement with a first-order process with offset and yielded a kinetic constant of $6.06 \cdot 10^{-5} s^{-1}$, while the analysis of the intensity of the broader peak at 2.55 ppm, relative to the **Down** isomer, shows, as expected, an opposite exponential trend with a rate constant of $7.65 \cdot 10^{-5} s^{-1}$ (see figure 4.16). When the experiment was carried out at T = 298 K, the trend observed was similar to that recorded at 288 K, but the interconversion between the two orientational isomers was faster. The fitting of the intensity variation for the two signals yielded a kinetic constant of $1.49 \cdot 10^{-4} s^{-1}$ for the decay of the **Down** isomer signal, and of $1.53 \cdot 10^{-4} s^{-1}$ for the growth of the **Up** isomer signal (see figure 4.17).

The final kinetic experiment, carried out at T = 333 K shows that a steady state is reached within one hour from the mixing of **WEtOEt** and **SC18N**. The calculated kinetic constants were of $1.92 \cdot 10^{-3} s^{-1}$ for the

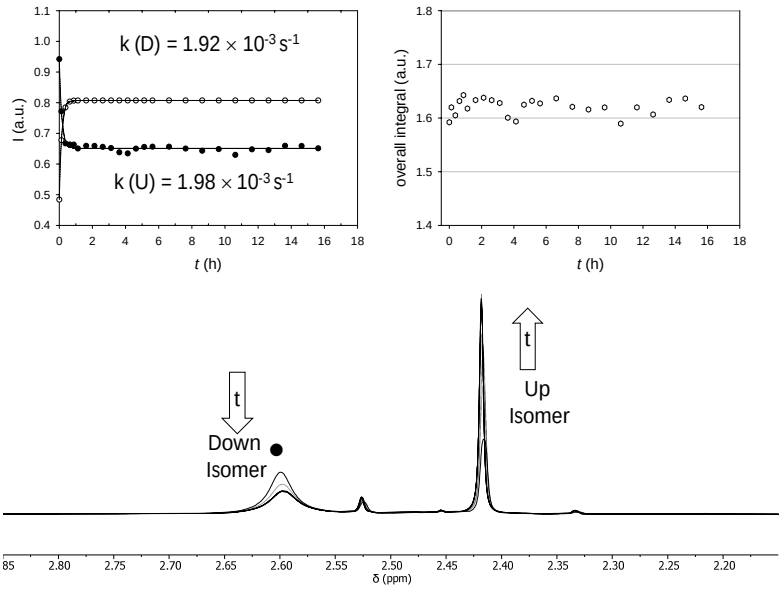

Figure 4.18: Variation of the intensities with time at T = 333 K of the N,N-dimethylamino signals of the orientational isomers **Down** (left) and **Up** (right). The plot on the right shows the variation of the overall integral intensity with time. The variation of the intensity of the two signals was fitted with a three-parameter exponential; the results are indicated on the relative plot on the left.

Solvent	Temperature (K)	**Up** isomer (%)	**Down** isomer (%)
$CDCl_3$	298	58	42
$CDCl_3$	228	50	50
C_6D_6	280[a]	17	83
C_6D_6	288	34	66
C_6D_6	298	39	61
C_6D_6	333	53	47

Table 4.1: Percentage of orientational isomers present in $CDCl_3$ and C_6D_6 solution at different temperatures for the complex between **WEtOEt** and **SC18N**. [a]The sample was removed from the fridge and immediately inserted in the spectrometer probe kept at 280 K.

decay of the **Down** isomer signal, and of $1.98 \cdot 10^{-3} s^{-1}$ for the growth of the **Up** isomer signal (see figure 4.18). It is worth to observe that at this temperature, the **Up** isomer is the predominant one in the solution (see also table 4.1). As expected, the wheel threading processes at this temperature are faster than in the previous experiments.

Comparing the results of the three experiments, it is possible to affirm that i) the overall intensity of the *guest* signals in the orientational isomers does not appreciably change with time; ii) the **Down** isomer is always formed faster and then slowly partially interconverts in the **Up**. At low temperature (288 K), the steady state is reached within ten hours, while at room temperature in half of the time. At high temperature (333 K), this interconversion is very fast, and the **Up** isomer becomes, even if slightly, the more abundant one. From the analysis of these results, it becomes also possible to formulate some hypotheses on the mechanism of the threading process of **SC18N** in the cavity of **WEtOEt**. First of all, the *guest* C18 alkyl chain may act as a kinetic stopper,[20] making the threading of **SC18N** through the wheel with the alkyl chain very slow and unfavoured. As a consequence, the formation of the **Up** isomer is likely due to the threading of the *guest* with its NMe_2 group through the wheel lower rim. Contrarywise, the threading of **SC18N** with its NMe_2 group through the upper rim of **WEtOEt**, leads to the fast formation of the **Down** isomer. The threading through the upper rim of the wheel is more favored since the lower rim is, on the NMR timescale, hindered from the methoxy groups oriented toward

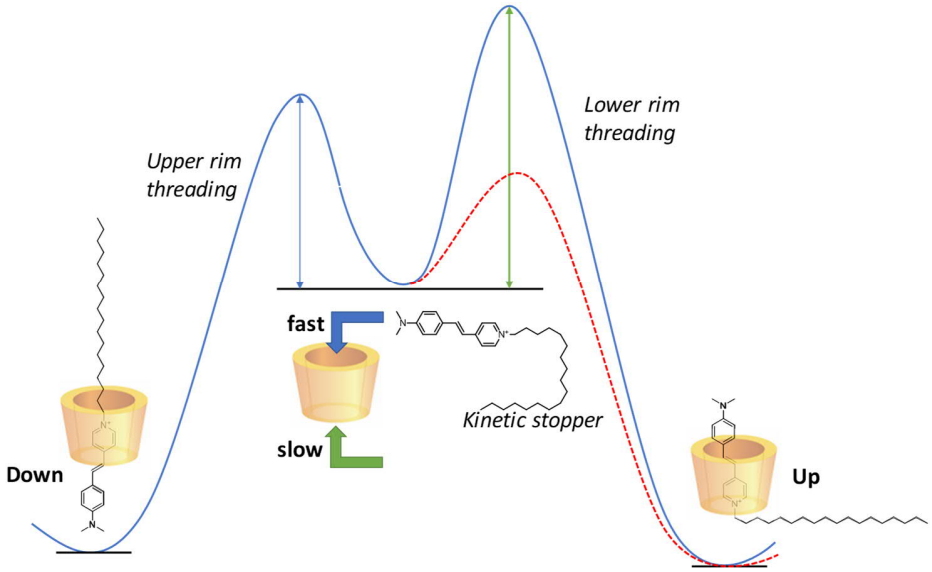

Figure 4.19: Schematic representation of the threading process in C_6D_6 solution of **SC18N** in **WEtOEt** as a function of the temperature (see text). The blue continuos line shows the energetic profile at low and room temperature for the inclusion of the *guest* in the wheel via its dimethylamino group since the C18 alkyl chain acts as a kinetic stopper. The red dashed line shows that at high temperature the *guest* is capable of threading the lower rim of the wheel, giving rise to the slightly more stable **Up** isomer.

the inner of the cavity. The increase of the temperature thus enhances the mobility of the methoxy group, and the threading through the lower rim becomes faster. Switching to the more polar deuterated chloroform, a speeding up of the interconversion process is observed. A steady-state is reached within a few minutes. It is reasonable to assume that a more polar solvent may loosen the ion pair, thus favoring the threading from the wheel lower rim, where the phenylureas are not present. Also in this case, the ratio between the **Up** and **Down** isomers changes with temperature: at T = 298 K the **Up** isomer is the more abundant, while at T = 228 K the two isomers have the same abundance. The relative ratio between **Up** and **Down** isomers with respect to the solvent and temperature are reported in table 4.1. Summarising, the **Up** isomer becomes the more favored one at high temperature and switching to a more polar solvent such as chloroform.

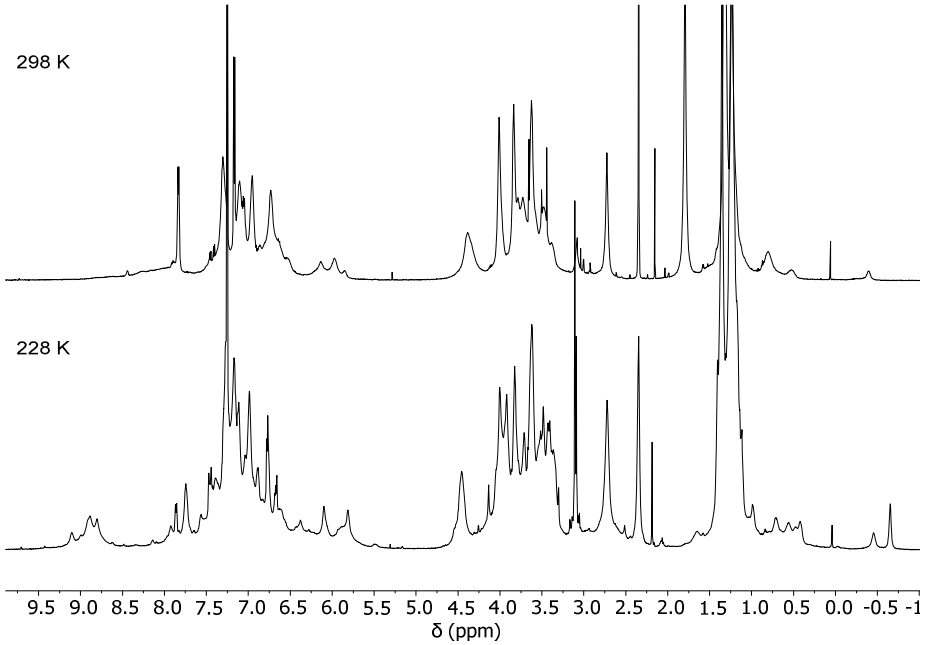

Figure 4.20: ^{1}H NMR stack plot (600 MHz, $CDCl_3$) of the 1:1 mixture between **WEtOEt** and **SC5N** taken at T = 298 K (top) and T = 228 K (bottom).

4.2.3 Effect of the Alkyl Chain of the Guest on the Threading Processes

To better understand the key factors governing the threading process, the complexation studies were also carried out with stilbazolium salts characterised by alkyl chains of different lengths (see scheme 4.1). In this new series, the first stilbazolium salt investigated was **SC5N**. Differently from **SC18N** this *guest* is characterised by a short C5 alkyl chain. This motif is known, for example, in N,N-dialkylviologen salts, to allow the insertion of the *guest* through its alkyl chain inside the calixarene cavity.[20] The ^{1}H NMR (see figure 4.20) and the 2D heterocorrelated HSQC spectra acquired in chloroform at T = 298 K allowed us to identify the presence in solution of both the orientational isomers **Up** and **Down**.

The dimethylamino signal relative to these isomers, resonating at δ = 2.09 ppm and 2.73 ppm for **Up** and **Down**, respectively, are in 7 to 3 ratio.

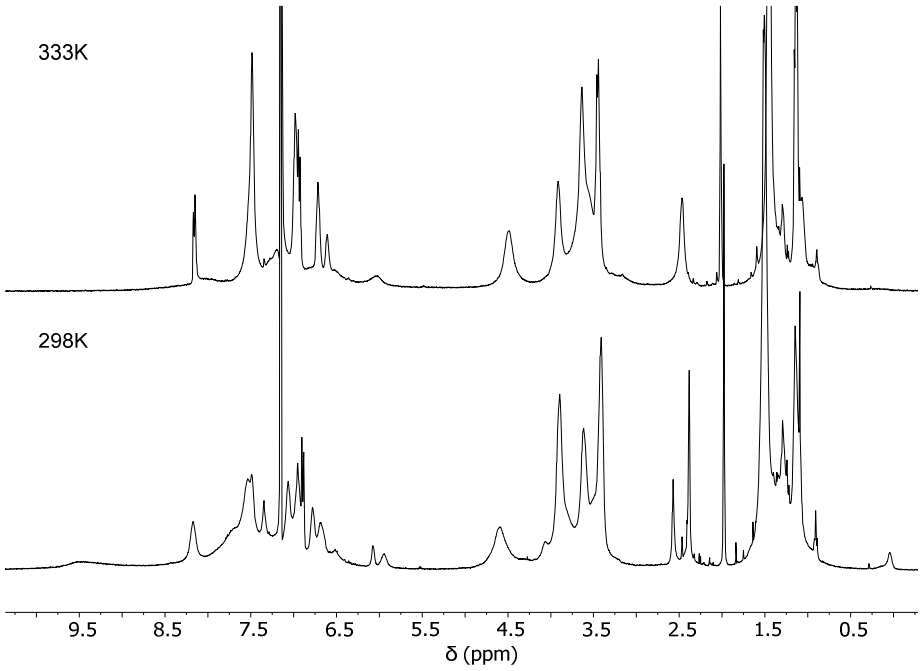

Figure 4.21: ^{1}H NMR stack plot (600 MHz, C_6D_6) of the 1:1 mixture between **WEtOEt** and **SC5N** taken at T = 333 K (top) and T = 298 K (bottom).

The ratio between the intensity of the two signals and thus between the amount of **Up** and **Down** isomers in solution became 6 to 4 lowering the temperature at T = 228 K. This finding strongly suggest that, as hypothesised above, the formation of **Up** isomer is influenced by the length and the steric hindrance, of the alkyl chain of the *guest*. The studies carried out in C_6D_6 support this hypothesis. Indeed, with this short alkyl chain, the equilibration process takes place, at room temperature, in few minutes (too fast to follow the kinetic through NMR) and at 333 K the two isomers are in fast exchange on the NMR timescale, and only one broad signal can be identified for the NMe_2 group (see figure 4.21). The complexation of **SC1N**, having just a methyl group appended to the pyridinium ring (see scheme 4.1), has been studied according to the other *guests* in the $CDCl_3$ solution. In figure 4.22 is reported the stack plot of the ^{1}H NMR spectrum acquired as usual at T = 298 K, and at 228 K.

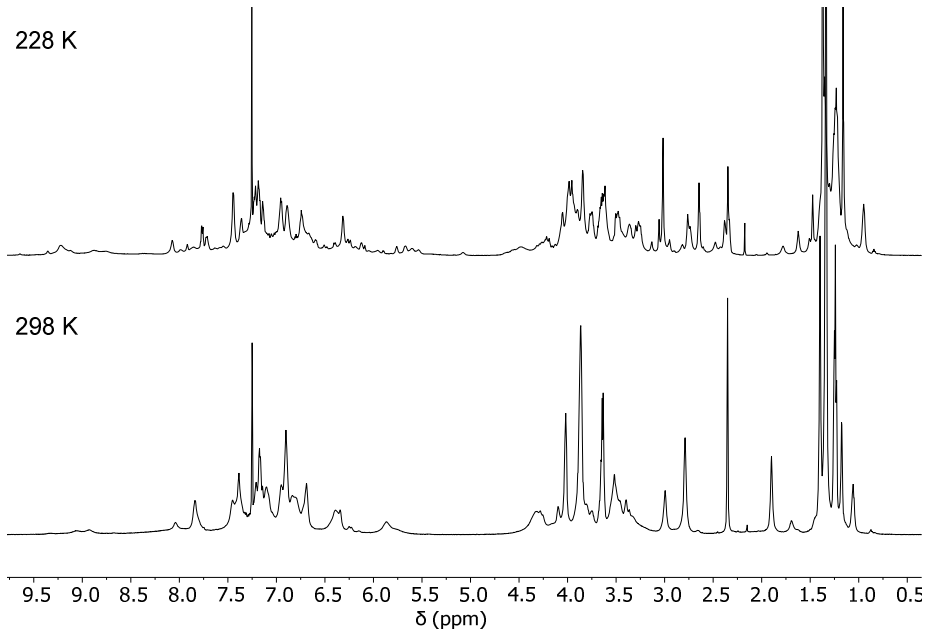

Figure 4.22: ^{1}H NMR stack plot (600 MHz, $CDCl_3$) of the 1:1 mixture between **WEtOEt** and **SC1N** taken at T = 228 K (top) and T = 298 K (bottom).

The spectrum taken at the latter temperature is rather complicated. However, two different sets of signals for the NMe_2 group and two for the ethoxyethyl chains of the wheel are still recognisable. Although in these two spectra it is not possible to carry out an accurate integration of the signals, the comparison of the results suggests that the ratio between **Up** and **Down** isomers is not affected by the temperature and remains constant at *ca.* 7 to 3, respectively. The *guest* **SCNCapped** (see scheme 4.1), bearing a diphenylacetyl stopper on the ending of its C6 alkyl chain, can thread the calix[6]arene wheel only with its dimethylamino group. In previous studies, it has been shown that this stopper is too bulky to pass through the calix[6]arene annulus.[18] The ^{1}H NMR spectrum acquired in chloroform at room temperature, reported in figure 4.23, shows the presence of two signals for the dimethylamino group. This finding is very important because it confirms that, at least in these conditions of temperature and solvent,

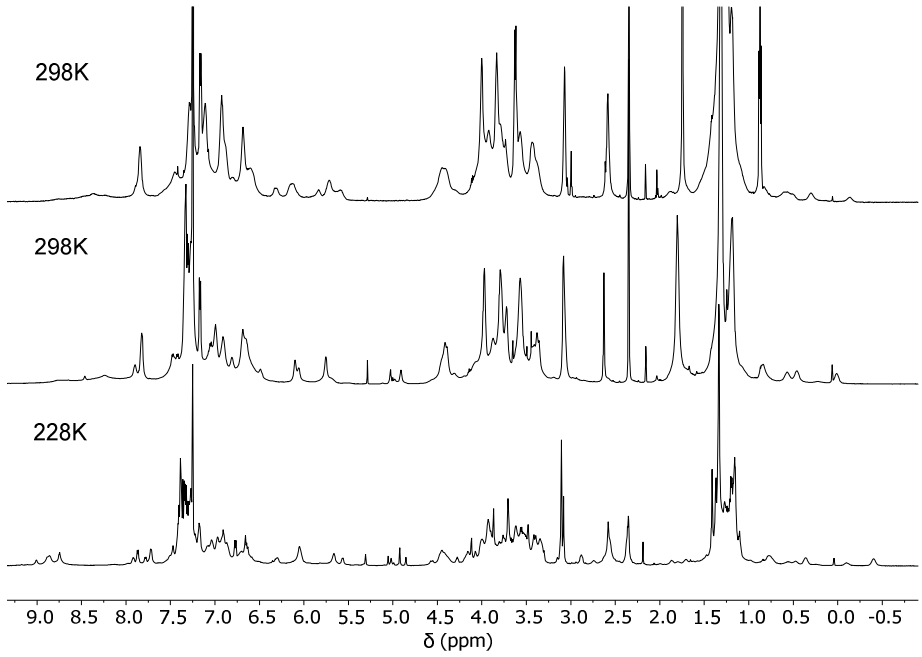

Figure 4.23: ^{1}H NMR stack plot (600 MHz, $CDCl_3$) of **WEtOEt⊃SC18N**, T = 298 K (top), **WEtOEt⊃SCNCapped**, T = 298 K (middle), and **WEtOEt⊃SCNCapped**, T = 228 K (down).

the threading also occurs through the calix[6]arene wheel lower rim. The integral ratio between the two signals of the dimethylamino group, which resonate at 2.63 ppm and 3.08 ppm, for the **Up** and **Down** isomers, respectively, is 3 to 7. Differently from what observed for **SC18N** at 298 K in $CDCl_3$, with **SCNCapped** the **Down** isomer is the preferred one. This could suggest that, because of the bulkiness of its stopper, with **SCNCapped** the two orientational isomers present different stability. Alternatively, it is possible to hypothesise that with **SC18N**, the **Up** isomer is formed either by the threading of the *guest* with i) the NMe_2 group through the wheel lower rim and ii) with its alkyl chain through the upper rim. This last threading mechanism is not obviously possible for **SCNCapped**, and thus the amount of **Up** isomer could be reduced.

4.2.4 Spectroscopic Characterisation of the Stilbazolium Salt

The optical properties of **SC18N** were initially studied in a toluene solution to evaluate the possible trans→cis isomerisation process. It is worth to mention that such isomerisation was not detected in all previous NMR measurements. As an example, the ^{1}H NMR spectrum of **SC18N** taken in $CDCl_3$ shows (see figure 4.6) only a pair of doublets at $\delta = 7.54$ and 6.77 ppm for the two olefinic protons. These doublets show a coupling constant J of 16.6 Hz, which is typical for isomers in the trans configuration.

The evolution of absorption and emission spectra were followed in the dark and in the light. The collection of absorption spectra acquired in the dark for 4 h at regular intervals of 3 min and after the exposition to light are reported in figure 4.24. It is interesting to note that the intensity of the main absorption band ($\lambda = 468$ nm) increased with time keeping the solution in the dark. The presence of two isosbestic points at 386 and 520 nm support the hypothesis of a cis/trans equilibrium and that the small amount of the cis isomer slowly interconverts in the trans one by keeping

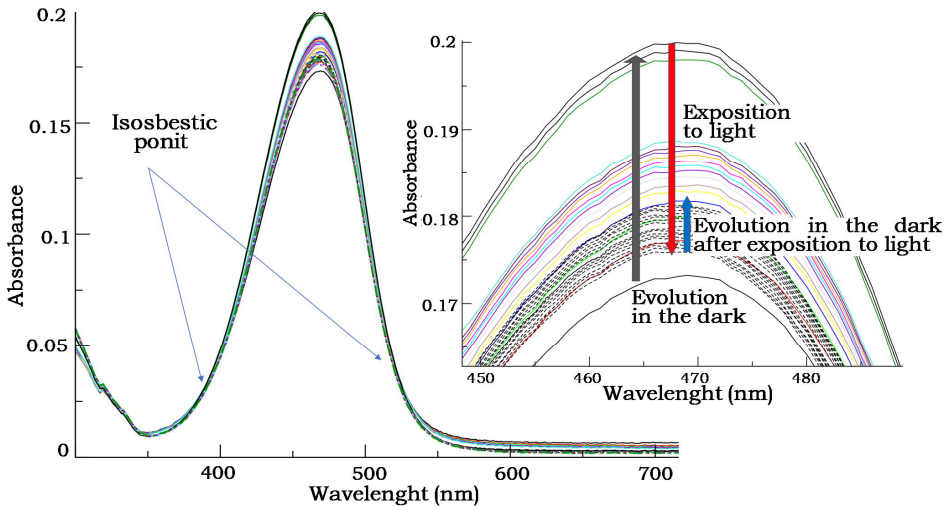

Figure 4.24: Absorption spectra of a solution of **SC18N** in toluene. The spectra were recorded with time intervals of 3 min (last measurement after 3 h) keeping the solution in the dark. In the inset, the evolution of the maximum of the band during the exposition of the solution to the light and, after this, in the dark.

the solution in the dark. The cuvette was then exposed to room light for about one hour, and a new absorption spectrum was then acquired. After the exposition to room light, a drop in the intensity of the absorption band at 468 nm was observed. The intensity of this band rises again hen the solution is kept again in the dark. The latter behavior suggests that the amount of cis-isomer formed during the exposition of the solution to the light interconverts back to its trans form in the dark.

4.2.5 Spectroscopic Studies on the WEtOEt/SC18N Complex

Due to the possible light-induced trans-cis isomerisation process for **SC18N**, all the solutions used for the complexation studies were prepared in a dark room. The concentrations of **WEtOEt** and **SC18N** used in the *host/guest* solution were $1.08 \cdot 10^{-3}$ M and $0.83 \cdot 10^{-4}$ M, respectively. The *host* **WEtOEt** was used in excess in order to favor the formation of the complex and, hence, the solubilisation of the *guest* **SC18N**. The excess of **WEtOEt** in the solution does not hinder the optical spectroscopic characterisation since **WEtOEt** only absorbs below 320 nm, *i.e.* outside the spectral region of interest. The concentration of **SC18N** in the *host/guest* solution required the use of short-path-length cells, both for absorption and fluorescence spectra. All the spectra have been recorded at room temperature ($\sim$ 291 K). While the solution of **SC18N** did not show any significant change over time, neither in absorption nor in fluorescence, absorption and fluorescence spectra of the *host/guest* solution showed a strong dependence according to the time delay with respect to the preparation of the solution. For this reason, absorption and fluorescence spectra of the *host/guest* solution were systematically collected over time, for a period of about 3 hours. The time indicated as "zero" corresponds to the minimum time required to completely solubilise **SC18N** into the flask containing **WEtOEt**, adjust the volume, fill the cells and start the measurements (a few minutes). Representative absorption spectra were reported in figure 4.25. While at time "0" has been mainly observed a single absorption band centered at 433 nm, for increasing time delays this band progressively loses intensity in favor of a new band appearing at $\sim$ 490 nm. The presence of a neat isosbestic point (at 455 nm) indicates that the equilibrium only involves two species. Neither of the two species corresponds to the isolated **SC18N**, whose ab-

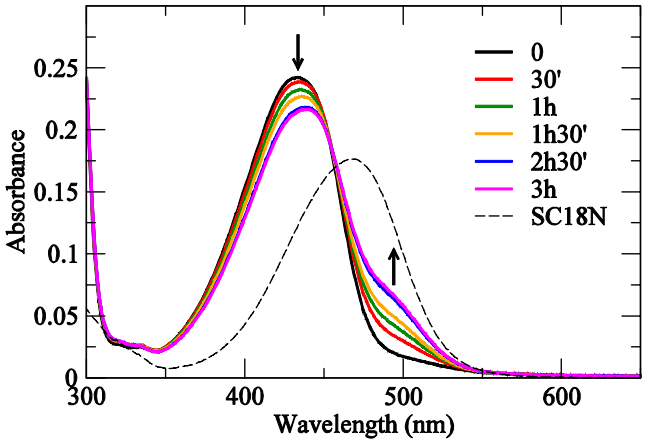

Figure 4.25: Absorption spectra of the **SC18N**/**WEtOEt** solution (path length 1 mm) for different time delays after preparation (see legend). The arrows indicate the time evolution. The black dashed line corresponds to the absorption spectrum of **SC18N** alone in toluene (saturated and filtered solution, path length 10 mm).

sorption is centered at 470 nm (in fact, **SC18N** is so poorly soluble in toluene that its concentration as a free species can be considered negligible with respect to complexed forms). The two bands are then related to two different **WEtOEt**/**SC18N** *host/guest* complexes: one is clearly kinetically favored, being formed promptly; the second species increases over time, at the expense of the first one, until the thermodynamic equilibrium is reached in about 3 hours.

Using the NMR data previously discussed, the promptly formed complex has been identified as the **Down** complex, while the one that increases in time as the **Up**. Interestingly, the absorption of the **Down** always stays more intense than the absorption of the delayed **Up**. Supposing that the oscillator strengths of the two complexes are similar (being related in either case to the absorption of **SC18N**), this suggests that complex **Down** always stays significantly more abundant than complex **Up**, *i.e.* that the promptly formed species is not only kinetically but also thermodynamically favored, with an energy difference a little bit greater than KT. Moreover, since experiments were performed in the dark, we can also conclude that thermal energy at room temperature is enough to overcome the activation barrier required for the conversion of one complex into the other. Repre-

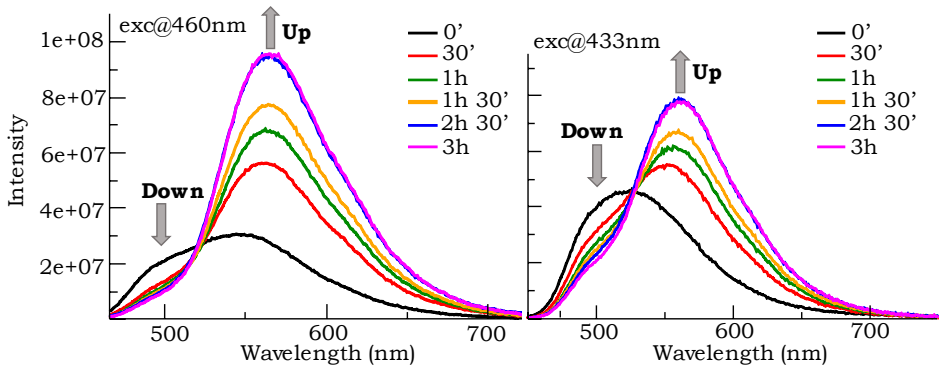

Figure 4.26: Corrected fluorescence emission spectra of the **SC18N**/**WEtOEt** solution collected at different time delays after preparation, for excitation wavelength fixed at 460 nm (left panel) or 433 nm (right panel). The arrows indicate the time evolution.

sentative fluorescence emission spectra of the *host/guest* solution in toluene are reported in figure 4.26, for two different excitation wavelengths. Consistently with the evolution observed in absorption spectra, we observe two emission bands: one at $\sim$ 490 nm, related to the species absorbing at 433 nm, the other at $\sim$ 560 nm, related to the species absorbing at 490 nm. The abundance of the species absorbing and emitting at shorter wavelength decreases with time, leading to the formation of the species absorbing and emitting at longer wavelength. The first excitation wavelength (433 nm, left panel) corresponds to the maximum absorption of complex **Down**. At t = 0 the direct excitation of the scarcely present complex **Up** is negligible so that emission (black line) only stems from complex **Down** (in fact the shape of this emission band coincides with the shape of the emission of **SC18N** alone in toluene. At increasing time delay, complex **Up** is gradually formed, even if its absorbance at 433 nm always stays much lower than the absorbance of complex **Down** (estimated 6:1 ratio at t = 3 h). However, complex **Up** absorbs at the same wavelengths where complex **Down** emits, so that, for increasing time delays, it plays a gradually increasing inner filter effect on the emission of complex **Down** (light emitted by complex **Down** can be reabsorbed by complex **Up**, in a radiative excitation energy transfer process).

The corresponding quenching of the emission of complex **Down** is taken into account by the correction for inner-filter effects (already applied in the

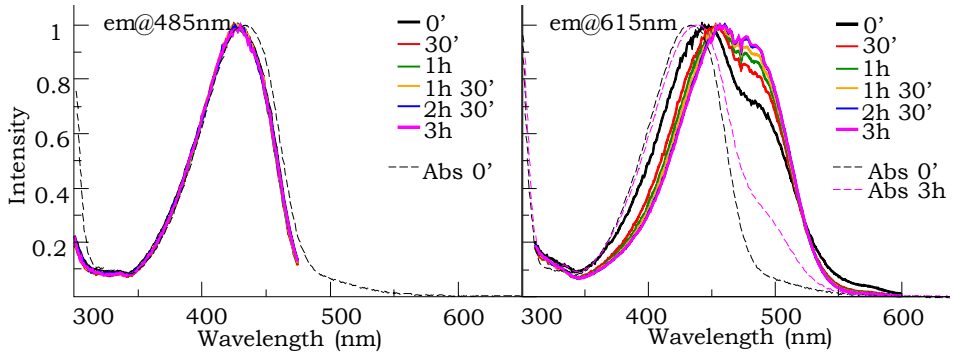

Figure 4.27: Normalised corrected fluorescence excitation spectra of the **SC18N/WEtOEt** solution collected at different time delays after preparation, for emission wavelength fixed at 485 nm (left panel) or 615 nm (right panel). Dashed lines correspond to normalised absorption spectra of the same solution (time delays in the legends).

spectra shown in figure 4.26), and amounts to less than 10% at t = 0 and to $\sim$ 30% at t = 3 h were found. The quenching of emission of complex **Down** is accompanied by a "sensitisation" of the emission of complex **Up**, because of the radiative energy transfer process: this effect shall lead to an amplification of the emission of the "acceptor" complex of the same amount as the quenching of the "donor" complex (*i.e.* never exceed 30%). Even taking the sensitisation of the emission of complex **Up** into account, fluorescence spectra reported in figure 4.26 suggest that complex **Up** is strongly more emissive than complex **Down**, dominating the fluorescence spectrum despite its scarce abundance at any time delay. Fluorescence spectra obtained for excitation wavelength fixed at 460 nm (figure 4.26, right panel) confirm this interpretation.

At this excitation wavelength, closer to the absorption maximum of complex **Up**, the emission spectra are even more dominated by the emission of complex **Up**. Fluorescence excitation spectra (figure 4.27) are consistent with the previous results. When detecting emission at 485 nm (left panel), the excitation profile corresponds to the absorption spectrum of complex **Down**. When detecting emission at 615 nm (right panel), the excitation profile shows the absorption bands of both complex **Down** and **Up**, with the component due to complex **Up** increasing with time. The presence

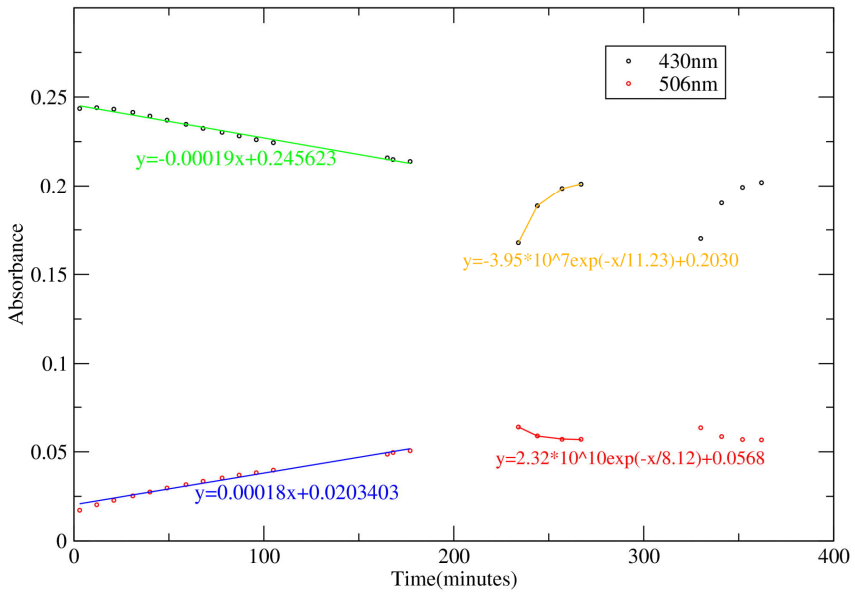

Figure 4.28: Fitting on the evolution of absorbance intensity at 403 nm (green) and 506 nm (blue) in the dark and in the light (yellow and red).

of the absorption band of complex **Down** in the excitation profile is due both to the fact that complex **Down** slightly emits at 615 nm and to the radiative energy transfer process from complex **Down** to complex **Up**. In figure 4.28 are reported the fitting performed on the absorbance intensity at $\lambda = 430$ nm and 506 nm, this data allowed to roughly estimate the kinetics of the corresponding processes. The kinetic in the dark is likely due to the interconversion between **Down** and **Up**, while the evolution in the light should depend on the trans/cis isomerisation.

4.3 Experimental

Materials: all solvents were dried using standard procedures; all other reagents were of reagent grade quality, obtained from commercial suppliers and were used without further purification. NMR spectra were recorded at 400 and 600 MHz for ^{1}H and 100 MHz for ^{13}C. Melting points are

uncorrected. Chemical shifts are expressed in ppm (δ) using the residual solvent signal as internal reference (7.16 ppm for C_6D_6; 7.26 ppm for $CDCl_3$ and 3.31 for CD_3OD). Mass spectra were recorded in ESI mode. Compound **S1**[16] was synthesised according to published procedures.

General procedure for the sinthesys of the stilbazolium salts: In a 100 mL round bottomed flask, **S1** (300 mg, 1.3 mmol) and the opportune alkylating agent (1.7 mmol) were dissolved in 40 mL of acetonitrile. The reaction mixture was stirred at reflux for 24 h, then the solvent was evaporated under reduced pressure.

SC1N: alkylation of **S1** with methyltosylate. The purification through column chromatography on silica gel (eluent: CH_2Cl_2/CH_3OH = 65/35) yields **SC1N** as a red solid in 30% yield. ^{1}H NMR (400 MHz, $CDCl_3$ + 10% CD_3OD): δ (ppm) = 8.28 (2H, d, ^3J = 6.9 Hz), 7.6-7.5 (m, 4H), 7.47 (d, 1H, ^3J = 15.9), 7.37 (d, 2H, ^3J = 8.9 Hz), (7.01 (d, 2H, J = 7.9), 6.71 (d, 1H, ^3J = 15.9 Hz), 6.56 (d, 2H, ^3J = 8.9 Hz), 4.0 (br. S., 3H), 2.92 (s, 6H), 2.18 (s, 3H).

SC5N: alkylation of **S1** with 1-pentyltosylate. Triturations of the crude mixture with ethyl acetate yield **SC5N** as a red solid in 68%. ^{1}H NMR (400 MHz, $CDCl_3$): δ (ppm) = 8.77 (d, 2H, ^3J = 6.7 Hz), 7.9 - 7.8 (m,4H), 7.59 (d, 1H, ^3J = 16.0 Hz), 7.52 (d, 2H, ^3J = 8.8 Hz), 7.16 (d, 2H, ^3J = 8.0 Hz), 6.84 (d, 1H, ^3J = 16.0 Hz), 6.79 (d, 2H, ^3J = 8.6 Hz), 4.52 (t, 2H, ^3J = 7.4 Hz), 3.09 (s, 6H), 2.34 (s, 3H), 1.94-1.89 (m, 2H), 1.3-1.2 (m, 4H), 0.86 (t, 2H, ^3J = 6.9 Hz). ^{13}C NMR (100 MHz, $CDCl_3$): δ (ppm) = 154.0, 152.3, 144.3, 143.7, 142.6, 139.3, 130.7, 128.9, 126.2, 123.0, 122.7, 116.9, 112.1, 60.3, 40.1, 31.3, 28.2, 22.3, 21.4, 14.0.

SC18N: alkylation of **S1** with 1-octadecyltosylate. Triturations of the crude mixture with ethyl acetate yield SC18N as a red solid in 63%. M.p. = 161 - 163 °C. ^{1}H NMR (400 MHz, $CDCl_3$): δ (ppm) = 8.74 (d, 2H, ^3J = 6.6 Hz), 7.86 (d, 2H, ^3J = 8.1 Hz), 7.83 (d, 2H, ^3J = 6.6 Hz), 7.57 (d, 1H, ^3J = 15.9 Hz), 7.50 (d, 2H, ^3J = 8.9 Hz), 7.17 (d, 2H, ^3J = 7.9 Hz), 6.80 (d, 1H, ^3J = 15.9 Hz), 6.69 (d, 2H, ^3J = 8.9 Hz), 4.50 (t, 2H, ^3J = 7.3 Hz), 3.09 (s, 6H), 2.35 (s, 3H), 1.94-1.83 (m, 2H), 1.1-1.4 (m,

30 H), 0.90 (t, 3H, ^3J = 6.8 Hz). ^{13}C NMR (100 MHz, $CDCl_3$): δ (ppm) = 153.9, 152.2, 144.1, 143.6, 142.6, 139.0, 130.6, 128.6, 126.1, 122.8, 122.5, 116.6, 112.0, 60.3, 40.1, 31.9, 31.5, 29.9-29.3 (multiple resonances), 29.1, 26.1, 22.7, 21.3, 14.1.

SCNCapped: alkylation of **S1** with **7a**. The purification through column chromatography on silica gel (eluent: CH_2Cl_2/CH_3OH = 90/10) yields **SCNCapped** as a red solid in 36% yield. M.p. = 144-146 °C. 1H NMR (300 MHz, $CDCl_3$): δ (ppm) = 8.67 (d, 2H, ^3J = 6.9 Hz), 7.84(d, 2H, ^3J = 8.1 Hz), 7.75(d, 2H, ^3J = 6.6 Hz), 7.46(d, 1H, ^3J = 15.9 Hz), 7.31 (d, 2H, ^3J = 9.0 Hz), 7.29 (m, 10H), 7.12(d, 2H, ^3J = 8.1 Hz), 6.74(d, 1H, ^3J = 15.9 Hz), 6.63 (d, 2H, ^3J = 9.0 Hz), 5.01(s, 1H), 4.35(t, 2H, ^3J = 5.4 Hz), 4.06 (t, 2H, ^3J = 5.1 Hz), 3.02 (s, 6H), 2.29 (s, 3H), 1.75 (m, 2H), 1.51 (m, 2H), 1.18 (m, 4H). ^{13}C NMR (100 MHz, $CDCl_3$): δ (ppm) = 172.5, 153.9, 152.1, 144.2, 143.5, 142.5, 139.1, 138.7, 130.5, 128.7, 128.6 (two resonances), 127.2, 126.0, 122.8, 122.5, 116.6, 111.9, 65.0, 59.8, 57.1, 40.1, 31.4, 28.4, 25.5, 25.2, 21.3. ESI-MS(+): m/z = 520.51 $[M\text{-}TsO]^+$.

NMR Kinetic Measurements: the spectrometer was stabilised at 288, 298 and 333 K. The sample was removed from the fridge, kept in hand until it was melted, gently shaken and then introduced in the magnet. The first spectrum was recorded within 15 min after removing the sample from the fridge (t = 0). The duration of each measurement was about 2 min, and all the spectra were recorded with the same acquisition parameters. Gradient shimming was applied before each measurement. The spectra were processed using one level of zero-filling (from 32k to 64k points) and exponential apodisation (lb = 1 Hz). The same first-order phase correction (PH1 = 70°) was applied to all the spectra. The zero-order correction was then finely adjusted for each spectrum. The spectra were baseline corrected using a simple first-order polynomial function (Filter 500). This yielded superimposable spectra with no chemical shift variation for the signal of the solvent. Chemical shift referencing was then applied (7.16 ppm for the signal of the solvent, C_6D_6).

Optical Spectroscopic Characterisation: due to the possible occurring of light-induced trans-cis isomerisation processes for **SC18N**, all the

solutions were prepared in a dark room only illuminated by a red light and were not exposed to room or daylight before the beginning of the sessions of measurements. Different portions of the stock solutions were used for absorption and fluorescence, in order not to expose the samples to light before any of the measurements. For the spectra measured at different time delays after the preparation of the solutions, the samples were kept in the dark, inside the instrument, in between any measurement and the following one. **SC18N** is poorly soluble in toluene so that a saturated solution was prepared and then filtered before pouring it into the quartz cuvette used for the absorption and emission measurements. Due to the poor solubility of **SC18N**, concentrated solutions of **WEtOEt** + **SC18N** could not be obtained by mixing the solutions of the isolated compounds, but were prepared as follows: **WEtOEt** and **SC18N** were weighted in amounts corresponding to final concentrations of $\sim 10^{-3}M$ and $10^{-4}M$, respectively, once in a 10 mL volume; the weighted amount of **WEtOEt** was dissolved in a 10 mL flask, using a <10 mL volume of toluene; the weighted amount of **SC18N** was added into the flask and the solution was vigorously shaken for a few seconds; after the complete dissolution of **SC18N** the volume of the solution was adjusted to reach 10 mL. The concentrations of **WEtOEt** and **SC18N** that were obtained in the *host/guest* solution were $1.08 \cdot 10^{-3}M$ and $0.83 \cdot 10^{-4}M$, respectively. The *host* **WEtOEt** was used in excess to favour the formation of the complex and, hence, the solubilisation of the *guest* **SC18N**. The excess of **WEtOEt** in the solution does not hinder the optical spectroscopic characterisation since **WEtOEt** only absorbs below 320 nm, *i.e.* outside the spectral region of interest. The concentration of **SC18N** in the *host/guest* solution required the use of short-path-length cells, both for absorption and fluorescence spectra. In particular, 1-mm quartz cuvettes were used for absorption, while a quartz tube having 4-mm internal diameter was used for fluorescence spectra. Despite the short path length, inner filter effects were not negligible in fluorescence spectra, so that both emission and excitation spectra were corrected:[21]

$$I_{corr}(\lambda_{exc}, \lambda_{em}) = I_{obs}(\lambda_{exc}, \lambda_{em}) \cdot 10^{[OD(\lambda_{exc})+OD(\lambda_{em})]\cdot d/2}$$

where OD is the optical density (absorbance per unit path length), and d is the path length relevant to the fluorescence measurements. The

time indicated as "zero" corresponds to the minimum time required to completely solubilise **SC18N** into the flask containing **WEtOEt**, adjust the volume, fill the cells and start the measurements (a few minutes).

Bibliography

(1) Doja, M. Q. *Chem. Rev.* **1931**, *11*, 273–321.

(2) Mishra, A.; Behera, R. K.; Behera, P. K.; Mishra, B. K.; Behera, G. B. *Chem. Rev.* **2000**, *100*, 1973–2012.

(3) Shindy, H. *Dyes and Pigments* **2017**, *145*, 505–513.

(4) Dong, H.; Zhang, C.; Zhao, Y. S. *J. Mater. Chem. C* **2017**, *5*, 5600–5609.

(5) Hao, F.; Zhu, D.; Ma, J.; Chai, L. *Spectrochimica Acta Part A: Molecular and Biomolecular Spectroscopy* **2014**, *123*, 46–53.

(6) Eaton, S. W.; Fu, A.; Wong, A. B.; Ning, C.-Z.; Yang, P. *Nature Reviews Materials* **2016**, *1*, 16028.

(7) Kuehne, A. J. C.; Gather, M. C. *Chem. Rev.* **2016**, *116*, 12823–12864.

(8) Samuel, I. D. W.; Turnbull, G. A. *Chem. Rev.* **2007**, *107*, 1272–1295.

(9) Dsouza, R. N.; Pischel, U.; Nau, W. M. In *Supramolecular Photochemistry*, Ramamurthy, V., Inoue, Y., Eds.; John Wiley & Sons, Inc.: 2011, pp 87–114.

(10) Sayed, M.; Pal, H. *J. Mater. Chem. C* **2016**, *4*, 2685–2706.

(11) Petrov, N. K.; Ivanov, D. A.; Alfimov, M. V. *ACS Omega* **2019**, *4*, 11500–11507.

(12) *Fluorescence of supermolecules, polymers, and nanosystems*; Berberan-Santos, M. N., Acuña, A. U., Eds.; Springer: 2008.

(13) Mourtzis, N.; Eliadou, K.; Yannakopoulou, K. *Supramol. Chem.* **2004**, *16*, 587–593.

(14) Zanichelli, V.; Ragazzon, G.; Orlandini, G.; Venturi, M.; Credi, A.; Silvi, S.; Arduini, A.; Secchi, A. *Org. Biomol. Chem.* **2017**, *15*, 6753–6763.

(15) Orlandini, G.; Ragazzon, G.; Zanichelli, V.; Secchi, A.; Silvi, S.; Venturi, M.; Arduini, A.; Credi, A. *Chem. Commun.* **2017**, *53*, 6172–6174.

(16) Pepitone, M. F.; Jernigan, G. G.; Melinger, J. S.; Kim, O.-K. *Org. Lett.* **2007**, *9*, 801–804.

(17) Binstead, R. A., *SPECFIT/32, fitting software, Spectrum Software Associates, Chapel Hill, 1996.* 1996.

(18) Arduini, A.; Calzavacca, F.; Pochini, A.; Secchi, A. *Chem. Eur. J.* **2003**, *9*, 793–799.

(19) Reichardt, C.; Welton, T. In *Solvents and Solvent Effects in Organic Chemistry*; John Wiley & Sons, Ltd: 2010; Chapter 6, pp 359–424.

(20) Arduini, A.; Bussolati, R.; Credi, A.; Secchi, A.; Silvi, S.; Semeraro, M.; Venturi, M. *J. Am. Chem. Soc.* **2013**, *135*, 9924–9930.

(21) Lakowicz, J. R., *Principles of Fluorescence Spectroscopy*, 3rd ed.; Springer: 2006.

Chapter 5

New Geometries for Calix[6]arene-based Hosts and Rotaxanes

5.1 Introduction

The importance of the "bottom-up" approach in the development of the field of nanotechnology is strictly related to the new knowledge acquired in supramolecular chemistry. The advancement achieved in the last decades allowed to develop of several stimuli-responsive devices.[1–3] As discussed in the general introduction, the nature, number and reciprocal orientation of the binding sites is fundamental to create assemblies able to perform a programmed function.[1–3] In analogy to the calix[6]arene derivative **WEtOEt** discussed in the previous chapters, the tris-(N-phenylureido)-trioctyloxy calix[6]arene **TPU** [4] (see figure 5.1) is characterised by the presence of three phenylureido groups that are, on the NMR time scale, at the upper rim of the *cone* conformation (as described in detail in the introduction). These groups can act as binding site for the anionic counteranion of the cationic *guest* engulfed in the cavity. Indeed, these groups play a crucial role in the complexation of viologen salts. They promote the separation of the ion pair of the *guest*, pivoting the unidirectional threading of the cationic viologen through the macrocycle upper rim.[4–7] The solid-state structure of pseudorotaxane **TPU⊃DOV**, formed by **TPU** and dioctylviologen di-

iodide (**DOV**) (see the Pluton view of the X-rays structure in figure 5.1),[4] shows the calix[6]arene macrocycle adopting a flattened *cone* conformation in which a defined π-rich aromatic cavity surrounds the viologen bipyridinium dication, while both the iodide counteranions are H-bonded to the ureido moieties at the upper rim of **TPU**.

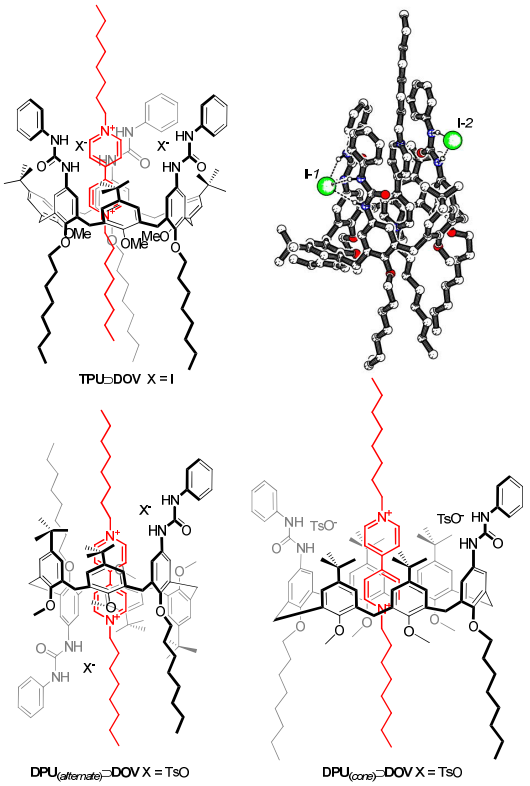

Figure 5.1: Schematic representation of the pseudorotaxanes formed between bis- and tris-(N-phenylureido) calix[6]arene **DPU** and **TPU** and viologen salts. On the right, the Pluton view of the X-ray structure of **TPU**$\supset$**DOV**$\cdot 2I^-$. [4]

However, the anions are in different situations: i) the first (I-1 in figure 5.1) forms hydrogen bonds with two phenylureido groups and it is completely separated from its countercation, ii) the other one (I-2 in figure 5.1), is H-bonded with the third phenylurea, remaining in intimate contact with the pyridinium ring protruding from the cavity. The role played by the

number and reciprocal orientation and position of the phenylureido binding groups on the complexation ability of the calix[6]arene *hosts* has never been investigated. Calix[6]arene-based *hosts* can assume different conformations in solution and in the solid state. In particular, Van Duynhoven *et al.* show that in low polarity solvents 1,3,5-trimethoxy-2,4,6-trialkoxy-para-tert-butylcalix[6]arenes slowly interconvert from the flattened *cone* conformation to the *1,2,3-alternate* conformation.[8] The two conformations are co-existent at room temperature, one slowly interconverting to the other. Such behaviour is explained considering an intra-annulus interconversion of the tert-butyl groups. However, **TPU** shows, on the NMR time scale, a strong preference for the *cone* conformation, probably thanks to the presence of the phenylureido groups. On the other hand, the preparation of calix[6]arene *hosts* in the *1,2,3-alternate* conformation, and decorated with H-bond-donor groups like phenylureas, might promote the formation of pseudorotaxanes and rotaxanes endowed with new properties. On these premises, in this chapter, the synthesis and characterisation of the novel hexa-O-alkylated heteroditopic calix[6]arene receptors **DPU** and **DSU** are presented. **DPU** is characterised by four methyloxy and two octyloxy groups in 2,3,5,6 and 1,4 positions respectively. The receptor is functionalised with two diametric N-phenylureido moieties in para position to the octyloxy groups (see scheme 5.1). **DSU** differs from **DPU** for the presence of two phenylthioureido groups, instead of phenylureido.

5.2 Results and Discussion

5.2.1 Synthesis of the Hosts

This work aims to study the properties of these new receptors and to establish their complexation ability toward viologen salts as well as their ability to form interwoven structures such as pseudorotaxanes and rotaxanes. **DPU** and **DSU** were synthesised starting from the known tetramethoxy-dinitro calix[6]arene derivative **30** (see scheme 5.1).[9] This compound was obtained in good yield from the tetramethoxy calix[6]arene derivative **4MeO**, which is obtained, in high amounts, as the main by-product during the synthesis of the **3MeO** derivative. This latter is the precursor for the synthesis of the tris(N-phenylureido)calix[6]arene *hosts* used so far. The reaction of

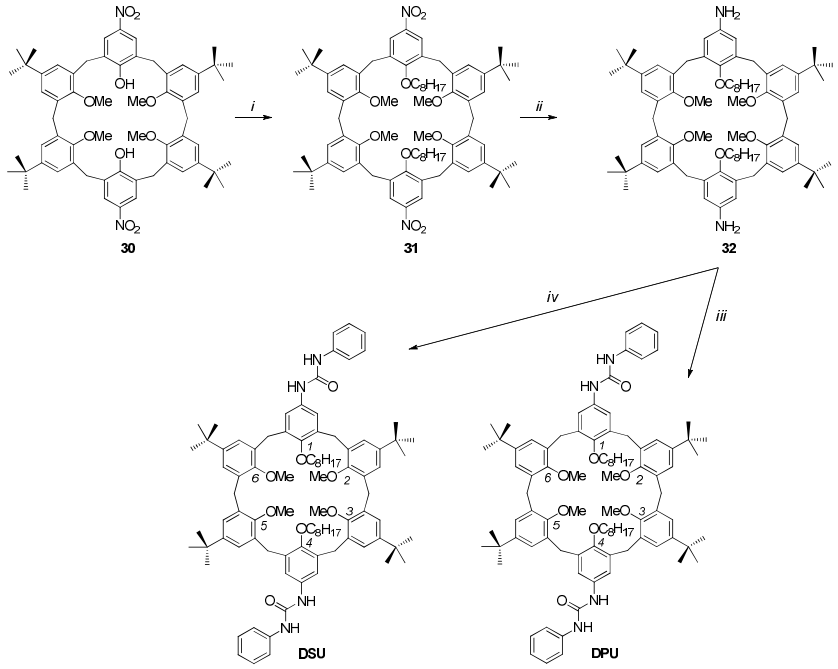

Scheme 5.1: Reagents and conditions: i) 1-Iodooctane, K_2CO_3, CH_3CN, reflux, 4 d, 70 %; ii) $NH_2NH_2{\cdot}H_2O$, Pd/C, EtOH, reflux, 24 h and iii) phenyl isocyanate, CH_2CH_2, RT, 2 h, 80 % (two steps) iv) phenyl isocyanate, CH_2CH_2, RT, 2 h, 69% (two steps).

30 with 1-iodooctane in dry acetonitrile at reflux for seven days, using K_2CO_3 as the base, led to the nitro derivative **31**, isolated by precipitation from ethyl acetate in 70% yield. The product **31** was fully characterised through NMR spectroscopy, ESI-MS, and X-RAY diffraction.

Figure 5.2 shows the 2D HSQC spectrum of **31**, taken in $CDCl_3$. In the aromatic region are present three broad signals at 7.6, 7.2 and 7.0 ppm in 1:1:1 integration ratio. The mid-field region of the spectrum shows: i) two broad doublets integrating for 4 protons each at 3.6 and 4.3 ppm ii) two overlapped broad signals whose total integral is 8 protons at *ca.* 3.9 ppm iii) a singlet integrating for 12 protons at *ca.* 3.0 ppm. Routinely 2D COSY and HSQC NMR experiments allowed to assign the two broad doublets to the AX system of coupled geminal protons of four bridging methylene groups of the macrocycle. In addition, it has been seen that the

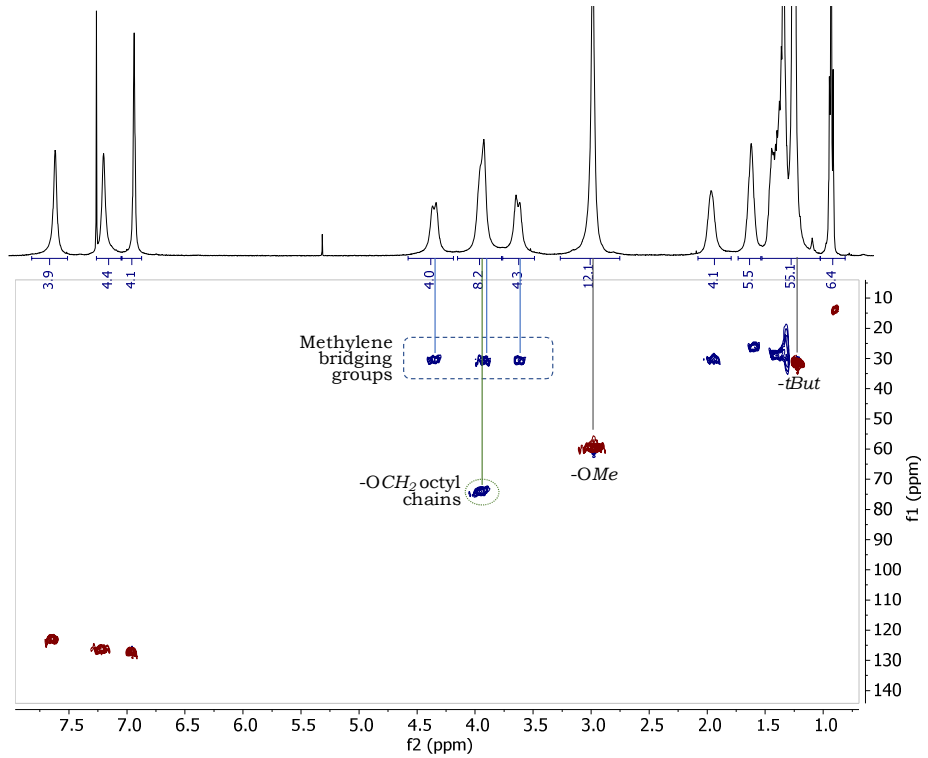

Figure 5.2: 2D edited HSQC spectrum ($CDCl_3$, 298 K, 400 MHz) of **31** (cross-peaks with red contours indicate CH couplings relative to tertiary and primary carbons, while those with blue contours the CH coupling of secondary carbons).

two overlapped signals belong: i) to the two remaining bridging methylenes, which are in this case magnetically equivalent, and ii) to the two methylene groups of the two octyl chains linked to the phenolic oxygen. The singlet at 3 ppm was assigned to the four methoxy groups, that is upfield-shifted of ~ 1 ppm with respect to its typical values. This shift at higher fields is also seen with **TPU**[10] and other trimethoxy calix[6]arene derivatives,[8] and it usually derives from the anisotropic shielding effect that the aromatic cavity of the macrocycle exerts on vicinal methoxy groups. The general broadness of the spectrum signals confirms a residual fluxionality of the macrocycle **31** on the NMR timescale. However, the overall pattern of signals is con-

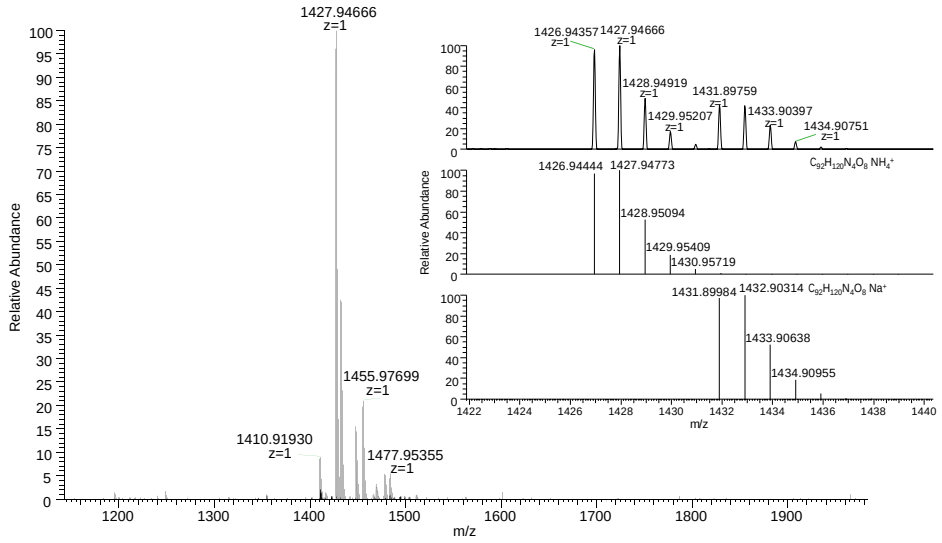

Figure 5.3: HR-MS spectrum of **DPU**, in the inset, the experimental isotopic distribution is compared with the calculated one.

sistent with a *1,2,3-alternate* conformation of the calix[6]arene macrocycle. The nitro groups of **31** were then reduced with hydrazine using Pd/C as catalyst. The reaction carried out in refluxing ethanol led to the diamino derivative **32**. Pd catalyst was removed by Schlenk filtration, while several washings with water allowed to eliminate the residual hydrazine. The reaction of **32** with phenylisocyanate and phenylthioisocyanate afforded the target calix[6]arenes **DPU** and **DSU** in 80% and 69% of overall yield, respectively.

Host **DPU** was characterised through high-resolution mass spectrometry and 1D and 2D NMR measurements. The HR-MS spectrum of **DPU** is reported in figure 5.3. It shows three principal singly charged peaks at 1410.91930, 1427.94666 and 1432.90314 D due, respectively, to the adducts of **DPU** with H^+, NH_4^+, and Na^+. Its 2D HSQC spectrum in $CDCl_3$ is reported in figure 5.4. The broad resonances observed in the ^{1}H NMR spectrum witness that on the NMR timescale also **DPU** has a certain fluxionality in solution.

The HSQC spectrum shows the presence of two different sets of signals.

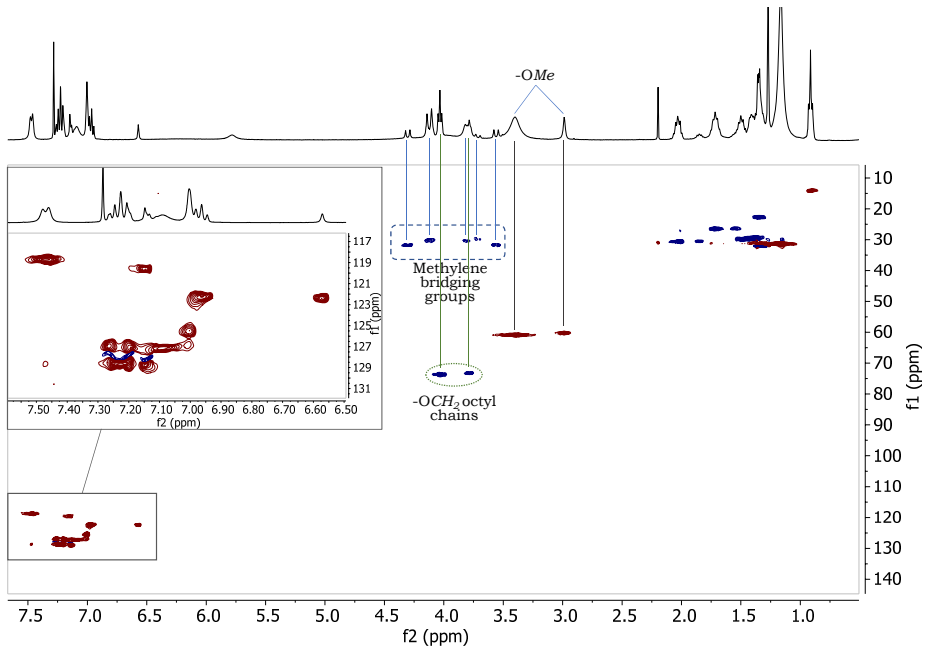

Figure 5.4: 2D edited HSQC spectrum ($CDCl_3$, 298 K, 400 MHz) of **DPU** (cross-peaks with red contours indicate CH couplings relative to tertiary and primary carbons, while those with blue contours correspond to the CH coupling of secondary carbons).

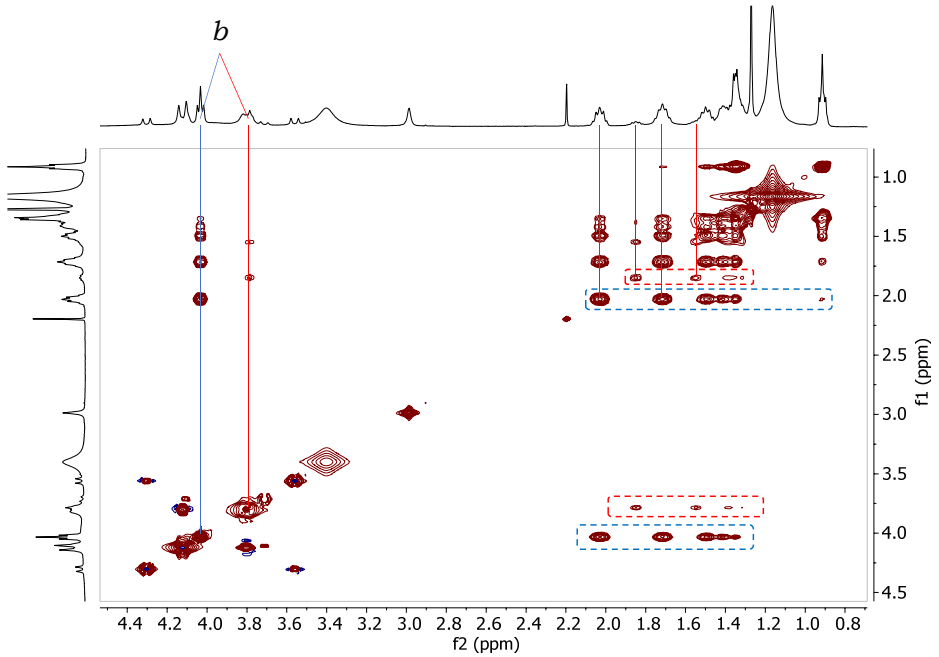

Figure 5.5: 2D TOCSY spectrum ($CDCl_3$, 298 K, 400 MHz) of **DPU**, expanded region 0.5 - 4.5 ppm. The blue dashed rectangle and lines indicate the correlations relative to the octyl chains of the major conformer, while the red ones the correlations relative to the less abundant conformer.

Through the projection of the two cross-peaks at F_1 ∼60 ppm, it is indeed possible to identify two signals for the -OMe groups *a*: a broad resonance at 3.4 ppm and a sharper singlet at 2.9 ppm (see figure 5-6 for compounds labelling). Two cross-peaks at F_1 ∼73 ppm also allow the identification of the methylene groups *b* of the octyl chains: an intense and a smaller triplet at 4.04 and 3.8 ppm respectively. In the corresponding ^{13}C-APT spectrum, the carbon nuclei of these two groups yield two signals each at 60.2 and *ca.* 61 ppm for *a* and at 73.7 and 73.3 ppm for *b*. The analysis of the upfield region of the 2D TOCSY spectrum (see figure 5.5) shows the presence of two series of multiple correlations, each starting from one of the two signals for the methylene *b* indicating the presence of two octyl chains experiencing different magnetic environmnent.

These findings, along with the splitting of several other resonances, sug-

gest the presence of two different conformers in solution in a 4:1 integration ratio. Through a perusal of the signals generated by the calix[6]arene bridging methylene groups, it has been possible to determine the two different geometries adopted by the macrocycle. It is known from the literature that, in low polarity solvents 1,3,5-trimethoxy-2,4,6-trialkoxy-para-tert-butylcalix[6]arenes may assume the *1,2,3-alternate* conformation, other than the more typical flattened *cone* one (see the introduction to this chapter). In addition, it has been just demonstrated that derivative **31** adopts in solution the *1,2,3-alternate* conformation. Based on these premises, it is reasonable to assume that also **DPU** might adopt at least these two conformations (see figure 5.1). The protons of the six bridging methylene groups of **DPU** would experience a different magnetic environment in response to the conformation adopted on NMR time scale. The *cone* conformation **C** would give rise to four doublets with geminal coupling, two for the axial and two for the equatorial protons in 2:1:1:2 ratio (see figure 5.6) because of the macrocycle symmetry. Based on the functionalisation of the aromatic nuclei, the existence of two different *1,2,3-alternate* conformations, **A-1** and **A-2** in figure 5.6, can be hypothesised. These two conformers differ for the position of the ring bearing the phenylureido groups with respect to the inversion points of the macrocycle and have different symmetry. The methylene bridging groups would thus yield two very different patterns of signals: conformer **A-1** would give a spectrum characterised by three signals in a 1:1:1 integration ratio: two doublets (equatorial and axial) and a singlet for the bridgings methylene of the inversion. A-2 would yield a more complicated pattern of two doublets (two types of axial protons), a singlet and two doublets (equatorial protons) in a 1:1:2:1:1 integration ratio (see figure 5.6).

Through a perusal of the 2D COSY and HSQC NMR spectra it has been possible to identify the bridging methylene groups of the minor conformer in two pairs of doublets at 4.31 and 4.1 ppm (axial) and 3.56 and 3.71 (equatorial), indicated by black circles in figure 5.7. This distribution of signals is in agreement with the *cone* conformation (**C**). On the contrary, the remaining pair of doublets resonating at 4.1 and 3.8 ppm with ^2J = 15 Hz belong to the axial and equatorial methylene protons of the major conformer (see white circles in figure 5.7). This pattern did not match any of the proposed conformations (see figure 5.6).

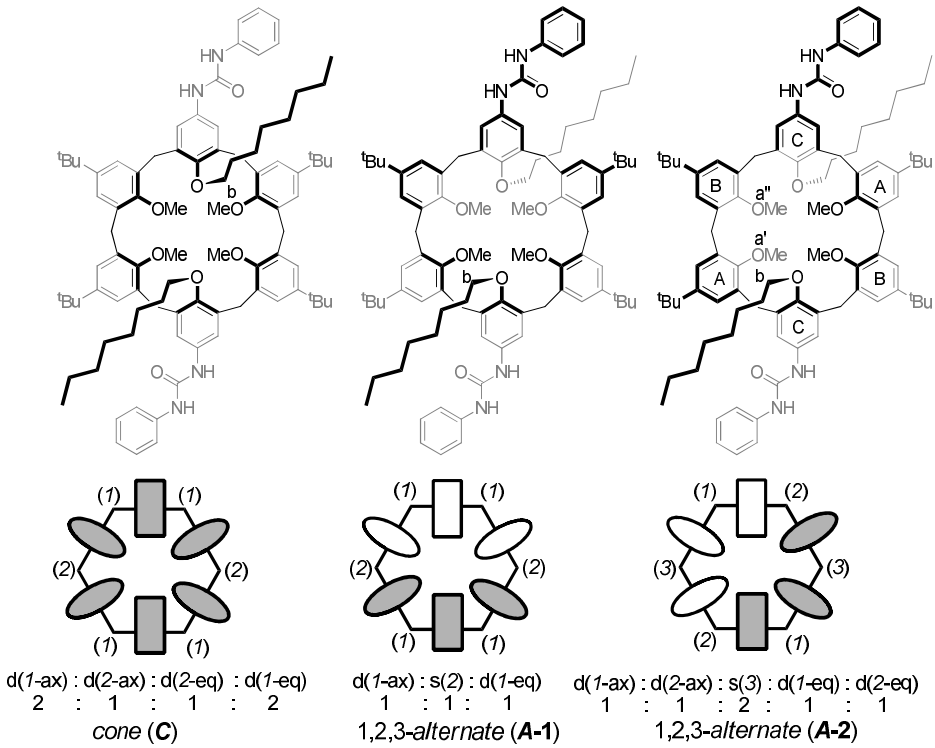

Figure 5.6: Schematic representation of the three possible conformations for **DPU**. The grey ovals/rectangles are upward with respect to the plane defined by the bridging methylene, while the white ones are downward. The rectangle identifies the phenolic ring bearing the octyloxy chains, while the ovals the rings functionalised with the methoxy groups. The pattern of the NMR signals of the bridging methylene groups with the relative integration ratio and the multiplicity (doublet or singlet) is reported below the schematic representation of each conformer. For diastereotopic protons, the axial (ax) or equatorial (eq) geometrical arrangement and multiplicity is indicated [*e.g.*: d(1-ax)].

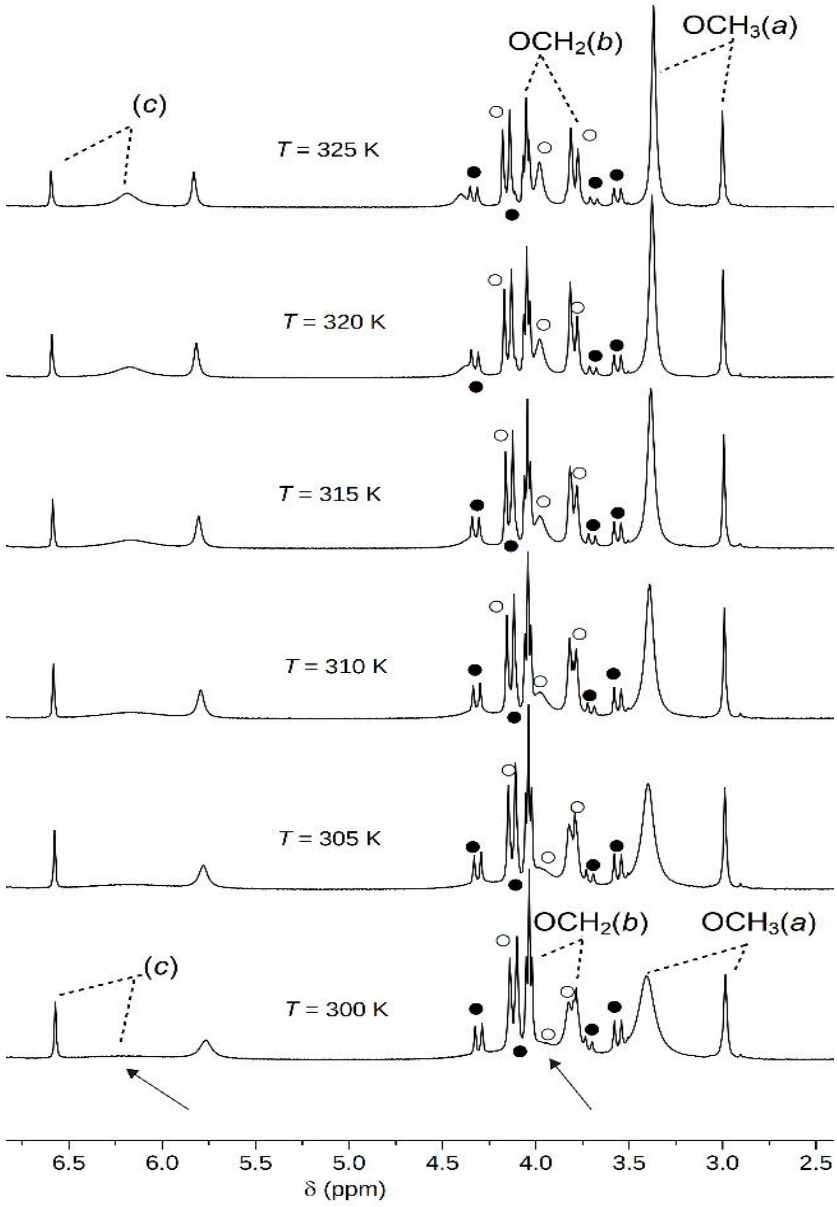

Figure 5.7: Stack plot of the variable temperature NMR experiment (T = 300→325 K, expanded region) carried out on **DPU** (400 MHz, **CDCl3**). The resonances of the bridging methylene protons belonging to conformers **C** and **A-1** (see figure 5.6) are labelled with black and white circles, respectively. Resonances marked as **a**, **b** and **c** have been indicated on the molecular sketches of figure 5.6

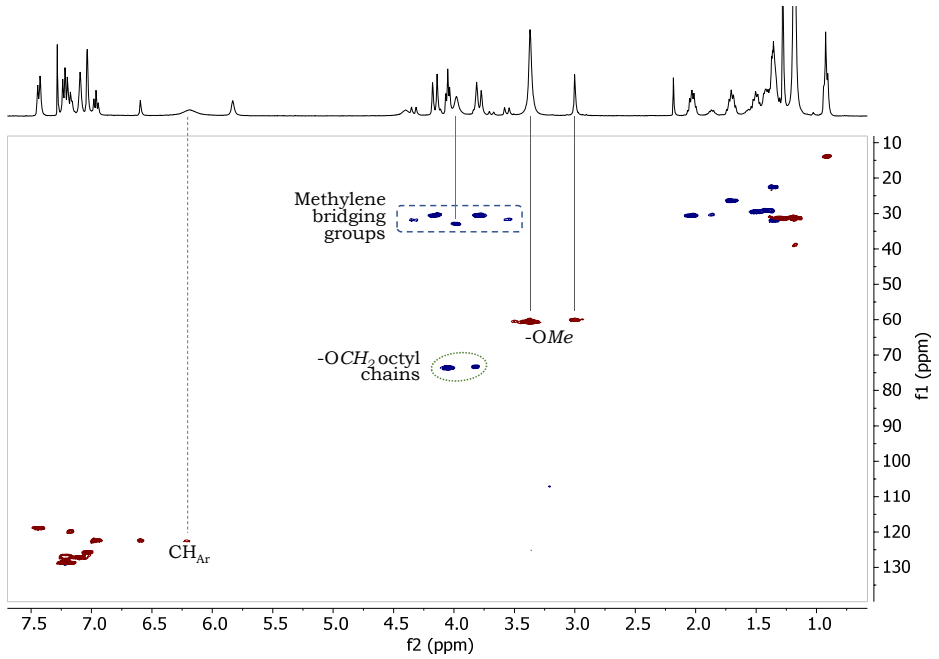

Figure 5.8: 2D edited HSQC spectrum ($CDCl_3$, 325 K, 400 MHz) of **DPU** (cross-peaks with red contours indicate CH couplings relative to tertiary and primary carbons, while those with blue contours correspond to the CH coupling of secondary carbons).

To better understand the distribution of **DPU** conformers in solution, variable temperature experiments were carried out (see figure 5.7). The relative abundance of the two conformers was not affected by the temperature rise, as can be seen from the intensity of the methoxy resonances in figure 5.7 that remains constant during the experiment. However, the conformation mobility of the more abundant conformer was significantly increased as can be see, for example, from the sharpening of the methoxy resonance at 3.4 ppm. Two other very broad resonances at *ca.* 6 and 4 ppm, barely recognisable at room temperature (see arrows in figure 5.7), gradually become sharper as the temperature increases. Through an analysis of the HSQC experiment carried out at T = 325 K (see figure 5.8) it was finally possible to assign the resonance at *ca.* 6 ppm to the aromatic protons, and the one at *ca.* 4 ppm to the bridging methylene group (2)

corresponding to the inversion points of the macrocycle (figure 5.6). Thus, the global pattern of signals for the bridging methylene groups of the more abundant conformer is doublet/singlet/doublet in a 1/1/1 integration ratio. This pattern is in agreement with the *1,2,3-alternate* conformation **A-1**.

To deepen the study on the conformation mobility of **DPU**, the effect of the temperature lowering has also been checked. The spectra collected lowering the temperature until T = 223 K are reported in the stack plot of figure 5.9. It is interesting to note that at T = 260 K signals coalescence was observed.[8–11] At T = 223 K, the signals are narrow enough to acquire an HSQC experiment (see figure 5.10). The identified pattern for the bridging methylene protons is two doublets (axial protons), one broad singlet (4.03 ppm), and two doublets (equatorial protons).

Independently by the overlapping between the central singlet and the signals of the octyl chains $-OCH_2$, the integration ratio between the resonances for the methylene bridges seems in agreement with an **A-2** conformation (see figure 5.6). In this conformation, the phenylureido groups are adjacent to the methylene bridges correspondent to the inversions; this makes this geometry less symmetric with respect to **A-1**. In the spectrum at T = 223 K, two signals in 1:1 ratio are visible for the methoxy groups *a'* and *a"* resonating at 3.83 and 3.45 ppm, respectively. Hence, the latter signal is $\sim$ 0.4 ppm up-field shifted. These findings suggest that one of the two methoxy groups experiences a higher shielding effect.

The observation that one of the aromatic signals resonates at 4.8 ppm was even more straightforward, which is unexpectedly largely up-field shifted ($\sim$ 2.5 ppm). To confirm such assignment, 2D NOESY and ROESY experiments have been carried out at T = 223 K. Among the multitude of NOE cross-peaks found in both spectra (see *e.g* the ROESY spectrum in figure 5.11), those correlating the signal of the methoxy protons *a"* with i) the tert-butyl signals at 0.9 and 1.35 ppm, ii) the aromatic signals at 4.8 and 7.0 ppm, and iii) the NH signal at 5.4 ppm (see figure 5.11 for a schematic representation of the NOE correlations) are all in agreement with a calix[6]arene macrocycle adopting the *1,2,3-alternate* conformation *A-2*. In fact, only in the geometrical arrangement described by this conformation, the methoxy protons of ring **A** can be simultaneously close to the tert-butyl group of the opposite ring **B** and to the NH protons of the vicinal ring **C**, which are both flipped with respect to **A** (see figure 5.6 for

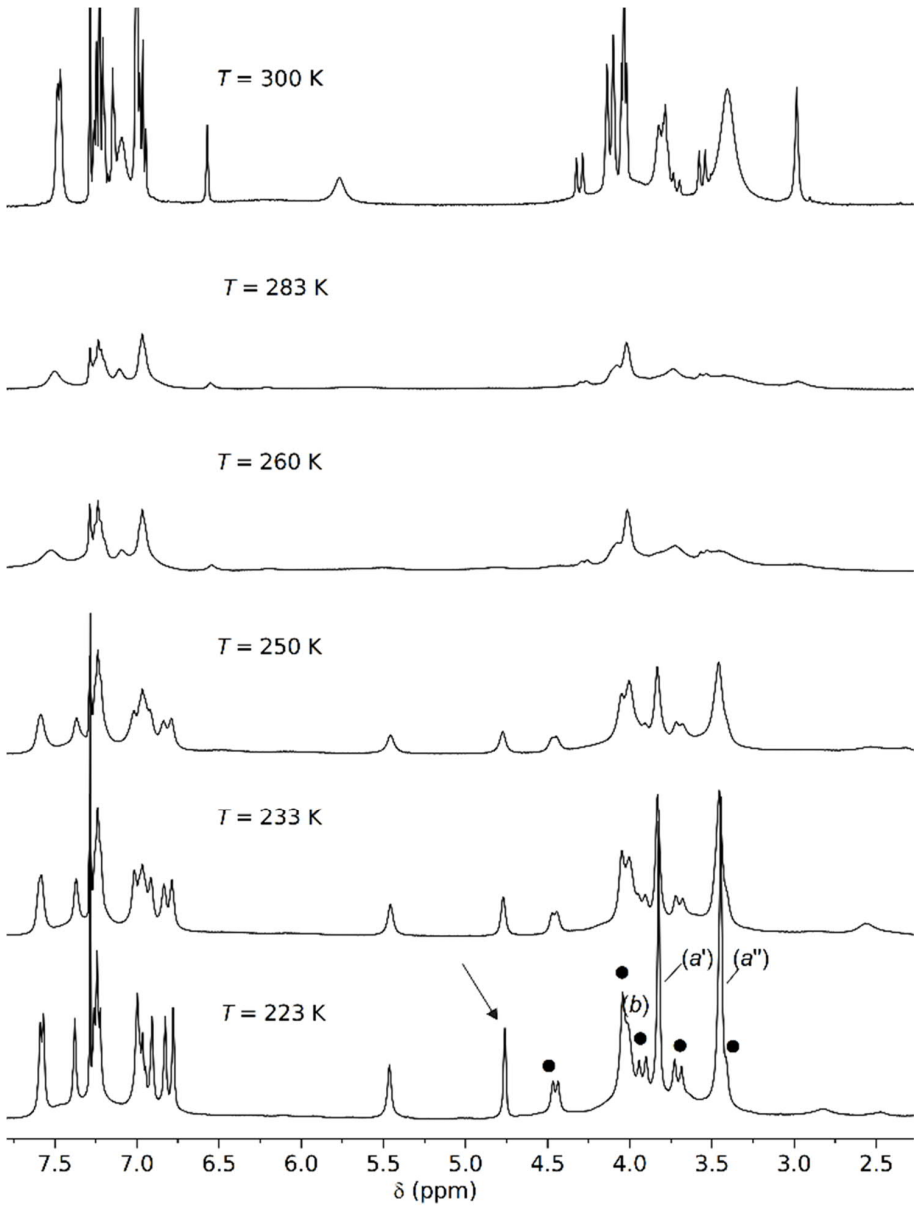

Figure 5.9: Stack plot of the variable temperature NMR experiment (T = 300→223 K, expanded region) carried out on **DPU** (400 MHz, $CDCl_3$). The resonances of the bridging methylene protons belonging to conformers **A-2** (see figure 5.6) are labelled with black circles, respectively. Resonances marked as *a* and *b* are indicated on the molecular sketches of figure 5.6. The arrow highlights one of the macrocycle aromatic protons resonating at unexpectedly high fields.

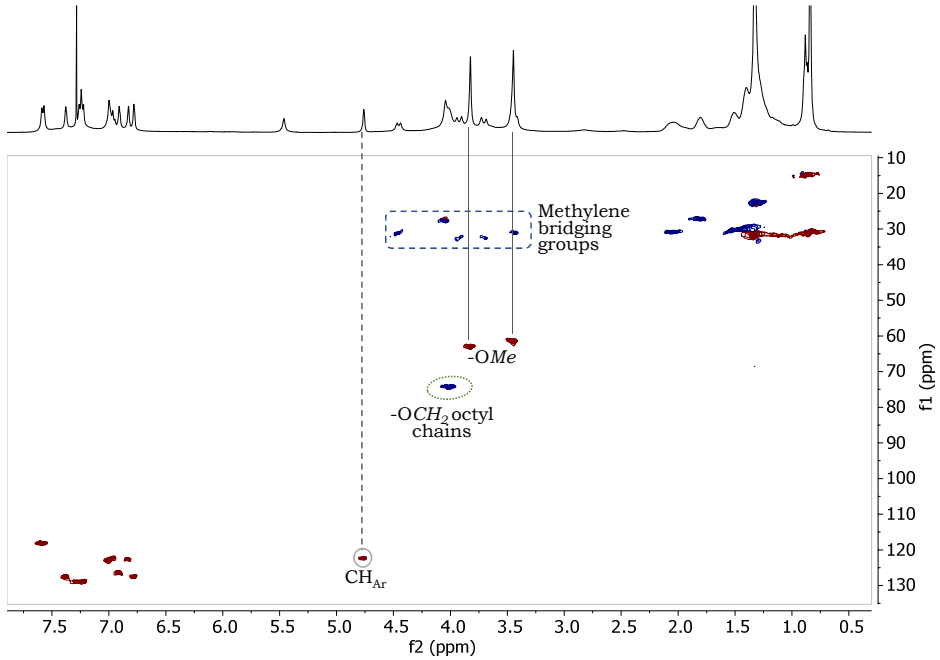

Figure 5.10: 2D edited HSQC spectrum ($CDCl_3$, 223 K, 400 MHz) of **DPU** (cross-peaks with red contours indicate CH couplings relative to tertiary and primary carbons, while those with blue contours correspond to the CH coupling of secondary carbons).

the rings' labels).

Finally, to verify the presence of aggregation phenomena promoted by the H-bond donor and acceptor nature of the phenylureas present in **DPU** has been verified through a simple NMR experiment. To a sample of **DPU** in $CDCl_3$, kept at room temperature, increasing amounts of deuterated methanol were added. The competition of the methanol for the H-bonding led to a progressive simplification of the NMR spectrum (see figure 5.12) with an upfield shift of the resonances of the methoxy (a) and methylene (b) groups of the major conformer (**A-1**). Although less marked, a similar upfield shift was also found for the corresponding resonances of the minor conformer. It thus seems that upon methanol addition, the protons of groups (a) and (b) experience a more shielding effect exerted by the aromatic units of **DPU**. On the other hand, the very broad and barely recog-

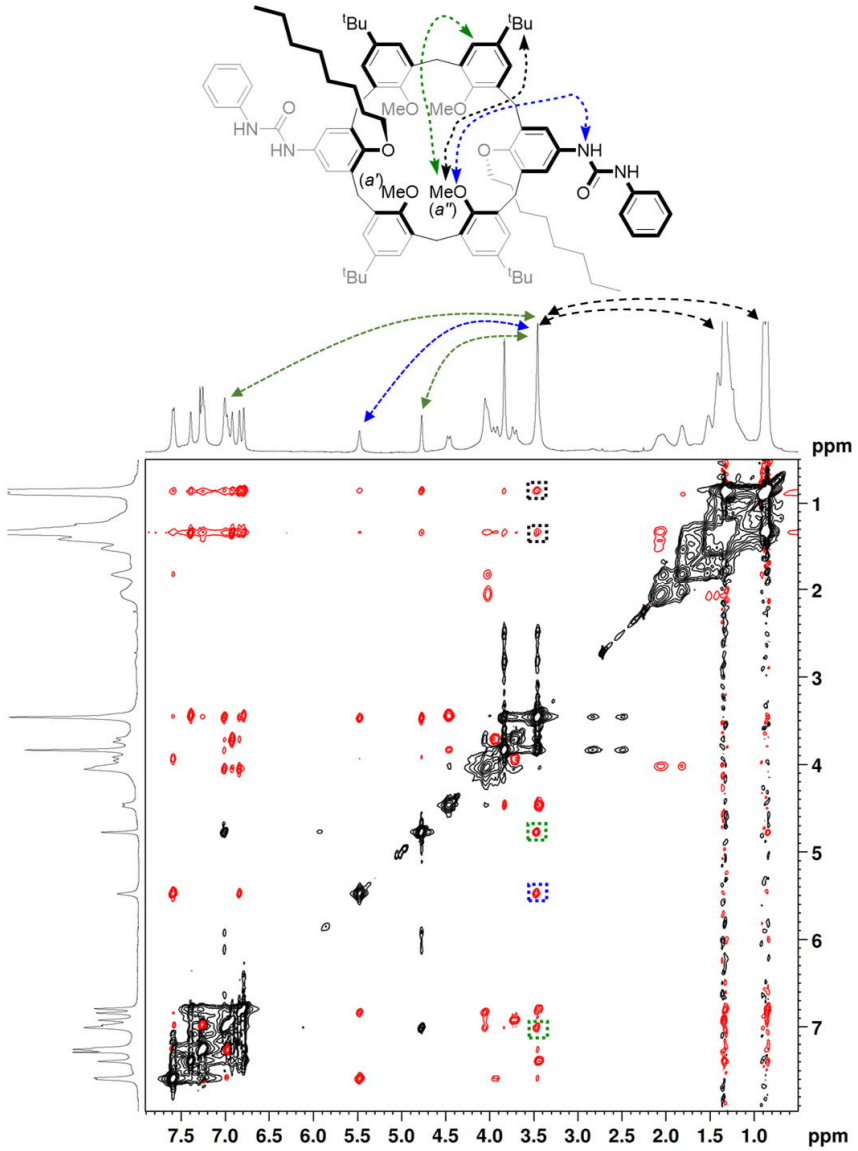

Figure 5.11: Expanded region of 2D ROESY spectrum of **DPU** (223 K, $CDCl_3$, 400 MHz, SL = 200 ms). Red cross-peaks (negative) evidence the spatial correlations, the black ones (positive) indicate that the aromatic nuclei bearing the methoxy groups exchange on the NMR time-scale. The dashed squares and double-headed arrows indicate the cross-peaks arising from the short contacts depicted in the sketch above the spectrum of conformer **A-2**.

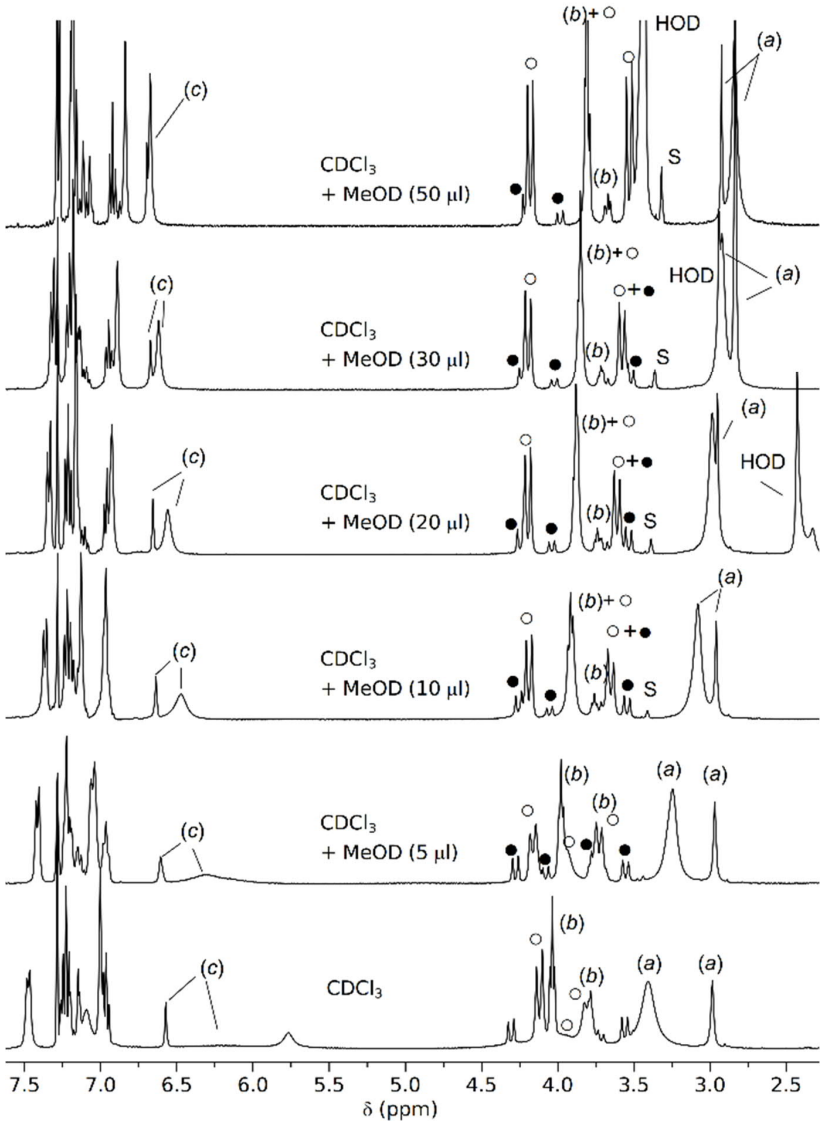

Figure 5.12: ^{1}H NMR stack plot (400 MHz, expanded region 2.3 - 7.6 ppm) recorded upon addition of increasing amount of CD_3OD to a solution of **DPU** in $CDCl_3$ at T = 300 K. The resonances more significantly affected by methanol addition are labeled as (a) for -OMe groups, (b) octyl chains $-OCH_2$ and (c) CH_{Ar}. The white circles indicate the methylene bridging groups for the **A-1** conformer, the black circles for the **C** conformer.

nisable aromatic resonance at *ca.* 6.4 ppm becomes sharper as methanol concentration increases and almost merges with the sharp resonance at 6.7 ppm which was previously ascribed to the minor conformer. The methanol addition also affects the abundance of the two conformers with a shift in favor of the major conformer **A-1** (from 4:1 to 5:1). This result can be tentatively explained supposing the flattened *cone* conformation is stabilised by an intramolecular H-bonding between the two phenylurea moieties on the macrocycle. Several 2D NMR experiments were successively accomplished on the sample with the highest amount of deuterated methanol added (50 μL, $CDCl_3/CD_3OD\sim$ 10/1). In particular, 2D COSY and HSQC experiments allowed us to unequivocally identify the three different signals relative to the bridging methylene protons – two doublets at 4.2 and 3.5 ppm and a broad singlet at 3.8 ppm - which are in full agreement with the structure of the *1,2,3-alternate* conformer (**A-1**) illustrated in figure 5.6. The *host* **DSU** was characterised through ESI-MS and 1D and 2DNMR experiments. The 2D HSQC spectrum of **DSU**, reported in figure 5.13, shows two different sets of signals in a $\sim$ 4:1 ratio.

Using a routinely COSY experiment (see figure 5.14b) and considering the relative integrals, it is possible to ascribe the two doublets at 4.34 and 3.57 ppm and the singlet at 3.76 ppm to the methylene bridging groups of the major conformer. On the contrary, the four small doublets at 4.25, 3.92, 3.81, 3.57 ppm (highlighted with black circles in the inset of figure 5.13) belong to to the minor conformer. Based on the data discussed above and on the found pattern of signals, **A-1** is the principal conformation present in chloroform solution while **C** is the less abundant. As previously seen for **DPU**, a 2D TOCSY allows to identify two different sets of signals for the octyl chains of the two conformers (see figure 5.14a).

5.2.2 Crystallographic studies

The crystal structure of compound **DPU** was determined via synchrotron X-ray diffraction data on single crystals obtained by slow evaporation of a $CHCl_3/CH_3OH$ solution. In the unit cell, three different molecules coexist, indicated in the discussion as I, II and III (see figure 5.15). For each calix[6]arene of general formula $C_{92}H_{120}N_4O_8$, 2/3 molecules of $CHCl_3$, 4/3 molecules of CH_3OH and 10/3 molecules of H_2O are present in the unit cell. For all the three macrocycles only half of the molecule is independent, while

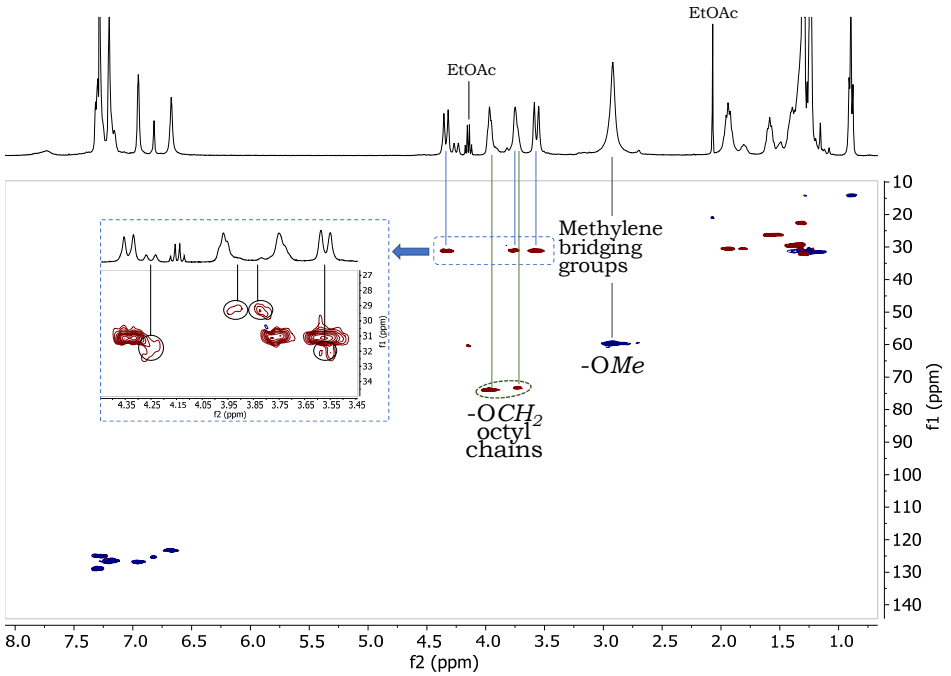

Figure 5.13: 2D edited HSQC spectrum ($CDCl_3$, 298 K, 400 MHz) of **DSU** (cross-peaks with blue contours indicate CH couplings relative to tertiary and primary carbons, while those with red contours the CH coupling of secondary carbons). In the inset, the expansion of the region of methylene bridging groups: the four signals in the black circles are relative to the less abundant conformer while the three principal peaks, also highlighted in the full spectrum, are relative to the major conformer.

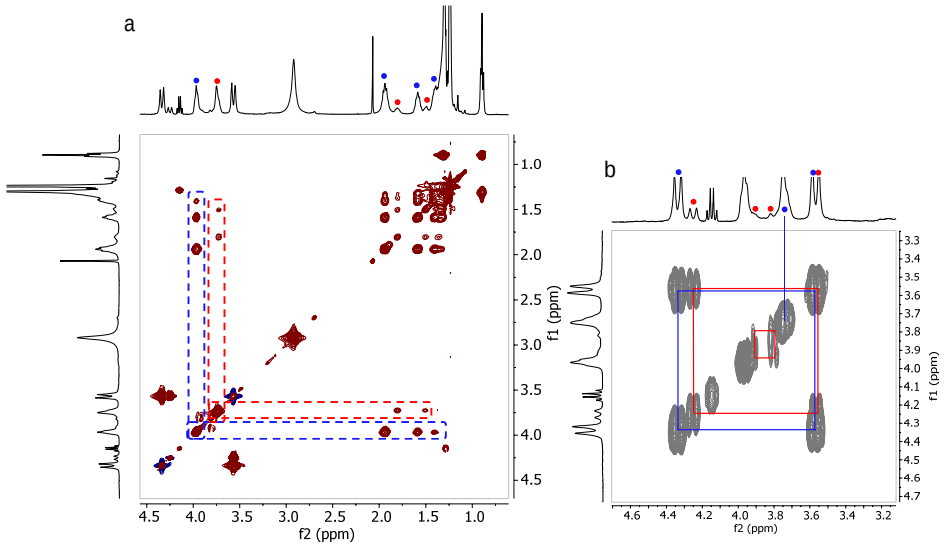

Figure 5.14: 2D NMR spectra ($CDCl_3$, 298 K, 400 MHz) of **DSU**: a) expanded region (0.2 - 4.6 ppm) of TOCSY spectrum: the blue dashed rectangles highlight the correlations of the octyl chains of the major conformer, the red dashed rectangles the correlations of the minor one; b) expanded region (3.1 – 4.7 ppm) of COSY spectrum: the blue lines and circles indicate the signals of methylene bridging groups of the major conformer, while in blue are indicated the signals of the minor one.

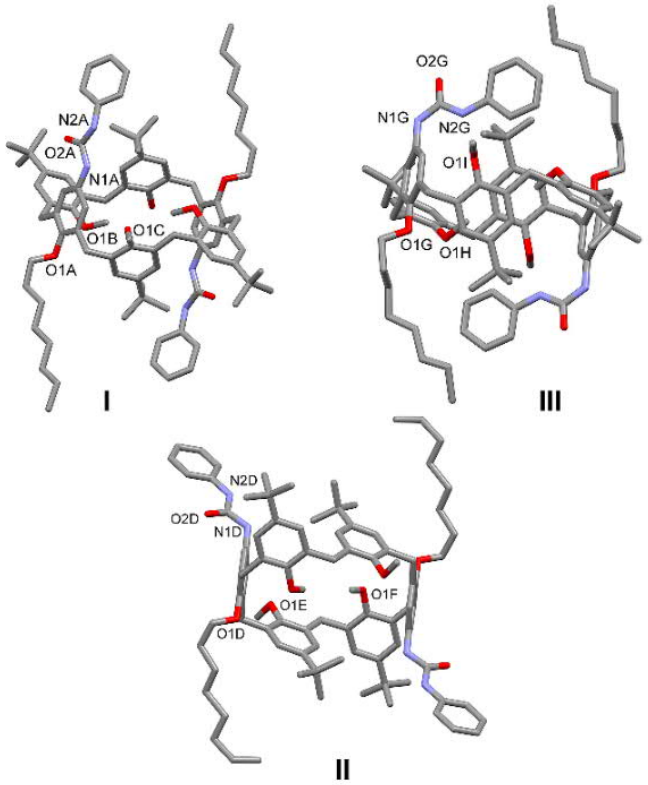

Figure 5.15: Molecular structure of I-III with partial labelling scheme for the atoms in the asymmetric unit. Hydrogen atoms and solvent molecules are omitted for clarity.

the other half is generated by symmetry [symmetry codes: (i) 1-x, 1-y, 2-z; (ii) = 1-x, 1-y, 1-z and (iii) = -x, y, 1-z for **I**, **II** and **III**, respectively]. The three independent aromatic rings forming the walls are labeled A, B, C (**I**), D, E, F (**II**) and G, H, I (**III**); the conformation of the cavity is always *1,2,3-alternate*.

The molecular structures **I-III** assume a geometry compatible with the *1,2,3-alternate* conformation indicated in the previous discussion as **A-2**. With respect to the mean plane passing through the six methylene bridges, the mean planes passing through the aromatic rings are inclined of 67.4(2), 36.8(3), 63.4(2), 74.3(4), 62.7(3), 40.7(3), 79.1(2), 44.2(2) and

68.8(3)°for A, B, C (**I**), D, E, F (**II**), G, H and I (**III**) (the values reported are always those smaller than 90°). In **III**, the phenylureido moiety is not parallel to the aromatic walls of the macrocycle like in **I** and **II**, but it is inclined towards the cavity as evidenced by the torsion angles C4-N1-C16-N2 [C4A-N1A-C16A-N2A = 176.6(3)°(**I**); C4D-N1D-C16D-N2D = -161.5(3)°(**II**); C4G-N1G-C16G-N2G = -9.2(4)°(**III**)]. These findings confirmed the results previously obtained in the variable temperature NMR experiment.

In each calixarene, two methoxy groups point inside the cavity, namely O1B-C8B (**I**), O1F-C8F (**II**), O1H-C8H (**III**) and their symmetry-related equivalents, forming $C-H\cdots\pi$ interactions with the aromatic walls which stabilise the **A-2** conformer [C8B-H8B3$\cdots$C5A, 3.576(2) Å and 132.2(3)°; C8B-H8B1$\cdots$C6C(1-x, 1-y, 2-z), 3.407(4) Å and 126.9(5)°; C8F-H8F1$\cdots$C2E, 3.451(3) Å and 128.0(5)°; C8F-H8F3$\cdots$C5D(1-x,1-y,1-z), 3.759(3) Å and 133.8(4)°; C8H-H8H3$\cdots$Cg1, 3.779(1) Å and 157.9(3)°; C8H-H8H2$\cdots$C2I(-x,-y,1-z), 3.526(5) Å and 143.8(3)°; C8H-H8H2$\cdots$C3I(-x,-y,1-z), 3.725(4) Å and 145.3(3)°. C6C, C2E, C5D C2I and C3I belongs to the rings C1A-C6A, C1C-C6C, C1E-C6E, C1D-C6D and C1I-C6I, respectively. Cg1 is the centroid of the benzene ring C1G-C6G]. In the lattice, the three molecules are connected through H bonds involving the ureido groups, with the N-H atoms behaving as donors and the oxygen atoms as acceptors [see figure 5.16; N1A-H1A$\cdots$O2D, 2.891(3) Å and 161.4(2)°; N2A-H2A$\cdots$O2D, 2.916(3) Å and 14.46(2)°; N1D-H1D$\cdots$O2G, 2.820(3) Å and 129.3(2)°; N2D-H2D$\cdots$O2G, 2.933(3) Å and 140.2(2)°]. The overall crystal packing results in a supramolecular sheet formed by the three independent molecules **I** (green), **II** (blue) and **III** (red). The sheet is parallel to the (1-10) plane and consists of alternating adjacent chains following the pattern ABAB, where the chain A is formed by H-bonded calixarenes **II** and **III**, while chains B comprise calixarenes **I**, H-bonded to water, methanol and chloroform molecules (not shown in the figure). In order to investigate the influence of the solvent on the crystal structure, calix[6]arene **DPU** was crystallised from ethyl acetate, yielding the monosolvate form **IV**, whose molecular structure can be seen in figure 5.17.

The asymmetric unit, crystallising in the monoclinic space group C2/c, comprises half of a molecule of the macrocycle and of ethyl acetate. With respect to the mean plane passing through the six methylene bridges, the

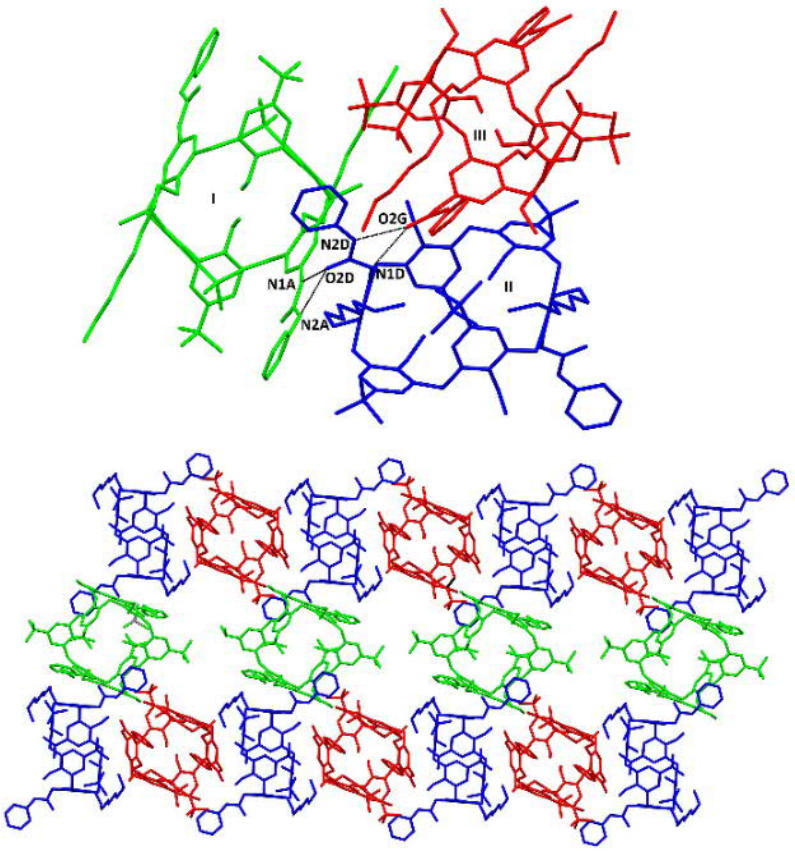

Figure 5.16: The set of H bonds, shown as black lines, involving the three independent molecules **I** (green), **II** (blue) and **III** (red) with partial labelling scheme (top). The view of the supramolecular sheet formed by **I**, **II** and **III** macrocycles (bottom). Hydrogen atoms and solvents molecules are omitted for clarity.

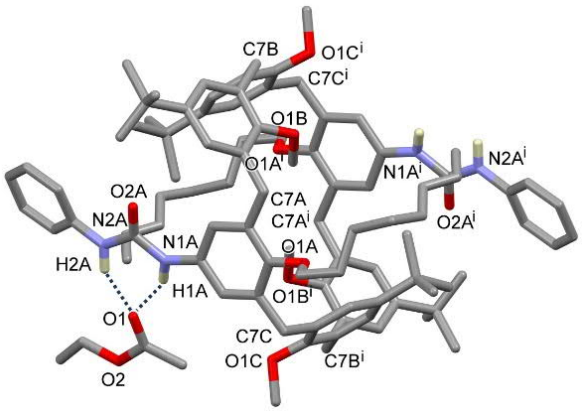

Figure 5.17: Molecular structure of **IV** with partial labelling scheme; symmetry code: (i) = 1-x, 1-y, 1-z. Only the H atoms involved in H bonding (blue dotted lines) are shown for clarity.

mean planes passing through the aromatic rings are inclined of 69.5(2), 45.3(3) and 68.8(3)°for rings A, B and C, respectively (in good agreement with the values found for **I**, **II** and **III**; the same labelling scheme has been used). The torsion angle C4A-N1A-C16A-N2A (which characterises the position of the phenylureido moiety with respect to the aromatic walls) is -177.8(3)°, similar to forms **I** and **II**. Also in this case, the methoxy group O1B-C8B and its symmetry-related equivalent point inside the cavity, forming C-H$\cdots$ interactions with the aromatic rings C1A-C6A and C1C-C6C [C8B-H8B1$\cdots$C6A, 3.510(2) Å and 145.0(4)°; C8B-H8B3$\cdots$C6C(1-x,1-y,1-z), 3.326(3) Å and 128.0(3)°], stabilising the A-2 conformer. The main supramolecular feature in **IV** is the presence of two strong H-bonds between the N-H groups of the phenylureido moiety and the oxygen atom O1 of the acetate solvent [N1A-H1A$\cdots$O1, 2.960(6) Å and 155.3(2)°; N2A-H2A$\cdots$O1, 2.904(5) Å and 153.5(5)°]. These strong interactions are also present in the crystal structure of the three independent calixarenes **I**, **II** and **III** but in that case, the H-bond acceptors are the oxygen atoms of the phenylureido unit of adjacent calixarenes, thus also influencing the packing of the compound. In IV, the overall crystal structure is mainly driven by van der Waals interactions, yielding layers parallel to the ab plane (see Figure 5 -18).

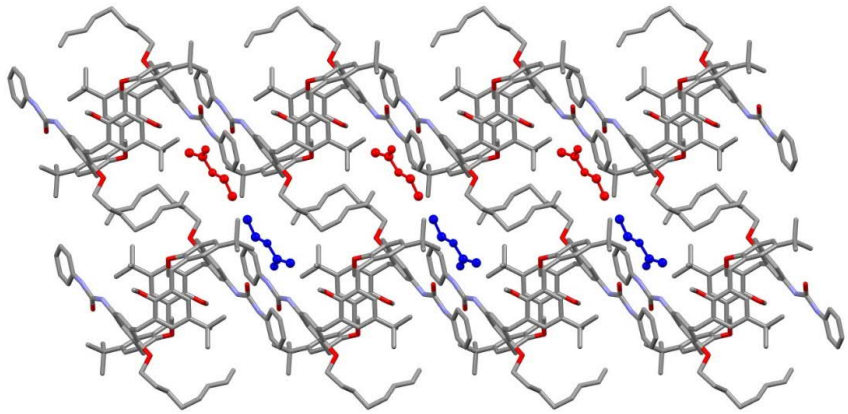

Figure 5.18: One of the layers forming the packing of compound **IV** viewed along the c-axis direction. H atoms have been omitted for clarity. Disordered acetate molecules are shown in red and blue. Since **IV** is a 1:1 solvate, with half acetate present in the asymmetric unit, only one of the two symmetry-related solvent molecules highlighted in red and blue can be present, but not at the same time

The crystal structure of compound **DSU** was determined *via* X-ray diffraction data on single crystals obtained by slow evaporation of a chloroform/methanol solution. The asymmetric unit consists of two independent half molecules and a crystallisation methanol molecule which could not be sensibly modeled and was hence removed with the program SQUEEZE (see the experimental part for the details). Figure 5.19 and figure 5.20 show the molecular structure of the two independent calix[6]arenes **I** and **II**, respectively; they both show a conformation of the type *1,2,3-alternate*, with the three independent aromatic rings forming the walls of the cavity labeled A, B, C (**I**) and D, E, F (**II**).

With respect to the mean plane passing through the six methylene bridges, the mean planes passing through the aromatic rings are inclined of 75.1(3), 64.3(4), 42.1(3), 79.6(4), 39.5(2) and 71.2(2)°for A, B, C (**I**) and D, E, F (**II**), respectively (the values reported are those smaller than 90°). In each calixarene, two symmetry-equivalent methoxy groups point inside the cavity, namely O1C-C8C (**I**) and O1E-C8E (**II**), which form C-H$\cdots\pi$ interactions with the aromatic walls [C8C-H8C3$\cdots$C6A, 3.355(2)Å and 127.5(3)°; C8E-H8E3$\cdots$C6D, 3.363(2) Å and 126.7(4)°.]

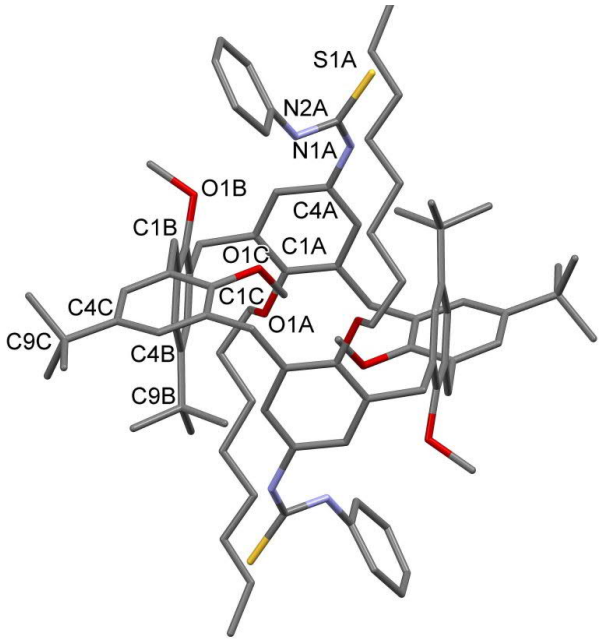

Figure 5.19: Molecular structure of **I** with partial labelling scheme for the atoms in the asymmetric unit. Hydrogen atoms and solvent molecules are omitted for clarity. The symmetry code to generate the whole molecule is 2-x, 1-y, 1-z.

The position of the phenylthioureido arm is different in **I** and **II**. In **I**, a weak hydrogen bond is formed between the N2A-H2N moiety and the methoxy oxygen atom O1B [N2A-H2N$\cdots$O1B, 3.157(1) Å and 125.9(1)°]. Besides, the phenyl group attached to N2A is inclined of 32.9(3)°with respect with the mean plane passing through the methylene bridges. In **II**, a weak interaction exists between the C19D-H19D group of the phenyl ring and the oxygen atom O1E of the methoxy group [C19D-H19D$\cdots$O1E, 3.300(1) Å and 135.4(1)°]. Differently from **I**, the phenyl ring is inclined of 67.1(4)°with respect to the mean plane passing through the methylene bridges. In the lattice, the two molecules **I** and **II** are connected through H bonds involving the thioureido groups, with the N-H atoms behaving as donors and the sulphur atoms as acceptors [N1A-H1N$\cdots$S1D, 3.497(2) Å and 170.6(1)°; N1D-H3N$\cdots$S1A, 3.231(1) Å and 145.5(1)°]. This motif

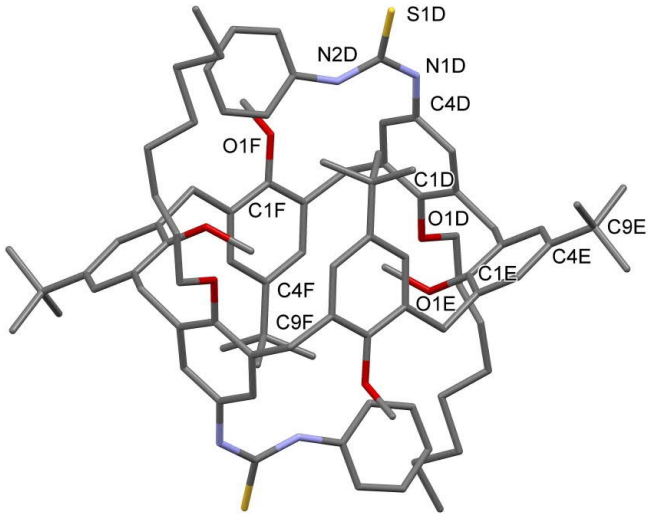

Figure 5.20: Molecular structure of **II** with partial labelling scheme for the atoms in the asymmetric unit. Hydrogen atoms and solvent molecules are omitted for clarity. The symmetry code to generate the whole molecule is 1-x, -y, 2-z.

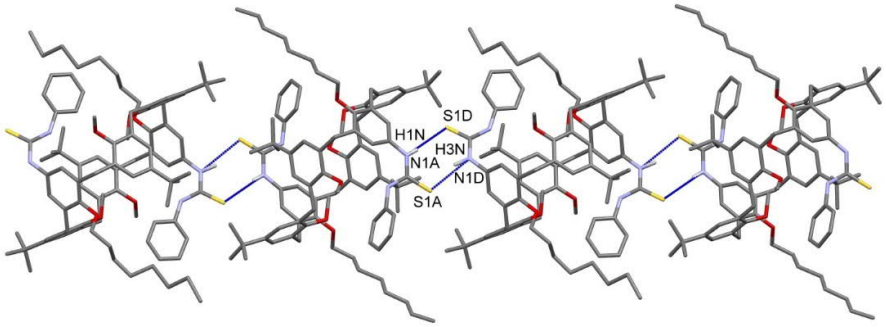

Figure 5.21: The set of H-bonds involving the two independent molecules **I** and **II** forming chains parallel to (101). Hydrogen atoms not involved in the interactions have been omitted for clarity. H bonds are shown as blue lines.

connects symmetry-related molecules **I** and **II** in a supramolecular chain parallel to the plane (101) (see figure 5.21). The overall packing in the three dimensions is dominated by dispersion interactions.

5.2.3 Synthesis and characterisation of the Intervowen Structures

In the second part of this study, the ability of **DPU** to act as a wheel in the formation of pseudorotaxane complexes with viologen salts was evaluated.

First of all, **DPU** was mixed with 1,1'-dioctyl-4,4'-bipyridinium ditosylate (**DOV**) in chloroform (see scheme 5.2). This led to the formation of a red-colored homogeneous solution, indicating that **DPU**, like **TPU**[8], is able to dissolve this unsoluble salt. The solution was analysed through NMR spectroscopy. The ^{1}H-NMR spectrum shows a highly complicated pattern of signals (see figure 5.22, middle), with respect to the spectra of the free components, see figure 5.22 top and bottom. With respect to the spectra of the free components (see figure 5.22 top and bottom), however, it is interesting to observe the presence of two new broad signals in the upfield

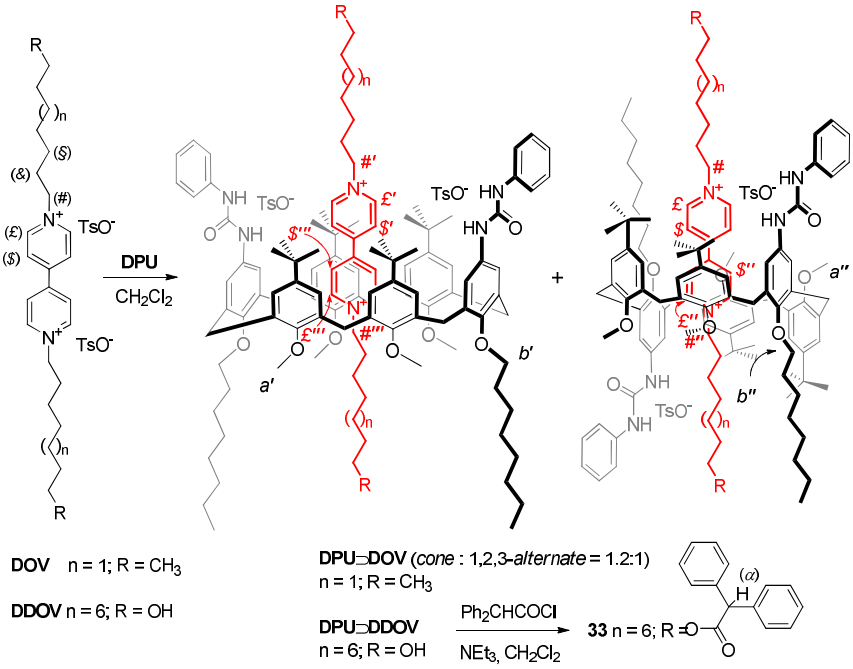

Scheme 5.2: Synthesis of the rotaxane **33**.

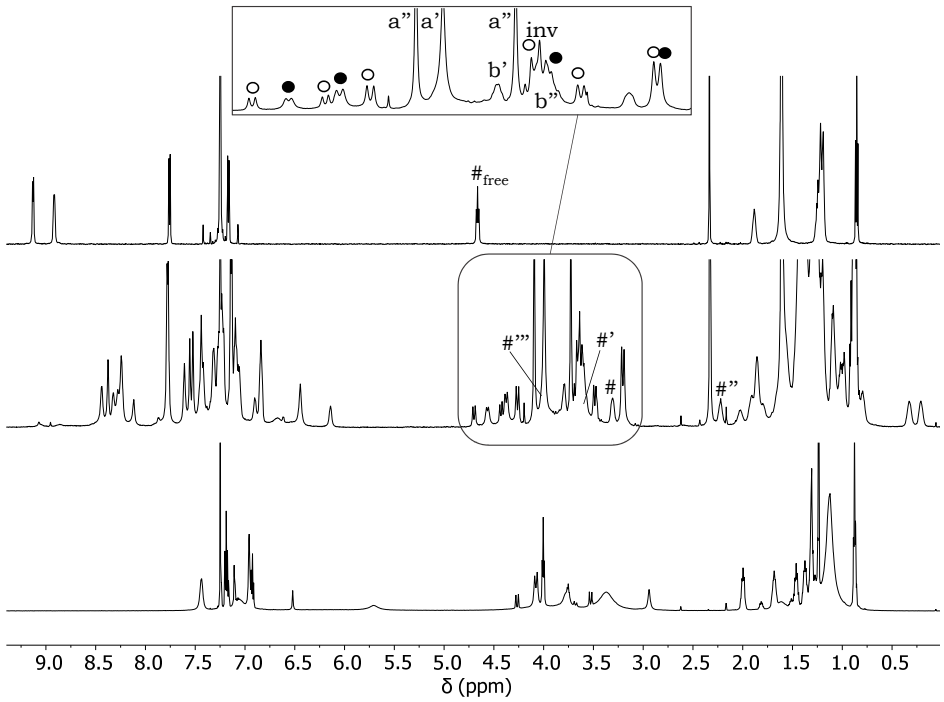

Figure 5.22: ^{1}H NMR stack plot (600 MHz, $CDCl_3$) of bottom) **DPU**, middle) pseudorotaxanes **DPU⊃DOV** and top) **DOV**. For the labels, see text and scheme 5.2.

region of the spectrum, at 0.3 and 0.4 ppm. Analysing the 2D COSY and HSQC spectra (see figure 5.23), these signals are assigned to some of the methylene groups of the **DOV** octyl chains (see scheme 5.2). As seen for **TPU**,[12–14] the appearance of these upfield shifted methylene resonances is indicative, along with the red color of the solution, of the formation of a pseudorotaxane complex. These signals are indeed due to methylene groups of the *guest* shielded by the pheylureido groups of the *host*.

In the pseudorotaxane complex formed with **TPU**, the **DOV** methylene groups, labelled as (#) in scheme 5.2, gives rise to two signals in response to the proximity to the two different rims of the *host*. Interestingly, in the complex with **DPU**, the methylene groups (#) originate four signals at 4.0, 3.6, 3.3 and 2.2 ppm. The integration is possible only for the signals at 2.2 and 3.3 ppm, resulting in a 1:1 ratio. All the four signals are upfield-shifted with

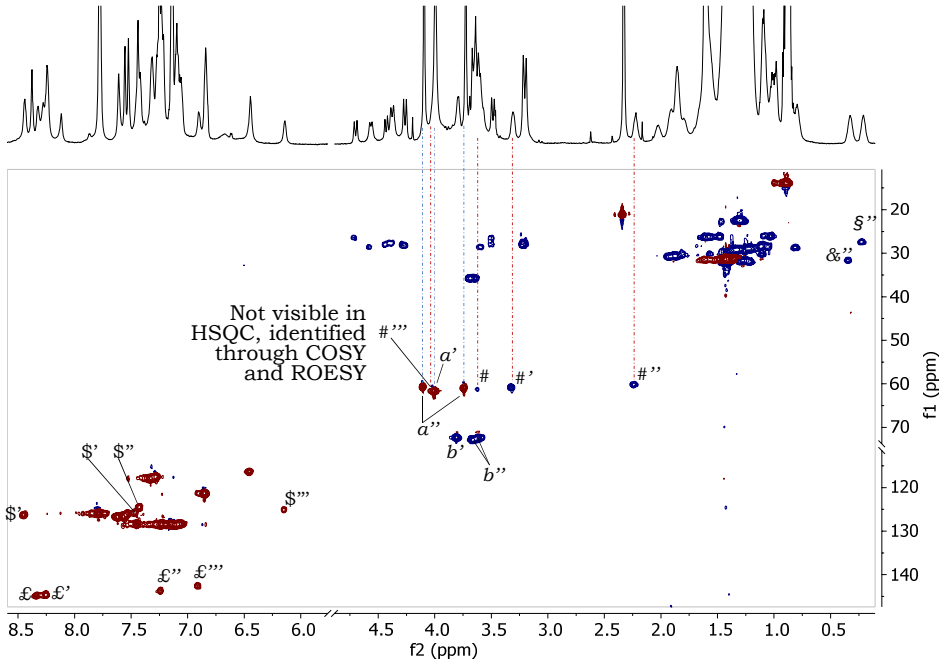

Figure 5.23: 2D Edited HSQC spectrum of **DPU⊃DOV** in $CDCl_3$ (600 MHz, T = 300 K), signals are labelled according to scheme 5.2.

respect to the chemical shift of the free **DOV** (4.6 ppm), and their number suggests the formation of more than one complex. Since **DPU** assumes both the *cone* and *1,2,3-alternate* conformation in chloroform solution, it is reasonable to hypothesise that both the conformations are able to form complexes with viologen salts leading to pseudorotaxanes with different geometrical features. This finding is confirmed also by the observation that in these conditions, the **DPU** wheel yields three resonances for the methoxy groups at 4.09 (*a"*), 3.99 (*a'*) and 3.73 (*a"*) ppm, and three for its OCH2 at 3.79 (*b'*), 3.66 (*b"*) and 3.61 (*b"*) ppm (the last two almost overlapped, see HSQC in figure 5.23).

The two signals with the same intensity at 3.31 and 2.24 ppm can be ascribed to the octyl chains of a *guest* threaded in an asymmetric magnetic environment. These findings are consistent with a pseudorotaxane complex in which the **DPU** *host* adopts a flattened *cone* conformation and a *1,2,3-*

alternate conformation in which the *guest* is displaced with respect to the mean plane of the *host* cavity. The 2D ROESY spectrum (not shown) presents weak correlations between the resonances of the methylene groups (#) at 3.31 ppm and those of the ortho aromatic protons (£) at 8.24 ppm of the pyridine rings. The resonance at 2.24 ppm (#") is spatially correlated with a resonance at 7.25 ppm (£"), partially hidden by the residual solvent signal, while the one at 3.63 ppm (#') is correlated with a small and broad aromatic signal at 8.33 ppm (£'). The resonance at 4.01 ppm (#"'), hidden by the signal of the methoxy group (a'), shows a spatial correlation with the signal at 6.90 ppm (£"'). The HSQC spectrum confirmed that these aromatic resonances correspond to the ortho protons of the pyridinium rings (see figure 5.23). Through a 2D COSY experiment, these signals were used to assign those of the other pyridinium protons (meta) ($) at 8.44 ppm, ($') at 7.46 ppm, ($") at 7.42 ppm and ($"') at 6.15 ppm. Differently from the isolated wheel, in this mixture of pseudorotaxanes, the ratio between the *1,2,3-alternate* and the *cone* conformation changes from 4:1 to 1.3:1. This shift in favor of the *cone* conformation can be explained considering that, in low polarity solvents, **DOV** is present as a tight ion pair that must be separated to allow the threading of the dication inside the aromatic cavity. This process will likely be more favoured for the *cone* conformer, since it has the urea moieties on the same side of the macrocycle.

To synthesise the rotaxane **33**, the 1,1'-bis(12-hydroxydodecyl)-4,4'-bipyridinium ditosylate (**DDOV**) was used as axle. Indeed, upon complexation, this thread is characterised by two terminal hydroxyl groups suitable for the rotaxanation reaction by the insertion of bulky diphenylacetyl groups. Following a procedure verified in previous studies,[6, 12, 14] an amount of solid **DDOV** was taken up with a solution of **DPU** in CH_2Cl_2 to promote the formation of pseudorotaxanes (**DPU⊃DDOV**). After 12 hours of mixing at room temperature, the undissolved salt was eliminated by filtration, and the resulting homogeneous solution treated with diphenylacetyl chloride to complete the stoppering reaction (see scheme 5.2). The chromatographic separation allowed to isolate rotaxanes 33 in 48% yield. HR-MS measurements confirmed the identity of the isolated product. The ^{1}H NMR spectrum in $CDCl_3$ of **33** (see figure 5.24) shares several common features with the spectrum of the pseudorotaxane **DPU⊃DOV**. In particular, the presence of two broad peaks (§' and &') in the upfield (0.1

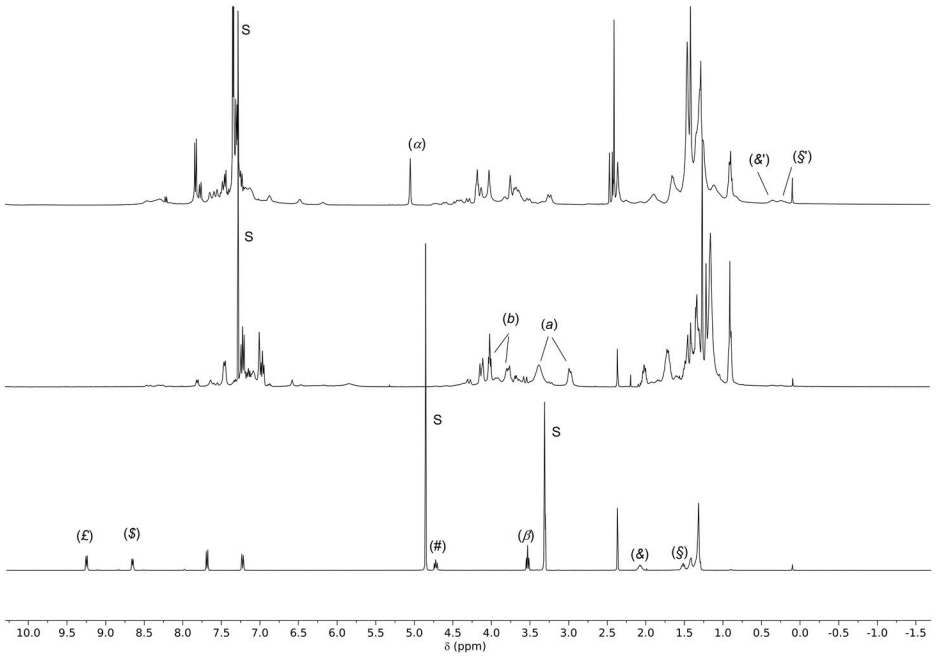

Figure 5.24: ^{1}H NMR stack plot (400 MHz) of a) rotaxane **33**, b) pseudorotaxanes **DPU⊃DOV** in $CDCl_3$ and c) **DDOV** in CD_3OD. For the labels see text and Scheme 5.2.

- 0.5 ppm) region of the spectrum is indicative of the formation of an interwoven structure, while the occurrence of a pattern of three signals for both the methoxy (a) and the octyloxy OCH2 methylene (b) groups is consistent with the presence in solution of approx. an equimolar mixture of two rotaxanes. As seen before for the pseudorotaxanes with **DOV**, what distinguishes also rotaxanes **33** is the *cone* and *1,2,3-alternate* conformation assumed in the solution by the calix[6]arene wheel surrounding the viologen thread. This hypothesis was verified by the analysis of a series of 1D and 2D NMR spectra. The effectiveness of the rotaxation reaction was verified by the presence in the spectrum of several signals belonging to the diphenylacetic stopper. The methine proton of the stopper (α) apparently yields a single signal at *ca.* 5 ppm, but the peak deconvolution revealed the presence of three resonances consistent with the above mixture of two

rotaxanes.

5.2.4 UV-Vis characterisation

The interwoven structures were characterised by UV-Vis spectroscopy. The absorption spectrum of **DPU** is characterised by an intense band in the UV, with λ max = 260 nm and ε= $38000 M^{-1} cm^{-1}$. This band is red-shifted and less intense with respect to the parent calixarene bearing three phenylureido moieties (**TPU**).[5] These differences can be ascribed to the lack of one chromophoric unit, but also to the different conformations assumed by the molecule in solution. Upon titration of a solution of **DOV** with **DPU**, the solution turns red, and a characteristic charge-transfer band, with a maximum around 500 nm, appears. This band was also observed in related pseudorotaxanes based on **TPU** calixarenes, and it is ascribed to the charge transfer interaction between the bipyridinium unit and the aromatic rings of **DPU** (figure 5.25). The association constant determined by fitting the data with a 1:1 binding model is $3.2 \cdot 10^6 M^{-1}$. Indeed, the results of the thermodynamic investigation would suggest that the number of phenylurea moieties does not affect the stability of the pseudorotaxane. The corresponding rotaxane **33** was characterised by UV-Vis spectroscopy, and, as expected, displays the same features of the pseudorotaxane: an intense band in the UV region of the spectrum and a weak and broad one in the visible region. In line with the observations reported on the **DPU** ring component, the absorption coefficient at λmax is lower with respect to the parent rotaxanes bearing a **TPU** macrocycle.[6, 14]

To investigate the dynamics of the threading process, kinetic experiments have been performed using a stopped-flow apparatus. **DPU** and **DOV** have been mixed in equimolar amounts, and the absorption changes have been followed in the UV and visible regions (figure 5.25 and 5.26). The kinetic traces were fitted with an equilibrium model by fixing the equilibrium constant to the value determined upon titration. The rate constants for threading and dethreading resulted to be $3.4 \cdot 10^3 M^{-1} s^{-1}$ and $1.1 \cdot 10^{-3} M^{-1} s^{-1}$ respectively. Such values are three orders of magnitude lower than in the parent pseudorotaxane with **TPU**.[5, 15] Phenylurea moieties are good anion receptors,[16, 17] and it is well known that, in this kind of systems, they play a crucial role in driving the formation of the supramolecular adduct. In particular, it has been hypothesised the involve-

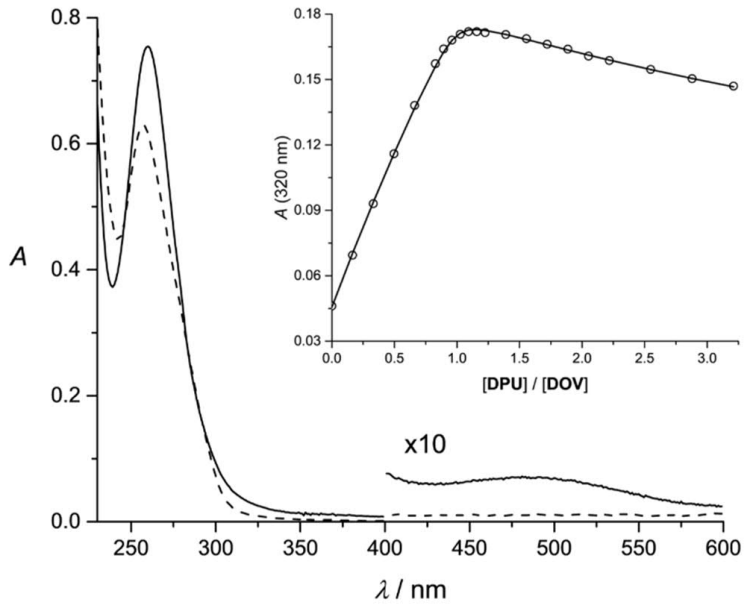

Figure 5.25: Sum of the absorption spectra (dashed line) and the absorption spectrum of the mixture (solid line) of CH_2Cl_2 solutions of **DOV** ($1.4 \cdot 10^{-5} M$) and **DPU** ($1.2 \cdot 10^{-5} M$). The inset shows the absorption changes at 320 nm together with the fitted curve upon titration of a $7.4 \cdot 10^{-5} M$ solution of **DOV** with concentrated **DPU**.

ment of a transition state wherein the counterions are no more paired with the bipyridinium unit, but they are already engaged with the calixarene.[5] The present results support this hypothesis, confirming the role of the phenylurea units in the stabilisation of the transition state. Since the electrochemical experiments have been performed in the presence of a 100-fold excess of tetrabutylammonium hexafluorophosphate ($TBAPF_6$) as supporting electrolyte (*vide infra*), also thermodynamic investigations have been performed in the same conditions. Indeed, the shape of the titration curve suggests a lower association, and the value of the stability constant determined by fitting the data with a 1:1 binding model is $7 \cdot 10^4 M^{-1}$. An effect of the concentration and the nature of the anions on the stability of the supramolecular complex is not unexpected, considering the double role played by the counterions in the formation and stabilisation of the pseudorotaxane:[5] not only the phenylurea moieties are good anion recep-

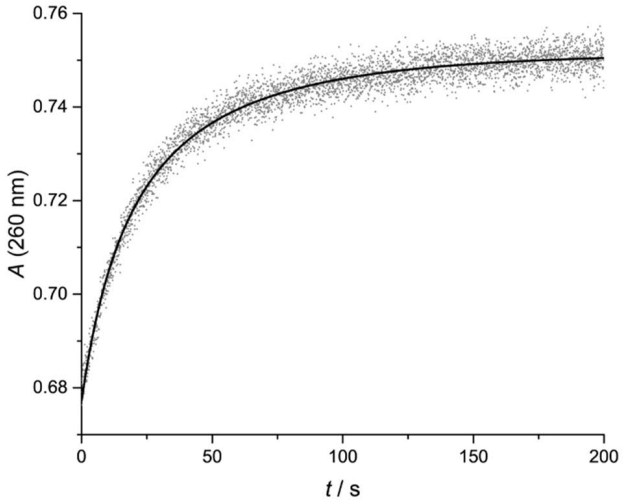

Figure 5.26: Absorption changes at 260 nm upon rapid mixing of equimolar amounts of **DOV** and **DPU**. The concentration of the reactants after mixing was $1.3 \cdot 10^{-5} M$.

tors, as mentioned above, but also the formation of the pseudorotaxane is in competition with the ion-pairing between the bipyridinium ion and its counteranions.[18, 19]

5.2.5 Electrochemical experiments

Cyclic voltammetry and differential pulse voltammetry experiments were performed in CH_2Cl_2 on the pseudorotaxane and rotaxane molecules, in the presence of a 100-fold excess of $TBAPF_6$ as supporting electrolyte. The bipyridinium moiety of **DOV** is characterised by two reversible and monoelectronic reduction processes, at $E_{1/2}$'= -0.27 V and $E_{1/2}$"= -0.83 V. When the viologen is included in the cavity of a calix[6]arene macrocycle, the reduction processes are shifted to more negative potential values, on account of the *host-guest* electron transfer interactions (Figure 11).[6, 14] Indeed, the cyclic voltammetric curves of rotaxane **33** are characterised by two quasi-reversible waves, with $E_{1/2}$' = -0.65 V and $E_{1/2}$" = -1.18 V. As observed for related **TPU**-based rotaxanes,[5] these processes are affected by slow heterogeneous electron-transfer kinetics. The pseudorotaxane ob-

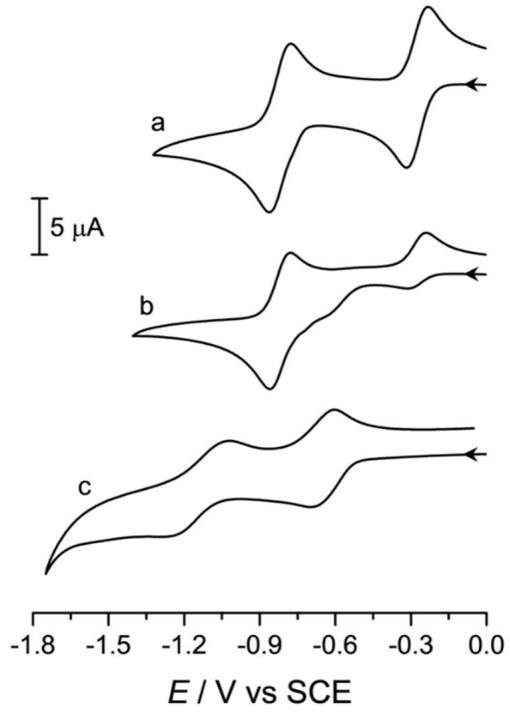

Figure 5.27: Cyclic voltammetric curves for the first and second reduction of the bipyridinium unit in (a) **DOV** (C = $3.0 \cdot 10^{-4} M$), (b) **DPU**⊃**DOV** (C = $3.0 \cdot 10^{-4} M$), and (c) **33** (C = $1.1 \cdot 10^{-4} M$) (CH_2Cl_2, 100-fold $TBAPF_6$, scan rate 100 mV/s).

tained by mixing **DPU** and **DOV** in equimolar amounts shows the typical cyclic voltammetry curves described by an electrochemical process followed by a chemical reaction (EC square scheme) (see figure 5.27).[5, 20, 21] A fraction of free **DOV** is still present in solution, as evidenced by the small cathodic process around -0.3 V. This is not unexpected from the association constant determined in the presence of an excess of PF_6^- ions and of the effect of the ion-pair dissociation on the formation of the complex.[18, 19] Indeed the intensity of this signal decreases when increasing the concentration of **DPU**. On the other hand, the encapsulated **DOV** is reduced at more negative potential values, but, after the first reduction, the complex dissociates and the second reduction process of free **DOV** is displayed at -0.82

V. Upon re-oxidation, only the processes of free **DOV** are observed: as a matter of fact, the first reduction process is characterised by a large separation between the cathodic and anodic peaks. This pattern can be modeled with an EC square scheme mechanism and is indicative of slow kinetics of the monoreduced bispyridinium.[5, 20, 21] Therefore, in analogy with parent **TPU**-based systems, pseudorotaxanes based on the **DPU** wheel can be disassembled by electrochemical reduction of the bipyridinium axle. The results of the electrochemical investigation suggest that the two different conformers behave in a similar way and the *1,2,3-alternate* and the *cone* conformation assumed by the interlocked structure cannot be distinguished in our experimental conditions.

5.3 Conclusions

The new calix[6]arene-based *hosts* **DPU** and **DSU**, functionalised with two phenylurea or phenylthiourea moieties in 1,4-diametral position have been synthesised and structurally characterised. Detailed NMR studies evidenced that in the solution of low polarity solvents, these *hosts* mainly adopt a *1,2,3-alternate* conformation. The determination of the crystal structure via X-ray diffraction on single crystals showed that **DPU** and **DSU** assume this conformation also in the solid-state. The ability of **DPU** to act as a wheel for the formation of pseudorotaxane and rotaxane species with viologen-based salts has been investigated in a solution of low polarity solvents through NMR, UV-vis and electrochemical measurements. The NMR studies evidenced that the formation of interwoven structures occurs with the *host* adopting both the *cone* and *1,2,3-alternate* conformation. Kinetic experiments showed that the rate constants for threading and dethreading of the viologen salts are three orders of magnitude lower with respect to the parent pseudorotaxane with **TPU** that, in low polarity solvents, is in the *cone* conformation. These findings thus account for the crucial role played by the number, orientation and reciprocal arrangement of the phenylurea binding groups in promoting the threading of the dicationic portion of the ion-paired viologen salts.

5.4 Experimental

5.4.1 Synthesis and Characterisation

Solvents were dried following standard procedures; all other reagents were of reagent grade quality, obtained from commercial sources and used without further purification. Chemical shifts are expressed in ppm using the residual solvent signal as an internal reference. Mass spectra were determined in ESI mode. Calix[6]arene **30**,[9] axles **DOV** [5] and **DDOV**[4, 6] ditosylate were synthesised according to reported procedures.

Calix[6]arene 31: In a 100 mL Schlenk flask, to a solution of calixarene **30** (1 g, 1 mmol) and 1-Iodooctane (0.72 g, 3 mmol) in dry acetonitrile (50 mL), K_2CO_3 (0.41 g, 3 mmol) was added. After two vacuum/nitrogen cycles, the flask was sealed and the heterogeneous reaction mixture was refluxed for 4 days. After cooling to room temperature, the solvent was evaporated to dryness under reduced pressure and the sticky residue was taken up with dichloromethane (50 mL) and with a 10% aqueous solution of HCl (30 mL). The separated organic phase was washed thrice with distilled water, dried over anhydrous Na_2SO_4, filtered and evaporated to dryness under reduced pressure. The solid residue was triturated with hot ethyl acetate to give, after Buchner filtration, 0.85 g of pure **31** (70% yield) as a white solid compound. ^{1}H NMR (400 MHz, $CDCl_3$): δ = 0.90 (t, 6 H, $^3J_{H,H}$ = 8 Hz, $-OCH_2CH_2(CH_2)_5CH_3$), 1.22, 1.3 - 1.5 and 1.6 (s, m, br. s, 56 H, tBu and $-OCH_2CH_2(CH_2)_5CH_3$), 1.9 (br. s, 4 H, $-OCH_2CH_2(CH_2)_5CH_3$), 3.0 (br. s, 12 H, $ArOCH_3$), 3.6 (br. d, 4 H, $Ar-CH_2-Ar$ (equatorial)), 3.92 (br. s, 8 H, $-OCH_2CH_2(CH_2)_5CH_3$ and $Ar-CH_2-Ar$), 4.3 (br. d, 4 H, $Ar-CH_2-Ar$ (axial)), 6.96 (s, 4 H, Ar-H), 7.22 (br. s, 4 H, Ar-H), 7.64 (br. s, 4 H, Ar-H); ^{13}C NMR (100 MHz, $CDCl_3$): δ = 14.0, 22.6, 26.2, 29.2, 29.5, 30.4, 30.7, 30.8, 31.3, 31.8, 34.2, 59.7, 74.0, 123.0, 126.4, 126.9, 132.1, 133.9, 136.5, 143.5, 146.4, 154.1, 160.0 ppm; ESI-MS(+): m/z (%) = 1253.9 (100) $[M+Na]^+$, 1254.9 (70) $[M+Na+1]^+$, 1269.9 (70) $[M+K]^+$, 1270.9 (60) $[M+K+1]^+$.

General procedure for the synthesis of *hosts* DPU and DSU: In a two-neck flask kept under inert atmosphere, to a solution of **31** (0.7 g, 0.57 mmol) in ethanol (150 mL), hydrazine monohydrate (1.42 g, 28 mmol)

and a tip of spatula of 10% Pd/C catalyst were added. The resulting mixture was refluxed for 48 h and then filtered, still warm and under an inert atmosphere, through a celite pad to remove the palladium catalyst. The filtered solution was evaporated to dryness under reduced pressure. The residue was diluted in dichloromethane (50 mL), and the resulting organic phase was washed thrice with water to remove the excess of hydrazine. The separated organic phase was dried over anhydrous $CaCl_2$, filtered and evaporated to dryness under reduced pressure. The residue was dissolved in anhydrous dichloromethane (50 mL) and placed in a two-neck flask kept under an inert atmosphere. To the resulting homogeneous solution, phenyl isocyanate (0.17 g, 1.4 mmol) or phenyl isothiocyanate (0.18 g, 1.4 mmol) was added. The reaction mixture was stirred at room temperature for 24 h; then the solvent was removed under reduced pressure.

DPU: purification of the residue by column chromatography (eluent n-hexane: ethyl acetate 75 : 25) afforded DPU in 80% yield as a white solid compound. Mp. 236 - 238 °C; ^{1}H NMR (400 MHz, $CDCl_3/CD_3OD$ = 10/1): δ = 0.8 (t, 6 H, $^3J_{H,H}$ = 8 Hz, $-OCH_2CH_2(CH_2)_5CH_3$), 1.1 (s, 36 H, tBu), 1.2 - 1.3 (m, 20 H, $-OCH_2CH_2(CH_2)_5CH_3$), 1.4 - 1.5 (m, 4 H, $-OCH_2CH_2(CH_2)_5CH_3$), 1,7 - 1.8 (m, 4 H, $-OCH_2CH_2(CH_2)_5CH_3$), 2.8 (br. s, 12 H, $ArOCH_3$), 3.5 (br. d, 4 H, Ar-CH2-Ar (equatorial)), 3.8 (br. S, 8 H, $-OCH_2CH_2(CH_2)_5CH_3$ and $Ar-CH_2-Ar$), 4.2 (br. d, 4 H, $Ar-CH_2-Ar$ (axial)), 6.7 (br. s, 4 H, Ar-H), 6.8 (br. s, 4 H, Ar-H), 6.9 (m, 2 H, Ar-H), 7.2 (br. s, 8 H, Ar-H), 7.3 (br. s, 4 H, Ar-H); ^{1}3C NMR (100 MHz, $CDCl_3/CD_3OD$ = 10/1): δ = 14.0, 22.6, 26.3, 29.3, 29.6, 30.5, 31.2, 31.8, 34.1, 59.7, 60.2, 73.7, 119.0, 121.1, 122.5, 122.9, 126.3, 126.7, 126.9, 128.7, 132.1, 132.8, 134.1, 135.4, 136.5, 138.9, 143.5, 146.4, 146.6, 150.4, 152.6, 154.1 ppm. HR-MS(+): m/z (%) = 1409.9155 (9) $[M+H]^+$, 1426.9436 (100) $[M+NH_4]^+$, 1431.8998 (45) $[M+Na]^+$.

DSU: crystallisation of the crude mixture from Ethyl Acetate afforded DSU in 69% yield as a white solid compound. ESI-MS(+): m/z (%) = 1441.8 $[M+H]^+$, 1465.0 $[M+Na]^+$, 1480.7 $[M+K]^+$. ^{1}H NMR (400 MHz, $CDCl_3$): δ = 7.35 - 7.13 (m, 18 H), 6.95 (br.s, 3H), 6.81 (br.s, 1H), 6.67 (br.s, 3H), 4.33 (d, 3H, ^{2}J = 14.5 Hz), 4.25 (d, 1H, ^{2}J = 14.2 Hz), 4.02 - 3.88 (m, 4H), 3.81 - 3.67 (br.s, 4H), 3.57 (d, 4H, ^{2}J = 15.4), 2.92 (br.s,

12H), 2.0 - 1.9 (m, 6H), 1.85 - 1.76 (m, 1.5H), 1.66 - 1.54 (m, 3.5H), 1.53 - 1.40 (m, 50H), 0.93 - 0.86 (m, 6H); ^{1}3C NMR (100 MHz, $CDCl_3$): 179.0, 154.1, 151.5, 146.5, 146.1, 138.0, 136.9, 133.8, 133.4, 132.6, 131.4, 129.1, 128.8, 126.8, 126.5, 126.2, 125.0, 123.2, 73.9, 60.6, 59.7, 34.1, 31.9, 31.4, 31.2, 30.6, 29.6, 29.3, 26.2, 22.7, 14.1.

Rotaxane 33: Calix[6]arene **DPU** (0.05 g, 0.035 mmol) was dissolved in dry dichloromethane and 1,1'-bis(12-hydroxydodecyl)-4,4'-bipyridinium ditosylate **DDOV** (0.034 g, 0.039 mmol) was added. The solution was stirred at room temperature for 12 hours, filtered to remove the undissolved salt, and then diphenylacetylchloride (0.021 g, 0.089 mmol) and triethylamine (0.011 g, 0.11 mmol) were added. The reaction mixture was stirred at room temperature overnight. The solvent was evaporated under reduced pressure, and the crude product was purified by column chromatography (eluent: CH_2Cl_2/CH_3OH = 92/2). To assure the total exchange of the viologen counteranions as tosylates, the solid residue recovered from the chromatographic separation was dissolved in 25 mL of dichloromethane and the resulting organic phase was washed thrice with a saturated solution of sodium tosylate and twice with distilled water. After evaporation of the organic phase under reduced pressure, rotaxane **33** was isolated in 48 % yield as a red solid compound. HR-MS (+): m/z (%) = 1161.7550 (78) $[M\text{-}2TsO]^{2+}$.

X-ray data collection and crystal structure determination: The crystal structures of the methanol/chloroform (**I-III**) and ethyl acetate (**IV**) solvates of **DPU** were determined by X-ray diffraction methods. Crystal data and experimental details for data collection and structure refinement are reported in Tables S1-S2 of the SI. Intensity data and cell parameters were recorded at 100(2) K at the ELETTRA Synchrotron Light Source (CNR Trieste, strada statale 14, Area Science Park, 34149, Basovizza, Trieste, Italy) for **I-III**, and at 150(2) K on a Bruker D8 Venture PhotonII diffractometer equipped with a CCD area detector, using a CuKα radiation (λ = 1.54178) for **IV**. The raw frame data were processed using the program package CrysAlisPro 1.171.38.41[22] for **I-III**, and the programs SAINT and SADABS[23] for **IV**. The structures were solved by Direct Methods using the SIR97 program[24] and refined on F_o^2 by full-matrix least-

squares procedures, using the SHELXL-2014/7[25] program in the WinGX suite v.2014.1.[26] All non-hydrogen atoms were refined with anisotropic atomic displacements, except for some disordered alkyl chains or solvent molecules. The carbon-bound and the nitrogen-bound H atoms were placed in calculated positions and refined isotropically using a riding model with C-H ranging from 0.93 to 0.97 Å and Uiso(H) set to 1.2–1.5Ueq(C), N-H equal to 0.86 and Uiso(H) set to 1.2Ueq(N), and O-H equal to 0.82 and Uiso(H) set to 1.5Ueq(O). The weighting schemes used in the last cycle of refinement were $\omega = 1/\ [\sigma^2 F_0^2 + (0.4534P)^2]$ and $\omega = 1/\ [\sigma^2 F_0^2 + (0.5768P)^2]$ where P = $(F_0^2 + 2F_c^2)/3$, for **I-III** and **IV**, respectively. Crystallographic data for the structures reported have been deposited with the Cambridge Crystallographic Data Centre as supplementary publication no. CCDC-1894692-1894693 and can be obtained free of charge on application to the CCDC, 12 Union Road, Cambridge, CB2 1EZ, UK (fax: +44-1223-336-033; e-mail deposit@ccdc.cam.ac.uk or http://www.ccdc.cam.ac.uk).

UV-Vis absorption spectroscopy: All spectroscopic measurements were performed on air-equilibrated CH_2CH_2 (Uvasol) solutions at room temperature in 1 cm path-length quartz cuvettes. UV-vis spectra were recorded with a Cary 300 (Agilent) spectrophotometer. Spectrophotometric titrations were performed adding a concentrated solution of the *host* to a more diluted solution of the *guest*. The apparent stability constants of the pseudorotaxanes were obtained by fitting the absorbance changes with software SPECFIT/32,[27] according to a 1:1 binding model.

Stopped-flow kinetics: Threading kinetics were investigated on air-equilibrated CH_2CH_2 (Uvasol) solutions at room temperature using a stopped-flow spectrophotometer equipped with a 1 cm pathlength cell and a driving ram for the mixing system at the N_2 pressure of 8.5 bar. Under these conditions, the time required to fill the cell is lower than 2 ms. The resulting absorption changes were then analysed with software SPECFIT/32[27] to obtain the rate constants for the threading process, according to a mixed order (second order threading–first order dethreading) kinetic model.

Electrochemical Measurements: Cyclic voltammetric (CV) experiments were carried out in argon-purged dry CH_2CH_2 (Sigma-Aldrich) with an Au-

tolab 30 multipurpose instrument interfaced to a PC. The working electrode was a glassy carbon electrode (Amel, 0.07 cm^2), carefully polished with an alumina-water slurry on a felt surface, immediately before use. The counter electrode was a Pt wire, separated from the solution by a frit, and an Ag wire was employed as a quasi-reference electrode. Ferrocene was present as an internal standard. Tetrabutylammonium hexafluorophosphate was added in a 100-fold proportion with respect to the sample concentration, as supporting electrolyte. Cyclic voltammograms were obtained at sweep rates varying from 0.05 to $5Vs^{-1}$. The IR compensation implemented within the software was employed to minimise the resistance of the solution. In any instance, the full electrochemical reversibility of the voltammetric wave of ferrocene was taken as an indicator of the absence of uncompensated resistance effects.

Bibliography

(1) Kassem, S.; Leeuwen, T. v.; S. Lubbe, A.; R. Wilson, M.; L. Feringa, B.; A. Leigh, D. *Chem. Soc. Rev.* **2017**, *46*, 2592–2621.

(2) Kay, E. R.; Leigh, D. A.; Zerbetto, F. *Angew. Chem. Int. Ed.* **2007**, *46*, 72–191.

(3) Balzani, V.; Credi, A.; Venturi, M. *Chem. Eur. J.* **2002**, *8*, 5524–5532.

(4) Arduini, A.; Ferdani, R.; Pochini, A.; Secchi, A.; Ugozzoli, F. *Angew. Chem. Int. Ed.* **2000**, *39*, 3453–3456.

(5) Credi, A.; Dumas, S.; Silvi, S.; Venturi, M.; Arduini, A.; Pochini, A.; Secchi, A. *J. Org. Chem.* **2004**, *69*, 5881–5887.

(6) Arduini, A.; Bussolati, R.; Credi, A.; Pochini, A.; Secchi, A.; Silvi, S.; Venturi, M. *Tetrahedron* **2008**, *64*, 8279–8286.

(7) Ugozzoli, F.; Massera, C.; Arduini, A.; Pochini, A.; Secchi, A. *CrystEngComm* **2004**, *6*, 227–232.

(8) Van Duynhoven, J. P. M.; Janssen, R. G.; Verboom, W.; Franken, S. M.; Casnati, A.; Pochini, A.; Ungaro, R.; de Mendoza, J.; Nieto, P. M. *J. Am. Chem. Soc.* **1994**, *116*, 5814–5822.

(9) De Mendoza, J.; Carramolino, M.; Cuevas, F.; Nieto, P. M.; Prados, P.; Reinhoudt, D. N.; Verboom, W.; Ungaro, R.; Casnati, A. *Synthesis* **1994**, *1994*, 47–50.

(10) Arduini, A.; Calzavacca, F.; Pochini, A.; Secchi, A. *Chem. Eur. J.* **2003**, *9*, 793–799.

(11) Gasparro, F. P.; Kolodny, N. H. *J. Chem. Educ.* **1977**, *54*, 258.

(12) Zanichelli, V.; Bazzoni, M.; Arduini, A.; Franchi, P.; Lucarini, M.; Ragazzon, G.; Secchi, A.; Silvi, S. *Chem. Eur. J.* **2018**, *24*, 12370–12382.

(13) Zanichelli, V.; Ragazzon, G.; Orlandini, G.; Venturi, M.; Credi, A.; Silvi, S.; Arduini, A.; Secchi, A. *Org. Biomol. Chem.* **2017**, *15*, 6753–6763.

(14) Zanichelli, V.; Ragazzon, G.; Arduini, A.; Credi, A.; Franchi, P.; Orlandini, G.; Venturi, M.; Lucarini, M.; Secchi, A.; Silvi, S. *Eur. J. Org. Chem.* **2016**, *2016*, 1033–1042.

(15) Arduini, A.; Bussolati, R.; Credi, A.; Secchi, A.; Silvi, S.; Semeraro, M.; Venturi, M. *J. Am. Chem. Soc.* **2013**, *135*, 9924–9930.

(16) Amendola, V.; Fabbrizzi, L.; Mosca, L. *Chem. Soc. Rev.* **2010**, *39*, 3889–3915.

(17) Pescatori, L.; Arduini, A.; Pochini, A.; Ugozzoli, F.; Secchi, A. *Eur. J. Org. Chem.* **2008**, *2008*, 109–120.

(18) Jones, J. W.; Gibson, H. W. *J. Am. Chem. Soc.* **2003**, *125*, 7001–7004.

(19) Huang, F.; Jones, J. W.; Slebodnick, C.; Gibson, H. W. *J. Am. Chem. Soc.* **2003**, *125*, 14458–14464.

(20) Kaifer, A.; Gómez-Kaifer, M., *Supramolecular Electrochemistry*; Wiley: 2008.

(21) Bard, A. J.; Faulkner, L. R., *Electrochemical Methods: Fundamentals and Applications, 2nd Edition*; John Wiley & Sons: 2000.

(22) *CrysAlisPro*; Rigaku Oxford Diffraction: 2015.

(23) Sheldrick, G. M., *SADABS v2.03: Area-Detector Absorption Correction*; University of Göttingen: Germany, 1999.

(24) Altomare, A.; Burla, M. C.; Camalli, M.; Cascarano, G. L.; Giacovazzo, C.; Guagliardi, A.; Moliterni, A. G. G.; Polidori, G.; Spagna, R. *J Appl Cryst* **1999**, *32*, 115–119.

(25) Sheldrick, G. M. *Acta Cryst A* **2008**, *64*, 112–122.

(26) Farrugia, L. J. *J Appl Cryst* **2012**, *45*, 849–854.

(27) Binstead, R. A., *SPECFIT/32, fitting software, Spectrum Software Associates, Chapel Hill, 1996.* 1996.

Acknowledgements

First and foremost, I want to thank my supervisor prof. Arturo Arduini for guiding me through this PhD and for sharing his experience with me. A special thank to prof. Andrea Secchi for all the suggestions, the encouragement and the valuable NMR tips. My highest gratitude goes to the people who worked with me to this project, in particular prof. Francesca Terenziani and Giuseppe for the help with UV-Vis and fluorescence measurements, the Credi group of University of Bologna for the electrochemical measurements, prof. Chiara Massera for the crystallographic data. Thanks to the people working at the CIM in Parma, Domenico, Stefano and Massimo, for their support in my hours of need. A special thank to prof. Michel Luhmer who *host*ed me at his group at CIREM (ULB), where I carried out most of the NMR studies reported in chapter 4 and many more. Thanks to Michel and the people who welcomed and supported me in Brussels, in particular prof. Ivan Jabin and Gael. They all helped me to grow up as a person and as a scientist. Thanks to Beatrice and to all the lab49 group who shared with me all the happy and though moments of these three years, in particular thanks to Francesco Rispoli who also gave an important contribution to this work. Thanks to the friends who supported me in this period in particular Francesca, Chiara and Martina. A special thank to those who found some time to check my thesis: Anna, Cecilia and Spez; and all those who shared lunch time with me. Thanks to my family for always being by my side and to Francesco for being here and support me.